Experimental and Modelling Studies on the Properties of Natural Rubber Reinforced with Conductive Hybrid Filler Systems

Thesis submitted in partial fulfillment of

Doctor of Philosophy

in

Chemistry

under the Faculty of Science

submitted to

University of Calicut

by

ABHISHA V S

Supervisor

Dr. Ranimol Stephen

Department of Chemistry
St. Joseph's College (Autonomous), Devagiri,
Calicut-673 008, Kerala, India.

January 2024

DECLARATION

I hereby declare that the work presented in the thesis entitled **Experimental and Modelling Studies on the Properties of Natural Rubber Reinforced with Conductive Hybrid Filler Systems** is based on the original work done by me under the guidance of **Dr. Ranimol Stephen,** Associate Professor, Department of Chemistry, St. Joseph's College (Autonomous), Devagiri, Calicut and has not been included in any other thesis submitted previously for the award of any degree. The contents of the thesis are undergone plagiarism check using iThenticate software at C.H.M.K. Library, University of Calicut, and the similarity index found within the permissible limit. I also declare that the thesis is free from AI generated contents.

Abhisha V S

Supervising Teacher
Dr. RANIMOL STEPHEN
Associate Professor
Department of Chemistry
St. Joseph's College (Autonomous) Devagi
Calicut-673 008

Calicut
16th June 2024

DR. RANIMOL STEPHEN
ASSOCIATE PROFESSOR
DEPARTMENT OF CHEMISTRY
ST. JOSEPH'S COLLEGE (AUTONOMOUS), DEVAGIRI
CALICUT- 673 008
Tel: 9446288448
E-mail: ranistephen@gmail.com

CERTIFICATE

This is to certify that the thesis entitled **Experimental and Modelling Studies on the Properties of Natural Rubber Reinforced with Conductive Hybrid Filler Systems** is an authentic record of the research work carried out by **Ms. Abhisha V S**, under my supervision and guidance in partial fulfilment of the requirements for the award of the degree of **Doctor of Philosophy in Chemistry** under the **Faculty of Science,** University of Calicut, Kerala. The work presented in this thesis has not been submitted for any other degree or diploma earlier. It is also certified that Ms. Abhisha V S has fulfilled the course requirements and qualified the coursework examination for the PhD degree of the University. I also certify that the corrections/suggestions recommended by the adjudicators have been incorporated in the thesis.

Ranimol Stephen

Calicut

16th June 2024

ACKNOWLEDGEMENT

I am genuinely grateful for the opportunities and circumstances that have allowed me to complete my dream. The untiring support from the incredible individuals around me has been truly god-like, and I am profoundly grateful for their impact on this journey.

First and foremost, I express my deepest gratitude to my guide, Dr. Ranimol Stephen, Associate Professor, Department of Chemistry, St. Joseph's College (Autonomous), Devagiri, Calicut, for her invaluable guidance and unwavering support throughout the entire process of completing this thesis. Her remarkable patience and problem-solving abilities have been critical in navigating challenges. She seamlessly put on multiple roles as an exceptional academic mentor and a pillar of support in my personal life, offering motivation and encouragement when I needed it most. I have learned a tremendous amount from her wealth of knowledge. I am truly grateful for her guidance, mentorship, and warmth, making this academic endeavour a rich and rewarding experience.

I am very grateful to the Management, the Principal, Dr. Satheesh George and the former Principal, Dr. Sibichen M Thomas, Dr. Sabu K Thomas, Dr. Jose John Mallikasseri and Dr. Boby Jose for their permission and valuable help and encouragement during my research tenure. I sincerely acknowledge and remember the support from the late Fr. Joseph Paikada CMI. I also thank Mr. Dominic and other office staff of St. Joseph's College (Autonomous), Devagiri for their support. I acknowledge the librarian and all the staff of St. Joseph's College (Autonomous, Devagiri Library for their help during the research programme.

I also wish to place on record my sincere thanks to Dr. Tania Francis, Head of the Department, and all my teachers and non-teaching staff of the Department of Chemistry, St. Joseph's College (Autonomous), Devagiri for their good wishes, support and generosity. I extend my heartfelt appreciation to my dedicated teachers, Dr. Jose John Mallikasseri, Dr. Joy Joseph, Dr. Babu I Maliakkal and Mr.Varkey Pattani, who have been instrumental in shaping my academic journey. Their kind words, blessings and warm support have helped me through my research journey. A special note of gratitude to Sreejith sir, Yoosuf sir and Anwar sir for their motivation and kind words that inspired my journey into research.

I am also thankful to Prof. (Dr.) Sabu Thomas for his expertise and feedback during the various stages of this research, which has been influential in shaping the thesis.

I also thank Mr. Sisanth KS, Ms. Prajitha V, Mr. Anu A S and Dr. Hanna J Maria for their invaluable help in characterising samples.

I want to extend my sincere gratitude to the staff of CFSC Manjeri, STIC CUSAT, Rubber Park Ernakulam, SAIF MGU, CSIF University of Calicut, IISER Trivandrum and CIF IIT Palakkad for helping to do various characterisations on time. I express my gratitude to Dr. Selvin P Thomas, Dr. Kishor Kumar Sadasivuni, and Dr. Mohamad Shahin Thayyil for their invaluable contributions in terms of resources and collaborative efforts.

Special thanks to the University Grants Commission (UGC), New Delhi, for the Junior Research Fellowship (JRF), which made this research possible.

I would like to acknowledge the support of research scholars, Dr. Meril Shelly, Dr. Anju K Sasidharan, Ms. Annie Stephy, Ms. Anjana K R, Ms. Sini KS, Ms. Farsana O P, Ms Jija Thomas, Ms. Vinatha Asokan, Ms. Reshma S Philip, Mr. Aswindas T P and Ms. Remya. I am also grateful for the caring, understanding and encouragement from Dr. Swapna V P, Ms. Theertha T, Ms. Amrutha K and Ms. Jeeshma R during the challenging times of my research period. I also thank Mr. Vincent Joseph for all his support and help.

I would like to mention my family's constant support and encouragement, without whom this research would not have been possible. I would like to thank my family, loving parents, brother, and mother-in-law, whose solid support and love have been my rock throughout this journey. Most importantly, my husband's encouragement and understanding sustained me during the late nights and challenging moments. Your belief in me gave me the strength to persevere. Thank you for creating a home environment that allowed me the space and time to focus on my studies. A special acknowledgement to my daughter Deva, who joined me halfway through this academic journey and remained my greatest motivation. Her presence motivated me to work hard to achieve my goals.

Thank you to everyone who played a role in making this thesis a reality.

ABHISHA V S

.....to us

ABSTRACT

Conductive elastomers have significant technological promise in the current world. The work focuses on the fabrication of high-performance conductive rubber composites by integrating natural rubber with a combination of carbon-based conductive fillers and ionic liquid-modified fillers. Unlike traditional metallic conductors, these elastomers offer advantages such as easy processability, flexibility, and cost-effectiveness.

The primary objective of this work is to enhance the electrical properties of natural rubber, focusing on improving interfacial interaction and dispersion of hybrid fillers within the rubber matrix. This is achieved through the incorporation of ionic liquid modification and the utilisation of two distinct processing techniques. The chosen carbon-based fillers include conductive carbon black, carbon nanotubes, and reduced graphene oxide.

The comprehensive investigation includes experimental and theoretical analysis, exploring dielectric, electrical and mechanical properties. The study probes into the reinforcement mechanisms of fillers in the rubber matrix, examining physical and chemical interactions. Viscoelastic properties and solvent transport characteristics are thoroughly examined, and the EMI shielding efficiency of the composites is measured. Thermal stability is evaluated via thermogravimetric analysis, with experimental findings compared to kinetic models to unveil underlying mechanisms. Additionally, this research involves the synthesis and characterisation of laboratory-synthesised thermally reduced graphene oxide. A comparative analysis is conducted on the properties of the natural rubber hybrid filler system, with carbon nanotubes and conductive carbon black, alongside both laboratory-synthesised and purchased reduced graphene oxide.

In essence, this work contributes to the advancement of conductive elastomers, shedding light on their potential applications as electromagnetic interference shielding devices. The findings offer a glimpse into the future of flexible, efficient, cost-effective conductors.

Keywords: Natural rubber, Conductive elastomer, Conductive fillers, Dielectric permittivity, EMI shielding

സംഗ്രഹം

ഇന്നത്തെ ലോകത്ത്, കണ്ടക്റ്റീവ് എലാസ്റ്റോമറുകൾക്ക് വളരെയധികം പ്രാധാന്യമുണ്ട്. കാർബൺ അധിഷ്ഠിത കണ്ടക്റ്റീവ് ഫില്ലറുകളും അയോണിക് ലിക്വിഡ് ഉപയോഗിച്ചു പരിഷ്ക്കരിച്ച ഫില്ലറുകളും പ്രകൃതിദത്ത റബ്ബറിൽ സംയോജിപ്പിച്ച്, മികച്ച പ്രകടനമുള്ള കണ്ടക്റ്റീവ് റബ്ബർ സംയുക്തങ്ങളുടെ നിർമ്മാണമാണ് ഈ ഗവേഷണത്തിന്റെ ഉദ്ദേശം. പരമ്പരാഗത മെറ്റാലിക് കണ്ടക്ടറുകളിൽ നിന്ന് വ്യത്യസ്തമായി, കണ്ടക്റ്റീവ് എലാസ്റ്റോമറുകൾ കുറഞ്ഞ ചിലവ്, വഴക്കം, എളുപ്പമുള്ള പ്രോസസ്സബിലിറ്റി തുടങ്ങിയ ഗുണങ്ങൾ വാഗ്ദാനം ചെയ്യുന്നു.

പ്രകൃതിദത്ത റബ്ബറിനുള്ളിൽ ഹൈബ്രിഡ് ഫില്ലറുകൾ തമ്മിലുള്ള ഇന്റെറാക്ഷൻ, ഡിസ്പർഷൻ എന്നിവ മെച്ചപ്പെടുത്തുന്നതിൽ ശ്രദ്ധ കേന്ദ്രീകരിച്ച്, പ്രകൃതിദത്ത റബ്ബറിന്റെ വൈദ്യുത ഗുണങ്ങൾ വർദ്ധിപ്പിക്കുക എന്നതാണ് ഈ ഗവേഷണത്തിന്റെ പ്രാഥമിക ലക്ഷ്യം. അയോണിക് ലിക്വിഡ് ഉപയോഗിച് പരിഷ്കരിച്ച ഫില്ലറുകളുടെയും, രണ്ട് വ്യത്യസ്ത പ്രോസസ്സിംഗ് സാങ്കേതിക വിദ്യകളുടെ ഉപയോഗത്തിലൂടെയും ഇതിനായി ശ്രമിക്കുന്നു. തിരഞ്ഞെടുത്ത കാർബൺ അധിഷ്ഠിത ഫില്ലറുകളിൽ കണ്ടക്റ്റിവ് കാർബൺ ബ്ലാക്ക്, കാർബൺ നാനോട്യൂബുകൾ, റെഡ്യൂസ്ഡ് ഗ്രാഫീൻ ഓക്സൈഡ് എന്നിവ ഉൾപ്പെടുന്നു.

സമഗ്രമായ ഈ ഗവേഷണത്തിൽ പ്രകൃതിദത്ത റബ്ബർ സംയുക്തങ്ങളുടെ ഗുണങ്ങളുടെ പരീക്ഷണാത്മകവും സൈദ്ധാന്തികവുമായ വിശകലനം ഉൾപ്പെടുന്നു. പ്രധാനമായും സംയുക്തങ്ങളുടെ ഇലക്ട്രോ മാഗ്നെറ്റിക് ഇന്റെർഫെറെൻസ് (ഇ. എം. ഐ.) ഷീൽഡിംഗ് കാര്യക്ഷമതയുടെ പഠനവും വിശകലനവും ചെയ്തിട്ടുണ്ട്. കൂടാതെ, ലബോറട്ടറിയിൽ ഉത്പാദിപ്പിച്ച റെഡ്യൂസ്ഡ് ഗ്രാഫീൻ ഓക്സൈഡിന്റെ സ്വഭാവ വിശകലനം ഉൾപ്പെടുത്തുകയും ചെയ്യുന്നു. കാർബൺ നാനോട്യൂബുകളും കണ്ടക്റ്റിവ് കാർബൺ ബ്ലാക്കും ഉൾപ്പെടുത്തിയ പ്രകൃതിദത്ത റബ്ബർ സംയുക്തങ്ങളിൽ ഇവ സമന്വയിപ്പിച്ച്, അവയുടെ ഗുണങ്ങളെക്കുറിച്ച് താരതമ്യ വിശകലനവും നടത്തിയിരിക്കുന്നു. സാരാംശത്തിൽ, കാര്യക്ഷമവും ചെലവ് കുറഞ്ഞതുമായ ഇ. എം. ഐ. ഷീൽഡിംഗ് ഉപകരണങ്ങളുടെ നിർമ്മാണത്തിനായി ഈ ഗവേഷണ പ്രബന്ധത്തിൽ പ്രതിപാദിച്ചിരിക്കുന്ന കണ്ടക്റ്റിവ് എലാസ്റ്റോമറുകൾ ഉപയോഗിക്കാവുന്നതാണ്.

CONTENTS

Symbols and Abbreviations

AC	-	Alternating current
ATR	-	Attenuated total reflectance
C	-	Volume fraction of constrained region
CB	-	Carbon black
CBS	-	N-cyclohexyl-2-benzothiazolesulpenaimde
CCB	-	Conductive carbon black
CNT	-	Carbon nanotubes
CR	-	Chloroprene
D	-	Diffusion coefficient
dB	-	Decibel
DC	-	Direct current
DMA	-	Dynamic mechanical analysis
dNm	-	Deci newton metre
DTG	-	Differential thermogram
E_a	-	Activation energy
E_m	-	Modulus of unfilled NR
EMI	-	Electromagnetic interference
EMIC	-	1-ethyl-3-methylimidazolium chloride
EPDM		Ethylene propylene diene monomer
FESEM	-	Field emission scanning electron microscopy
FKM	-	Viton
FTIR	-	Fourier transform infrared spectroscopy
GO	-	Graphene oxide
IIR	-	Butyl rubber
IL	-	Ionic liquid
m_0	-	Mass of the sample before immersion
MBT	-	2-mercaptobenzothiazole
M_H	-	Maximum torque
M_L	-	Minimum torque
MPa	-	Mega pascal
M_s	-	Molecular mass of solvent
m_t	-	Mass of the sample at the time t of immersion
MWCNT	-	Multi-walled carbon nanotubes
N	-	Entanglement density
NR	-	Natural rubber
P	-	Permeability coefficient
phr	-	Parts per hundred rubber
P_I	-	Incident power

P_T	-	Transmitted power
Q	-	Swell ratio
Q_∞	-	Equilibrium absorption
Q_t (%)	-	Mol % uptake of solvent per unit mass of polymer
r	-	Reinforcing efficiency
R	-	Universal gas constant
RBM	-	Radial breathing mode
RGO	-	Reduced graphene oxide
S	-	Sorption coefficient
SAED	-	Selected area electron diffraction
SE_A	-	Shielding by absorption
SEM	-	Scanning electron microscopy
SE_M	-	Shielding by mutiple reflections
SE_R	-	Shielding by reflection
SE_T	-	Total shielding effectiveness
SWCNT	-	Single walled carbon nanotubes
syTRGO	-	Synthesised thermally reduced graphene oxide
T	-	Temperature
T_{90}	-	Cure time
TEM	-	Transmisssion electron microscopy
TGA	-	Thermogravimetric analysis
T_{max}	-	Temperature of maximum weightloss
TRGO	-	Thermally reduced graphene oxide
UV	-	Ultra-violet
V	-	Voltage
V_{rf}	-	Volume fraction of rubber in the solvent- swollen filled sample
V_s	-	Molar volume of solvent
W_1	-	Weight of the sample after swelling
W∞	-	Weight of the sample at equilibrium swelling
Wo	-	Weight of the sample before swelling
XPS	-	X-ray photoelectron spectroscopy
XRD	-	X-ray diffraction
Z	-	Impedance
z	-	Weight fraction of filler
α	-	Swelling coefficient
α_f	-	Westlinning-Wolff constant
β	-	Heating rate
ΔM	-	Torque difference
δp	-	Solubility paramter of polymer
δs	-	Solubility paramter of solvent

ε'	-	Dielectric permittivity
ε''	-	Dielectric loss
ε''_D	-	Dielectric loss due to dipole orientations
ε''_{DC}	-	Dielectric loss due to DC conductance
ε''_{MW}	-	Dielectric loss due to interfacial polarizations
ε_o	-	Permittivity of air
ν	-	Crosslink density
ρ_r	-	Density of polymer
ρ_s	-	Density of solvent
σ	-	Tensile strength
σ_{AC}	-	AC conductivity
σ_{DC}	-	DC conductivity
ϕ	-	Volume fraction of filler
χ	-	Interaction parameter

Preface

The main focus of the work is the fabrication of conductive elastomer composites using natural rubber (NR) integrated with carbon-based conductive fillers, and ionic liquid (IL) modified fillers, with the primary goal of enhancing the electrical properties of NR. A comprehensive analysis of the dielectric and electrical properties of these composites is conducted, evaluating their potential as electromagnetic interference (EMI) shielding devices. Furthermore, the study explores the mechanical properties, examining the reinforcement mechanism of fillers in the NR matrix through physical and chemical interactions. Viscoelastic properties and solvent transport characteristics of the composites are examined. The thermal stability of the composites is assessed using thermogravimetric analysis. Experimental findings are compared with kinetic models to gain insights into the underlying mechanisms. Additionally, laboratory-synthesised thermally reduced graphene oxide is prepared and characterised. A comparative analysis is performed on the properties of the NR hybrid filler system, incorporating both carbon nanotubes (CNT) and conductive carbon black (CCB) with laboratory-synthesised reduced graphene oxide (syTRGO) and commercially available reduced graphene oxide (RGO).

In **Chapter 1**, a concise exploration is undertaken on conductive elastomers, specifically focusing on NR and diverse carbon-based conductive fillers. A comprehensive literature review explores the incorporation of conductive fillers in NR composites. Additionally, the discussion extends to the motivation behind the present research and identifies areas of gap within the existing literature.

Chapter 2 discusses the materials and fabrication methods used for making NR composites. The specifications of conductive fillers and IL employed for the present study are discussed. The detailed procedure for synthesising thermally reduced graphene oxide (syTRGO) and fabrication of NR composites are included. It also details the characterisation techniques used to analyse the properties of fillers and NR composites.

Chapter 3 discusses the curing characteristics of NR composites filled with carbon-based conductive fillers and IL-modified fillers. The characterisation of the IL-

modified fillers and the filler-incorporated composites are also discussed. Rheological analysis on the NR composites suggests the reinforcement effect of rubber matrix in the presence of filler.

Chapter 4 discusses the mechanical properties, morphological analysis and dynamic mechanical properties of NR filled with carbon-based conductive fillers and IL-modified fillers. Experimental and theoretical studies of the mechanical properties were done.

Chapter 5 focuses on the dielectric properties, EMI shielding effectiveness and DC and AC conductivity of the NR hybrid filler systems. These properties are evaluated in terms of the homogeneous dispersion of fillers and the physicochemical interfacial interactions established between the fillers and the polymer matrix.

Chapter 6 focuses on the solvent transport properties of NR hybrid filler systems as a function of filler concentration and its comparison. Experimentally obtained transport data are evaluated using different kinetic models.

Chapter 7 evaluates the thermal degradation stability of NR hybrid filler systems using thermogravimetric analysis (TGA) and discusses the thermal degradation mechanisms using various kinetic models.

Chapter 8 explores the morphological and structural characteristics of thermally reduced graphene oxide, which is synthesised in the laboratory using Hummer's method **(**syTRGO**)**. Also, the characterisation and properties of the syTRGO-incorporated NR/CCB-CNT hybrid filler systems are discussed in detail.

The thesis concludes by summarising the findings derived from both experimental and theoretical analysis of the properties of NR composites, as discussed across multiple chapters. Finally, the future outlook of the current research work is also presented.

Chapter 1

Introduction

Conductive elastomers hold significant technological promise in the current world. Their advantages include easy processability, flexibility, and cost-effectiveness compared to traditional metallic conductors, which are heavy and prone to corrosion. The flexibility of conducting elastomers makes them ideal for applications in electronic devices, where they can serve as gaskets to prevent electromagnetic interference (EMI) radiation leakage and function as materials for shielding against microwaves. (1–5) Conductive elastomers are utilised in touch control switches, low-temperature heaters as antistatic materials, and various energy storage devices such as supercapacitors, batteries, and fuel cells. Their adjustable piezoresistive properties and flexibility render them compatible for producing flexible electrodes, pressure-sensitive sensors, transducers, and actuators. (6–9) Insulating rubbers can attain conductivity by creating a consistent network of conducting fillers within the rubber matrix. Frequently employed conducting fillers include carbon nanotubes, graphene, carbon dots, metal fillers and their oxides, and conductive carbon black (CCB). (10–17)

Natural rubber latex-based composites are utilised in tissue engineering, drug delivery, dentistry, wound healing and antibacterial applications. In the electronics industry, rubber-based materials are used to seal and insulate various components of machines and instruments. Natural rubber (NR) reinforced with conductive fillers offers improved electrical and thermal conductivity and additional advantages of bendability, stretchability and tear strength under frequent elastic deformations. Rubber composites are used to make electronics gaskets, insulations for electrical wires, deep sea cables and electronic components designed to endure intense vibrations and pressure, as encountered in applications like washing machines, automotive engine seals, and belts. A combination of good elasticity, mechanical hysteresis, dynamic properties, abrasive resistance, tear and tensile strength makes rubber composites an inevitable factor in the tire and automotive industries and other engineering applications. (18) High-performance tires for race cars, buses and aircraft are also made from NR. Other conductive rubber composite-based products include antivibration mounts, drive couplings, springs, bearings, rubber bands and adhesives. Many NR composites incorporated with graphene,(19) natural fibres,(20) CNT,(21) and CB(22) are potential choices for strain sensors. The high flexibility and sensitivity of NR composites are also appropriate for wearable sensors.

The main focus of the work is the fabrication of conductive elastomer composites using natural Rubber (NR) integrated with carbon-based conductive fillers and ionic liquid (IL) modified fillers, with the primary goal of enhancing the electrical properties of NR.

1.1. Natural rubber

1.1.1. History

Natural rubber, also known as cis- polyisoprene, is an elastomer obtained as latex from the tree species *Hevea brasiliensis*. NR is the homopolymer of 2-methylbuta-1,3-diene (isoprene), the empirical formula is C_5H_8 and has cis 1-4 configuration. It is a straight-chain polymer with high molecular weight and has a density of 0.93g/cm^3.

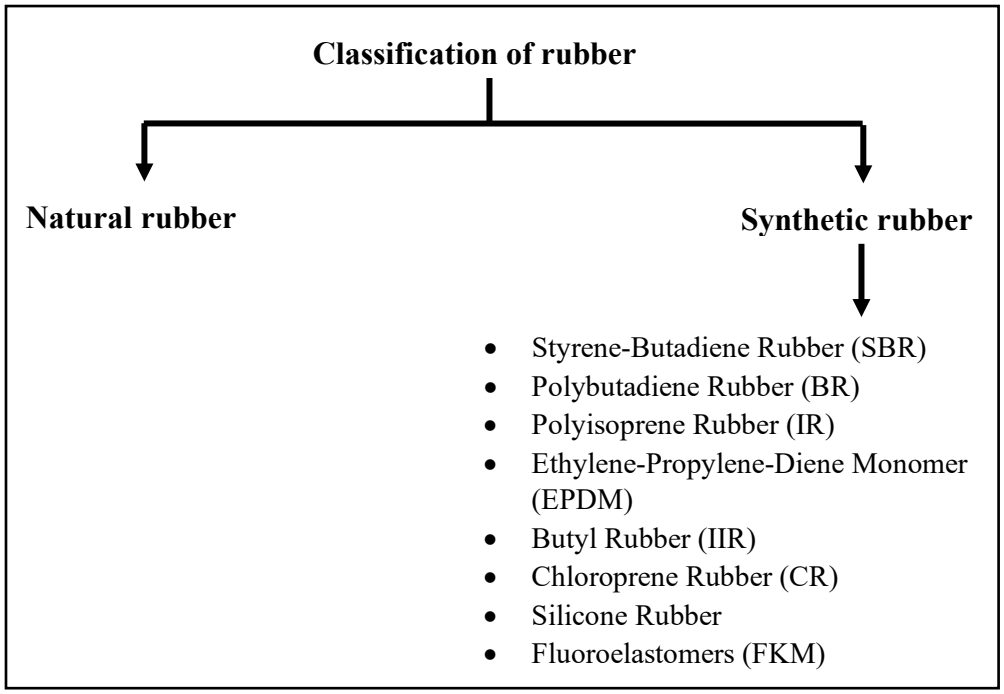

Figure 1.1 Classification of rubber

Intrinsic properties of NR include oil resistance, low gas permeability, wet grip, rolling resistance, tensile and tear properties and resistance to heat build-up. Also, it can recover its original dimension after deformation in compression or tension. The characteristic viscoelastic properties of elastomers enable their use in tyres, damping, and shock absorption. Rubber exhibits excellent toughness under dynamic or static stresses, impermeability to air and water and high resistance to solvents and chemicals. Another classification of rubber is called synthetic rubber. Synthetic rubber is an artificial elastomer created from petroleum by-products, serving as an alternative to NR. The most important synthetic rubbers are nitrile-butadiene rubber (NBR),

styrene-butadiene rubber (SBR), butadiene rubber, butyl rubbers and silicones. **Figure 1.1** presents the classification of rubber.

1.1.2. Processing technique

Natural rubber latex is collected from the rubber tree through tapping. The addition of acid coagulates the latex, and further processing steps are carried out after air-drying the resulting mass. This involves mastication to break down polymer molecules and mixing with various additives, ultimately enhancing rubber properties and broadening its applicability. Subsequently, the viscous rubber mass undergoes shaping through extrusion or molding. Finally, crosslinks are introduced during the curing process. The process of selecting and adding the optimum number of various additives to the rubber matrix in order to achieve desired chemical and physical properties is called compounding. Internal mixers or mill mixers are used for conventional rubber compounding. Various ingredients, such as curing agents, accelerators, activators, antioxidants, plasticizers and fillers, are added to the rubber during compounding. **Table 1.1** presents the list of compounding ingredients used in elastomers.

Commonly used curing agents are sulfur, peroxides and metal oxides. Curing introduces carbon-carbon, carbon-sulfur and sulfur-sulfur bonds in the rubber matrix and a three-dimensional network is formed by the polymer chains. Accelerators are employed to decrease the curing time by enhancing the rate of curing. Accelerators are classified as primary and secondary accelerators. Accelerators belonging to the group of thiazoles and sulfenamides are primary accelerators. Secondary accelerators are used to activate primary accelerators, and guanidines, thiurams, and dithiocarbamates belong to the class of secondary accelerators. Another group of rubber compounding ingredients are activators, which are the organic or inorganic chemicals that boost the curing of rubber. Antidegradants are used during rubber compounding to slow down the ageing of rubber and to prevent degradation due to ozone, oxygen, light and heat.(23) Antidegradants also include antiozonants, specifically added to prevent rubber degradation by ozones. Rubber processing oils are added as plasticizers during mixing to reduce the viscosity and improve flow characteristics of rubber. Processing oils also helps to disperse filler homogeneously in the rubber matrix. Some specific purpose ingredients, such as dyes, odorants, retarders, blowing agents, etc., are also added during rubber compounding for definite applications.

Table 1.1- Compounding ingredients for NR

Compounding ingredients	Class	Examples	Function
Vulcanising agents	Sulfur compounds	Sulfur	Increase crosslinking
	Peroxides	Dicumyl peroxide	
Accelerators	Primary	Sulphanamides, Thiazoles	Speed up the vulcanisation process
	Secondary	Dithiocarbamates, Thiurams, Guanidines	
Activators	Inorganic	Zinc Oxide, Magnesium Oxide	Promote cross-linking of polymer chains
	Organic fatty acids	Stearic acid	
Fillers	Black	Carbon black	Reinforce Enhance properties Reduce cost
	Non black	Silica, ZnO	
	Conducting	Metals, CNT	
Plasticizers	Mineral oils	Parafinic oil Naphthenic oil, Aromatic oil	Increase softness or flexibility Aid in the breakdown of the elastomer, Reduce crystallization, Increase dispersion
	Esters	Phthalates Sebacates, Adipates	
Antidegradants	Antioxidants	Amines, Phenolics, Quinolines	Prevent degradation due to oxidation, ozone and heat
	Antiozonants	Waxes, p-phenylenediamine derivatives	
Retarders	Organic acids	Benzoic acid, Maleic acid	Slow down vulcanisation
Processing Aids	Oils and waxes	Pine tar, Mineral oil, Phenolic resins, Petroleum resins	Improve processing characteristics

Both synthetic rubbers and NR are vulcanised to improve the crosslinking of chains. Processing technique employed, the nature and properties of incorporated filler have a major role in determining the final properties of rubber composites. Apart from filler characteristics, the dispersion of filler in rubber matrix and filler-rubber interfacial properties are also important factors in influencing the properties of final rubber compound. All these factors make rubber composite suitable for multifunctional applications. **Table 1.2** presents the widely used elastomers and their characteristics.

1.2. Fillers

There are many conventional and novel types of filler that can reinforce and expand the properties of elastomers. **Table 1.3** lists the different classes of fillers and their properties.

Silica, nano clay, conducting fillers like carbon black (CB), carbon nanotubes (CNT), and graphene are generally used for the fabrication of rubber composites. Silica is a non-black, widely used conventional filler. These reinforcing fillers can boost the mechanical properties of NR, such as elastic modulus, fracture toughness, fracture strength, abrasion resistance and friction properties. It minimises rolling resistance and enhances wet traction of tire tread compounds better than CB. Hydrophilic nature of silica creates a significant filler-filler network and fails to form a strong filler-elastomer network with the nonpolar matrix. (24,25) Moreover, silica requires a long processing time and consumes high energy. Another class of widely used fillers in the rubber industry are nanoclays, which are layered mineral silicates like montmorillonite (MMT), bentonite, kaolinite, hectorite and halloysite nanotubes(HNT). Clay or modified clay-filled composites have enhanced flame and barrier retardant properties, storage modulus, accelerated vulcanisation process, high crosslinking density, and superior mechanical properties. (26–30) Also, an optimum amount of iron or nickel nanoparticles can be included in the rubber matrix to form magnetic composite materials with improved rheometric and physico-mechanical properties that depend on the type and concentration of magnetic filler. (31)

1.2.1. Conducting fillers

Conducting fillers are added to polymers to enhance the thermal and electrical conductivity of polymer composites. The electrical conductivity of the elastomer composites depends on the resistivity of incorporated fillers.

Table 1.2- Elastomers and characteristics

Elastomers	Abbreviation	Important properties	Service temperature range	Applications
Natural				
Natural Rubber	NR	Elasticity and resilience, High tensile strength, Good abrasion resistance, Poor resistance to oil and ozone	-50°C to +70°C	Tires, Adhesives, Gloves, Insulation, Automotive parts, Medical devices, Surgical gloves, Pacifiers, Cloths
Synthetic Rubber				
Styrene-Butadiene Rubber	SBR	Abrasion resistance, Moderate resistance to oils and chemicals, Water swell resistance, Compression set	-40°C to 100°C	Seals integrated into hydraulic brake systems. Cutting boards, Gaskets, Shoe soles
Nitrile Butadiene Rubber	NBR	Excellent oil resistance, Good abrasion resistance	-30°C to +100°C	Automotive gaskets and seals, O-rings, Engine hoses, Surgical gloves
Polyurethane	PU	High load-bearing capacity, Excellent abrasion resistance, Wide range of hardness options, Good resistance to oils and solvents	-40°C to +90°C	Building and construction, Insulation, Coatings, Adhesives, Sealants, Medical devices, Technical laboratory equipment

Ethylene Propylene Diene Monomer	EPDM	Excellent weather resistance, Resistant to acids and alkalis, Superior noise and thermal insulation properties	-40°C to +120°C	Roofing sealants, Hoses, Seals
Butyl Rubber	IIR	Low permeability to gas and moisture, High resistance to weather, heat, ageing, chemical exposure, abrasion, flexing and tearing.	-55°C to +105°C	Inner tubes, Sport balls, Sealants, Additive in diesel and petroleum fuels Chewing gums
Neoprene (Chloroprene)	CR	Moderately resistant to petroleum oils and weather, Low compression set, Excellent resilience and abrasion resistance, Resistance to flex cracking	-40°C to +135°C	Adhesives corrosion-resistant coatings. High-pressure gaskets, Belts, Window and door seals.
Silicone rubber	Q	Chemically inert, Biocompatible, Resistant to extreme temperatures, fire and weather	-84°C to +232°C	Gloves, Respiratory masks, Implants, Medical products, Baby care items, Cosmetic applicators, Food containers
Viton (Brand name - DuPont)	FKM	Durable, Exceptional temperature stability, Swell in fluorinated solvents, High cost	-20°C to +205°C	Aircraft engines, Automotive fuel handling systems, Fuel system seals, Gaskets, O-rings, Aerospace, Military

Conductive fillers can act as the channels for the transport of electrons through the insulating matrix. Commonly used conducting fillers are carbon, metal, and metal-coated fillers.

1.2.2. Carbon black

Carbon black (CB) is produced from hydrocarbons or natural gas by partial combustion or thermal decomposition. The conductivity of CB-incorporated polymer composites depends on the type of carbon black, filler loading, size and structure of the particles. CB, along with its high reinforcing ability, possesses the advantage of low cost and easy availability. Viscoelastic properties of rubber are tremendously influenced by CB, and it is important for designing rubber compounds for tires, power transmission belts and vibration isolation mountings. (32,33)

Farida et al. (34) studied the effect of CB composition in NR compound and found a transition of amorphous structure to the semi-crystalline form with increasing CB loading. Homogeneous dispersion of filler in NR is obtained by open mill mixing. The study of carbon black filled NR composites gives insight into the nature of filler-filler and filler-polymer interactions.

1.2.3. Graphite

Graphite is the stable crystalline form of elemental carbon, constituting stacked layers of carbon. Its unique structure and high thermal conductivity make it an effective reinforcing filler, leading to improved stiffness and heat resistance in NR. Swelling measurements of graphite incorporated NR showed that the volume fraction of natural rubber in the swollen gel, the interaction parameter, and the crosslink density decreased by increasing graphite loadings. (35) Cheng *et al.* (36) studied the flame retardant and thermal properties of NR composites with expandable graphite (EG) microcapsules. In-situ polymerisation and boron nitride doped organic shell of EG increases the compatibility and thermal conductivity of NR.

1.2.4. Carbon nanotubes (CNT)

Carbon nanotubes (CNT) (single walled carbon nanotubes (SWCNT) or multi walled carbon nanotubes (MWCNT) are well studied fillers in rubber composites. CNT exhibit remarkable characteristics such as high electrical and thermal conductivity and tensile strength. Utilizing CNT as fillers in rubber composites improves their electrical, thermal, and mechanical characteristics.

Table 1.3- Different classes of fillers used in elastomers

Classification	Examples		Properties
Reinforcing fillers	Carbon black	Furnace black	High tensile strength
		Thermal black	Abrasion resistance
		Channel black	
		Lamp black	
	Non-black fillers	Silica	Impart unique properties like colour, permeability and oil resistance
		ZnO	Reduction of cost
		Talc	
		Kaolin clay	
Inert fillers	Calcium Carbonate		Reduction of cost
	Barium sulfate		Dimensional stability
	Aluminium trihydrate		
Conducting fillers	Carbon nanotubes		High mechanical properties at low loadings
	Graphene		Barrier properties
	Metal fillers		Electrical properties
	Liquid metal fillers		
	Metal coated fillers		

However, CNT tends to agglomerate in rubber matrix due to the van der Waals force of attraction, resulting in low performance of the composites. Nevertheless, the structure of CNT allows extensive chemical functionalisation in order to prevent agglomeration and ensure uniform dispersion in any polymer matrix. CNT possesses a high aspect ratio and surface area that provides stress transfer in composites. MWCNT can decrease the volume resistivity of NR at a lower percolation threshold. MWCNT can form conductive pathways in the composites, but at higher filler loading, the Payne effect causes the breakdown of filler-filler network. CNT forms a conduction network in epoxidised natural rubber (ENR) also. CNT loaded rubber exhibit high electrical conductivity than neat or CB- filled rubber matrix. The reinforcing effect of CNT is attributed to its high aspect ratio. These properties make CNT an excellent choice for fillers in polymer composites. High Young's modulus and electrical and thermal properties are obtained in the case of SBR, acrylonitrile butadiene rubber (NBR), ENR and silicone rubber in the presence of CNT when it is used as such or after chemical modification.(37–40) The exceptional mechanical strength and flexibility, make CNT-reinforced NR composites highly suitable for developing anthropomorphic prosthetic foot. This composite exhibits high tensile strength of 6.02 MPa, better wear resistance, storage modulus of 200-7500 MPa and loss moduli of 500-1413 MPa. They also have high heat energy dissipating capacity. (41) CNT incorporated NR composites can be made used for large deformation monitoring sensors. Also, the resistance-strain sensitivity developed can be used to monitor the strain load of rubber isolation bearing used in seismic protection systems.(42)

1.2.5. Graphene

Graphene possesses high surface area, improved mechanical properties, high electrical and thermal conductivity, and good gas barrier performance. Uniform dispersion of graphene in rubber matrix also imparts these properties to rubber composites. More excellent graphene-rubber interaction will bring about the best of NR composites. Electrically and thermally conductive elastomers with good mechanical performance can be prepared by incorporating graphene as filler. (43) Graphene networks also have the ability to overcome the poor thermal conductivity of NR. Graphene has a reinforcing effect on elastomers by inducing fast strain-induced crystallization. Besides, higher crystallinity and the planar structure enable more interaction with the

matrix. Superior mechanical properties, weathering resistance and electrical properties make graphene/elastomer composites suitable for potential applications in various fields. (44–46)

The addition of even 0.1 phr reduced graphene oxide (RGO) in NR resulted in a 14% improvement in stress at 700% elongation. Likewise, the thermal conductivity reached 0.236 W/(m. K) with an enhancement of 36%. (47) Natural rubber/graphene composites can be used to fabricate flexible ultrasensitive and wearable strain sensors by simple and low-cost methods. These sensors exhibited good compression performance and can detect various human activities. (48) Graphene nanosheets can also increase the electrical conductivity by four orders of magnitude and thermal conductivity by 50% compared to pure NR. Similarly, good thermal stability and an obvious increase in mechanical properties are also observed. Graphene networks constructed in the NR matrix improve the tensile and dynamic storage modulus. At a low percolation threshold of 0.21 vol%, electrical conductivity improved several orders. Excellent strain sensitivity and repeatability can be used to detect cyclic movements of human joints, which makes it suitable for fabricating sensitive and stretchable strain sensors. (49) 25 wt% of graphene loading has improved the thermal conductivity of NR to 0.891 W/(m.K), along with good mechanical and antistatic properties. Such types of NR composites are suitable for thermal management devices. (50)

1.2.6. Metal fillers

Solid metal fillers in elastomer composites offer advantages like low density, low cost and easy processing.(51) Particle fillers separate from each other in the composite upon stretching and cause the lowering of electrical conductivity. Carbon-based fillers offer better oxidative resistance and higher mechanical strength over conventional metal fillers. However, metal filler incorporated elastomers are more sensitive to mechanical deformation.

1.2.7. Liquid metal fillers

Apart from solid metal fillers, liquid metal fillers are also broadly employed in fabricating elastomer composites. Liquid metal fillers tend to break into microdroplets in the elastomer upon mixing. These droplets can deform along with the matrix, which enables them to retain the high conductivity of elastomer composites at high strains. Liquid metal fillers increase the toughness of composites by propagating the tears in

the matrix. However, liquid metal limits the applicability of composites as sensors due to its insensitivity to strain. Commonly used liquid metal fillers include gallium based liquid metal alloys like EGaIn a mixture of 75% Gallium and 25% Indium. (52,53)

1.2.8. Metal coated fillers

Pure ferromagnetic materials are highly inert to elastomeric matrices. Metal coating on carbon fillers like CB and CNT provides a promising route to combine both magnetic property and reinforcement in rubber matrix. Metals like iron and nickel have high permeability, low remanent magnetization and high saturation magnetization. Iron and nickel coated CB filler simultaneously imparts ferromagnetic property and reinforcement in NR.(54) However, metal coated CB lowers the mechanical properties in NR compared to neat CB and it is more compatible with NR than SBR. Similarly, nickel coated carbon fibre incorporated in silicone rubber is conducive to electromagnetic shielding interference applications. (55) Copper coated carbon fibre increases thermal and electrical conductivity in silicon rubber. (56)

1.2.9. MXenes

MXene is a newly emerged category of stacked two-dimensional (2D) layered materials comprising early transition metal carbides and/or nitrides, with the general formula of $M_{n+1}X_n$ (M being an early transition metal, and X being carbon or nitrogen). MXene possesses high conductivity, biocompatibility and large surface area. (57) MXene ($Ti_3C_2T_x$) nanosheet incorporated NR serves as an excellent choice for EMI shielding materials due to the formation of lightweight, hydrophobic conductive elastomer composites. MXene/NR system containing 60% MXene with a thickness of 65.6 μm demonstrates exceptional EMI shielding efficiency at 47.8 dB. Even after undergoing water immersion for 15 days and enduring 6000 bending cycles, the film maintains an EMI shielding efficiency of 32.8 dB, indicating high durability. (58) 6.71 vol% of MXene exhibits electrical conductivity of 1400 S m^{-1} and EMI shielding efficiency of 53.6 dB. The interconnected network of MXenes in the NR favours efficient electron transport and load transfer at low filler content. (59)

1.3. Conducting hybrid fillers in natural rubber (NR)

Integrating hybrid fillers in a rubber matrix is an excellent technique to produce high-performance polymer materials by combining two or more fillers. Hybrid fillers can include a combination of conventional fillers or chemically or physically modified

fillers.(60) Incorporating hybrid filler system in rubber matrix gives the chance to utilise the synergistic effect of combining fillers. Proper selection and pairing of fillers is an essential factor in developing final composite material with desired properties. Many of the study reports reveal that the hybrid fillers can perform well better than the single filler system.(61) Rubber composites with hybrid filler of CB, silica, CNT and various other carbon allotropes have been thoroughly studied. The synergistic effect of the combination of fillers in an elastomer matrix can preserve the superior properties of all fillers and can complement each other.

High-performance damping material suitable for seismic application was prepared using hybrid NR nanocomposites. Organically modified MMT was added to NR containing MWCNT, which showed improved mechanical properties. In this work, low-quantity MWCNT was added to enhance the mechanical properties of NR, and then different quantities of expanded organo-modified montmorillonite (EOMt) were added to tune the properties.(62) Organically modified clay-CB hybrid filler in NR can influence the properties of NR compounds. Replacement of CB by modified nano clay induces the dispersion of CB in NR matrix. The incorporation of nanoclay decreases the activation energy of the networking process. Thus, strong interactions are formed between CB, nanoclay and NR.(63) Synergistic effects of CB and expanded nanoclay in NR are used in the model tire truck formulation. Stearic acid-modified nanoclay helps in the intercalation of rubber between the silicate layers of nanoclay, resulting in the enhancement of mechanical properties and decrease of rolling resistance at reduced CB loading.(64) The cut tensile strength, tear strength and thermal ageing resistance of NR vulcanisates with CB and clay is increased as the clay/CB ratio is decreased owing to the higher reinforcing efficiency of CB than clay.(65) In 2010, Liu *et.al*.(66) reported that the reinforcement of NR by the integration of CB/organoclay hybrid filler is because of the synergistic effect of hybrid filler network as revealed by DMA and tensile tests. The storage modulus increases with hybrid filler content. Maximum value of G' is obtained for composite with 15 phr CB and 10 phr nanoclay. Drop of tan δ peak height for the same indicates strong filler- rubber interaction and reinforcing ability of hybrid filler. In 2012, Thimmaiah *et.al.*(67) optimized the amount of metakaolin in NR/CB system by studying thermal and mechanical properties. Metakaolin acts as a non-reinforcing filler in NR and lacks filler matrix interaction.

NR/Silica/MWCNT hybrid nanocomposites can provide better properties due to the synergistic effect of both fillers. In the absence of agglomeration of both fillers, NR/Silica/MWCNT hybrid nanocomposites exhibited decreased scorch and curing temperatures and increased elongation at break, tensile strength and fatigue. Addition of cheaper silica like reinforcing filler into NR composites with expensive CNT fillers helps to reduce the cost of nanotube-based composites without compromising the improved mechanical properties. Silica has further advantages such as reduced heat build-up, enhancements in tear strength and improved adhesion of compounds in multi-component products. (69)

Dual phase hybrid filler system of carbon and silica could control and tailor the dielectric and microwave absorption properties of NR composites. Hybrid filler was synthesised by the impregnation of conventional CB in various amounts of silica sol which helped regulate the quantitative ratio of two phases within the fillers.(70) Incorporation of silica in CNT filled NR composites results in better dispersion of CNT and exhibits improved mechanical stiffness, tensile strength, increased modulus and electrical conductivity at low CNT loading itself. But a slight reduction in the tear resistance under dynamical loading is observed. Height of the peak corresponding to glass transition temperature (~-60^{o} C) is decreasing with CNT content and value of G' at high temperature is sensitive to CNT content ; both indicates the increasing effect of CNT- rubber interface with CNT content.(71) ENR containing 25 mol% epoxide groups having nanoclay (NC) and CB fillers exhibited synergistic mechanical and dynamic mechanical property developments. Later, the influence of hybrid microstructures and CB-NC interfaces upon the electrical and mechanical properties of ENR was verified.(72) Organo modified kaolin/ silica hybrid filler was used in NR/polybutadiene (BR) blend and rubber-filler interaction increased as the organo modified kaolin content is increased. Tensile strength, tear strength, flux resistance and elongation at break show definite improvement, and there is a reduction in heat buildup, while tensile modulus shows a slight decrease.(73)

1.3.1. Graphene and carbon nanotubes (CNT)

The combination of graphene and CNT increased the mechanical properties of NR and thereby expanded the versatility of NR composites in practical applications. Hybrid filler system developed a compact network of physical interactions which act as sacrificial bonds that absorb energy prior to material failure. The substantial energy

dissipation not only enhances fracture toughness and tensile strength but also inhibits the rate of crack growth in NR composites. Compact hybrid filler network comprising of π-π interactions is conducive for high performance devices that demands long term sustainability.(74) Tangled structure of CNT in host matrix leads to the failure to construct a conductive network which in turn elevates the percolation threshold. The synergistic effect of this hybrid filler augments the electrical and mechanical properties of various elastomers(75) and unlocks an array of applications like tunable strain sensors.(76) Hybrid filler network of graphene and CNT was used for toughening of NR aiming practical applications that require long term sustainability of materials employing modified latex mixing method to ensure homogeneous dispersion of fillers. Physical interactions in this network has lower bond energy and has high heat dissipation leading to the increase in fracture toughness and tensile strength and suppression of crack growth rate in NR/GE (graphene)/CNT composites.(77)

Piezoresistance based sensors can be fabricated by tailoring the piezoresistivity of elastomers by incorporating hybrid nanofillers. A combination of a few layers of thermally reduced graphite oxide (TRGO) and MWCNT in NR exhibits nonlinear piezoresistive behaviour depending on the nanostructure of the hybrid filler system.(78) Synergistic effect of reduced graphene oxide and CNT was also found to impart solvent sensing to NR. TRGO sheets can induce polarity and reduces the interactions between CNT and lead to sensing of aromatic solvents.(79) TRGO and MWCNT has interconnected percolation network in rubber matrix. The morphology and structure of fillers are found to play a prominent role in the electrical and piezoresistive behaviour of nanocomposites. Thus the tailored combination of platelet type graphene and rod shaped MWCNT can be used to fabricate piezoresistive- based sensors.(80)

1.3.2. Conductive carbon black (CCB) and carbon nanotubes (CNT)

Comparative study of properties of NR composites with CB as primary filler with fixed amount and CCB and CNT as secondary filler with varying amounts shows increased viscosity, vulcanisation rate, hardness, crosslink density, and modulus, thermal and electrical conductivities by sacrificing elasticity. CB/CNT hybrid composites have greater strength and rebound resilience than CB/CCB composites, provided both have similar hardness. CCB increased the tensile and tear strengths at lower filler loading, while CNT does not have any significant effect on strength. (81)

NR/CNT/CCB hybrid elastomer systems exhibited improved optimal conductivity at a particular CNT-CCB composition due to the high electron tunnelling when CNT encapsulates are bridged by CCB aggregates. Three dimensional filler network was formed at low percolation threshold due to the reduced inter particle gap between CNT and CCB.(82) Employing ultrasonic assisted latex mixing process for the fabrication of NR/CB/ hydroxyl MWCNT composites ensured uniform dispersion of CNT in the rubber matrix, resulting in synergistic reinforcing effect. Increase in the elastic modulus, storage modulus and complex viscosity of the rubber composites was observed while shear thinning index decreased as the CNT contents increased. Mechanical properties, compression stress and crosslink density reached maximum when weight ratio of CNT/CB was 20:5. (83)

1.4. Properties of NR- hybrid filler composites

1.4.1. Electrical properties

Natural rubber cannot conduct electricity without any assistance as its electrons are tightly bound. Addition of conducting fillers like CB, CNT or metallic fillers impart electrical properties to NR. Electrical conductivity of NR is in the range 10^{-9} – 10^{-15} S/m. CB has a conductivity of 10^{4}-10^{5} S/m. The addition of CB boosts the conductivity of NR by several orders.(84)

Conducting single fillers or hybrid fillers form a continuous conductive network in rubber matrix above the threshold concentration. Continuous network enables less hindered transport of electrons across the rubber matrix. This filler network can also upgrade the electrical conductivity by a quantum mechanical phenomenon called tunnelling. The percolation threshold is the minimum quantity of filler required to establish a three-dimensional conductive filler network in the polymer matrix. Percolation value is influenced by the filler type, size, geometry and state of dispersion. DC conductivity of rubber composites is frequency independent and can be determined from DC resistance measurements using multi probe method. AC current is frequency dependent and is determined by impedance spectroscopy. Volume resistivity provides a direct assessment of charge transport within the bulk of the material, while surface resistivity measures transport along the surface of the material. Volume resistivity of composites can be measured using two probe method and using below equation,

$$\rho_v = R_v \frac{S}{h} \tag{1.1}$$

where R_v rhomic resistance between electrodes, h is the sample thickness between electrodes, S is the cross-sectional area of measuring electrodes. The inverse of volume resistivity gives the dc conductivity.

Study of hybrid filler system of CNT and graphite in NR shows that infinite conductive network formation of CNT and graphite aided in increased conductivity and dielectric constant. However, continuous network formation could be achieved only when graphite was added over 20 phr and CNT 3 phr. They proposed a partly connected "dead arm" structure for NR composites with hybrid filler concentration lower than optimal level. (85) CNT/ZnO hybrid filler system provides high electrical conductivity compared to the CNT/NR. This can be attributed to the electrostatic interaction between ZnO and CNT with the optimum amount of 3 phr ZnO, giving a finer distribution of CNT in the matrix. (86) Conductive epoxidized NR composites with nano structures of MWCNT and few layer graphene (FLG) also exhibits high electrical properties along with mechanical properties. The π-π interactions between fillers and rubber filler interactions decreased the electrical percolation threshold by 70%. (87)

1.4.2. Dielectric properties

The dielectric constant of a material is defined as the ratio of the electrical permeability of the material and the electric permeability of the vacuum. NR is inherently dielectric. NR composites incorporated with hybrid fillers (conducting or dielectric) enables to control its dielectric properties by varying the ratio and type of fillers. The focus is to develop dielectric elastomer with high dielectric constant and low dielectric loss (tan δ). Dielectric characteristics are measured using an impedance analyser in varying frequency ranges at a constant voltage.

A novel hybrid filler system containing silicon and carbon obtained from biomass gives enhanced electrical properties when incorporated in NR. This filler system attained improved interfacial and dipole polarizability, which resulted in high dielectric constant of the rubber composite.(88) Other hybrid systems of biological origin that improve the dielectric constant include sisal/coir hybrid fibre,(89), sisal-oil palm hybrid biofibre.(90) Hybrid conductive fillers found to enhance the dielectric properties include porous reduced graphene oxide and molybdenum sulphide (MoS_2),(91) modified bentonite clay/carbon black,(92) CNT and zinc particles,(86) MWCNT decorated with nanosilica. (93)

1.4.3. Microwave absorption and EMI shielding

Electromagnetic interference (EMI) is an undesirable property exhibited in electronic and telecom devices, which adversely affects the electronic performance of the devices, causes economic loss and has a negative impact on human health. Pure NR is transparent to electromagnetic radiation. The addition of conducting and/or magnetic fillers in the matrix helps fabricate high-performance shielding materials. Pristine CNT have poor microwave absorption which can be overcome by the designing of hybrid filler system with various metal oxide compounds. Synergetic effect of one dimensional MWCNT and two-dimensional molybdenum disulphide (MoS_2) showed excellent microwave absorption capacity in NR composites. The reflection loss exhibited is 9.2 and 21.9 times stronger than the MWCNT or MoS_2 alone filled NR composites.(94) Another hybrid filler combination of CNT with nickel oxide (NiO) can improve the microwave absorption properties of NR. The core shell structured CNT-NiO fabricated by modified atomic layer deposition method attains a reflection loss of -43.6 dB in natural rubber composites. This improvement in microwave absorption can be attributed to the multiple interfacial polarization, higher impedance matching and multiple reflection and scattering.(95) Magnetite- Titania hybrid containing natural rubber composite could attain maximum microwave attenuation of 28.1 dB for 1 vol% of hybrid filler dispersed in NR. This hybrid system also possesses the advantage of high tensile strength and thermal stability.(96) Hybrid system of thermally reduced graphene and ionic liquid (1-ethyl-2,3-dimethyl imidazolium bis(trifluoromethylsulfonyl)imide modified CNT filled NR matrix is able to attain a reflection loss -30 dB at 2 mm thickness.(97)

1.4.4. Mechanical properties

NR composites have high tensile strength, tear strength, resilence and compression set. In addition to that, it also possesses impact resistance, abrasion resistance and vibration damping. Rubber can also be adhered to metal and other rigid materials. Vulcanisation imparts structural stability, strength and resilience to rubber. Reinforcing fillers like clay, silica and CB in optimum amounts can help to attain superior mechanical properties of composites without compromising their processability and applicability. Reinforcing nanofillers like layered silicates, spherical nano silica, CNT, bio nanofillers, graphene and GO possess some advantages over reinforcing microfillers like clay, CB and silica. Nano filler reinforced composites offer high hardness,

modulus, antiaging and gas barrier properties than micro filler reinforced rubber composites.(98) Polymer chains of NR align themselves in the direction of deformation and forms crystalline microstructure known by the phenomenon of strain induced crystallisation. High strength and toughness of NR can be accounted to this phenomenon. (99) Graphene derivative hybrid nanocomposites in NR establishe unique microstructures that improve the properties of the system. (100) Combination of CB with natural fibres like palm kernel seed shell and sand box seed shell reinforces effectively and also provides environment friendly alternative to conventional fillers. (101) Alumina coated graphene oxide hybrid fillers produced by electrostatic self-assembly method forms an interconnected filler network in NR matrix. This filler system could attain a tensile strength of 25.6 MPa at a filler loading of 18 vol %. (102)

1.4.5. Dynamic mechanical analysis

Dynamic mechanical analysis gives storage modulus, loss modulus and loss factor values. Storage modulus represents recoverable or elastic energy; loss modulus represents energy loss by dissipation. At low temperature, NR is in glassy state characterised by high storage modulus attributed to the semi-crystalline nature followed by the rubbery plateau. Introduction of hybrid fillers can enhance the storage modulus of NR. Hybrid filler system of CNT and graphite in NR could increase the storage modulus, lower the glass transition temperature and damping. This is due to the synergetic effect of CNT and graphite to increase the chain flexibility and elasticity of polymer chains. Moreover, stronger interface formation facilitates lower energy dissipation also. (85) The extent of reinforcement of the filler system on the polymer matrix can be deducted from the peak height of plot of tan δ versus temperature. Filler –filler and rubber- filler interaction can be further analysed from the strain sweep plot of storage modulus against strain amplitude. As the strain increases, filler –filler networks start to break down leading to decrease in storage modulus. This is observed for nano clay –jute fibre and CNT modified jute fibre hybrid system.(103,104)

1.4.6. Solvent transport

Rubber composites possess unique ability to resist the diffusion of solvent molecules. This property makes the rubber composites suitable candidate for barrier applications. The transport of molecules of various organic solvents are studied extensively. Addition of hybrid fillers cause dramatic effect on the transport properties of polymer composites. Hybrid filler network formed in the polymer hinders the solvent transport

by providing a tortuous path for diffusing solvent molecules. Uniformly dispersed fillers decrease the major amount of total voids in the rubber matrix. This is further aided by the stronger rubber-filler interaction. Extent of filler network formation, dispersion and dimension of fillers have major role in altering the transport properties of composites. The transport/sorption behavior of rubber composites are studied using various organic solvents such as toluene, xylene, and benzene at various filler loadings. Marble sludge/silica and marble sludge/ rice husk derived silica hybrid fillers are developed from industrial and agricultural waste. NR reinforced with this system provides enhanced swelling characteristics. Solvent absorption is highly restricted in hybrid NR composites. Highly dispersed hybrid filler system creates strong crosslinks in the system.(105) Transport properties of sisal coir/hybrid fibre reinforced NR composites are studied in benzene, toluene and xylene. Addition of bonding agents to these composites has increased the restriction of solvents in the system. Furthermore, increase in fibre content and penetrant size also diminish the solvent uptake.

1.4.7. Thermal stability

Unvulcanised rubber is unstable for a wide range of temperatures. Vulcanisation enhances the thermal stability of the rubber matrix. Thermal stability of the samples can be studied by thermogravimetric analysis (TGA) in a wide temperature range from 30ºC to high temperature such as 600ºC or 900ºC by varying heating rate in N_2 or O_2 atmosphere. TGA plots include weight loss versus temperature and its derivative plots. TGA also helps to calculate activation energy for thermal degradation of rubber composites. Hybrid filler incorporation on the NR matrix can improve the thermal stability. Porous reduced graphene oxide and molybdenum disulphide hybrid conductive filler system is effective in improving the thermal stability.(106) Hybrid filler system of CNT modified with silver nanoparticles improved the thermal resistance of composites. Weight loss curves of the composites show two decomposition steps. The first step of degradation is in the N_2 atmosphere, and it marks the degradation of low molecular weight additives and NR molecules. Second degradation step in the O_2 atmosphere is anticipated to be due to the degradation of hybrid filler and ZnO activator. Degradation of functional groups in the hybrid filler gives an additional degradation step in thermogram.(107) The weight of residue present is directly proportional to the amount of filler in reinforced composites.

1.5. Modification of fillers using ionic liquids

Ionic liquids (IL) are salts which exists as liquids below 100°C or even at room temperature. Ionic liquids consist of organic cations and inorganic anions. They are characterised by the low viscosity, low toxicity, nonflammability, nonvolatility, high chemical and thermal stability. High ionic conductivity of ionic liquids is exhibited up to their decomposition temperature. Ionic liquids maintain small lattice enthalpies and significant entropy changes that are justified by their large size and conformational flexibility. Consequently, the liquid state of ionic liquid is thermodynamically favorable. (108,109) Ionic liquids are widely used as green reagents in chemical synthesis, catalysis, separation and electrochemistry. The first room temperature ionic liquid, $[EtNH_3][NO_3]$ was discovered in 1914. (110) Later, binary ionic liquids made from mixtures of aluminium (III) chloride and N-alkylpyridimium or 1,3-dialkylimidazolium chloride was discovered. The melting point and properties of binary ionic liquids depends upon its components and ionic species present. The ability to tune properties like polarity, hydrophilicity/hydrophobicity gives its name 'designer solvents'. Ionic liquids are also known by the name of molten salts, neoteric solvents and ionic fluids. Ionic liquids can be formulated according to the requirement by the suitable choice of ions. Regularly, used ionic liquid cations are alkylammonium, dialkylimidazolium and N-alkyl pyridinium.(111). Frequently used anions include inorganic anions like halides, tetrafluoroborates, hexafluorophosphates and organic anions like methane sulfonate and bis(trifluoromethylsulfonylimides). (112,113)

Ionic liquids have been used for the surface modification of CB (114–117), CNT (118–122), graphene (97), and GO(123,124). This helps to improve their dispersion in elastomer matrix which in turn creates a superior balance among mechanical, thermal and electrical properties to fabricate multifunctional advanced materials. Ionic liquid-modified CB and CNT improves flexibility, filler dispersion, electrical conductivity and even piezoresistive response as a result of the improved rubber-filler interaction. The presence of ionic liquids also influences the cure kinetics of rubber composites. Ionic liquids can refine the ZnO dispersion in the elastomer matrix and can accelerate sulfur vulcanisation of NBR and NR. Alkylimidazolium ionic liquids also catalyses crosslinking reactions at interface.(120) Further, more imidazole based ionic liquids can be exploited in the fabrication of blend composites also. (125) NR/ bromobutyl

rubber (BIIR) blends with butyl imidazole and CNT significantly enhance the tensile strength and delivers self-healing properties. Ionic liquid acts as a physical crosslinker for the BIIR phase and offers non-covalent bonds that are responsible for the self-healing properties of materials .(126)

1.5.1. Ionic liquid modified carbon nanotubes

Chemical modification of carbon nanotubes by imidazolium based ionic liquid (1-ethyl-2,3-dimethylimidazolium bis(trifluoromethylsulfonyl)) enhances the mechanical properties (tensile strength, hardness and abrasion resistance) and electrical properties (dielectric constant and conductivity) of SBR composites. Ionic liquid modified CNT also improves the EMI shielding effectiveness and separation performance of SBR composites.(118,127,128) Microstructural conductive network formation and uniform dispersion of CNT improves the interfacial interaction of filler and rubber chains and this accounts for the enriched properties of rubber composites. IL modified CNT can be integrated in natural rubber latex as well. Imidazolium-based ionic liquids (1-ethyl-3-methylimidazolium bromide and 1-hexyl-3-methylimidazolium bromide) homogeneously distribute CNT in latex and facilitate improved fatigue resistance and mechanical properties. (119) The ionic liquid-carbon nanotube interaction can be better understood using various characterisation techniques. Raman spectroscopy is a widely used powerful and non-destructive technique for the characterisation of graphitic structural materials. Raman spectroscopy can be employed to study the physical interactions arising between ionic liquid and CNT. Raman spectra confirm the physical modification of nanotubes without any chemical deterioration.(122,129–132) Furthermore, it proves that the chemical structure of CNT is intact after modification and hence surface modification by ionic liquid is purely physical in nature. Generally, two strong peaks are observed for both pristine and modified CNT; the G band around 1600 cm^{-1} and D band around 1300cm^{-1}. G band is attributed to the in-plane vibrations of graphitic wall and D band originates from the defects in the graphitic structure. Radial breathing mode (RBM) around 100-200 cm^{-1} is also observed in the spectra of carbon nanofillers. IL modification also induces a subtle shift of 3-4 cm^{-1} for D and G bands with no emergence of new vibrations. The upshift may be due to the cation–π interactions and/or perturbation of π-π stacking of multiwall of the tubes. Raman spectra provide another parameter called the D/G intensity ratio to assess the structure of pristine and

modified CNT. The D/G intensity ratio serves as an indicator for assessing the degree of crystallinity and purity of nanotubes. This also indicates the structural defects when both D and G peaks have similar intensity. Modified CNT shows a decreased D/G intensity ratio, which supports surface modification without any structural destruction. Cations of AMICL can interact with π- electrons of graphtic structure in CNT, and this results in enhanced properties of rubber composites.(133) Ionic liquid employed in butadiene-styrene elastomer filled with CNT shortened the optimal vulcanisation time and decreased the vulcanisation temperature compared to ZnO containing rubber compound. A considerable increase in the crosslink density of vulcanisates is also observed.(114)

1.5.2. Ionic liquid modified carbon black

The ionic liquid can be employed to modify carbon black in order to produce conducting polymer composites. Ionic liquid ensures homogeneous dispersion and better interface interaction of filler and elastomer matrix. Imidazole based ionic liquid, 1-allyl-3-methyl imidazolium chloride (AMICL) modified CB exhibited enhanced dispersion in elastomers.

Conductive rubber composites are made use as strain sensors or stretchable conductors based on their response to external stimuli. Ionic liquid modification overcomes the stiffness effect associated with CNT filled elastomers and aids the construction of conducting composites with improved flexibility and electrical conductivity conducive for the fabrication of small strain sensors.1-decyl-3-methyl imidazolium chloride is employed for the modification of CCB and it is loaded in SBR to fabricate composite with tuneable electrical- strain behavior. Here, the alignment of CNT aggregates was extended during stretching, reaching maximum conducting strain and heightened sensitivity at small strains. The tuneable electrical strain behaviour enables the efficient use of conducting composites as stretchable conductors and /or small strain sensors.(116)

1.5.3. Ionic liquid modified graphene

Ionic liquid modification of graphene can be done by simple technology such as solid grinding. Ionic liquid (1-allyl-3-methylimidazolechloride) can be used to modify graphene oxide to develop environment friendly tire tread materials with high wear resistance. Hydrogen bonding and π-cation interaction between graphene oxide and ionic liquid creates a strong interface in rubber vulcanisate. (134) Ionic liquid modified

GO gives excellent mechanical and healing performance in carboxylated nitrile rubber (XNBR).(135) Ionic liquid modified graphene incorporated natural rubber has yet not been reported.

1.6. Motivation of work

Conductive elastomers represent a promising class of materials with diverse applications, including microwave absorption, EMI shielding, piezoresistivity, flexible electronics, wearable technology, soft robotics, and medical devices in bio-sensing and prosthetic technology. Their flexibility, low cost, and ease of processing make them a compelling alternative to traditional metal counterparts in EMI shielding. While metals have proven effective in this role, they have drawbacks such as limited corrosion resistance, high processing costs, and substantial weight. Insulating elastomers are transformed into conductive or semiconducting materials through the strategic integration of conducting fillers. This versatile approach allows for the fine-tuning of polymer properties, enabling customisation to meet specific application requirements. These tailor-made materials find extensive use in diverse fields of electronics.

Natural rubber is an insulating material with good flexibility, low cost, and easily available. Introducing conducting fillers can significantly change the applicability of NR. Carbon black is a conventional reinforcing filler used to improve the mechanical properties of NR. Employing conductive carbon black (CCB) filler is economical, and can also impart conductivity in NR. Nano-dimensional CNT and graphene are also used as conducting fillers. Ionic liquid modification on these fillers can strengthen the rubber-filler interphase, leading to enriched properties.

In this work, hybrid filler NR composites are fabricated with a focus on high-performance conducting rubber composites for EMI shielding applications. Synergistic effect of conducting hybrid fillers could help to attain the goal. The challenge of this work is to improve the interfacial interaction and dispersion of hybrid filler in rubber matrix. Combination of fillers can reduce the aggregation and result in the formation of a continuous conducting network through the interaction of functional groups present on the surface of fillers. Also, chemical modifications of the fillers and the processing techniques adopted can enhance the filler dispersion. For this, ionic liquid modification and two types of processing techniques are employed. Theoretical studies on the experimental analysis give better insight into the underlying rubber-

filler and filler-filler interactions. A comprehensive analysis of the dielectric and electrical properties of these composites is conducted, evaluating their potential as EMI shielding devices. Knowing the challenges in fabrication and its application, we have prepared hybrid fillers of CCB-CNT, CCB-CNT-RGO, and ionic liquid modified fillers incorporated NR using two-step processing. A comparative analysis is performed on the properties of the NR hybrid filler systems.

1.7. Gap areas

- Development of economical and environment-friendly conducting NR composites.
- Attainment of homogeneous dispersion of filler in the matrix to get a continuous conducting pathway.

1.8. Objectives of the work

The main objective of the research work is to develop conducting NR composites incorporated with hybrid fillers. Although many studies have been carried out in this field, our aim is to utilise the synergistic effect of hybrid filler to enhance the conductivity of the NR matrix. Various strategies are adopted to get a homogeneous dispersion of nanosized filler with a continuous conducting network. The objectives are:

1. Synthesis of conducting fillers such as reduced graphene oxide (RGO) using Hummer's method.
2. To prepare NR/CCB and NR/hybrid filler systems using RGO, CNT and CCB by employing two-step processing and analysis of the properties.
3. Modifying filler surface using ionic liquid, 1-ethyl-3-methylimidazoliumchloride and its characterization using spectroscopic and microscopic methods.
4. Preparation of NR hybrid filler systems using laboratory synthesised RGO and analysis of properties.
5. Preparation of modified filler incorporated NR hybrid systems and its characterisation.
6. To study cure, dielectric, mechanical, viscoelastic, solvent transport and thermal properties of the fabricated systems. Theoretical studies of the experimental data by applying various models.
7. To investigate the properties in terms of the EMI shielding application.

1.9. Scope of the work

Conductive elastomers will benefit significantly in the electronic industry, sensors, actuators, intelligent clothes, artificial muscles and dielectric materials. It has been proved that the conducting fillers can create an electrical pathway by the formation of filler-filler networks within the rubber matrix. In the present work, conducting hybrid fillers are incorporated in the NR matrix and attained composites with high EMI shielding and mechanical and thermal stability. It is found to be a potential material for application in electronics domain.

1.10. References

1. Zhan Y, Oliviero M, Wang J, Sorrentino A, Buonocore GG, Sorrentino L, et al. Enhancing the EMI shielding of natural rubber-based supercritical CO 2 foams by exploiting their porous morphology and CNT segregated networks. Nanoscale. 2019;11(3):1011–20.
2. Jia LC, Li YK, Yan DX. Flexible and efficient electromagnetic interference shielding materials from ground tire rubber. Carbon. 2017;121:267–73.
3. Jia LC, Yan DX, Yang Y, Zhou D, Cui CH, Bianco E, et al. High Strain Tolerant EMI Shielding Using Carbon Nanotube Network Stabilized Rubber Composite. Adv Mater Technol. 2017;2(7):1–6.
4. Sheng A, Yang Y, Ren W, Duan H, Liu B, Zhao G, et al. Ground tire rubber composites with hybrid conductive network for efficiency electromagnetic shielding and low reflection. J Mater Sci Mater Electron. 2019;30(15):14669–78.
5. Rohini R, Bose S. Electromagnetic wave suppressors derived from crosslinked polymer composites containing functional particles: Potential and key challenges. Nano-Struct Nano-Objects. 2017;12:130–46.
6. Yee MJ, Mubarak NM, Abdullah EC, Khalid M, Walvekar R, Karri RR, et al. Carbon nanomaterials based films for strain sensing application—A review. Nano-Struct Nano-Objects. 2019;18:100312.
7. Kumar V, Alam MN, Manikkavel A, Song M, Lee DJ, Park SS. Silicone Rubber Composites Reinforced by Carbon Nanofillers and Their Hybrids for Various Applications: A Review. Polymers. 2021 Jul 15;13(14):2322.
8. Dhakal KN, Khanal S, Krause B, Lach R, Grellmann W, Le HH, et al. Electrically conductive and piezoresistive polymer nanocomposites using multiwalled carbon nanotubes in a flexible copolyester: Spectroscopic, morphological, mechanical and electrical properties. Nano-Struct Nano-Objects. 2022;29:100806.
9. Giannone P, Graziani S, Umana E. Investigation of carbon black loaded natural rubber piezoresistivity. In: 2015 IEEE International Instrumentation and Measurement Technology Conference (I2MTC) Proceedings. 2015. p. 1477–81.
10. Jin X, Feng C, Ponnamma D, Yi Z, Parameswaranpillai J, Thomas S, et al. Review on exploration of graphene in the design and engineering of smart sensors, actuators and soft robotics. Chem Eng J Adv. 2020;4:100034.
11. Ganapathy T, Sathiskumar R, Sanjay MR, Senthamaraikannan P, Saravanakumar SS, Parameswaranpillai J, et al. Effect of Graphene Powder on Banyan Aerial Root Fibers Reinforced Epoxy Composites. J Nat Fibers. 2021 Jul 3;18(7):1029–36.
12. Sreenath PR, Mandal S, Panigrahi H, Das P, Dinesh Kumar K. Carbon dots: Fluorescence active, covalently conjugated and strong reinforcing nanofiller for polymer latex. Nano-Struct Nano-Objects. 2020;23:100477.
13. Basheer B V, George JJ, Siengchin S, Parameswaranpillai J. Polymer grafted carbon nanotubes—Synthesis, properties, and applications: A review. Nano-Struct Nano-Objects. 2020;22:100429.
14. Al-Sehemi AG, Al-Ghamdi AA, Dishovsky NT, Malinova P, Atanasov NT, Atanasova GL. Natural rubber composites containing low and high dielectric constant fillers and their application as substrates for compact flexible antennas. Polym Polym Compos. 2020 Mar 18;29(4):233–45.

15. Nanda M. Physico-mechanical and electrical properties of conductive carbon black reinforced chlorosulfonated polyethylene vulcanizates. Express Polym Lett - EXPRESS POLYM LETT. 2008 Nov 28;2:855–65.
16. Wang YB, Huang ZX, Qin Y, Du M, Zhang LM. Experimental Investigation on the Electrical and Dynamic Mechanical Properties of PMN/Electrically Conductive Carbon Black/Butyl Composites. Composite Materials V. Trans Tech Publications Ltd.; 2007. p. 171–5.
17. Alarifi IM. Investigation the conductivity of carbon fiber composites focusing on measurement techniques under dynamic and static loads. J Mater Res Technol. 2019;8(5):4863–93.
18. Jayalakshmy MS. Applications of Rubber Based Biocomposites and Bionanocomposites. In: Visakh P. M., editor. Rubber Based Bionanocomposites: Preparation [Internet]. Cham: Springer International Publishing; 2017. p. 167–76. Available from: https://doi.org/10.1007/978-3-319-48806-6_8
19. Liu H, Gao H, Hu G. Highly sensitive natural rubber/pristine graphene strain sensor prepared by a simple method. Compos Part B Eng. 2019 Aug 15;171:138–45.
20. Tang B, Chen X, He Y, Zhou J, Zhao H, Chen W, et al. Fabrication of kapok fibers and natural rubber composites for pressure sensor applications. Cellulose. 2021 Mar 1;28(4):2287–301.
21. R. Torres, A. Venugopalarao, I. Neckel, R. Ramalingame, C. Müller, O. Kanoun. Strain Sensor Based on MWCNT-Natural Rubber Composite for Wearable Electronics. In: 2016 Nanotechnology for Instrumentation and Measurement (NANOfIM). 2016. p. 5–16.
22. Job A, Oliveira F, Alves N, Giacometti J, Mattoso L. Conductive composites of natural rubber and carbon black for pressure sensors. Synth Met - Synth Met. 2003 Apr 1;135:99–100.
23. Datta RN, Huntink NM, Datta S, Talma AG. Rubber Vulcanizates Degradation and Stabilization. Rubber Chem Technol. 2007 Jul 1;80(3):436–80.
24. Boonkerd K, Chuayjuljit S, Abdulraman D, Jaranrangsup W. Silica-Rich Filler for the Reinforcement in Natural Rubber. Rubber Chem Technol. 2012;85(1):1–13.
25. Kaewsakul W, Sahakaro K, Noordermeer JWM. Optimization of mixing conditions for silica-reinforced natural rubber compounds. Chem Listy. 2011;105(15 SPEC. ISSUE):277–94.
26. Ľalíková S, Pajtášová M, Chromčíková M, Liška M, Šutinská V, Olšovský M, et al. Investigation of natural rubber composites with addition of montmorillonite fillers using thermal analysis. J Therm Anal Calorim. 2011;104(3):969–73.
27. Avalos F, Ortiz JC, Zitzumbo R, López-Manchado MA, Verdejo R, Arroyo M. Effect of montmorillonite intercalant structure on the cure parameters of natural rubber. Eur Polym J. 2008;44(10):3108–15.
28. Hrachová J, Komadel P, Chodák I. Effect of montmorillonite modification on mechanical properties of vulcanized natural rubber composites. J Mater Sci. 2008;43(6):2012–7.
29. Jincheng W, Yuehui C, Jihu W. Novel Reinforcing Filler: Application to Natural Rubber (NR) System. J Elastomers Plast. 2005;37(2):169–80.
30. Abhisha V, Augustine A, Joseph J, Thomas SP, Stephen R. Effect of halloysite nanotubes and organically modified bentonite clay hybrid filler system on the properties of natural rubber. J Elastomers Plast. 2020 Aug;52(5):432–52.
31. El-Nashar DE, Mansour SH, Girgis E. Nickel and iron nano-particles in natural rubber composites. J Mater Sci. 2006;41(16):5359–64.
32. Medalia AI. Effect of Carbon Black on Dynamic Properties of Rubber Vulcanizates. Vol. 51, Rubber Chemistry and Technology. 1978. p. 437–523.
33. Kato A, Ikeda Y, Tsushi R, Kokubo Y, Kojima N. A new approach to visualizing the carbon black/natural rubber interaction layer in carbon black-filled natural rubber vulcanizates and to elucidating the dependence of mechanical properties on quantitative parameters. Colloid Polym Sci. 2013;291(9):2101–10.
34. Farida E, Bukit N, Ginting EM, Bukit BF. The effect of carbon black composition in natural rubber compound. Case Stud Therm Eng. 2019 Dec;16:100566.
35. Al-Mutairi N, Braihi A, Ahmed J, J.Khadim B. Effect of Graphite on the Properties of Natural Rubber. 2017.
36. Cheng J, Niu S, Zhao Y, Liu Y, Kang M, Guan Y, et al. The flame retardant and thermal conductivity properties of high thermal conductivity expandable graphite microcapsule filled natural rubber composites. Constr Build Mater. 2022 Feb 7;318:125998.
37. Bokobza L. Multiwall carbon nanotube-filled natural rubber: Electrical and mechanical properties. Express Polym Lett. 2012;6(3):213–23.
38. Azira AA, Hassim DHAI, Verasamy D, Suriani AB, Rusop M. Properties of Natural Rubber Nanocomposites Reinforced with Carbon Nanotubes. Adv Mater Res. 2015;1109:195–9.

39. Girun N, Ahmadun FR, Rashid SA, Atieh MA. Multi-wall carbon nanotubes/Styrene Butadiene Rubber (SBR) nanocomposite. Fuller Nanotub Carbon Nanostructures. 2007;15(3):207–14.
40. Katihabwa a. Multi-walled carbon nanotubes/silicone rubber nanocomposites prepared by high shear mechanical mixing. J Reinf Plast Compos. 2011;30(12):1007–14.
41. Medupin RO, Abubakre OK, Abdulkareem AS, Muriana RA, Abdulrahman AS. Carbon Nanotube Reinforced Natural Rubber Nanocomposite for Anthropomorphic Prosthetic Foot Purpose. Sci Rep. 2019 Dec 27;9(1):20146.
42. Liu X, Guo R, Lin Z, Yang Y, Xia H, Yao Z. Resistance-strain sensitive rubber composites filled by multiwalled carbon nanotubes for structuraldeformation monitoring. Nanomater Nanotechnol. 2021 Jan 1;11:18479804211011384.
43. Araby S, Zhang L, Kuan HC, Dai J Bin, Majewski P, Ma J. A novel approach to electrically and thermally conductive elastomers using graphene. Polym U K. 2013;54(14):3663–70.
44. Fu DH, Zhan YH, Yan N, Xia HS. A comparative investigation on strain induced crystallization for graphene and carbon nanotubes filled natural rubber composites. Express Polym Lett. 2015;9(7):597–607.
45. Frasca D, Schulze D, Wachtendorf V, Huth C, Schartel B. Multifunctional multilayer graphene/elastomer nanocomposites. Eur Polym J. 2015;71:99–113.
46. Lin Y, Dong X, Liu S, Chen S, Wei Y, Liu L. Graphene-Elastomer Composites with Segregated Nanostructured Network for Liquid and Strain Sensing Application. ACS Appl Mater Interfaces. 2016;8(36):24143–51.
47. Lim LP, Juan JC, Huang NM, Goh LK, Leng FP, Loh YY. Enhanced tensile strength and thermal conductivity of natural rubber graphene composite properties via rubber-graphene interaction. Mater Sci Eng B. 2019;246:112–9.
48. Zhang W, Yin B, Wang J, Mohamed A, Jia H. Ultrasensitive and wearable strain sensors based on natural rubber/graphene foam. J Alloys Compd. 2019;785:1001–8.
49. Dong B, Wu S, Zhang L, Wu Y. High Performance Natural Rubber Composites with Well-Organized Interconnected Graphene Networks for Strain-Sensing Application. Ind Eng Chem Res. 2016 May 4;55(17):4919–29.
50. Duan X, Cheng S, Li Z, Liang C, Zhang Z, Zhao G, et al. Flexible and environmentally friendly graphene natural rubber composites with high thermal conductivity for thermal management. Compos Part Appl Sci Manuf. 2022 Dec 1;163:107223.
51. Bhattacharya SK. Metal filled polymers. Vol. 11. CRC Press; 1986.
52. Bartlett MD, Fassler A, Kazem N, Markvicka EJ, Mandal P, Majidi C. Stretchable, high-k dielectric elastomers through liquid-metal inclusions. Adv Mater. 2016;28(19):3726–31.
53. Kazem N, Hellebrekers T, Majidi C. Soft multifunctional composites and emulsions with liquid metals. Adv Mater. 2017;29(27):1605985.
54. Ruße M. Elastomere mit metallbeschich- teten Rußen. :8.
55. Akesson J, Seal S, Shukla S, Rahman Z. Copper plating process control by SEM. Adv Mater Process. 2002;160(2):33.
56. Zhang Y long, Zang C guang, Jiao Q jie. Electrical and thermal properties of silicone rubber composites filled with Cu-coated carbon fibres and functional carbon nanotubes. Plast Rubber Compos. 2019;
57. Kumar YR, Deshmukh K, Kennedy LJ, Keçili R, Hussain CM, Kesarla MK, et al. Chapter 7 - MXenes and their composites: emerging materials for gas sensing and biosensing. In: Sadasivuni KK, Deshmukh K, Pasha SKK, Kovářík T, editors. Mxenes and their Composites [Internet]. Elsevier; 2022. p. 241–79. Available from: https://www.sciencedirect.com/science/article/pii/B9780128233610000162
58. Yang W, Liu JJ, Wang LL, Wang W, Yuen ACY, Peng S, et al. Multifunctional MXene/natural rubber composite films with exceptional flexibility and durability. Compos Part B Eng. 2020 May 1;188:107875.
59. Luo JQ, Zhao S, Zhang HB, Deng Z, Li L, Yu ZZ. Flexible, stretchable and electrically conductive MXene/natural rubber nanocomposite films for efficient electromagnetic interference shielding. Compos Sci Technol. 2019;182(July):107754.
60. Wypych G. 5 - FUNCTIONAL FILLERS – STRUCTURE. In: Wypych G, editor. Functional Fillers [Internet]. ChemTec Publishing; 2018. p. 101–51. Available from: https://www.sciencedirect.com/science/article/pii/B9781927885376500072
61. Mehra N, Mu L, Ji T, Zhu J. Chapter 3 - Thermal Conduction in Polymer Composites. In: Song K, Liu C, Guo JZ, editors. Polymer-Based Multifunctional Nanocomposites and Their

Applications [Internet]. Elsevier; 2019. p. 77–110. Available from: https://www.sciencedirect.com/science/article/pii/B9780128150672000032
62. Ivanoska-Dacikj A, Bogoeva-Gaceva G, Rooj S, Wie??ner S, Heinrich G. Fine tuning of the dynamic mechanical properties of natural rubber/carbon nanotube nanocomposites by organically modified montmorillonite: A first step in obtaining high-performance damping material suitable for seismic application. Appl Clay Sci. 2015;118:99–106.
63. Mangalath S, Abraham S, Joseph J. pH-Responsive Fluorescence Enhancement in Graphene Oxide – Naphthalimide Nanoconjugates : A Fluorescence Turn-On Sensor for Acetylcholine. 2017;11404–9.
64. Das A, Stöckelhuber KW, Rooj S, Wang DY, Heinrich G. Synergistic effects of expanded nanoclay and carbon black on natural rubber compounds. KGK Kautsch Gummi Kunststoffe. 2010;63(7–8):296–302.
65. Rattanasom N, Prasertsri S. Mechanical properties, gas permeability and cut growth behaviour of natural rubber vulcanizates: Influence of clay types and clay/carbon black ratios. Polym Test. 2012;31(5):645–53.
66. Liu YB, Li L, Wang Q. Reinforcement of natural rubber with carbon black/nanoclay hybrid filler. Plast Rubber Compos. 2010;39(8):370–6.
67. Thimmaiah SR, Siddaramaiah. Investigation of carbon black and metakaolin cofillers content on mechanical and thermal behaviors of natural rubber compounds. J Elastomers Plast. 2013;45(2):187–98.
68. Ahmed K, Nizami SS, Riza NZ. Reinforcement of natural rubber hybrid composites based on marble sludge/Silica and marble sludge/rice husk derived silica. J Adv Res. 2014;5(2):165–73.
69. Ismail H, Ramly AF, Othman N. Effects of silica/multiwall carbon nanotube hybrid fillers on the properties of natural rubber nanocomposites. J Appl Polym Sci. 2013;128(4):2433–8.
70. Al-Ghamdi AA, Al-Hartomy OA, Al-Solamy FR, Dishovsky N, Mihaylov M, Malinova P, et al. Dielectric and microwave properties of elastomer composites loaded with carbon-silica hybrid fillers. J Appl Polym Sci. 2016;133(7):1–9.
71. Fritzsche J, Lorenz H, Klüppel M. CNT based elastomer-hybrid-nanocomposites with promising mechanical and electrical properties. Macromol Mater Eng. 2009;294(9):551–60.
72. Chattopadhyay PK, Das NC, Chattopadhyay S. Influence of interfacial roughness and the hybrid filler microstructures on the properties of ternary elastomeric composites. Compos Part Appl Sci Manuf. 2011;42(8):1049–59.
73. Sreelekshmi R V., Sudha JD, Menon ARR. Novel organomodified kaolin/silica hybrid fillers in natural rubber and its blend with polybutadiene rubber. Polym Bull. 2017;74(3):783–801.
74. Li H, Yang L, Weng G, Xing W, Wu J, Huang G. Toughening rubbers with a hybrid filler network of graphene and carbon nanotubes. J Mater Chem A. 2015;3(44):22385–92.
75. Tan QC, Shanks RA, Hui D, Kong I. Functionalised graphene-multiwalled carbon nanotube hybrid poly(styrene-b-butadiene-b-styrene) nanocomposites. Compos Part B Eng. 2016;90:315–25.
76. Liu H, Gao J, Huang W, Dai K, Zheng G, Liu C, et al. Electrically conductive strain sensing polyurethane nanocomposites with synergistic carbon nanotubes and graphene bifillers. Nanoscale. 2016;8(26):12977–89.
77. Li H, Yang L, Weng G, Xing W, Wu J, Huang G. Toughening rubbers with a hybrid filler network of graphene and carbon nanotubes. J Mater Chem A. 2015;3(44):22385–92.
78. Aguilar-Bolados H, Yazdani-Pedram M, Contreras-Cid A, López-Manchado MA, May-Pat A, Avilés F. Influence of the morphology of carbon nanostructures on the piezoresistivity of hybrid natural rubber nanocomposites. Compos Part B Eng. 2017 Jan;109:147–54.
79. Ponnamma D, Sadasivuni KK, Strankowski M, Guo Q, Thomas S. Synergistic effect of multi walled carbon nanotubes and reduced graphene oxides in natural rubber for sensing application. Soft Matter. 2013;9(43):10343–53.
80. Aguilar-Bolados H, Yazdani-Pedram M, Contreras-Cid A, López-Manchado MA, May-Pat A, Avilés F. Influence of the morphology of carbon nanostructures on the piezoresistivity of hybrid natural rubber nanocomposites. Compos Part B Eng. 2017;109:147–54.
81. Thaptong P, Sirisinha C, Thepsuwan U, Sae-Oui P. Properties of Natural Rubber Reinforced by Carbon Black-based Hybrid Fillers. Polym - Plast Technol Eng. 2014;53(8):818–23.
82. Nakaramontri Y, Pichaiyut S, Wisunthorn S, Nakason C. Hybrid carbon nanotubes and conductive carbon black in natural rubber composites to enhance electrical conductivity by reducing gaps separating carbon nanotube encapsulates. Eur Polym J. 2017;90:467–84.

83. Zhan YH, Liu GQ, Xia HS, Yan N. Natural rubber / carbon black / carbon nanotubes composites prepared through ultrasonic assisted latex mixing process. 2011;40(1).
84. Roland CM. Electrical and dielectric properties of rubber. Rubber Chem Technol. 2016;89(file:///E:/Work Data/aa NR_CCB_CNT/references ccb cnt/natarajan2017.pdf):32–53.
85. Kitisavetjit W, Nakaramontri Y, Pichaiyut S, Wisunthorn S, Nakason C, Kiatkamjornwong S. Influences of carbon nanotubes and graphite hybrid filler on properties of natural rubber nanocomposites. Polym Test. 2021 Jan 1;93:106981.
86. Thongkong N, Wisunthorn S, Pichaiyut S, Nakason C, Kiatkamjornwong S. Natural rubber nanocomposites based on hybrid filler of zinc nanoparticles and carbon nanotubes: Electrical conductivity and other related properties. Express Polym Lett. 2020;14(12):1137–54.
87. Salaeh S, Kao-ian P. Conductive epoxidized natural rubber nanocomposite with mechanical and electrical performance boosted by hybrid network structures. Polym Test. 2022 Apr 1;108:107493.
88. Qian M, Zou B, Shi Y, Zhang Y, Wang X, Huang W, et al. Enhanced mechanical and dielectric properties of natural rubber using sustainable natural hybrid filler. Appl Surf Sci Adv. 2021 Dec 1;6:100171.
89. Haseena A, Unnikrishnan G, Kalaprasad G. Dielectric properties of short sisal/coir hybrid fibre reinforced natural rubber composites. Compos Interfaces. 2007;14(7–9):763–86.
90. Jacob M, Varughese KT, Thomas S. Dielectric characteristics of sisal–oil palm hybrid biofibre reinforced natural rubber biocomposites. J Mater Sci. 2006 Sep 1;41(17):5538–47.
91. Pan H, Wang Z, Cui Y, Cao L, Zong C. Influences of porous reduction graphene oxide/molybdenum disulfide as filler on dielectric properties, thermal stability, and mechanical properties of natural rubber. J Vinyl Addit Technol. 2021 Nov 1;27(4):868–80.
92. Ravikumar K, Palanivelu K, Ravichandran K. Vulcanization, Mechanical and Dielectric Properties of Carbon Black/Nanoclay Reinforced Natural Rubber Hybrid Composites. Appl Mech Mater. 2015;766–767:377–82.
93. George N, Venugopal B, John H, Mathiazhagan A, Joseph R. Nanosilica decorated multiwalled carbon nanotubes (CS hybrids) in natural rubber latex. Polymer. 2019 Jan 14;161:170–80.
94. Geng H, Zhao P, Mei J, Chen Y, Yu R, Zhao Y, et al. Improved microwave absorbing performance of natural rubber composite with multi-walled carbon nanotubes and molybdenum disulfide hybrids. Polym Adv Technol. 2020 Nov 1;31(11):2752–62.
95. Zhou M, Wan G, Mou P, Teng S, Lin S, Wang G. CNT@NiO/natural rubber with excellent impedance matching and low interfacial thermal resistance toward flexible and heat-conducting microwave absorption applications. J Mater Chem C. 2021;9(3):869–80.
96. Prabhahar M, S J, Arun Prakash VR. Role of Magnetite (Fe3O4)-Titania (TiO2) hybrid particle on mechanical, thermal and microwave attenuation behaviour of flexible natural rubber composite in X and Ku band frequencies. Mater Res Express. 2020 Jan 1;7.
97. Yaragalla S, Sindam B, Abraham J, Raju KCJ, Kalarikkal N, Thomas S. Fabrication of graphite-graphene-ionic liquid modified carbon nanotubes filled natural rubber thin films for microwave and energy storage applications. J Polym Res. 2015;22(7).
98. Posadas P, Gonzalez-Jimenez A, Valentin JL. Natural rubber: Properties, behavior and uses. In: Natural Rubber: Properties, Behavior and Applications. 2016. p. 1–24.
99. Rao IJ, Rajagopal KR. A study of strain-induced crystallization of polymers. Int J Solids Struct. 2001 Feb 1;38(6):1149–67.
100. Sethulekshmi AS, Jayan JS, Saritha A, Joseph K. Recent developments in natural rubber nanocomposites containing graphene derivatives and its hybrids. Ind Crops Prod. 2022 Mar 1;177:114529.
101. Comparison of Mechanical Properties of Natural Rubber Vulcanizates Filled with Hybrid Fillers (Carbon Black/Palm Kernel Shell and Palm Kernel Shell/Sandbox Seed Shell). :7.
102. Li J, Zhao X, Zhang Z, Xian Y, Lin Y, Ji X, et al. Construction of interconnected Al2O3 doped rGO network in natural rubber nanocomposites to achieve significant thermal conductivity and mechanical strength enhancement. Compos Sci Technol. 2020 Jan 20;186:107930.
103. Roy K, Chandra Debnath S, Das A, Heinrich G, Potiyaraj P. Exploring the synergistic effect of short jute fiber and nanoclay on the mechanical, dynamic mechanical and thermal properties of natural rubber composites. Polym Test. 2018;67:487–93.
104. Tzounis L, Debnath S, Rooj S, Fischer D, Mäder E, Das A, et al. High performance natural rubber composites with a hierarchical reinforcement structure of carbon nanotube modified natural fibers. Mater Des. 2014 Jun 1;58:1–11.

105. Ahmed K, Nizami SS, Riza NZ. Reinforcement of natural rubber hybrid composites based on marble sludge/Silica and marble sludge/rice husk derived silica. J Adv Res. 2014;5(2):165–73.
106. Pan H, Wang Z, Cui Y, Cao L, Zong C. Influences of porous reduction graphene oxide/molybdenum disulfide as filler on dielectric properties, thermal stability, and mechanical properties of natural rubber. J Vinyl Addit Technol. 2021 Nov 1;27(4):868–80.
107. Krainoi A, Kummerlöwe C, Vennemann N, Nakaramontri Y, Pichaiyut S. Effect of carbon nanotubes decorated with silver nanoparticles as hybrid filler on properties of natural rubber nanocomposites. J Appl Polym Sci. 2018 Nov 25;136:47281.
108. Krossing I, Slattery JM, Daguenet C, Dyson PJ, Oleinikova A, Weingärtner H. Why Are Ionic Liquids Liquid? A Simple Explanation Based on Lattice and Solvation Energies [J. Am. Chem. Soc. 2006, 128, 13427−13434]. J Am Chem Soc. 2007 Sep 1;129(36):11296–11296.
109. El Seoud OA, Koschella A, Fidale LC, Dorn S, Heinze T. Applications of Ionic Liquids in Carbohydrate Chemistry: A Window of Opportunities. Biomacromolecules. 2007 Sep 1;8(9):2629–47.
110. Walden, P. Ueber die Molekulargr¨osse und elektrische Leitf¨ahigkeit einiger geschmolzenen Salze. 1914. 8(6):405–22.
111. Wasserscheid P, Keim W. Ionic Liquids-New “Solutions” for Transition Metal Catalysis. Angew Chem Int Ed Engl. 2000 Nov 3;39(21):3772–89.
112. Hallett JP, Welton T. Room-Temperature Ionic Liquids: Solvents for Synthesis and Catalysis. 2. Chem Rev. 2011 May 11;111(5):3508–76.
113. Goujon LJ, Khaldi A, Maziz A, Plesse C, Nguyen GTM, Aubert PH, et al. Flexible Solid Polymer Electrolytes Based on Nitrile Butadiene Rubber/Poly(ethylene oxide) Interpenetrating Polymer Networks Containing Either LiTFSI or EMITFSI. Macromolecules. 2011 Dec 27;44(24):9683–91.
114. Maciejewska M, Zaborski M. Ionic liquids as coagents for sulfur vulcanization of butadiene–styrene elastomer filled with carbon black. Polym Bull. 2018 Oct;75(10):4499–514.
115. Silva TA. Electrochemical sensor based on ionic liquid and carbon black for voltammetric determination of Allura red colorant at nanomolar levels in soft drink powders. :44.
116. Narongthong J, Le HH, Das A, Sirisinha C, Wießner S. Ionic liquid enabled electrical-strain tuning capability of carbon black based conductive polymer composites for small-strain sensors and stretchable conductors. Compos Sci Technol. 2019 Apr;174:202–11.
117. Narongthong J, Wießner S, Hait S, Sirisinha C, Stöckelhuber KW. Strain-rate independent small-strain-sensor: Enhanced responsiveness of carbon black filled conductive rubber composites at slow deformation by using an ionic liquid. Compos Sci Technol. 2020 Mar;188:107972.
118. Abraham J, Jose T, Moni G, George SC, Kalarikkal N, Thomas S. Ionic liquid modified multiwalled carbon nanotube embedded styrene butadiene rubber membranes for the selective removal of toluene from toluene/methanol mixture via pervaporation. J Taiwan Inst Chem Eng. 2019 Feb;95:594–601.
119. Ge Y, Zhang Q, Zhang Y, Liu F, Han J, Wu C. High-performance natural rubber latex composites developed by a green approach using ionic liquid-modified multiwalled carbon nanotubes. J Appl Polym Sci. 2018 Oct 10;135(38):46588.
120. Krainoi A, Kummerlöwe C, Nakaramontri Y, Wisunthorn S, Vennemann N, Pichaiyut S, et al. Influence of carbon nanotube and ionic liquid on properties of natural rubber nanocomposites. Express Polym Lett. 2019;13(4):327–48.
121. Sahoo BP, Naskar K, Tripathy DK. Multiwalled Carbon Nanotube‐Filled Ethylene Acrylic Elastomer Nanocomposites: Influence of Ionic Liquids on the Mechanical, Dynamic Mechanical, and Dielectric Properties. :13.
122. Subramaniam K, Das A, Heinrich G. Development of conducting polychloroprene rubber using imidazolium based ionic liquid modified multi-walled carbon nanotubes. Compos Sci Technol. 2011 Jul;71(11):1441–9.
123. Kim TY, Lee HW, Stoller M, Dreyer DR, Bielawski CW, Ruoff RS, et al. High-performance supercapacitors based on poly (ionic liquid)-modified graphene electrodes. ACS Nano. 2011;5(1):436–42.
124. Lyu Q, Yan H, Li L, Chen Z, Yao H, Nie Y. Imidazolium ionic liquid modified graphene oxide: as a reinforcing filler and catalyst in epoxy resin. Polymers. 2017;9(9):447.
125. Yin Q, Wen Y, Jia H, Hong L, Ji Q, Xu Z. Enhanced mechanical, dielectric, electrical and thermal conductive properties of HXNBR/HNBR blends filled with ionic liquid-modified multiwalled carbon nanotubes. J Mater Sci. 2017 Sep;52(18):10814–28.

126. Le HH, Hait S, Das A, Wiessner S, Stoeckelhuber KW, Boehme F, et al. Self-healing properties of carbon nanotube filled natural rubber/bromobutyl rubber blends. Express Polym Lett. 2017;11(3):230–42.
127. Abraham J, P. MA, Kailas L, Kalarikkal N, George SC, Thomas S. Developing highly conducting and mechanically durable styrene butadiene rubber composites with tailored microstructural properties by a green approach using ionic liquid modified MWCNTs. RSC Adv. 2016;6(39):32493–504.
128. Abraham J, Arif P M, Xavier P, Bose S, George SC, Kalarikkal N, et al. Investigation into dielectric behaviour and electromagnetic interference shielding effectiveness of conducting styrene butadiene rubber composites containing ionic liquid modified MWCNT. Polymer. 2017 Mar;112:102–15.
129. Yin Q, Wen Y, Jia H, Hong L, Ji Q, Xu Z. Enhanced mechanical, dielectric, electrical and thermal conductive properties of HXNBR/HNBR blends filled with ionic liquid-modified multiwalled carbon nanotubes. J Mater Sci. 2017 Sep;52(18):10814–28.
130. Carrión FJ, Espejo C, Sanes J, Bermúdez MD. Single-walled carbon nanotubes modified by ionic liquid as antiwear additives of thermoplastics. Compos Sci Technol. 2010 Dec;70(15):2160–7.
131. Wang B, Tang W, Liu X, Huang Z. Synthesis of ionic liquid decorated muti-walled carbon nanotubes as the favorable water-based lubricant additives. Appl Phys A. 2017 Nov;123(11):680.
132. Pamies R, Espejo C, Carrión FJ, Morina A, Neville A, Bermúdez MD. Rheological behavior of multiwalled carbon nanotube-imidazolium tosylate ionic liquid dispersions. J Rheol. 2017 Mar;61(2):279–89.
133. Kreyenschulte H, Richter S, Götze T, Fischer D, Steinhauser D, Klüppel M, et al. Interaction of 1-allyl-3-methyl-imidazolium chloride and carbon black and its influence on carbon black filled rubbers. Carbon. 2012 Aug 1;50(10):3649–58.
134. Chu L, Kan M, Jerrams S, Zhang R, Xu Z, Liu L, et al. Constructing Chemical Interface Layers by Using Ionic Liquid in Graphene Oxide/Rubber Composites to Achieve High-Wear Resistance in Environmental-Friendly Green Tires. ACS Appl Mater Interfaces. 2022 Feb 2;14(4):5995–6004.
135. Das M, Aswathy TR, Pal S, Naskar K. Effect of ionic liquid modified graphene oxide on mechanical and self-healing application of an ionic elastomer. Eur Polym J. 2021 Sep 5;158:110691.

Chapter 2

Materials, Fabrication Methods and Characterisation Techniques

Summary

This chapter discusses the materials and fabrication methods for making natural rubber (NR) hybrid filler systems. The specifications of conductive fillers and ionic liquid employed for the present study are discussed. The detailed procedure for synthesising thermally reduced graphene oxide (syTRGO) and fabrication of NR composites are included. It also details the characterisation techniques used to analyse the properties of fillers and NR hybrid filler systems.

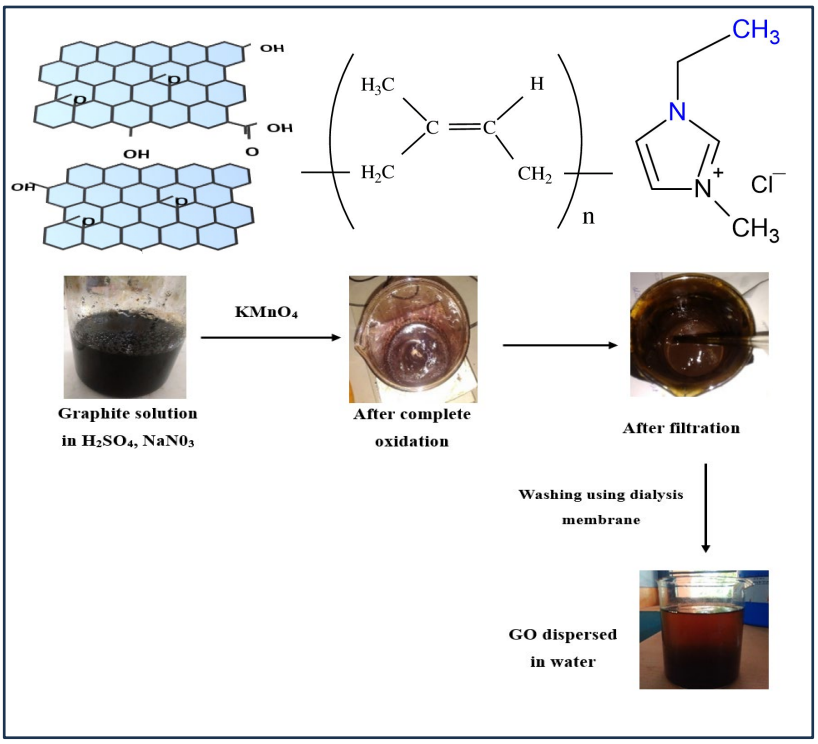

2.1. Materials

2.1.1. Natural rubber (NR)

Natural rubber (NR) is obtained as latex from the *Hevea Brasiliensis* tree. It is composed of cis-1,4-polyisoprene, which is a stereoregular polymer derived from the monomer isoprene. Notably, NR possesses a glass transition temperature (Tg) of -71°C and an approximate molecular weight of 1.5 x 10^6 g/mol. (1) For the present study, NR, specifically the ISNR 20 variant, was purchased from the Rubber Research Institute of India (RRII) in Kottayam, Kerala. Other contents in the NR include dirt, ash, volatile mass and nitrogen in the percentages 0.20, 1, 0.80 and more than 0.60, respectively. **Figure 2.1** shows the chemical structure of NR.

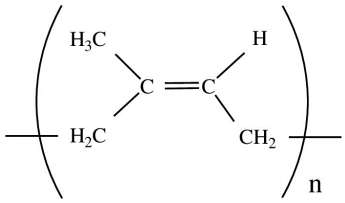

Figure 2.1-Structure of NR

2.1.2. Conductive fillers

2.1.2.1. Conductive carbon black (CCB)

Continental Carbon India Limited (CCIL) in Uttar Pradesh, India, generously supplied the conductive carbon black (CCB). The specific properties of this CCB are iodine number 240±10 mg/g, B.E.T surface area 260±10 m^2/g, ash content of less than 0.60 wt.%, and density 320 ± 20 kg/m^3.

2.1.2.2. Carbon nanotubes (CNT)

Multiwalled carbon nanotubes (CNT) were purchased from Ad-Nano Technologies Pvt Ltd, Karnataka, India. It has a purity greater than 99%, a diameter ranging from 10-15 nm, a length of ~ 5µm, and a surface area close to 400 m^2/g.

2.1.2.3. Reduced graphene oxide (RGO)

Carborundum Universal Limited in Kakkanad, Kerala, India, gifted the thermally reduced graphene oxide (RGO) powder. RGO is a black, fluffy powder with fewer than 15 layers. It has a bulk density of 0.01g/cm^3 and oxygen content under 7%. Its lateral dimensions are roughly 8-10 microns, and BET surface area ranges from 200-240 m^2/g.

2.1.2.4. Thermally reduced graphene oxide (syTRGO)

Thermally reduced graphene oxide (syTRGO) was prepared in the laboratory. Details of the preparation method are given in **section 2.2.1**. **Figure 2.2** shows the expected schematic structure of syTRGO.

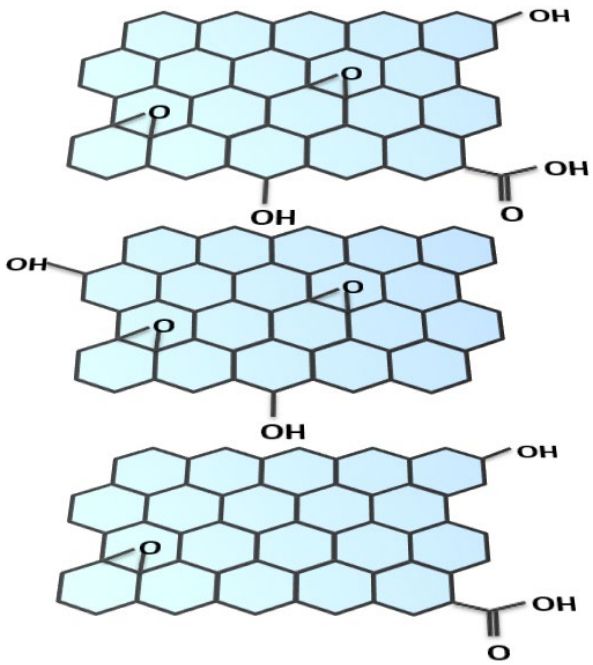

Figure 2.2-Schematic structure of thermally reduced graphene oxide

2.1.3. Ionic liquid

For the present work, the ionic liquid employed was 1-ethyl-3-methylimidazolium chloride, commonly referred to as EMIC. This product was procured from Sigma-Aldrich.

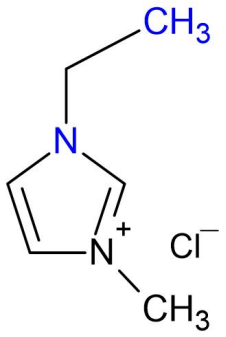

Figure 2.3-Structure of EMIC

EMIC is a colourless and odourless viscous liquid that remains in the liquid state at room temperature. Its molecular weight is 146.62 g/mol, with the chemical formula

being $C_6H_{11}ClN_2$, and it solidifies in the temperature range 77 to 79°C. **Figure 2.3** is the structure of EMIC.

2.1.4. Materials for the synthesis of thermally reduced graphene oxide (syTRGO)

Materials used for the synthesis of thermally reduced graphene oxide (syTRGO) is presented in **Table 2.1**.

Table 2.1-Materials for the synthesis of syTRGO

Ingredients	**Manufacturers, State/ Country**
Natural graphite flakes (mwt- 12.01g/mol)	Sigma-Aldrich, Germany
Sulphuric acid (H_2SO_4)	Fisher Scientific, India
Potassium permanganate ($KMnO_4$)	Spectrum, India
Hydrogen peroxide (H_2O_2) 30% w/v	Merck, India
Sodium nitrate ($NaNO_3$)	Spectrum, India
Dialysis membrane	HiMedia, India
Mwt cut-off 12000-14000	

2.2. Fabrication methods

2.2.1. Synthesis of thermally reduced graphene oxide (syTRGO)

Graphene oxide (GO) was synthesised from natural graphite flakes using Hummer's method. (2) In this procedure, graphite flakes (3g, 1 wt. equiv.), sodium nitrate ($NaNO_3$)(1.5g, 0.5 wt. equiv.) and concentrated sulfuric acid (H_2SO_4)(72 ml) were stirred together for 15 minutes. Subsequently, potassium permanganate ($KMnO_4$)(15g, 5 wt. equiv.) was added gradually, ensuring the temperature remained below 20°C. The mixture was then placed in a water bath set at 35°C and continuously stirred for 2 hours. 125 ml of water was slowly introduced, and the temperature was raised to 95°C for an additional hour. Then, 225 ml of water and hydrogen peroxide (H_2O_2) were added. To remove sulfate ions, the reaction mixture was washed with 5% hydrochloric acid (HCl). A dialysis membrane was employed to neutralise the pH of the solution. Ultimately, the mixture was centrifuged, and the resultant material was dried at 60°C overnight, yielding brown sheets of GO. The scheme for the synthesis of GO is given in **Figure 2.4.**

To produce reduced graphene oxide, the dried GO samples were placed in a crucible and then subjected to heating in a muffle furnace at 200°C for 2 hours. This procedure ensured the efficient reduction of GO. (3,4)

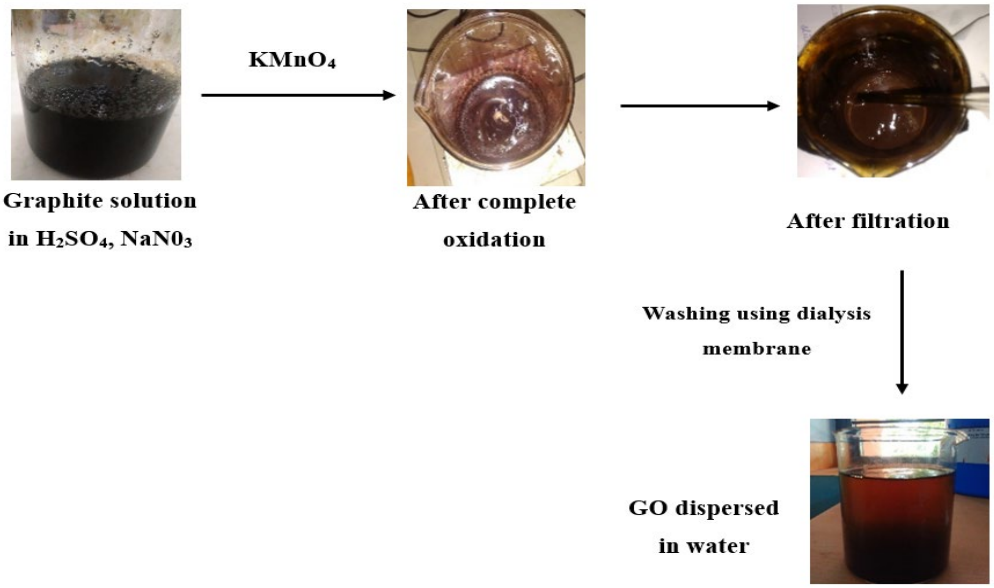

Figure 2.4-Scheme of synthesis of GO

2.2.2. Ionic liquid modification of fillers

Ionic liquid modification of the filler was performed by grinding the filler and ionic liquid in an agate mortar for 30 minutes. Subsequently, ethanol was added to the mixture, followed by sonication for 30 minutes. The resulting mixture was then subjected to overnight drying at 60°C in a hot air oven. Ionic liquid-modified composites were prepared with a filler-to-ionic liquid ratio of 1:1 and 1:3.

2.2.3. Compounding procedure of NR hybrid filler systems

NR hybrid filler systems were fabricated using a Brabender (Plastograph EC Plus, GmbH & CO. KG, Duisburg, Germany) under specific conditions: 8 minutes at 100°C and a rotation speed of 60 rpm. Following this, curatives were incorporated using an open two-roll mill maintained at ambient temperature, and the entire mixing process was completed in 15 minutes. The order of addition of filler in the composite fabrication process varied depending on the specific composite being produced. The fabrication of NR hybrid filler systems was carried out by mixing NR, fillers and curatives in various compositions (as given in **Table 2.2).** In the sample designations, 'N' stands for natural rubber and 'B' signifies conductive carbon black (CCB).

NR/CCB systems were given designations NB0, NB5, NB10, NB15 and NB20, and the numbers (0, 5, 10, 15 and 20) represent the weight percentage of CCB in the respective composite.

Table 2.2-Formulation of NR hybrid filler systems

Ingredient	**Quantity**
Natural rubber (NR)	100
Conductive carbon black (CCB)	5, 10, 15, 20
Multi-walled carbon nanotubes (CNT)	0.5, 1, 3, 5
Ionic liquid	1, 3
Reduced graphene oxide (RGO)	1
Synthesised thermally reduced graphene oxide (syTRGO)	1
Zinc oxide (ZnO)	5
Stearic acid ($C_{18}H_{36}O_2$)	3
N-cyclohexyl-2-benzothiazolesulpenaimde (CBS) ($C_{13}H_{16}N_2S_2$)	1.3
2-Mercapto benzothiazole (MBT) ($C_7H_5NS_2$)	0.1
Sulfur	2.8

NR/CCB-CNT hybrid filler systems were labelled NB20C0.5, NB20C1, NB20C3, and NB20C5. In these notations, 'C' indicates multi-walled carbon nanotubes (CNT). Specifically, the samples NB20C0.5, NB20C1, NB20C3, and NB20C5 incorporated 20 phr CCB along with 0.5, 1, 3, and 5 phr CNT, respectively.

For the production of the NR/ILCCB system, IL-modified CCB was incorporated into the NR matrix. The samples were labelled as NB20IL1 and NB20IL3. Here, 'IL' stands for the ionic liquid used, and the numbers (1 and 3) denote the ratio of the ionic liquid to the CCB in the composite. Both samples contain 20 phr of CCB. The CCB to IL ratio for NB20IL1 is 1:1, while for NB20IL3, the ratio is 1:3.

All the NR/CCB-ILCNT hybrid filler systems contain 20 phr of CCB with varying amounts of ILCNT. Specifically, the samples NB20C3IL1 and NB20C3IL3 each have 3 phr of CNT, with CNT to IL ratios of 1:1 and 1:3, respectively. Likewise, the samples NB20C5IL1 and NB20C5IL3 each have 5 phr of CNT, with IL to CNT ratios of 1:1 and 1:3, respectively.

NR/CCB-CNT-RGO hybrid filler systems were labelled NB20C1R1 and NB20C5R1. In these labels, 'R' signifies reduced graphene oxide (RGO). Specifically, both samples

incorporate 20 phr CCB and 1 phr RGO, but NB20C1R1 contains 1 phr CNT, whereas NB20C5R1 has 5 phr CNT.

NR/CCB-CNT-syTRGO hybrid filler systems were designated as NB20C1syR1 and NB20C5syR1. In these labels, 'syR' represents the laboratory-synthesised thermally reduced graphene oxide (syTRGO). These samples contain 20 phr CCB and 1 phr syTRGO. However, NB20C1syR1 and NB20C5syR1 include 1 and 5 phr CNT, respectively.

Compounded NR samples were moulded in a compression moulding hydraulic press (Santosh Rubber Machinery PVT.LTD.) at 150°C and pressure close to 120 bar. The optimum cure time (T_{90}) for the moulding of each sample was obtained from the rheograph.

2.3. Characterisation techniques

2.3.1. Characterisation of fillers and composites

2.3.1.1. X-ray diffraction (XRD) analysis

X-ray diffraction analysis of the samples was done using a Bruker AXS D8 Advance model equipped with a Cu Kα source. Key parameters included a 1.5406 A° wavelength and 0.028° resolution. This technique provides insight into the crystalline structure of the carbonaceous fillers.

2.3.1.2. Scanning electron microscopy (SEM)

Structural characteristics of the hybrid filler systems were examined using scanning electron microscopy (SEM), specifically the Jeol 6390LA/OXFORD XMX N model, which operated within an accelerating voltage range of 0.5 to 30 kV and offered a magnification capacity of up to 300,000x. SEM analysis of the tensile fracture surface of rubber composites is carried out by ASTM E982-10. Additionally, a high-resolution image of the samples was taken using a field emission scanning electron microscope (FESEM), employing the ZEISS GeminiSEM 300 instrument. This device worked within an acceleration voltage spectrum of 0.02 - 30 kV and provided a remarkable magnification range from 12x to 2,000,000x.

2.3.1.3. Transmission electron microscopy (TEM)

The dispersion of fillers within the NR matrix was examined using transmission electron microscopy (TEM) on a JEOL-JEM 2100 instrument from Japan, operating at an accelerating voltage of 200 kV. For sample preparation, an ultra-microtome

(Leica Ultracut UCT) was employed. This allowed for the precise cryo-cutting of the specimens into ultrathin sections, which were then placed on 300 mesh copper grids for examination, all at ambient room temperature. The examination procedure of TEM for rubber composites is based on the general ASTM standards for electron microscopy ASTM E7-19.

2.3.1.4. Raman spectroscopy

Raman spectroscopy is used to study the defects and ordering in the carbon structures. Analysis was conducted on fillers at room temperature on a WITec alpha300 RA Raman microscopy system with a 532 nm DPSS (diode-pumped solid-state) laser for enhanced spectral resolution.

2.3.1.5. X-ray photoelectron spectroscopy (XPS)

The surface chemistry of GO and syTRGO was examined using X-ray photoelectron spectroscopy (XPS) on a PHI 5000 VersaProbe II system by ULVAC-PHI Inc., USA. This equipment featured a micro-focused, monochromatic Al-Kα X-ray source (200 μm, 15 KV) with a photon energy of 1486.6 eV. Comprehensive assessments included a broad survey of spectra, set at 50W power and 187.85 eV pass energy, and high-resolution scans for significant elements tuned to 46.95 eV pass energy. XPS will offer a detailed elemental and bonding state analysis of the carbonaceous filler surface.

2.3.1.6. Fourier transform infrared spectroscopy (FTIR)

Fourier transform infrared (FT-IR) spectroscopy, a fundamental tool in analysing molecular structures and interactions, was employed to study the fillers and NR hybrid filler systems. FT-IR spectra of the modified fillers were acquired using Nicolet iS5 (Thermo Fischer Scientific) spectrometer with KBr pellets of spectroscopic grade. The NR hybrid filler systems were explicitly analysed in the attenuated total reflectance (ATR) mode, ensuring a comprehensive view of the various functional groups present in the NR hybrid filler systems. ASTM E168 - 16 covers the general procedures for infrared spectroscopy. Measurements were taken at a resolution of 4 cm^{-1}, covering a frequency range between 4000 and 400 cm^{-1} with 32 scans. All acquired spectra were baseline-corrected to eliminate any potential instrumental or background variations.

2.3.1.7. Ultraviolet-visible spectroscopy

Jasco-V-730 UV-visible spectrophotometer was employed to investigate the oxidative and reductive transformations of graphite and GO. For this, sample dispersions were

prepared in water using a bath sonicator and subsequently scanned within a 200 to 800 nm wavelength range.

2.3.2. Analysis of properties of NR hybrid filler systems

2.3.2.1. Cure characteristics

Cure properties of the composite specimens were evaluated with a Moving Die Rheometer (Rheoline MDR 100). ASTM D5289-95 is commonly employed to assess the vulcanisation properties of rubber compounds using a rotorless rheometer. This instrument was calibrated to operate at a precise temperature of 150°C. A frequency of 167 Hz was maintained alongside a deformation angle set at 0.5°. Three critical parameters were closely monitored throughout this evaluation: the minimum torque, denoted as M_L; the peak torque, referred to as M_H; and the time it takes for the sample to reach 90% of its total curing, labelled as T_{90}.

2.3.2.2. DC conductivity

Keithley 2450 Source Meter, a sophisticated instrument integral for electrophysical measurements, was employed to systematically procure current-voltage (I-V) plots of the NR composite specimens. Each specimen was prepared with dimensions of 1cm x 1cm. Measurements were conducted at ambient room temperature, in the voltage range of 0 to 5 V. A precise step voltage of 0.05 V was adopted. These I-V curves offer quantitative insight into the electronic behaviour of the NR under varying voltage conditions. The DC (direct current) conductivity (σ) of the samples was determined using the slope of the I-V curves, considering the length l and area of cross-section A of the sample.

$$\sigma = \frac{l}{A} \times (slope\ of\ I - V\ plot) \tag{2.1}$$

2.3.2.3. Dielectric studies

Dielectric analysis used the Wayne Kerr Electronics-6500B series Precision Impedance Analyzer. It is operated in the frequency sweep mode from 20 Hz to 30 MHz at room temperature. From the composite sheets, disc-shaped samples with 12 mm diameter and 2 mm thickness were used for the analysis. During the evaluation, essential parameters such as capacitance (C), impedance (Z), and dielectric loss tangent (tan δ) were carefully measured and plotted against the frequency spectrum. Representation of complex permittivity for materials is commonly given as

$$\varepsilon = \varepsilon' - j\varepsilon'' \quad (2.2)$$

where ε' represents the real part of dielectric permittivity, indicating the ability of the material to store energy in an alternating field, and ε" represents the dielectric loss factor, which signifies the ability of the material to dissipate energy. The real part of dielectric permittivity (ε') can be determined by using the capacitance (C) of the sample and the sample's thickness (t). The equation used for this determination is as follows:

$$\varepsilon' = \frac{C.t}{A\varepsilon_o} \quad (2.3)$$

where A represents the electrode's area and ε_0 is the permittivity of air, approximately equal to 8.854 x 10^{-12} F/m.

Loss tangent, also known as the dissipation factor, is the ratio of the imaginary part of the dielectric permittivity (ε") to the real part. It can be expressed as:

$$\text{Tan}\,\delta = \frac{\varepsilon''}{\varepsilon'} \quad (2.4)$$

AC conductivity (σ_{ac}) was calculated using the equation,

$$\sigma_{ac} = 2\pi f.\varepsilon_o.\varepsilon'' \quad (2.5)$$

where f is the frequency, ε_o is the permittivity of air (8.854 x 10^{-12} F/m) and ε" is the imaginary part of dielectric permittivity (ε' x tan δ).

2.3.2.4. Mechanical properties

Tensile properties were determined in accordance with the ASTM D 412-06a Tension with Extensometer standard. Dumbbell-shaped specimens were tested at room temperature and a 500 mm/min crosshead speed. Five samples from each composite sheet are tested.

2.3.2.5. Dynamic mechanical analysis

Viscoelastic properties of the samples were examined utilising a temperature sweep approach with a Dynamic mechanical analyser (DMA Q800 V20.26 Build 45). Rectangular specimens were analysed in tension mode at a frequency of 1 Hz in the temperature range -80° to +80°C, with a controlled heating rate of 5°C/min. Dynamic mechanical properties were determined by following the general guidelines of ASTM D4065-12, which refer to the dynamic mechanical properties of plastics and rubber.

2.3.2.6. Electromagnetic interference (EMI) shielding.

Electromagnetic interference (EMI) shielding capabilities of the rubber composite samples were gauged using a two-port PNA network analyser (Agilent E8362B, with a frequency range of 10 MHz-20 GHz). This analyser was integrated with a Keycom waveguide, operating specifically in the X-band region (from 8.2 to 12.4 GHz). By tracing the scattering parameters of the specimens, we deduced the total shielding effectiveness using prescribed equations.

EMI shielding effectiveness of the samples can be expressed in terms of total shielding effectiveness (SE_T). From the perspective of classical electromagnetic wave theory, SE_T of the composite samples can be defined logarithmically. It is quantified as the ratio of the power incident on the sample (P_I) to the power that ultimately transmits through it (P_T).

$$SE_T = -10 \log \frac{P_I}{P_T} \tag{2.6}$$

Total shielding efficiency is the sum of shielding by absorption (SE_A), reflection (SE_R) and multiple reflections (SE_M). SE_M can be neglected in all practical applications when $SE_T > 10$ dB. This occurs due to the growing absorption of reflected waves from the internal surface when shield thickness is greater than the skin depth. (5) In this context, total shielding efficiency can be expressed as,

$$SE_T = SE_A + SE_R \tag{2.7}$$

Total shielding effectiveness (SE_T in dB) and reflective shielding effectiveness of the composite surface (SE_R in dB) can be obtained by the following equations.

$$SE_T = -10 \log T, \text{ where } T = \left|\frac{P_I}{P_T}\right| = |S_{21}|^2 \tag{2.8}$$

$$SE_R = -10 \log(1 - R), \text{ where } R = \left|\frac{P_R}{P_I}\right| = |S_{11}|^2 \tag{2.9}$$

Vector network analyser (VNA) provides the complex scattering parameters S_{11} and S_{21}, which are the representatives of reflected, absorbed and transmitted power. S_{11} is the forward reflection coefficient, and S_{21} is the forward transmission coefficient.

Absorptive shielding effectiveness (SE_A in dB) was calculated from SE_T and SE_R.

$$SE_A = SE_T - SE_R \tag{2.10}$$

2.3.2.7. Transport studies

The transport behaviour of samples in toluene was studied at room temperature. Circular-shaped samples were immersed in 20 ml toluene and taken in closed diffusion bottles. The weight and thickness of the samples before immersing in solvent were measured and recorded. The weight of the samples was taken in specific intervals until equilibrium swelling was reached. Each weighing was completed within 30 seconds to minimise the error due to the evaporation of solvent during weighing. The mol % uptake of solvent per unit mass of polymer, Q_t of the samples was computed using the following equation,

$$Q_t\,(\%) = \frac{(m_t - m_o)/M_S}{m_o} \times 100 \tag{2.11}$$

where m_t is the mass of the sample at the time t of immersion and m_o is the mass of the sample before immersion in solvent. M_S is the molecular mass of solvent. Here, the molecular mass of toluene is 92.14g/mol. Diffusion coefficient of the composites is calculated from the equation derived from second Fickian law. (6)

$$D = \pi\left(\frac{h\theta}{4Q_\infty}\right)^2 \tag{2.12}$$

where h is the thickness of the sample, θ is the slope of the initial linear portion of the plot of Q_t (%) against $t^{1/2}$, and $Q_\infty$the equilibrium absorption. Permeability coefficient (P) of toluene in the composites is determined using the following equation,

$$P = D.S \tag{2.13}$$

where D is the diffusion coefficient and S is the sorption coefficient. The sorption coefficient is calculated from the following equation,

$$S = \frac{m_\infty}{m_O} \tag{2.14}$$

where m_∞ is the mass of the solvent absorbed at equilibrium and m_O is the mass of the sample before immersion in solvent.

2.3.2.8. Swelling studies and crosslink density

Swelling index indicates the swelling resistance of the rubber composites and is obtained using equation,

$$Swelling\ index(\ \%) = \frac{W_1 - W_O}{W_O} \times 100 \quad (2.15)$$

where W_1 and W_O are weight of the samples after swelling and before swelling in toluene. Swelling behaviour of rubber composites can also be analysed from the swelling coefficient value ($\propto$), which is an index of the ability with which the samples swell and is given by following equation,

$$\propto = \left[\frac{W_\infty - W_O}{W_O}\right] \times \left[\frac{1}{\rho_S}\right] \quad (2.16)$$

where W_∞ is the weight of the sample at equilibrium swelling in solvent, W_O is the weight of the samples before swelling and ρ_S is the density of the solvent used. Here density of toluene used is 0.866g/cm^3.

Toluene swelling method defined in ASTMD-0471-16a was used to determine the crosslink density of the samples. Circular-shaped samples are weighed and allowed to swell in toluene until equilibrium. Then, after weighing, swelled samples are air-dried for 72 hours to measure the de-swollen weight. The apparent crosslink density value is given by $\frac{1}{Q}$, where Q is the swell ratio and is given by the following equation,

$$Q = \frac{W_1 - W_O}{W_O} \quad (2.17)$$

Actual crosslink density of the samples is calculated using the Flory-Rehner equation (7)

$$v = \frac{\ln[1 - V_{rf}] + V_{rf} + \chi V_{rf}^{\,2}}{-2\rho_r V_S V_{rf}^{\,1/3}} \quad (2.18)$$

where V_{rf} is the volume fraction of rubber in the solvent- swollen filled sample, χ is the interaction parameter given by **Equation 2.19** (8), ρ_r is the density of the polymer and V_s is the molar volume of solvent. Here molar volume of toluene is 106.3cm^3/mol.

$$\chi = \beta + \frac{Vs}{RT}\left(\delta_p - \delta_s\right)^2 \quad (2.19)$$

where β is the lattice constant (0.34), R is the universal gas constant, T is the temperature, $and\ \delta_p$ and δ_s are the polymer and solvent solubility parameters, respectively.

2.3.2.9. Thermogravimetric analysis (TGA)

Thermogravimetric analysis of the samples was performed in alignment with ASTM E1131-08, a standard test method for compositional analysis by thermogravimetry. TGA was conducted using the STA7200 Thermal Analysis System from Hitachi.

Samples weighing around 7 mg were placed in an aluminium pan and subjected to a temperature range of 30° to 580°C. It is also conducted at varying heating rates, i.e.,10, 15, and 20 °C per minute, all under a consistent nitrogen flow rate of 100 ml per minute.

2.4. References

1. Brüning K. Natural Rubber. In: Encyclopedia of Polymeric Nanomaterials [Internet]. Springer, Berlin, Heidelberg; 2015 [cited 2023 Aug 15]. p. 1377–82. Available from: https://link.springer.com/referenceworkentry/10.1007/978-3-642-29648-2_302
2. Hummers WSJr, Offeman RE. Preparation of Graphitic Oxide. J Am Chem Soc. 1958 Mar 1;80(6):1339–1339.
3. Yaragalla S, A.P. M, Kalarikkal N, Thomas S. Chemistry associated with natural rubber–graphene nanocomposites and its effect on physical and structural properties. Industrial Crops and Products. 2015 Nov;74:792–802.
4. Ponnamma D, Sadasivuni KK, Strankowski M, Guo Q, Thomas S. Synergistic effect of multi-walled carbon nanotubes and reduced graphene oxides in natural rubber for sensing application. Soft Matter. 2013;9(43):10343–53.
5. Bhattacharjee Y, Biswas S, Bose S. Thermoplastic polymer composites for EMI shielding applications. In: Materials for Potential EMI Shielding Applications [Internet]. Elsevier; 2020 [cited 2023 May 5]. p. 73–99. Available from: https://linkinghub.elsevier.com/retrieve/pii/B9780128175903000051
6. Abraham J, Maria HJ, George SC, Kalarikkal N, Thomas S. Transport characteristics of organic solvents through carbon nanotube filled styrene butadiene rubber nanocomposites: The influence of rubber-filler interaction, the degree of reinforcement and morphology. Physical Chemistry Chemical Physics. 2015;17(17):11217–28.
7. Flory PJ, Rehner J. Statistical Mechanics of CrossLinked Polymer Networks II . Swelling Statistical Mechanics of Cross-Linked Polymer Networks. 1943;521.
8. James J, Thomas GV, Pramoda KP, Thomas S. Transport behaviour of aromatic solvents through styrene butadiene rubber/poly [methyl methacrylate] (SBR/PMMMA) interpenetrating polymer network (IPN) membranes. Polymer. 2017 May 5;116:76–88.

Chapter 3

Cure Properties and Characterisation of Fillers and NR Hybrid Filler Systems

Summary

This chapter discusses the cure properties of natural rubber (NR) hybrid filler systems incorporated with carbon-based conductive fillers and ionic liquid (IL) modified fillers. The characterisation of the ionic liquid-modified fillers and the filler-incorporated composites is also discussed. FTIR and Raman spectroscopic analysis confirmed the IL modification of fillers. Morphological analysis of the fillers was done using SEM. IR spectroscopic analysis helps identify the functional groups in NR hybrid filler systems. Rheological analysis on the NR hybrid filler systems suggests the reinforcement effect of rubber matrix in the presence of filler.

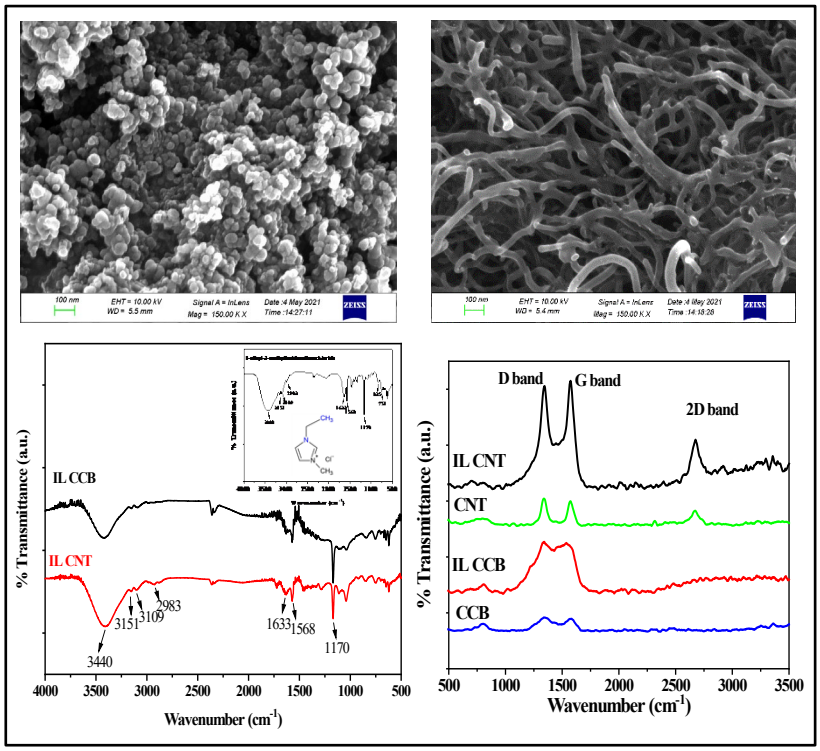

3.1. Introduction

Curing process involves the crosslinking of polymer chains, forming a three-dimensional network that defines the structural integrity of the composite. Curing, also known as vulcanisation, is the process in a which plastic rubber compound changes into the highly elastic final product through physical and chemical reactions at high temperature and pressure. Among the many curatives used for natural rubber (NR), sulfur and peroxide are commonly used. Sulfur curing is a complex process which requires a combination of activators and accelerators to introduce crosslinking in NR chains. This results in the formation of monosulfidic, disulfidic and polysulfidic crosslinks between macromolecular chains that contribute to the enhancement of properties. The presence of conductive fillers impacts the crosslinking density and, in turn, alters the properties of the NR composite. The analysis of cure kinetics enables the optimisation of properties of NR hybrid filler systems. Cure characteristics involve cure time (T_{90}), minimum torque (M_L), maximum torque (M_H), and torque difference (ΔM). Minimum torque is the measure of stiffness of the composite before curing, and maximum torque is the measure of stiffness after vulcanisation. This chapter also deals with the characterisation of fillers and NR hybrid filler systems using various microscopic and spectroscopic techniques and also discusses the curing properties of NR compounds.

3.2. Theoretical models applied for cure characteristics

3.2.1. Westlinning-Wolff equation

Westlinning-Wolff (1) equation can be used to analyse the extent of rubber-filler interaction. The equation is presented below,

$$\propto_f = \frac{\frac{\Delta M_f}{\Delta M_g} - 1}{z} \tag{3.1}$$

where ΔM_f and ΔM_g are the rheometric torque differences between maximum and minimum torque values (M_H-M_L) for filled composites and unfilled NR, respectively, and z is the weight fraction of filler in composites. The $\propto_f$ is the filler specific constant which is determined by filler structure in the vulcanisate after possible structure breakdown during mixing and vulcanisation (1).

3.3. Results and discussion

3.3.1. Characterisation of fillers

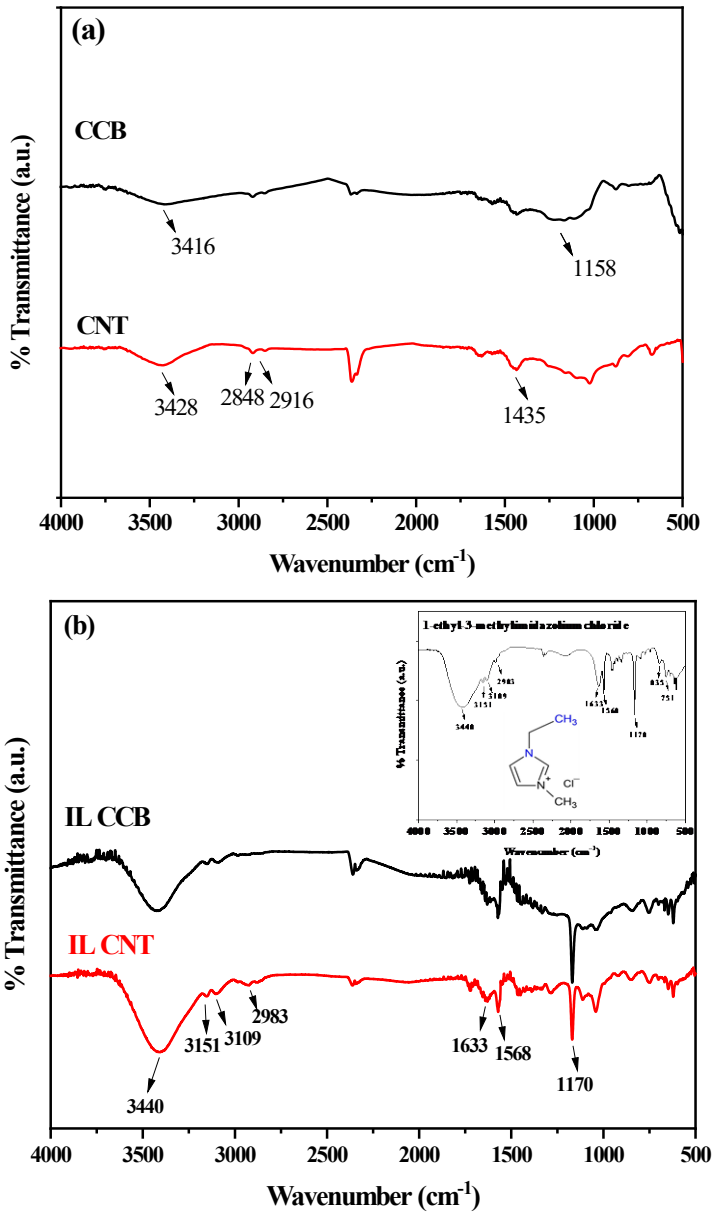

Figure 3.1-FTIR spectra of fillers (a) CNT and CCB (b) IL, ILCNT and ILCCB

Figure 3.1 (a and **b)** presents the FTIR spectra of unmodified CCB and CNT and 1-ethyl-3-methylimidazoliumchloride modified CCB and CNT. FTIR of CNT and CCB has O-H stretching band around 3400 cm^{-1}, and peaks in the range of 1300-950 cm^{-1}, corresponding to the C-O bonds. (2) FTIR spectra of IL, 1-ethyl-3-

methylimidazoliumchloride (inset of **Figure 3.1(b)**) displays a prominent peak around 3400 cm^{-1} assigned to the O-H stretching vibration, which is characteristic of quarternary ammonium salts. (3) The other vibration peaks present in the spectra of IL are at 1633cm^{-1} corresponding to the stretching of the N=C bond, 1564 cm^{-1} corresponding to the vibration of the positively charged nitrogen atom, 1174 cm^{-1} corresponding to the C-C stretching vibration of alkyl chain of IL and the peak at 1034 cm^{-1} corresponds to the N-C ring stretching vibration. (4,5) The appearance of these peaks in the FTIR spectra of IL modified CCB and CNT confirms that the fillers are modified by IL.

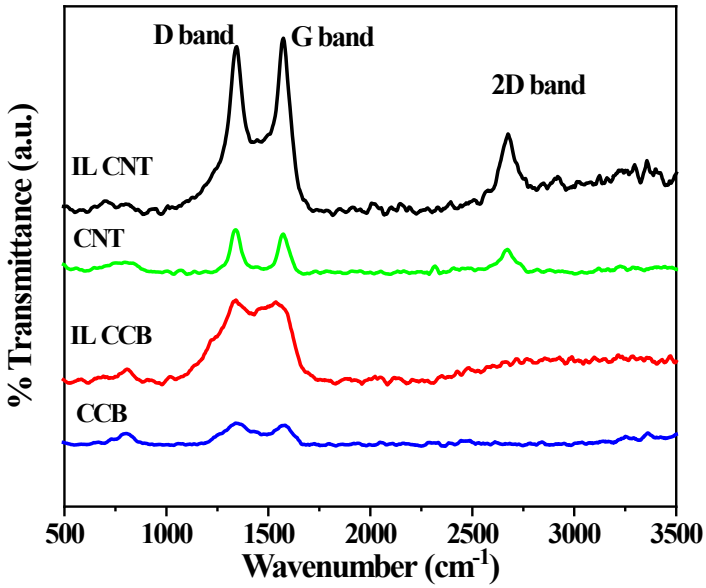

Figure 3.2-Raman spectra of fillers

Figure 3.2 presents the Raman spectra of CCB, CNT, and IL modified CCB and CNT. The modification process exhibits notable changes in the structural and vibrational characteristics of both IL modified CNT, and IL modified CCB. A blue shift is observed in the D band, indicating alterations in the sp^3 carbon content. In the case of IL modified CNT, there is an increase in the intensity of the G band, highlighting changes in the graphitic structure. Additionally, the sharp and distinguished peaks associated with CCB undergo broadening upon modification, suggesting a modification-induced impact on its crystalline structure. These

spectroscopic changes signify the successful modification of CNT and CCB by 1-ethyl-3-methylimidazoliumchloride.

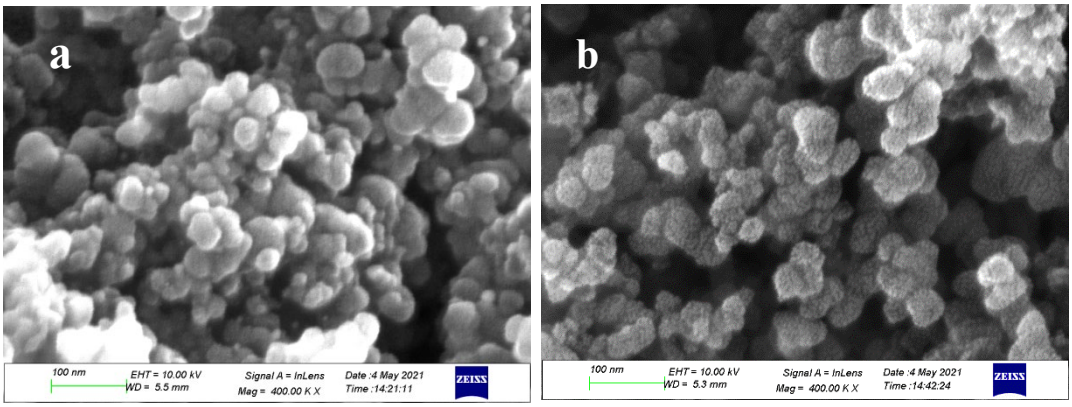

Figure 3.3-SEM images (a) CCB (b) IL modified CCB

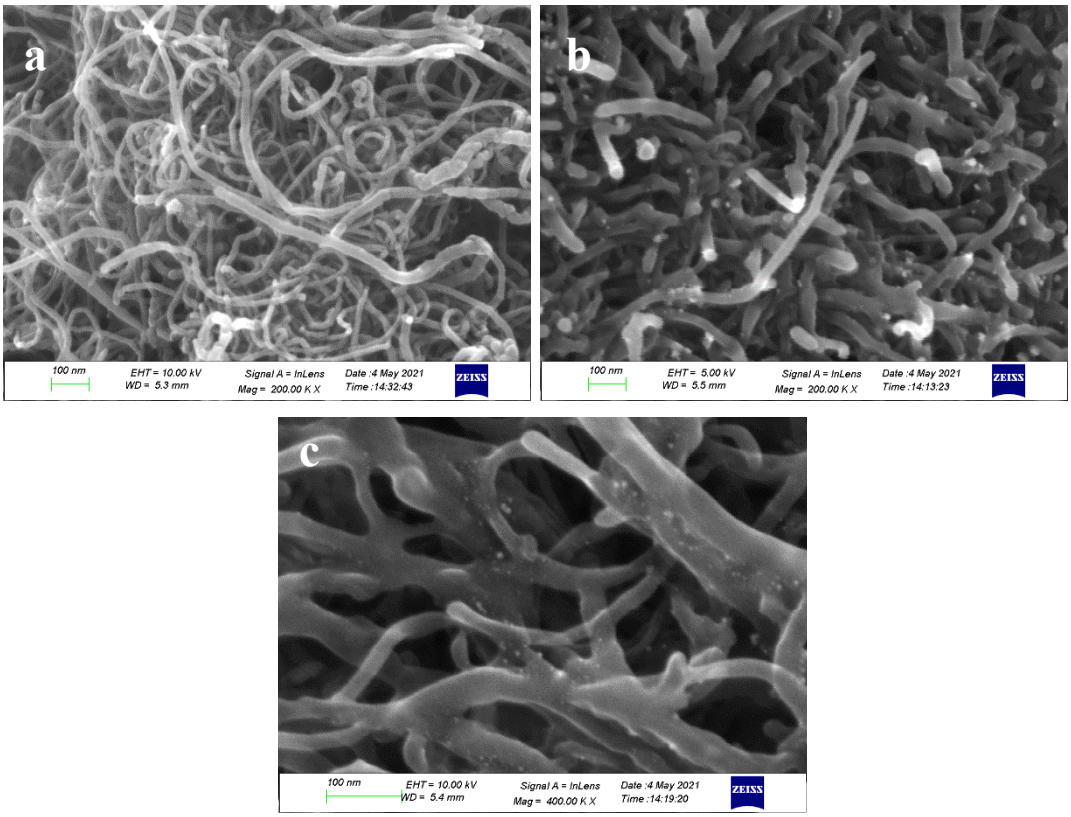

Figure 3.4-SEM images (a) CNT (b) IL modified CNT at 200 Kx and (c) IL modified CNT 400 Kx magnifications

Figure 3.3 (a) and **(b)** present the SEM images of unmodified CCB and 1-ethyl-3-methylimidazolium chloride modified CCB. SEM images suggest that the IL modification has not affected the spherical morphology of CCB. The high degree of

aggregation is observed in the case of unmodified CCB. However, it decreases upon IL modification due to the interaction between functional groups on the surface of CCB and IL. **Figure 3.3 (b)** indicates that the IL modification has reduced the CCB aggregation due to the presence of IL molecules at the surface of CCB. **Figure 3.4 (a)** presents the SEM image of unmodified CNT, and **(b)** and **(c)** presents the 1-ethyl-3-methyl-imidazolium chloride modified CNT at lower and higher magnifications. SEM images clearly depict the difference in morphology of CNT upon modification. **Figure 3.4 (b)** shows the reduced length of the modified CNT resulting from the grinding and sonication process used for IL modification. **Figure 3.4 (c)** shows the fused CNT tubes upon IL modification. Increased thickness of the walls of CNT suggests IL modification on the surface of CNT.

3.3.2. Characterisation of NR hybrid filler systems

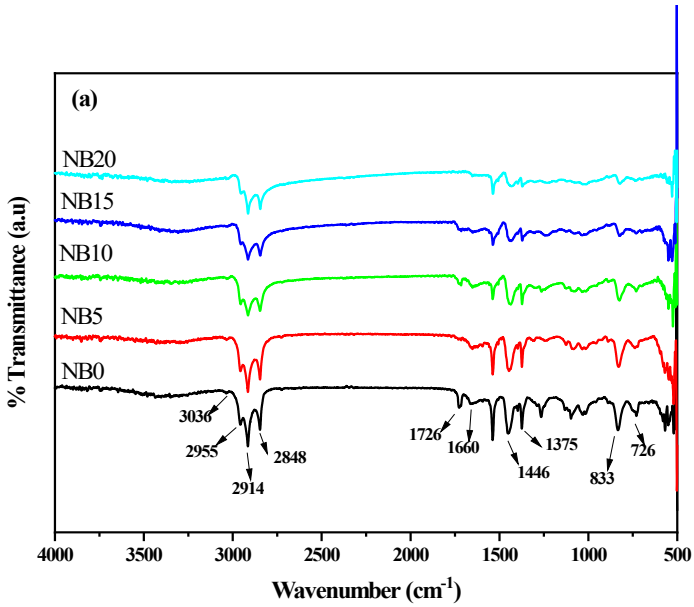

Figure 3.5-ATR spectra of (a) NR/CCB systems

ATR has been used to characterise the NR hybrid filler systems for evaluating the filler interaction (6,7) and composition. (8,9) **Figure 3.5 (a-e)** gives the ATR spectra of NR hybrid filler systems with different filler systems. The characteristic peaks of NR are weak =C-H stretching peak at 3036 cm^{-1}, asymmetric CH_3 stretching peak at 2955 cm^{-1}, CH_2 vibrational peaks at 2914 cm^{-1} (asymmetric stretching), 2848 cm^{-1}(symmetric stretching), C=C stretching peak at 1660 cm^{-1}, C-H deformation peaks of CH_3 (asymmetric deformation) and CH_2 at 1375 $cm^{-1}$and 1446 cm^{-1} respectively,

=C-H out of plane bending peak at 833 cm^{-1} and CH_2 rocking peak at 726 cm^{-1}. (10) Characteristic peaks of NR are identified in the ATR spectra of all NR/filler composites.

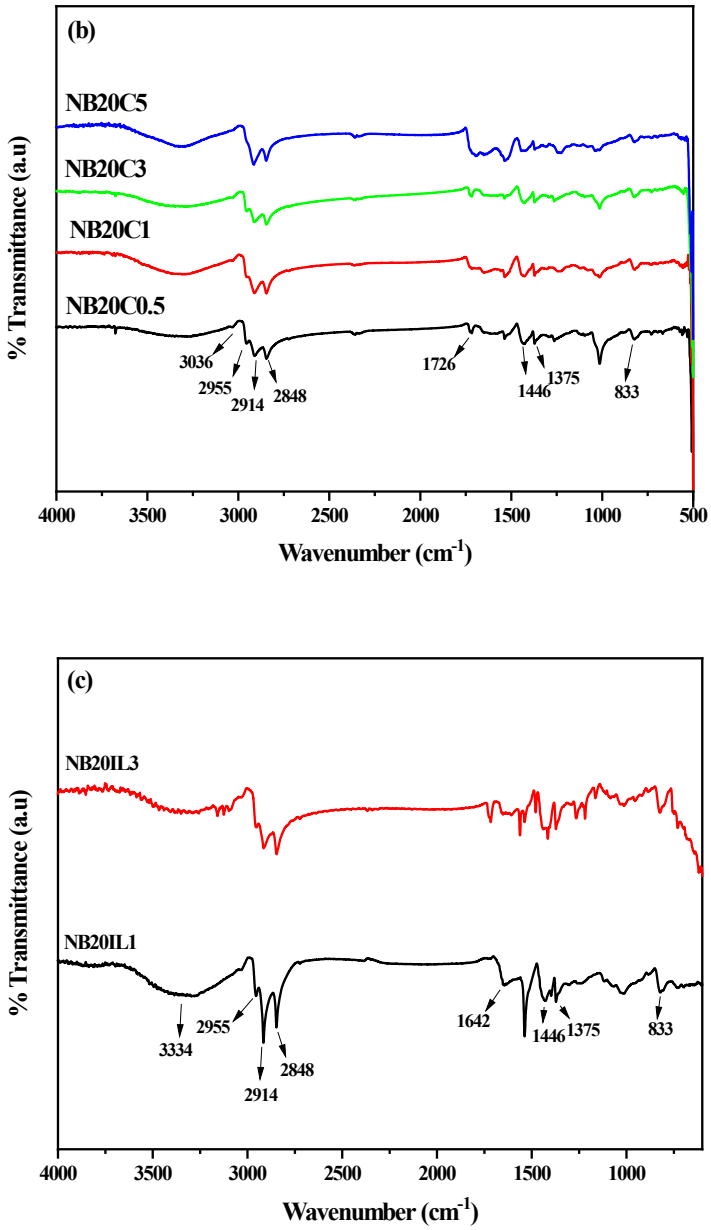

Figure 3.5-ATR spectra of (b) NR/CCB-CNT composites and (c) NR/ILCCB systems

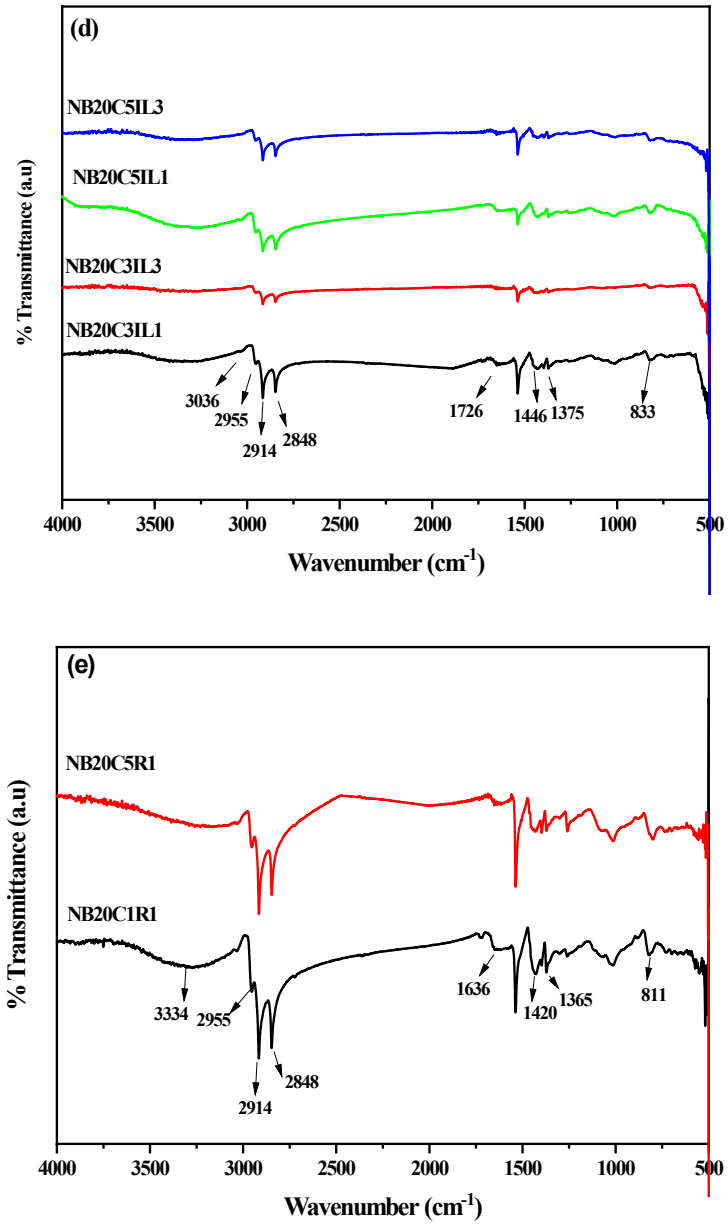

Figure 3.5-ATR spectra of (d) NR/CCB-ILCNT and (e) NR/CCB-CNT-RGO hybrid filler systems

Table 3.1-Density (g/cm^3) of NR hybrid filler systems

NR/CCB composites		NR/CCB-CNT composites		NR/ILCCB composites		NR/CCB-ILCNT composites		NR/CCB-CNT-RGO composites	
NB0	0.96	NB20C0.5	1.04	NB20IL1	1.04	NB20C3IL1	1.07	NB20C1R1	1.04
NB5	0.99	NB20C1	1.05	NB20IL3	1.05	NB20C3IL3	1.05	NB20C5R1	1.06
NB10	1	NB20C3	1.05			NB20C5IL1	1.07		
NB15	1.02	NB20C5	1.06			NB20C5IL3	1.06		
NB20	1.04								

The density of all NR composite systems is presented in **Table 3.1**. Unfilled NR has a density of 0.96 (g/cm^3)**.** Incorporation of inorganic fillers has increased the composite density for all filler systems than unfilled NR.

3.3.3. Cure properties

3.3.3.1. NR/CCB systems

Torque profile during curing indicates crosslinks in the system formed by the rubber-rubber and rubber-filler interaction. **Figure 3.6** is the torque–time plot of the unfilled and CCB filled NR composites. Torque experienced by the samples is increasing linearly with an increase in filler. As the filler incorporation increases, the rubber composites have a tendency for reversion. Reversion occurs when crosslinks formed during vulcanisation start to break down. (11) **Table 3.2** shows the cure characteristics of NR/CCB systems. Minimum torque (M_L), maximum torque (M_H) and cure time (T_{90}) of the rubber samples are increasing with respect to CCB filler content. High surface area of CCB enables the entanglement of rubber chains into its surface and reducing mobility. This, in turn, increases the M_L and M_H, which is an indication of physical crosslinks in the system. (12) Torque difference, ΔM gradually increases from 10.29 dNm for unfilled NR to 17.02 dNm for 20 phr CCB filled NR. This shows the improvement in rubber-filler interaction and directly correlates to the crosslinks in the system. Maximum torque values demonstrate the extent of rubber–filler interaction. Westlinning-Wolff equation (**Equation 3.1)** provides the value $\propto_f$, that can be used to analyse the extent of rubber-filler interaction. The $\propto_f$ values of NR/CCB systems are given in **Table 3.2**. It is found to be increasing as a function of filler loading, which is an indication of the improved polymer-filler interaction.

Table 3.2-Cure characteristics of NR/CCB systems

Sample	M_L (dNm)	M_H (dNm)	ΔM	T_{90}(min)	$\propto_f$
NB0	0.12	10.41	10.29	6.14	-
NB5	0.17	11.66	11.49	6.89	2.45
NB10	0.21	13.07	12.86	6.94	2.75
NB15	0.25	15.08	14.83	7.05	3.38
NB20	0.36	17.38	17.02	7.57	3.92

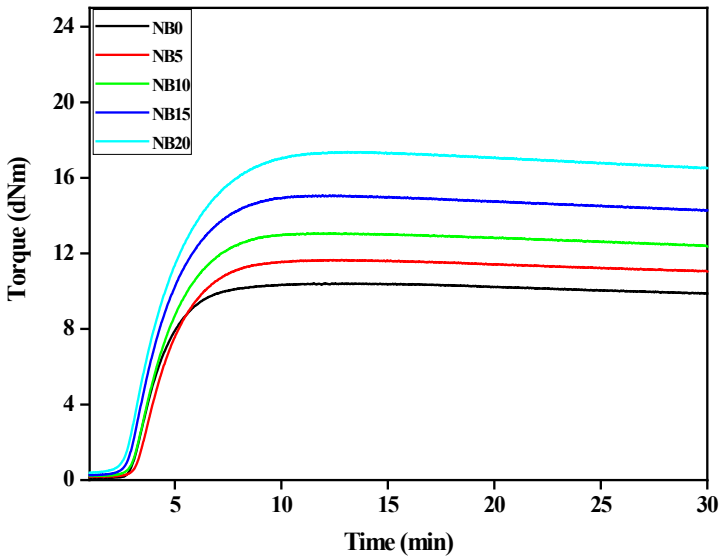

Figure 3.6-Torque-time curves of NR/CCB systems

3.3.3.2. NR/CCB-CNT hybrid filler systems

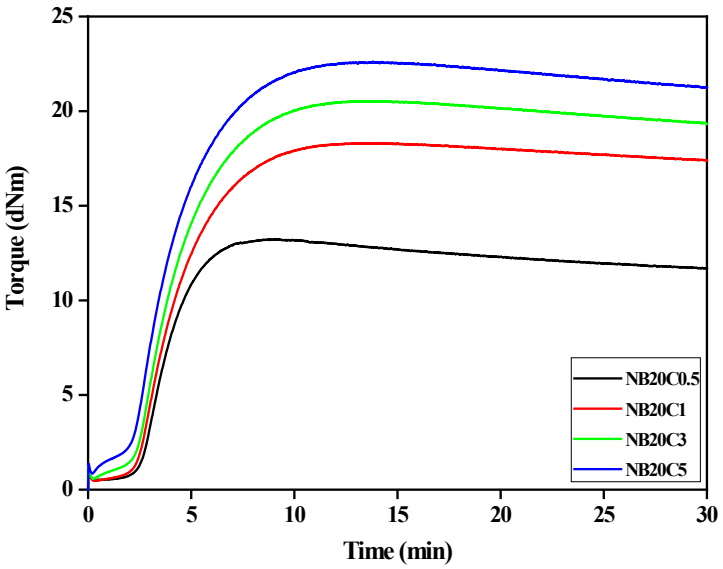

Figure 3.7-Torque-time curves of NR/CCB-CNT hybrid filler systems

Figure 3.7 is the torque–time plot of the NR/CCB-CNT hybrid filler systems. Torque of composites filled with CCB-CNT hybrid filler is found to be higher in the presence of CNT. **Table 3.3** shows the effect of CCB-CNT hybrid filler in the cure characteristics of NR composites. Minimum and maximum torque increases upon the

addition of CNT. CNT has a high aspect ratio, consequently the contact surface area of matrix and the filler increases. Highest M_H is obtained for NB20C5, which indicates increased rubber-filler interaction and torque difference reflects the increased crosslinks in the composites due to rubber-filler interaction. These values markedly increase after 1 phr addition of CNT. This indicates the increased network density of rubber after CNT addition. Cure time of NB20C1, NB20C3 and NB20C5 are around 7 min, while NB20C0.5 has a lower value of 5.74 min. Here, CCB-CNT hybrid filler loading has negligible effect on the cure time of the composites. The $\propto_f$ values obtained from torque of NR hybrid filler systems are given in **Table 3.3**. It signifies the extent of rubber-filler interaction in the composites. The $\propto_f$ values are increasing after 1 phr CNT addition. The $\propto_f$ value obtained for NR/CCB-CNT hybrid filler systems indicates that the hybrid filler system of CCB and CNT has made better interaction with the NR matrix.

Table 3.3-Cure characteristics of NR/CCB-CNT hybrid filler systems

Sample	M_L (dNm)	M_H (dNm)	ΔM	T_{90} (min)	$\propto_f$
NB20C0.5	0.51	13.25	12.74	5.74	1.40
NB20C1	0.46	18.32	17.86	7.53	4.24
NB20C3	0.57	20.54	19.97	7.64	5.03
NB20C5	0.85	22.62	21.77	7.57	5.58

3.3.3.3. NR/1-ethyl-3-methylimidazolium chloride modified CCB (NR/ILCCB) systems

Figure 3.8 depicts the cure curves of NR/ILCCB systems**.** It demonstrates that NB20IL1 exhibits a higher torque than NB20IL3. Cure parameters such as M_L, M_H, ΔM and T_{90} of NR/ILCCB systems are presented in **Table 3.4**. Minimum torque value recorded during the curing process indicates the initial resistance to flow or the stiffness of the material. In NB20IL3, as the IL content is higher, the initial resistance to flow is higher than NB20IL1. Maximum torque is the indication of the material's viscosity or resistance to further deformation. ΔM represents the torque change or the overall torque response of the material during curing. NB20IL1 has the highest ΔM value, indicating a significant shift in torque during curing. NB20IL1 and NB20IL3

exhibit higher maximum torque values than NB0, indicating increased viscosity or resistance to further deformation due to the interaction between IL and CCB. These samples also have higher T_{90} values compared to NB0, as it requires more time for optimum curing. Imidazolium based IL can enhance the dispersion of fillers in the NR matrix. (13) Carbon black surface is characterised by oxygen-containing chemical groups such as lactons, phenolic, carboxylic and ketonic, which can form bonds with IL.(14,15) Another possibility is the π-π interaction of CCB and IL.

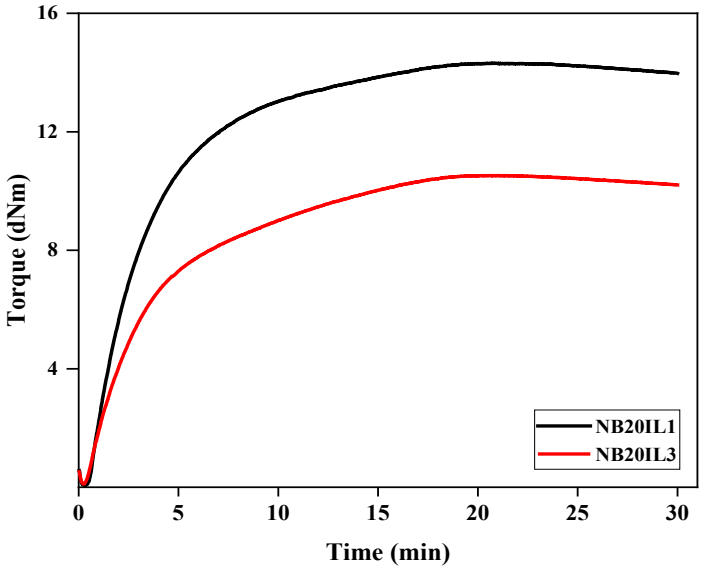

Figure 3.8-Torque-time curves of NR/ILCCB systems

Table 3.4-Cure characteristics of NR/ILCCB systems

Sample	M_L (dNm)	M_H (dNm)	ΔM	T_{90} (min)	$\propto_f$
NB20IL1	0.07	14.32	14.25	9.46	2.06
NB20IL3	0.11	10.52	10.41	12.07	0.05

3.3.3.4. NR/ CCB-1-ethyl-3-methylimidazolium chloride modified CNT `(NR/CCB-ILCNT) hybrid filler systems

Cure curves of NR/CCB-ILCNT hybrid filler systems are given in **Figure 3.9**. NB20C5IL3 demonstrates the high torque value with a CNT: IL ratio of 1:3. In general, the torque increases with CNT loading and CNT: IL ratio, except for NB20C3IL3. **Table 3.5** presents the cure parameters of NR/CCB-ILCNT hybrid filler systems. In the presence of IL modified CNT, the minimum and maximum

torque decreases for hybrid filler incorporated NR. This can be attributed to the plasticizing effect of the IL in the NR matrix. In general, a decrease in cure time is observed for NR/CCB-ILCNT systems, which means that the IL accelerate the vulcanisation process. Notably, the torque increases as a function of the weight percentage of CNT owing to the interaction of functional groups on the surface of CNT and IL. Moreover, IL has reduced the chance of adsorption of curatives and accelerators on the surface of fillers and thereby aided in curing process. (16)

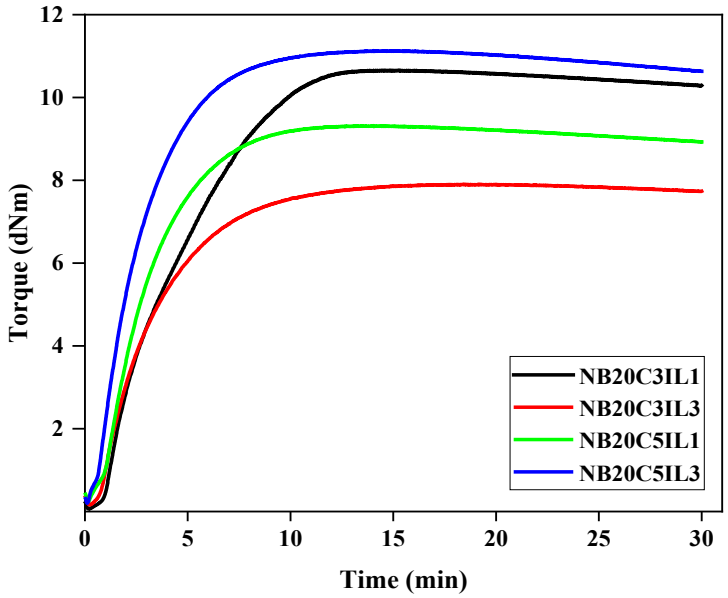

Figure 3.9-Torque-time curves of NR/CCB-ILCNT hybrid filler systems

Table 3.5-Cure characteristics of NR/CCB-ILCNT hybrid filler systems

Sample	M_L (dNm)	M_H (dNm)	ΔM	T_{90} (min)	$\propto_f$
NB20C3IL1	0.06	10.66	10.60	9.00	0.16
NB20C3IL3	0.16	7.90	7.74	7.64	-1.27
NB20C5IL1	0.24	9.31	9.07	6.46	-0.58
NB20C5IL3	0.20	11.13	10.93	6.02	0.29

3.3.3.5. NR/CCB-CNT-RGO hybrid filler systems

Figure 3.10 is the cure profile of NR/CCB-CNT-RGO hybrid filler systems, which illustrates the effect of hybrid filler on the rubber matrix. The M_L, M_H and T_{90} of the samples were determined and presented in **Table 3.6**. Presence of RGO enhances the torque values of NR due to filler-filler and rubber-filler interactions.

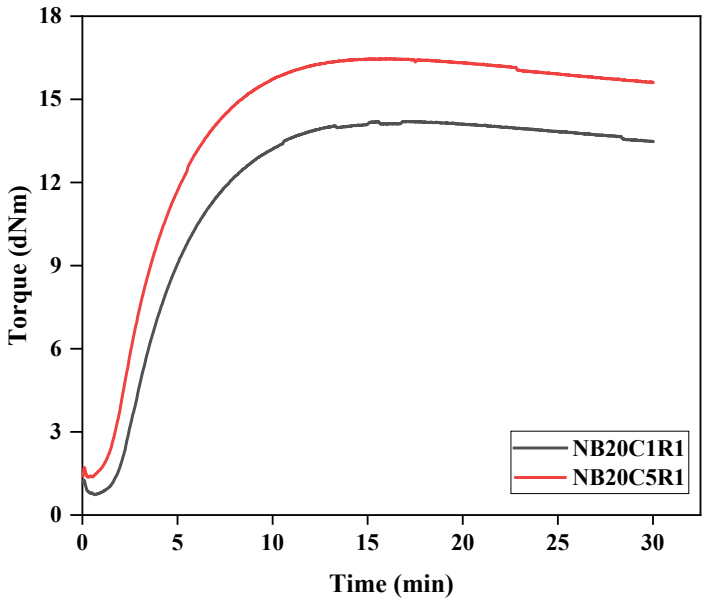

Figure 3.10-Torque-time curves of NR/CCB-CNT-RGO hybrid filler systems

Table 3.6-Cure characteristics of NR/CCB-CNT-RGO hybrid filler systems

Sample	M_L (dNm)	M_H (dNm)	ΔM	T_{90}(min)	$\propto_f$
NB20C1R1	0.73	14.2	13.47	9.15	1.71
NB20C5R1	1.36	16.47	15.11	8.28	2.27

An increase in the minimum torque values indicates the number of physical crosslinks, which enhances the stiffness of the composite. Conversely, the maximum torque and torque difference represent the increased crosslink density resulting from the interaction between the rubber and hybrid fillers. **Table 3.6** displays the $\propto_f$ values of hybrid filler systems. The $\propto_f$ values are found to be higher than IL modified system which signifies the greater degree of interaction between rubber matrix and filler. Generally, π-π interaction of sp^2 hybridised carbon atoms of RGO

layers causes stacking of graphene layers. However, in composites, these van der Waals interactions between the RGO layers and CNT can create a conductive network in the NR matrix, which can improve the cure kinetics. The functional groups on the surface of CCB, CNT and RGO lead to the formation of a filler-filler network. The expected interactions between the hybrid filler system of CCB, CNT and RGO are represented schematically in **Figure 3.11**. Consequently, the contact surface area of the filler and NR increases and is reflected in the $\propto_f$ values.

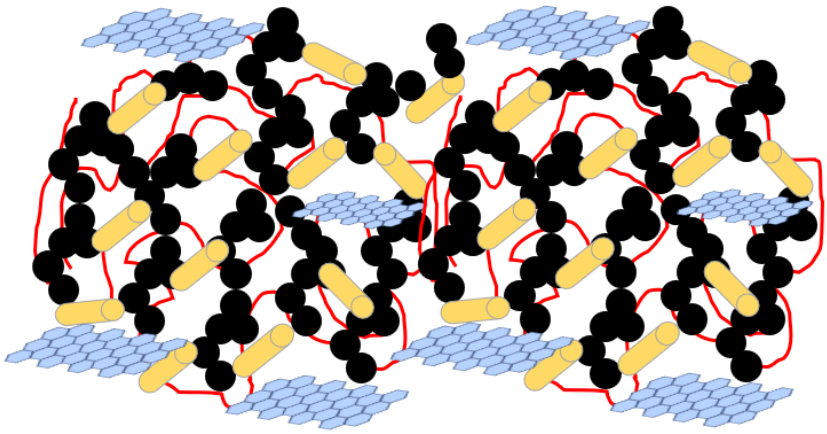

Figure 3.11-Schematic representation of filler interaction in NR/CCB-CNT-RGO hybrid filler systems

3.4. Comparative analysis of cure properties

Table 3.7-Cure characteristics of NR hybrid filler systems

Sample	M_L (dNm)	M_H (dNm)	ΔM	T_{90} (min)
NB0	0.12	10.41	10.29	6.14
NB20	0.36	17.38	17.02	7.57
NB20C5	0.85	22.62	21.77	7.57
NB20IL1	0.07	14.32	14.25	9.46
NB20C5IL3	0.20	11.13	10.93	6.02
NB20C5R1	1.36	16.47	15.11	8.28

Table 3.7 compares cure characteristics of NR hybrid filler systems with different filler systems. Rheograph analysis reveals the torque response during curing. Cure time of all filled composites is higher than unfilled NR except for NB20C5IL3. This can be attributed to the fact that the fillers like CCB, CNT and RGO can act as

physical barriers to the penetration of curing agents into the NR matrix. This slows down the curing process and results in a longer cure time for composites. (17) Torque experienced by filled composites is higher than the unfilled NR. Hybrid filler system of CCB-CNT has the highest torque values. This increase in torque value indicates the formation of filler-filler and polymer-filler networks. The nanosize and high aspect ratio of CNT allow increased contact surface area and improved interfacial interactions with NR. (18) CNT can also act as a nucleating agent and results in enhanced cross link density, leading to high torque of composites.

3.5. Conclusion

Characterisation of conductive and IL modified fillers were carried out to understand the extent of modification using ionic liquid. FTIR, Raman, and SEM analysis confirmed the successful modification of CNT and CCB using 1-ethyl-3-methylimidazolium chloride. Characterisation of NR hybrid filler systems using ATR helped identify the functional groups in the NR matrix. Cure characteristics revealed that the incorporation of fillers has improved the torque experienced by the composites. Maximum torque value is obtained for CCB-CNT filler system due to filler-filler and filler-matrix interaction. The torque difference obtained for ionic liquid modified filler and CCB-CNT-RGO filler systems is higher than NB0.

3.6. References

1. Wolff S. Chemical Aspects of Rubber Reinforcement by Fillers. Rubber Chemistry and Technology. 1996 Jul 1;69(3):325–46.
2. Stobinski L, Lesiak B, Kövér L, Tóth J, Biniak S, Trykowski G, et al. Multiwall carbon nanotubes purification and oxidation by nitric acid studied by the FTIR and electron spectroscopy methods. Journal of Alloys and Compounds. 2010 Jul;501(1):77–84.
3. Lupa L, Voda R, Popa A. Adsorption behavior of cesium and strontium onto chitosan impregnated with ionic liquid. Separation Science and Technology. 2018 May 3;53(7):1107–15.
4. Babicka M, Woźniak M, Dwiecki K, Borysiak S, Ratajczak I. Preparation of Nanocellulose Using Ionic Liquids: 1-Propyl-3-Methylimidazolium Chloride and 1-Ethyl-3-Methylimidazolium Chloride. Molecules. 2020;25(7).
5. Sarmad S, Zafarani-Moattar MT, Nikjoo D, Mikkola JP. How Different Electrolytes Can Influence the Aqueous Solution Behavior of 1-Ethyl-3-Methylimidazolium Chloride: A Volumetric, Viscometric, and Infrared Spectroscopy Approach. Frontiers in Chemistry [Internet]. 2020;8. Available from: https://www.frontiersin.org/articles/10.3389/fchem.2020.593786
6. Jarnthong M, Liao L, Zhang F, Wang Y, Li P, Peng Z, et al. Characterization of interaction between natural rubber and silica by FTIR. AIP Conference Proceedings. 2017;1846.
7. Agrebi F, Ghorbel N, Bresson S, Abbas O, Kallel A. Study of nanocomposites based on cellulose nanoparticles and natural rubber latex by ATR/FTIR spectroscopy: The impact of reinforcement. Polymer Composites. 2019;40(5):2076–87.

8. Manohar N, Jayaramudu J, Suchismita S, Rajkumar K, Babul Reddy A, Sadiku ER, et al. A unique application of the second order derivative of FTIR–ATR spectra for compositional analyses of natural rubber and polychloroprene rubber and their blends. Polymer Testing. 2017;62:447–53.
9. Kralevich ML, Koenig JL. FTIR analysis of silica-filled natural rubber. Rubber Chemistry and Technology. 1998;71(2):300–9.
10. Gorassini A, Adami G, Calvini P, Giacomello A. ATR-FTIR characterization of old pressure sensitive adhesive tapes in historic papers. Journal of Cultural Heritage. 2016;21:775–85.
11. Milani G, Leroy E, Milani F, Deterre R. Mechanistic modeling of reversion phenomenon in sulphur cured natural rubber vulcanization kinetics. Polymer Testing. 2013;32(6):1052–63.
12. Li ZH, Zhang J, Chen SJ. Effects of carbon blacks with various structures on vulcanization and reinforcement of filled ethylene-propylene-diene rubber. Express Polymer Letters. 2008;2(10):695–704.
13. Zhou J, Wang W, Song Y, Zheng Q. Effect of ionic liquid on structure and properties of carbon black filled natural rubber vulcanizates. Composites Part A: Applied Science and Manufacturing. 2023 Apr 1;167:107432.
14. Lin JH. Identification of the surface characteristics of carbon blacks by pyrolysis GC–MASS. Carbon. 2002 Feb 1;40:183–7.
15. Boehm HP. Some aspects of the surface chemistry of carbon blacks and other carbons. Carbon. 1994 Jan 1;32(5):759–69.
16. Maciejewska M, Sowińska A. Influence of Fillers and Ionic Liquids on the Crosslinking and Performance of Natural Rubber Biocomposites. Polymers. 2021 May 19;13(10):1656.
17. Pichaiyut S, Kitisavetjit W, Nakason C. Synergistic Effects of Graphite and Carbon Nanotube Hybrid Fillers on Key Properties of Epoxidized Natural Rubber Nanocomposites.
18. Siriwas T, Pichaiyut S, Susoff M, Petersen S, Nakason C. Enhancing curing, mechanical and electrical properties of epoxidized natural rubber nanocomposites with graphene and carbon nanotubes hybrid fillers. J Mater Sci [Internet]. 2023 Oct 24 [cited 2023 Oct 31]; Available from: https://doi.org/10.1007/s10853-023-09003-3

Chapter 4

Morphology, Mechanical and Dynamic Mechanical Properties of NR Hybrid Filler Systems

Summary

This chapter discusses the mechanical properties, morphological analysis and dynamic mechanical properties of natural rubber (NR) hybrid filler systems filled with carbon based conductive fillers and ionic liquid (IL) modified fillers. Theoretical predictions of mechanical modulus were made using the Rule of mixtures, Einstein, Guth and Kerner model. Also, Nicolais-Narkis, Kunori-Geil and Turcsanyi models are employed to compare experimental and theoretical values of the tensile strength of the composites. DMA showed that the hybrid filler network of CCB and CNT effectively restricted molecular chain mobility, resulting in a higher storage modulus. CNT-CCB hybrid system also shows improved tensile strength, and the highest tensile strength is exhibited by the incorporation of 20 phr CCB. Viscoelastic studies and the examination of various parameters, such as the volume fraction of the constrained region, the degree of entanglement, and the reinforcing efficiency, were employed to understand the interactions between the rubber matrix and filler in the composites.

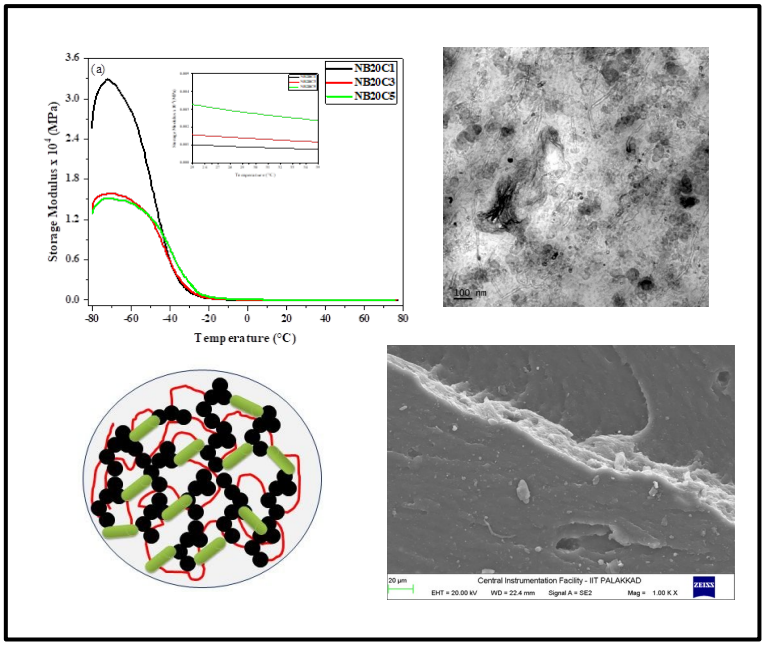

A part of this chapter is published in the Journal of Applied Polymer Science. Vol. 139., No.47., Pages e53197, 2022. https://doi.org/10.1002/app.53197

4.1. Introduction

Study on the static and dynamic physical properties of rubber is essential because of the elastic and viscous nature. Elastomers are widely used as shock absorbers or damping materials. Therefore, an insight into the mechanical and viscoelastic properties is relevant in designing products for various applications. In the present study, NR is reinforced with conducting fillers such as CCB, CNT and RGO. This chapter provides the effect of these conducting fillers on the mechanical and dynamic mechanical properties of NR as a function of filler weight percentage, filler modification and hybrid systems.

4.2. Theoretical models applied for various studies

4.2.1. Mechanical properties

The modulus of NR hybrid filler systems is evaluated theoretically and compared with experimental findings using the following models.

4.2.1.1. Rule of mixtures model

Rule of mixtures model is used for the prediction of the modulus of composite by the incorporation of fillers. The equation employed is given below,

$$E = E_m (1 + \varphi) \tag{4.1}$$

where E is the modulus of composites, E_m is the modulus of the unfilled NR and φ is the volume fraction of filler.

4.2.1.2. Einstein model

Einstein model (1) is developed by introducing an adhesion parameter to the rule of mixtures model, which is 2.5 for spherical fillers. Einstein assumed the dilute suspension and perfect adhesion between the spherical filler and matrix of the composite. This model is expressed as the following equation,

$$E = E_m (1 + 2.5\varphi) \tag{4.2}$$

4.2.1.3. Guth model

Guth model (2) is extensively used for analysing the mechanical properties of composites reinforced with spherical fillers. Guth model considered filler-filler interaction and assumed that at higher concentration, the modulus of composites can be expressed as a power series in φ as given below (3),

$$E = E_m (1 + \alpha_1\varphi + \alpha_2\varphi^2 + \alpha_3\varphi^3 + \cdots) \tag{4.3}$$

where α_1, α_2, α_3 etc. are numeric factors that depends on the shape and interaction between fillers. For spherical particles $\alpha_1 = 2.5$ and it expresses the independent action of filler particles up to 10 vol% of filler concentration. At higher concentration, α_2, α_3, α_4 etc., represent mutual interaction among pairs, triplets and quadruplets of filler particles respectively.

4.2.1.4. Kerner model

Kerner model (4) is used with spherical fillers, and it takes into account the Poisson's ratio of matrix. It is used for rigid particles incorporated polymer matrix featuring some adhesion. Kerner model assumes a homogeneous distribution of spherical filler particles surrounded by a uniform layer of the matrix. Kerner equation is given by,

$$E = E_m \left[1 + \left(\frac{\varphi}{1-\varphi}\right)\left\{\frac{15\,(1-v)}{8-10v}\right\}\right] \tag{4.4}$$

where ν is the Poisson's ratio and is 0.4999 for NR (5).

4.2.1.5. Nicolais-Narkis model

Nicolais-Narkis (6) model is employed for the theoretical prediction of tensile strength of composites using the equation given below

$$\sigma = \sigma_m\,(1 - k\varphi^{2/3}) \tag{4.5}$$

where σ is the tensile strength of the composite and σ_m is the tensile strength of the unfilled NR and k is the stress concentration factor. As the k values decreases the adhesion between filler and polymer matrix increases (7).

4.2.1.6. Kunori-Geil model

The equation for Kunori and Geil (8) model is given by,

$$\sigma = \sigma_m\,(e^{-a\varphi}) \tag{4.6}$$

Kunori and Geil model relates the tensile strength of the composites to a proportionality constant "a," which is the stress concentration parameter. Increased "a" value indicates improved adhesion between filler and matrix.

4.2.1.7. Turcsanyi model

Turcsanyi model (9) calculates the tensile stress in composites using the equation given below,

$$\sigma = \frac{1-\varphi}{1+A\varphi}\sigma_m\, f(\varphi) \tag{4.7}$$

The value of A in this method is 2.318 for both face-centred cubic and hexagonal close

packing. By applying this equation to different polymer/filler systems, the researchers found that the best fit was an exponential function, which was expressed as the equation given below,

$$\sigma = \sigma_m \frac{1-\varphi}{1+2.5\,\varphi} e^{B\varphi} \quad (4.8)$$

The parameter B in this equation represents the interfacial properties and was determined through fitting.

4.2.2. Dynamic mechanical properties

4.2.2.1. Coefficient β_f

Coefficient β_f is introduced for the indication of effectiveness of fillers on the moduli of the composites (10). β_f is calculated using following equation,

$$\beta_f = \frac{\frac{E'_g}{E'_r}\, filled\ composites}{\frac{E'_g}{E'_r}\, gum\ vulcanizate} \quad (4.9)$$

where E_g' and E_r' are the storage modulus values in the glassy and rubbery regions of the composites respectively.

4.2.2.2. Volume fraction of the constrained region

For linear viscoelastic behaviour, the energy loss fraction of the composites is given by the following equation (11),

$$W = \frac{\pi\, tan\delta}{\pi\, tan\delta+1} \quad (4.10)$$

where the dynamic viscoelastic data gives the energy loss fraction W at the tan δ peak as given below,

$$W = \frac{(1-C)W_o}{1-C_O} \quad (4.11)$$

where C is the volume fraction of the constrained region, (1-C) is the volume fraction of the amorphous region, W_o is the energy loss fraction of the unfilled NR and C_O is the volume fraction of the constrained region in the pure polymer. C_O is taken as 0 for gum vulcanizate. The fraction of the constrained region of the composite can be calculated by modifying the above equation as follows,

$$C = 1 - \frac{(1-C_O)W}{W_O} \quad (4.12)$$

4.2.2.3. Entanglement density

Interaction between NR matrix and fillers can be calculated from the rubbery region using the given equation for entanglement density,

$$N = \frac{E_r}{\varphi RT} \tag{4.13}$$

where E_r is the modulus at T_g+ 30 in K, φ is the front factor and φ = 1, R is the gas constant and T is T_g+ 30 in K.

4.2.2.4. Reinforcing efficiency

Reinforcing efficiency of filler in polymer matrix is calculated from the following equation,(12)

$$E_c = E_m \left(1 + r\, V_f\right) \tag{4.14}$$

E_c and E_m are the storage modulus values of filled composites and unfilled NR respectively, r is the reinforcing efficiency of fillers and V_f is the volume fraction of filler.

4.3. Results and discussion

4.3.1. NR/CCB systems

4.3.1.1. Mechanical properties and morphological analysis

Mechanical properties such as tensile strength, elongation at break (%), and modulus at 100, 200, and 300 % elongation of NR/CCB systems are given in **Table 4.1**. The tensile strength of NR/CCB systems has increased significantly due to filler-filler and filler-matrix interactions(13). CCB aggregates, after mixing, disperse into the polymer matrix and reinforce the NR by forming a filler network. Reinforcement of CCB in NR based on physical, mechanical and dynamic filler rubber interactions. The hydrodynamic interaction between rigid CCB aggregates and NR molecules where rigid fillers increase the stiffness and lead to significant local strains which can reinforce the matrix and improve the mechanical properties of NR/CCB systems. (14) In addition, the physical interaction between CCB chains and NR molecules also contribute to the reinforcement of NR matrix. The high surface area of carbon black allows the adsorption of rubber chains, which leads to more rubber–filler interactions. Adsorbed rubber chains occur in a glassy state around spherical CCB particles. (15) Consequently, the improved contact area of filler and rubber at the interface results in the enhanced physical properties of NR/CCB systems. (16,17) The surface of CCB is

characterised by the presence of oxygen functionalities such as lactons, phenols and carboxylic groups. Chemical interactions happen when the acidic groups on the CCB surface react with the basic functional groups on the surface of the rubber. (18) The double bonds in the CCB react with S atoms, olefins and radicals of rubber to form chemical bonds and result in reinforcement. (19) The dynamic reinforcement is explained by the slippage postulation by Dannenberg in 1966. (20) Slippage on the rubber chains and CCB interface redistributes the strain and prevents the molecular rupture of the matrix. The interface slippage phenomenon occurs under stress and is a proposed reinforcement mechanism under strain.

Elongation at the break of the samples is gradually decreased with CCB filler loading. Modulus at 100, 200, and 300% elongation are gradually increasing with an increase in filler loading due to the increased rubber-filler interaction. **Figure 4.1** shows the possible physical and chemical interactions of CCB and NR chains.

Table 4.1-Mechanical properties of NR/CCB systems

Sample	Elongation at break (%)	Tensile strength (MPa)	Modulus at 100% (MPa)	Modulus at 200% (MPa)	Modulus at 300% (MPa)
NB0	1184 ±22	17.1 ±0.9	0.9 ±0.01	1.4 ±0.01	2.0±0.00
NB5	1126 ±47	23.2 ±0.5	1.1 ±0.02	1.7 ±0.03	2.4 ±0.04
NB10	991 ±49	22.4 ±0.5	1.2 ±0.04	2.0 ±0.05	3.0 ±0.07
NB15	913 ±10	23.7 ±0.6	1.4 ±0.02	2.5 ±0.04	3.8 ±0.09
NB20	893 ±25	26.3 ±0.9	1.6 ±0.02	2.9 ±0.04	4.5 ±0.08

Figure 4.2 shows the SEM image of the tensile fracture surface of NR/CCB systems. CCB can act as stress transferring agents in the matrix. Consequently, it necessitates high crack propagation energy to fracture the NR/CCB systems, as evidenced by the presence of the matrix fracture lines in the tensile fracture surfaces (21). Also, homogeneous dispersion of filler is seen in the SEM images. HRTEM images of NR/CCB systems provide an insight into the distribution of CCB in NR matrix and are presented in **Figure 4.3**. TEM images of B20 show a homogeneous distribution of CCB in the rubber matrix.

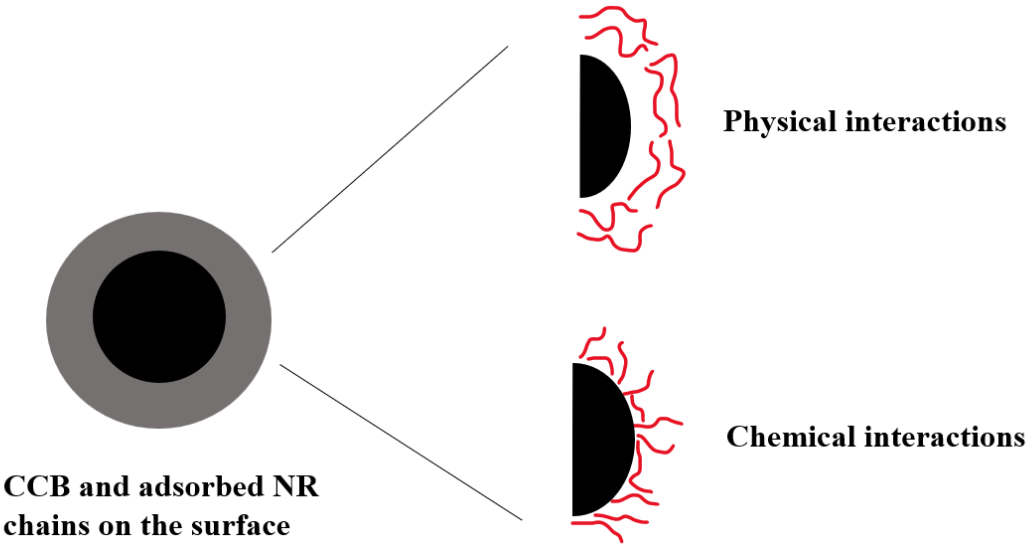

Figure 4.1-Schematic representation of interactions between CCB and NR

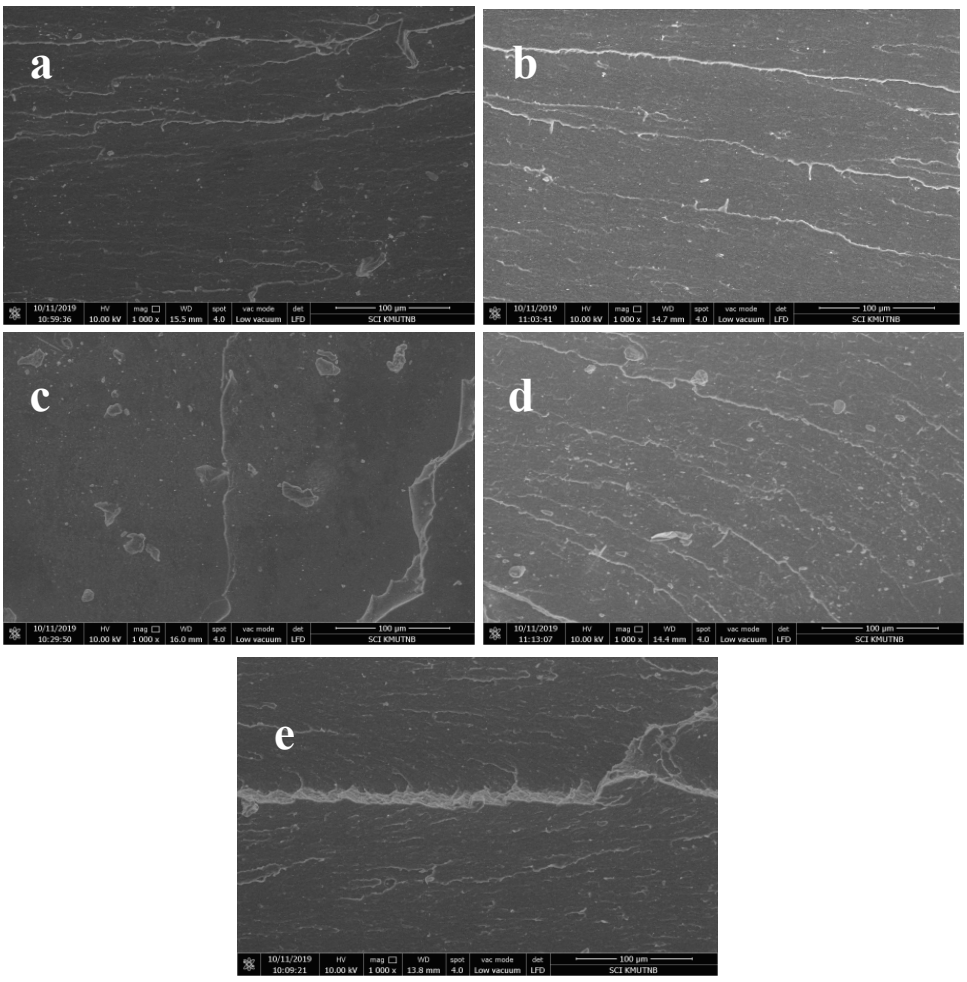

Figure 4.2-SEM of tensile fracture surface (1000 x) of (a) NB0 (b) NB5 (c) NB10 (d) NB15 (e) NB20

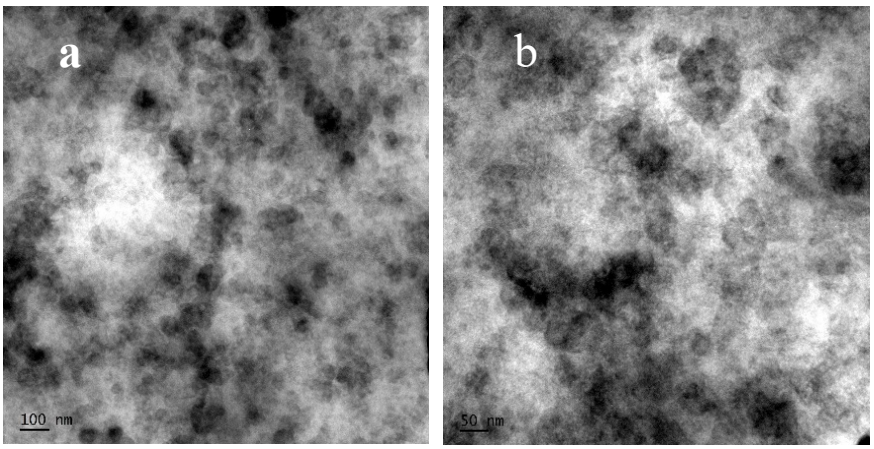

Figure 4.3-HRTEM images of NB20 at (a) low and (b) high magnifications

Theoretical models such as the Rule of mixtures, Einstein, Guth and Kerner have been applied to predict the mechanical properties of filler reinforced elastomer composites. Filler characteristics like particle geometry, dimension, surface area, and distribution in polymer matrix influence the mechanical properties of composites. Hence, properties of fillers are also considered in these theoretical models while predicting composite properties. Experimentally and theoretically predicted modulus values of NR/CCB systems are given in **Figure 4.4**. Experimental values are lower than the moduli predicted by Rule of mixtures and Einstein model. Kerner model predicts lower modulus values than experimental results, while the Guth model is in good agreement with experimental values. Agreement of theoretical predictions using Guth model with experimental values suggests filler-filler interaction as well as filler-matrix interaction even up to a higher concentration of filler, ie, 20 phr. Guth model also considers the increase in viscosity of matrix due to filler addition and its uniform dispersion(22). Theoretical predictions of tensile strength using Nicolais-Narkis, Kunori-Geil, and Turcsanyi models and experimental values are compared in **Figure 4.5.** Theoretically predicted tensile strength is lower or almost same as that of experimental results. Stress concentration factor, k obtained for NR/CCB systems is -0.85, which indicates strong adhesion between spherical CCB and NR matrix. Nicolais-Narkis model is based on the assumption that there is a lack of adhesion between filler particle and polymer matrix. In that case, filler particles cannot endure the stress, and the stress is completely carried by the polymer matrix. Then, the stress concentration parameter will be 1.21.

However, when strong adhesion exists between filler and polymer matrix the stress concentration parameter will be less than 1.21 (23).

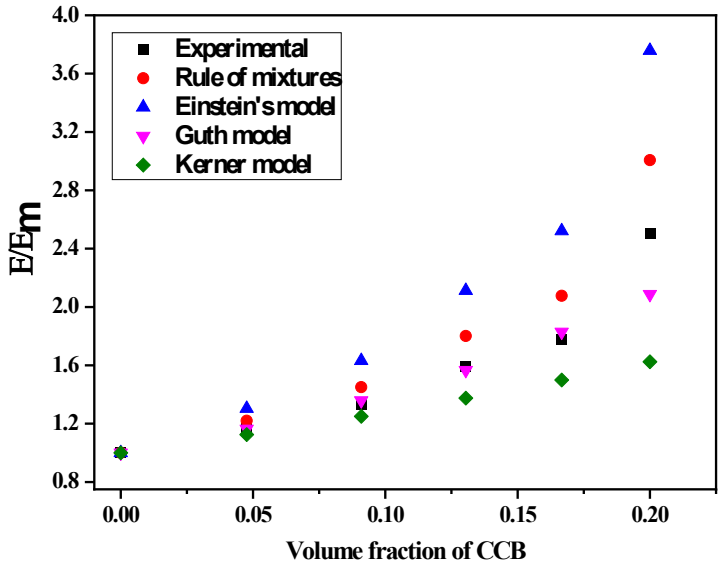

Figure 4.4-Theoretical comparison of modulus as a function of volume fraction of CCB in NR/CCB systems

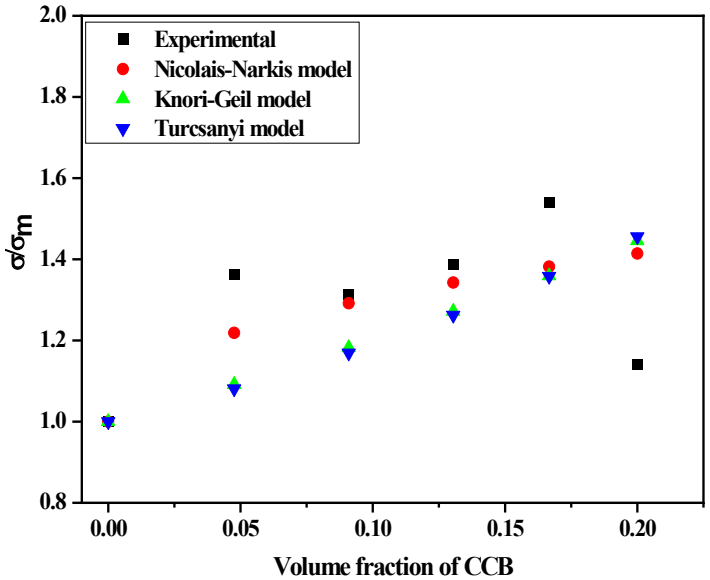

Figure 4.5-Theoretical comparison of tensile strength as a function of volume fraction of CCB in NR/CCB systems

4.3.1.2. Dynamic mechanical analysis (DMA)

Storage modulus (E′) is an indication of the segmental mobility and also signifies the energy stored in a viscoelastic material. At low temperatures, restricted molecular motion leads to higher storage modulus. Also, higher viscosity at low temperature leads to very small free volume in the polymer matrix, which consecutively results in negligible segmental motion. As the temperature increases, polymer chains exhibit high mobility; therefore, storage modulus decreases with temperature. The region where an increase in free volume of the polymer matrix is higher than the volume expansion of molecules marks the glass transition. Glass transition region illustrates the change of the polymer matrix from a glassy restricted state to a more elastic rubbery state. In the glass transition region, the chain dynamics of the NR matrix are changed when various relaxations of long chains of NR come into action. This causes high dissipation of energy indicated by the tan δ peak. Storage modulus values exhibit a sudden drop in the glass transition region and continue as a plateau in the rubbery region. The molecular motions in the glassy region are confined to vibrational and rotational motions. In the rubbery region, rapid viscosity drop with increasing temperature leads to segmental motion, causing low energy dissipation and storage modulus. Filler incorporation can enhance the storage modulus and reduce energy dissipation by restricting the chain mobility of the polymer matrix.

Storage modulus and loss tangent of NR/CCB systems are presented in **Figure 4.6 (a) & (b),** respectively. Storage modulus decreases with an increase in temperature in the range of -60°C to -30°C, where the transition from a glassy to rubbery state occurs. Storage modulus values at 25°Care 1.99, 2.45 and 7.07 MPa for unfilled NR, 10 and 20 phr CCB filled NR, respectively. This is attributed to the hindered chain mobility of polymer segments due to the adsorption of NR molecules on the CCB surface. This is associated with the reinforcing ability of filler. As the reinforcing activity of filler increases, chain mobility decreases and thereby, storage modulus increases (24). In the rubbery zone, unfilled NR exhibits low energy dissipation, and increases with filler loading. The energy dissipation or damping in the glass transition region is caused by the polymer component. Hence, it decreases with filler incorporation, while in the rubbery zone, damping increases with filler loading.

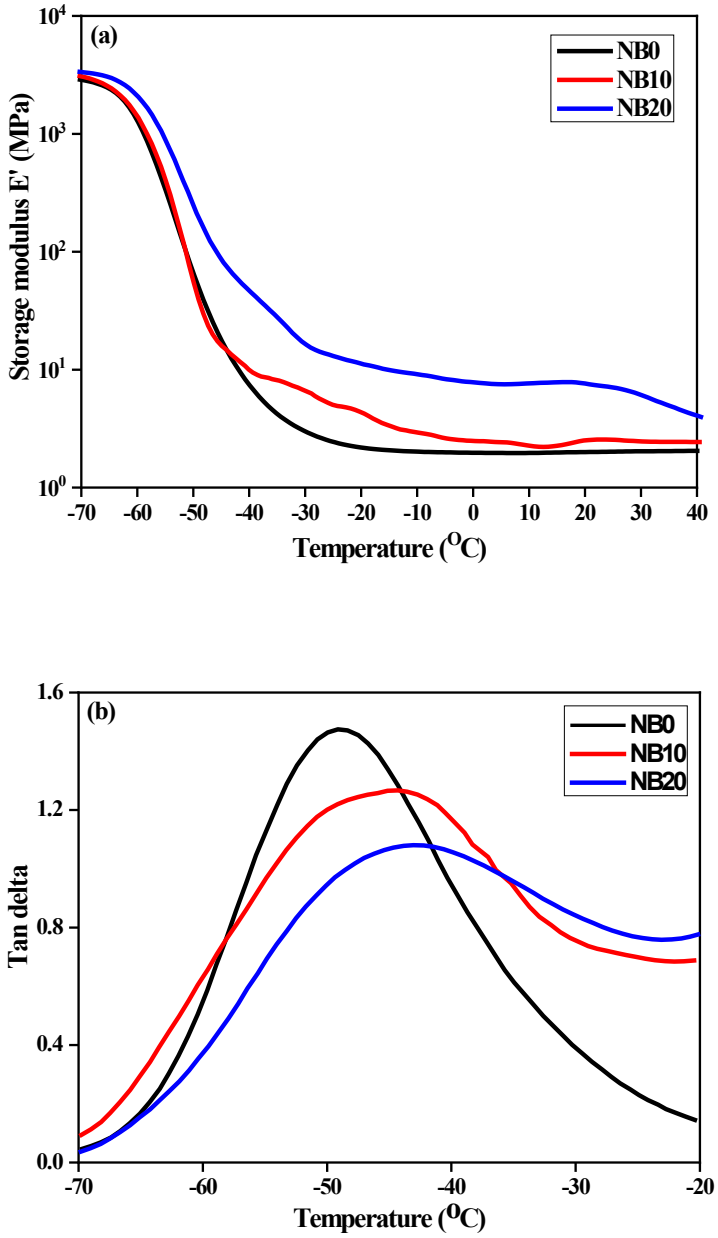

Figure 4.6-(a) Storage modulus and (b) Loss tangent of NR/CCB systems

Loss tangent (tan δ) represents the viscous response of the material and is given by the ratio of dynamic loss modulus (E″) and dynamic storage modulus (E′) (tan $\delta = \frac{E''}{E'}$). Tan δ peak value varies with polymer matrix and filler. However, tan δ, in general, represents the dissipation of energy due to the internal friction and molecular motions. Tan δ peak occurs in the transition region where the viscoelastic material changes from a glassy to a rubbery state. The constraints of chains in the glassy region can cause less

damping, which increases upon passing through glass transition temperature. Again, the damping is decreased, and the molecular chains are free to move in the rubbery state. The extent of reinforcement in the filled composites can be understood from the peak height of the tan δ plots (25). Damping gradually decreases after filler addition, indicating better reinforcement at the filler-matrix interface. The broadening and reduced magnitude of damping peak is an indication of restricted mobility of NR chains due to the inclusion of CCB fillers and broader distribution of chain relaxations in NR.

Different theoretical parameters are employed to analyse the DMA data of the NR/CCB systems. The coefficient, β_f of the composites are calculated to analyse the effectiveness of the filler in the polymer matrix. Calculated β_f values are given in **Table 4.2.** The low value of β_f indicates the higher effectiveness of filler. β_f values decrease with filler content, and NB20 has the lowest β_f value signifying the highest effectiveness of the filler. Immobilisation of NR polymer chains occurs on the surface of CCB particles. Quantitative estimation of volume fraction of constrained region is important to understand the role of confined polymer chains in improving the mechanical properties of NR/CCB systems. The constrained region in the composites can be estimated from the decrease in the height of tan δ peaks. Estimated values of constrained regions are given in **Table 4.2.** There is a linear relationship between volume fraction of constrained region and amount of filler incorporated. Increasing volume fraction of constrained region, C with increasing CCB in the NR composites suggests improved interfacial interaction between CCB surface and NR chains. Polymer confinement in the surface of CCB filler particles leads to restricted chain mobility, which in turn results in enhanced reinforcement of composites.

Table 4.2-Various theoretical parameters from DMA analysis

Sample	β_f	N (mol/dm^3)	C	r
NB0	1.00	0.10×10^{-2}	-	
NB10	0.50	0.15×10^{-2}	0.0275	0.71
NB20	0.08	0.45×10^{-2}	0.0596	11.53

Another parameter to understand the interaction between polymer and the filler is given by the entanglement density denoted by N. The degree of entanglement in rubber

composites can be measured using various techniques, including rheological measurements and dynamic mechanical analysis. The entanglement density, which describes the number of entanglements per unit volume of the material, is a key parameter that affects the mechanical behaviour of the composite. **Table 4.2** gives the values of N in mol/dm^3. The N values are found to increases with increase in concentration of CCB in the NR matrix, indicating the progressive enhancement in interfacial interaction with respect to filler loading. Larger N values are an indication of the strong interfacial interaction (26). Increased storage modulus values of NB20 as shown in **Figure 4.6 (a)** is further confirmed from the computed N value. Reinforcing efficiency of the filler can also be understood from the DMA data, which is presented in **Table 4.2,** and there is a 15% enhancement when the CCB content is increased from 10 to 20 phr.

4.3.2. NR/CCB-CNT hybrid filler systems

4.3.2.1. Mechanical properties and morphological analysis

Mechanical properties such as density, tensile strength, elongation at break % and modulus at 100, 200, and 300 % elongation of NR/CCB-CNT hybrid filler systems are given in **Table 4.3**. The highest tensile strength of NR/CCB-CNT is 24 MPa for NB20C1. Elongation at break of composites decreases with filler loading. Modulus values at 100, 200 and 300 % elongation gradually increase for all composites, indicating the increased filler-rubber interaction.

Table 4.3-Mechanical properties of NR/CCB-CNT hybrid filler systems

Sample	Elongation at break (%)	Tensile strength (MPa)	Modulus at 100% (MPa)	Modulus at 200% (MPa)	Modulus at 300% (MPa)
NB20C0.5	639 ±43	21.4 ±0.3	2.1 ±0.04	3.9 ±0.08	6.5±0.19
NB20C1	699 ±7	24.0 ±0.1	2.2 ±0.06	4.0±0.13	6.6±0.24
NB20C3	629 ±8	22.3 ±0.4	2.5 ±0.01	4.8 ±0.01	7.8±0.06
NB20C5	561 ±33	21.3 ± 0.5	3.1 ±0.06	6.1±0.05	9.7±0.04

Figure 4.7 shows the theoretical comparison of tensile strength as a function of the volume fraction of CNT of NR/CCB-CNT hybrid filler systems. Theoretically predicted tensile strength using Nicolais-Narkis and Turcsanyi model is in agreement

with experimental results for NB20C0.5 and NB20C3. Stress concentration factor, k, obtained using Nicolais-Narkis model is -0.94, which indicates strong adhesion between filler particles and NR matrix. However, experimental tensile strength values of NB20C1 and NB20C5 show slight deviations from theoretical model predictions.

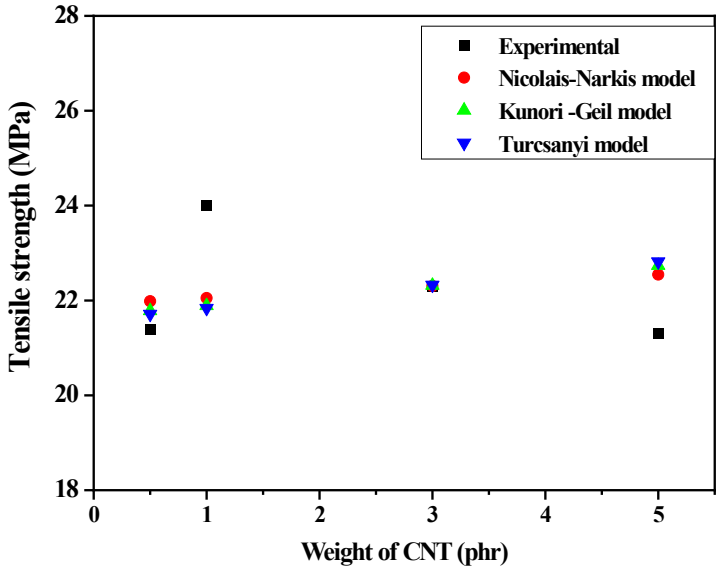

Figure 4.7-Theoretical comparison of tensile strength as a function of volume fraction of CNT of NR/CCB-CNT hybrid filler systems

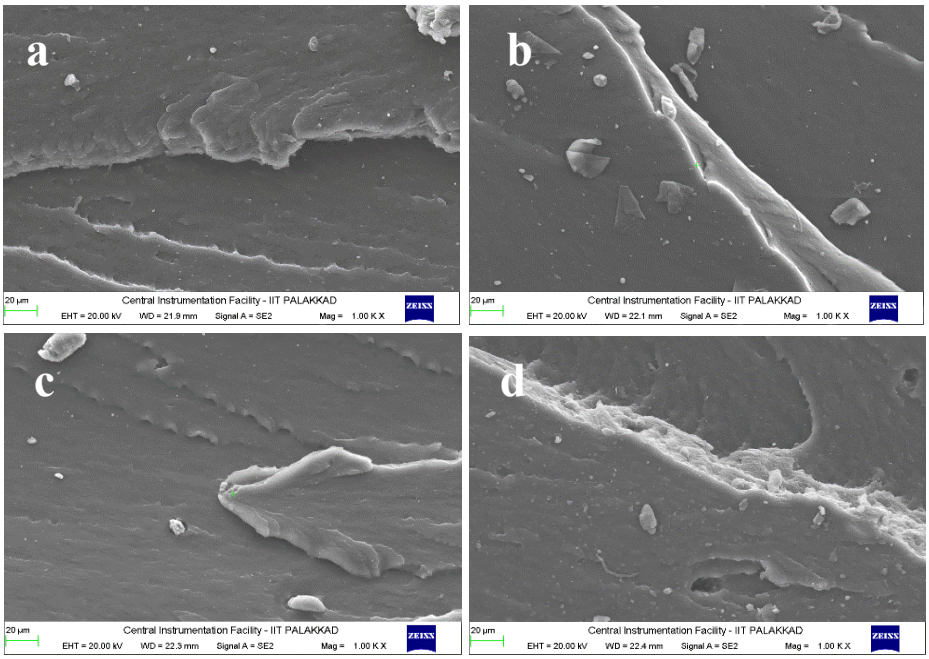

Figure 4.8-SEM of tensile fracture surface of (a) NB20C0.5 (b) NB20C1 (c) NB20C3 (d) NB20C5

Figure 4.8(a-d) presents the SEM images of the tensile fracture surface of NR/CCB-CNT hybrid filler systems. Matrix fracture lines are seen upon the incorporation of CCB-CNT filler, which indicates the resistance of NR matrix to crack propagation due to the presence of a hybrid filler system.

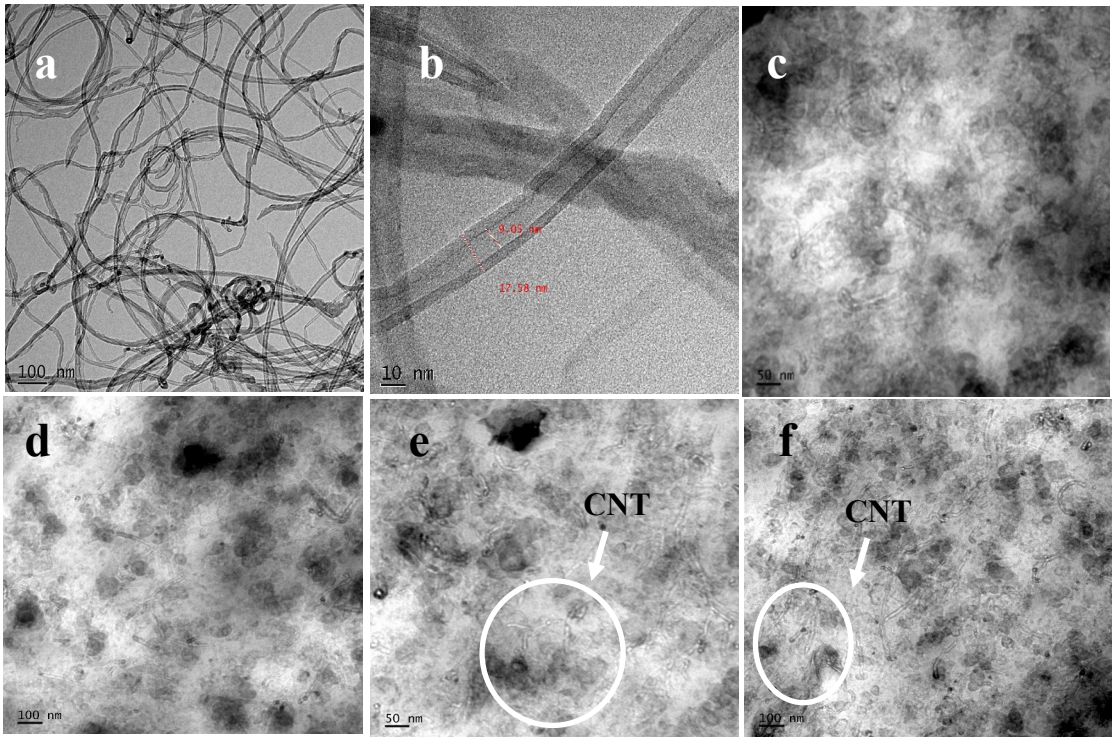

Figure 4.9-HRTEM images of (a & b) CNT (c & d) NB20C3 and (e & f) NB20C5 at different magnifications

Figure 4.9(a) shows the TEM images of unmodified CNT at different magnifications. **Figure 4.9(b)** marks the inner diameter as 9.05nm and outer diameter as 17.58 nm and shows the inner walls of multiwalled carbon nanotubes. **Figure 4.9 (c-f)** shows the HRTEM images of NB20C3 and NB20C5 at low and high magnifications. TEM images clearly show the CNT tubes distributed among the CCB aggregates. **Figure 4.9 (c)** and **(d)** show higher concentrations of the CCB aggregates, while **(e)** and **(f)** show an increase in the concentration of CNT tubes that forms an extensive network with CCB aggregates. The network formation of CNT and CCB is evident in TEM images.

4.3.2.2. Dynamic mechanical analysis (DMA)

Storage modulus of NR hybrid filler systems in the temperature range of -70°C to +70°C is illustrated in **Figure 4.10 (a)**. Higher storage modulus is obtained for NB20C1 at low temperatures. At higher CNT, the storage modulus decreases due to the probable agglomeration of nanofillers in the matrix. However, the modulus of higher CNT loading composites is still much higher than unfilled NR. As the temperature increases, an abrupt drop in modulus is obtained with the transition from glassy to rubbery state. **Figure 4.10 (b)** presents the plot of tan δ against temperature. Tan δ peak shows that the glass transition temperature shifts to higher temperatures for hybrid filler NR composites. The damping peak of all hybrid filler composites is around -25°C while the tan δ peak of NB20 is at -38°C (**Figure 4.10 (b)**). Also, a noticeable decrease in peak height and broadening of peaks are observed upon the incorporation of fillers. This is attributed to the restricted mobility of polymer chains in composites in the glass transition region. (27,28) At low temperatures, the modulus values are high because the spherical CCB and tubular CNT effectively restrict the motion of polymer chains. Storage modulus of the hybrid systems at ambient temperature increases proportionally with CNT content (inset of **Figure 4.10(a)**).

Table 4.4-Various theoretical parameters from DMA analysis

Sample	β_f	N (mol/dm^3)	C	r
NB20C1	0.14	2.93 x10^{-2}	0.18	18.94
NB20C3	0.14	4.09 x10^{-2}	0.22	30.27
NB20C5	0.06	9.05 x10^{-2}	0.27	63.04

Table 4.4 presents the calculated β_f values of NR/CCB-CNT hybrid filler systems which give the effectiveness of filler. Lower β_f indicates the higher efficiency of filler in the NR matrix. NB20C1 and NB20C3 have similar β_f values. However, a further increase in the CNT has decreased the β_f value. Quantitative estimation of the volume fraction of constrained region is important to understand the role of confined polymer chains in improving the mechanical properties of NR hybrid filler systems. Decrease in the height of the $tan\delta$ peak gives the extend of the constrained region. The calculated volume fraction of constrained region, C, is presented in **Table 4.4**. The filler content increases, the constrained region in the NR matrix increases. This indicates the increased interfacial interaction of the hybrid filler network and rubber

chains. The homogeneous network of CNT and CCB is able to immobilize polymer chains on the surface, giving a more constrained region. Volume fraction of constrained region also depends on the nature of the polymer and polymer–filler interaction. (10)

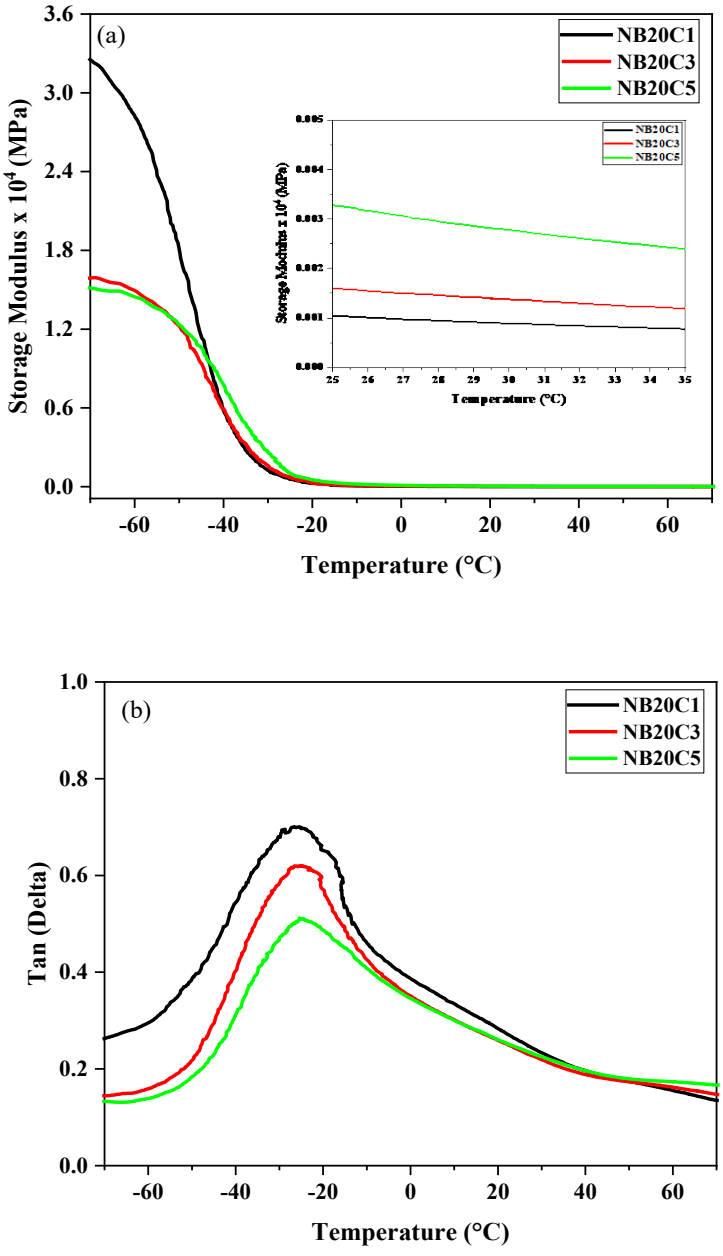

Figure 4.10 (a) Storage modulus [Inset: Storage modulus above 0°C] and (b) loss tangent of NR/CCB-CNT hybrid filler systems

Figure 4.11 shows the linear relationship between the volume fraction of the constrained region and the amount of CNT. Entanglement density values, N, are presented in **Table 4.4**, which also support the enhancement of interfacial interaction with filler loading. N value gives an insight into the extent of entanglement between NR and hybrid fillers and is found to be higher for 5 phr CNT and 20 phr CCB containing composite due to the strong hybrid filler network-matrix interaction.

Reinforcing efficiency, r of the composites is also presented in **Table 4.4.** The r values also suggest the increasing reinforcement offered by the hybrid filler network. The CNT and CCB effectively form a strong interface with the NR matrix. This is supported by the β_f and r values. Volume fraction of constrained region calculated from the decreasing height of tan δ peak also supports the observation that increasing the strength of hybrid filler-matrix interface. The volume of constrained region shows 45.5% increase for 5 phr CNT compared to 1 phr. Similarly, degree of entanglement increases by approximately 209% and reinforcing efficiency increases by 233% for NB20C5.

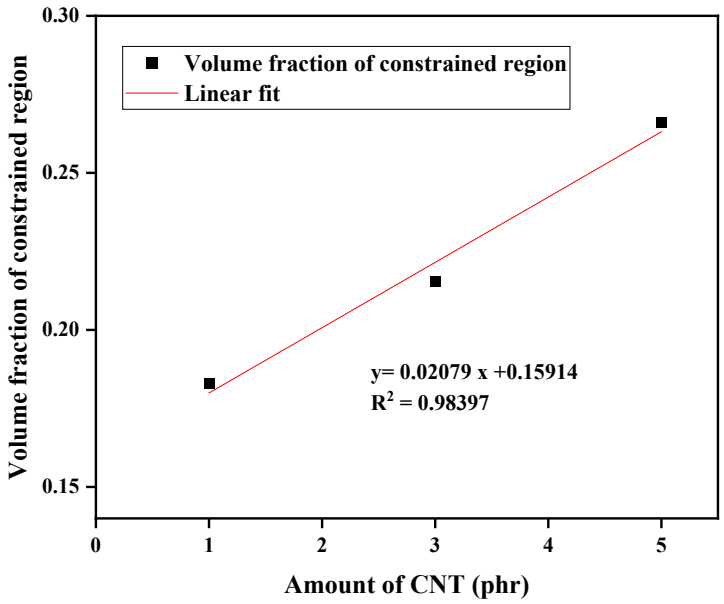

Figure 4.11-Linear variation of volume of constrained region with amount of CNT in NR/CCB-CNT hybrid filler systems

4.3.3. NR/1-ethyl-3-methylimidazolium chloride modified CCB (NR/ILCCB) systems

4.3.3.1. Mechanical properties and morphological analysis

Table 4.5-Mechanical properties of NR/ILCCB systems

Sample	Break strain (%)	Tensile strength (MPa)	Modulus at 100% (MPa)	Modulus at 200% (MPa)	Modulus at 300% (MPa)
NB20IL1	886 ± 29	15.92 ± 0.08	1.19 ± 0.1	2.09 ± 0.16	3.17 ± 0.24
NB20IL3	1119 ± 6	15.52 ± 0.34	0.80 ± 0.04	1.31 ± 0.05	1.92 ± 0.08

Table 4.5 presents the mechanical properties of NR/ILCCB systems. IL modified CCB incorporated NR has lower tensile modulus owing to the plasticising action of IL. (29) Modulus values at 100, 200 and 300 % elongation represent the stiffness or elasticity of the material. The composite sample NB20IL3 consistently exhibits lower modulus values, indicating lower stiffness. The break strain represents the maximum strain the material can undergo before failure or breaking. NB20IL3 exhibits the highest break strain percentage (1119 ± 6%) and possess good flexibility and stretchability. Theoretical prediction of tensile strength of composites using the Nicolais-Narkis, Knori-Geil and Turcsanyi model and comparison with experimental values are presented in **Table 4.6.** Theoretically, predicted tensile values are close to the experimentally determined values. Nicolais-Narkis model gives a correlation coefficient of 0.99 with a k value of 0.22. Knori-Geil model offers a correlation coefficient of 0.99 with K value of 0.40. Turcsanyi model parameter B less than 1 suggests insufficient adhesion at the interface of the filler and matrix, whereas the value between 1 and 3 indicates a certain degree of interfacial adhesion between the filler and matrix. (30) The Turcsanyi model parameter obtained for NR/ILCCB systems is 2.73, which indicates the adhesion between ILCCB filler particles and the NR matrix.

Figure 4.12 presents the FESEM images of NB20IL3. Tensile surface morphology of NB20IL3 shows that the stress transfer is not concentrated in any particular area. This suggests that the ionic liquid modification has facilitated a uniform distribution of

CCB, which in turn reduce the localised failure during the application of stress. This is possible through the homogenous dispersion of IL modified CCB in NR.

Table 4.6-Theoretical comparison of tensile strength (MPa) of NR/ILCCB systems

Sample	Experimental	Nicolais-Narkis model	Knori-Geil model	Turcsanyi model
NB20IL1	15.92	15.79	15.83	15.76
NB20IL3	15.52	15.63	15.60	15.66

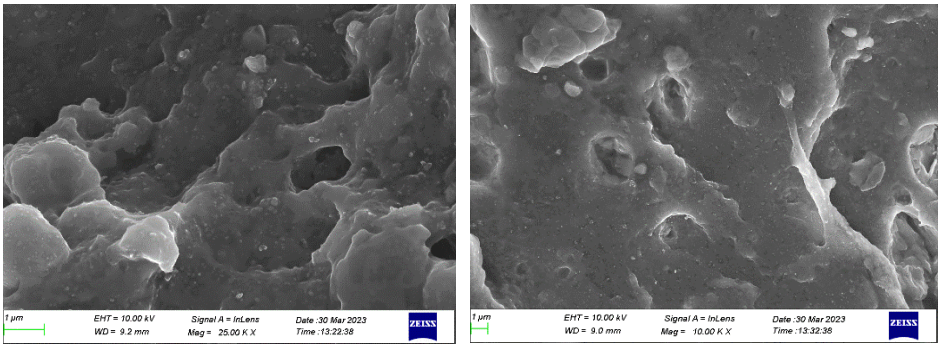

Figure 4.12-FESEM images of tensile fracture surface of NB20IL3

4.3.3.2. Dynamic mechanical analysis (DMA)

Figure 4.13(a) illustrates the storage modulus of NR/ILCCB systems. It demonstrates a gradual increase in storage modulus with ionic liquid modification and filler loading. Inset of **Figure 4.13** specifically displays the storage modulus values at room temperature, indicating a direct increase with modified CCB. Tan delta is a measure of the efficiency with which a material or system dissipates energy in the form of heat. Tan delta peaks of NR/ILCCB systems are given in **Figure 4.13 (b)**. The tan delta of rubber composites with fillers represents the mobility of macromolecules within the polymer matrix and the occurrence of phase transitions in the polymer system. (24) The addition of fillers can affect the viscoelastic behaviour of the polymer matrix, owing to the interaction between polymer chains and the filler particles. This can result in changes in the mobility and dynamics of the macromolecules, leading to variations in the occurrence and temperature range of these phase transitions.

Theoretical parameters obtained from storage modulus values are presented in **Table 4.7.** Calculations of various parameters such as the coefficient "β_f," volume fraction of the constrained region, and estimation of entanglement between filler and matrix, as

well as reinforcement efficiency, which helps to analyse the viscoelastic behaviour of composites. The constant β_f indicates that the effectiveness of filler has increased as the amount of IL increased in the NR composites. The entanglement density and reinforcing efficiency are also increased in NB20IL3. This indicates the improved interfacial interaction between filler and NR matrix. Volume fraction of constrained region shows a slight decrease as the ILCCB content is increased.

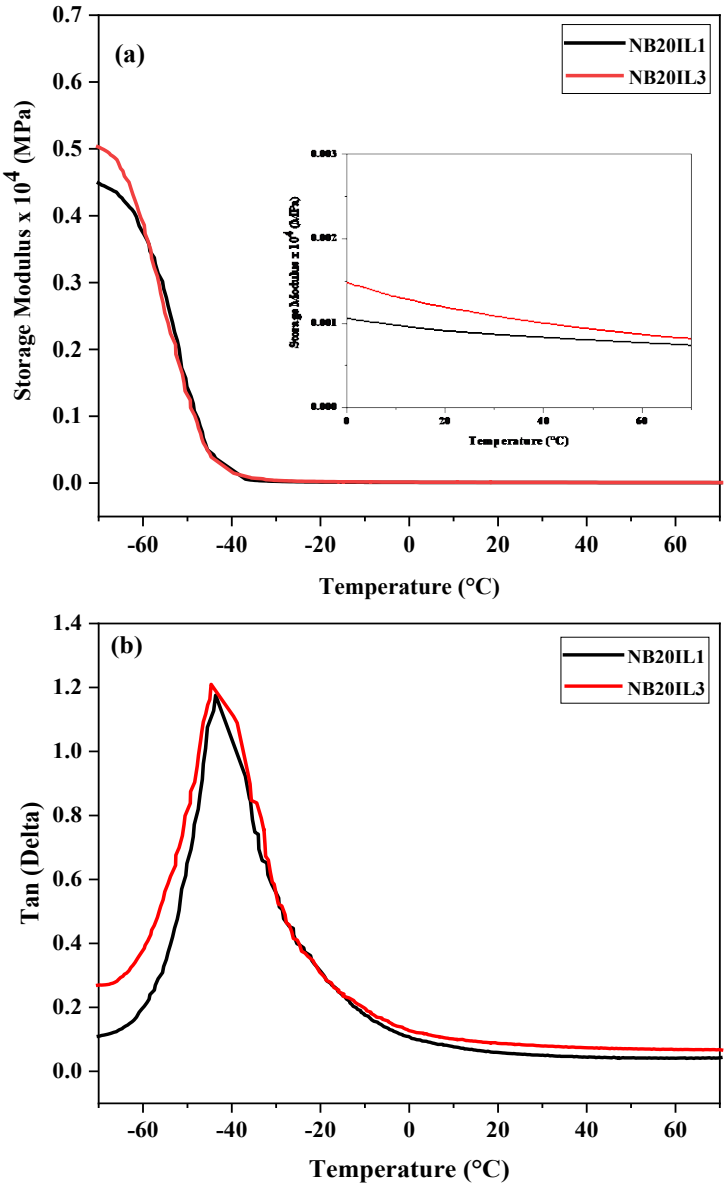

Figure 4.13-(a) Storage modulus [Inset: Storage modulus above 0°C] and (b) Loss tangent of NR/ILCCB systems

Table 4.7-Various theoretical parameters of DMA analysis

Sample	β_f	N (mol/dm^3)	C	r
NB20IL1	0.26	0.62 x 10^{-2}	7.11 x 10^{-2}	7.35
NB20IL3	0.19	0.94 x 10^{-2}	6.62 x 10^{-2}	18.06

4.3.4. NR/CCB-1-ethyl-3-methylimidazolium chloride modified CNT (NR/CCB-ILCNT) hybrid filler systems

4.3.4.1. Mechanical properties and morphological analysis

Table 4.8 presents the mechanical properties of NR/CCB-ILCNT hybrid filler systems. Ionic liquid modification of CNT and CCB has a detrimental effect on the tensile strength of the NR matrix. The ionic liquid acts as plasticiser in the NR composites and can cause a reduction in the tensile modulus. The modulus at 100, 200 and 300 % elongation represent the stiffness or elasticity of the material. Modulus values at different elongations are highest for NB20C5IL3, indicating superior stiffness and resistance to deformation.

Table 4.8-Mechanical properties of NR/CCB-ILCNT hybrid filler systems

Sample	Elongation at break (%)	Tensile strength (MPa)	Modulus at 100% (MPa)	Modulus at 200% (MPa)	Modulus at 300% (MPa)
NB20C3IL1	706 ± 47	11.7 ± 0.68	1.34 ± 0.03	2.40 ± 0.05	3.66 ± 0.06
NB20C3IL3	642 ± 41	11.7 ± 0.68	1.558 ± 0.02	2.92 ± 0.02	4.54 ± 0.02
NB20C5IL1	631 ± 52	10.52 ± 0.85	1.39 ± 0.04	2.61 ± 0.04	4.02 ± 0.03
NB20C5IL3	588 ± 60	11.18 ± 0.34	1.72 ± 0.05	3.15 ± 0.06	4.82 ± 0.07

Comparison of the experimental results with theoretical models helps in a better understanding of the underlying filler-polymer interaction. Effective filler polymer interaction is essential for reinforcement and improved physical properties of NR. **Figure 4.14** presents the comparison of experimental tensile strength with theoretical models. Theoretically predicted tensile strength values are close to the experimental data obtained for the NR composite. Nicolais-Narkis model predicts the tensile strength with a correlation coefficient 0.99. The Knori-Geil model also predicts the tensile strength values close to experimentally determined values with a correlation coefficient of 0.99. the Turcsanyi model parameter B, has a value of 1.08, suggesting adhesion of filler and NR matrix.

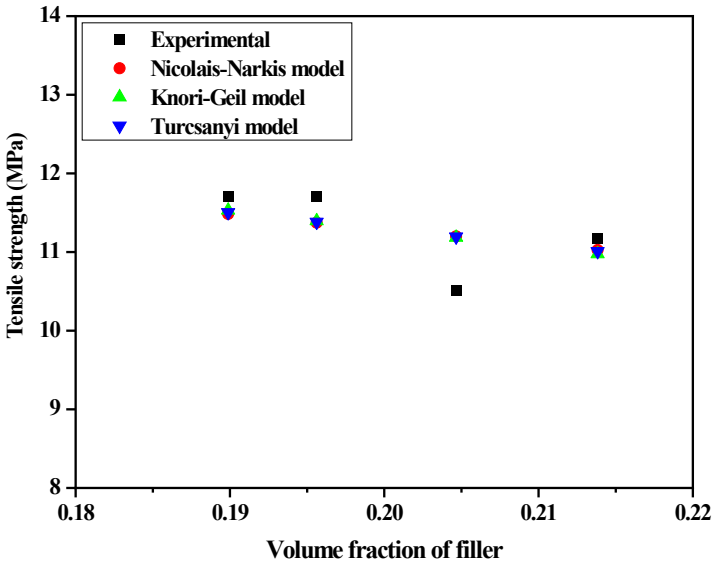

Figure 4.14-Theoretical comparison of tensile strength as function of volume fraction of filler

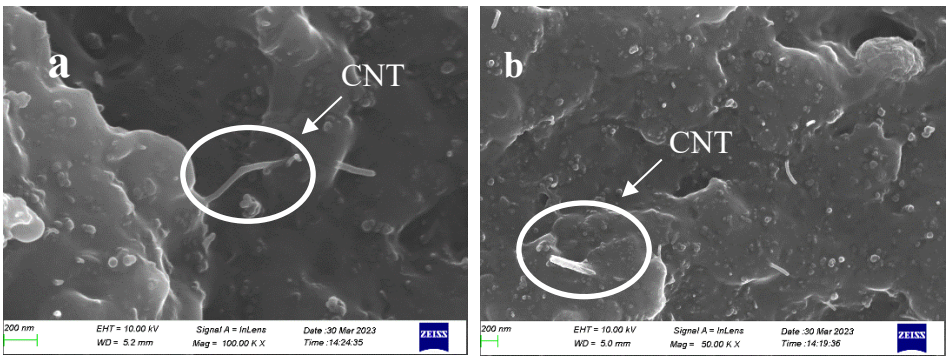

Figure 4.15-FESEM images of tensile fracture surface of NB20C5IL3

FESEM images of the tensile fracture surface of NR/CCB-ILCNT hybrid filler systems are shown in **Figure 4.15(a)** and **(b)**. It is mentioned that IL can shield the CNT molecules from π-π interaction, which can lead to the formation of agglomerates.(31) The presence of individual CNT tubes in the NR matrix, as observed in the FESEM images, indicates that the filler is uniformly dispersed and distributed throughout the composite. Additionally, the fracture surface morphology, as depicted in **Figure 4.16**, shows uniform stress transfer across the membrane. This suggests the absence of CNT or CCB agglomerates, further indicating the successful dispersion and distribution of the fillers within the composite. Uniform stress transfer is desirable as

it ensures the load is effectively distributed and shared among the reinforcement elements. **Figure 4.17** shows the HRTEM images of NB20C3IL3. The uniform distribution of CCB and CNT is evident from the morphological analysis. The presence of IL has decreased the CCB agglomeration in the matrix.

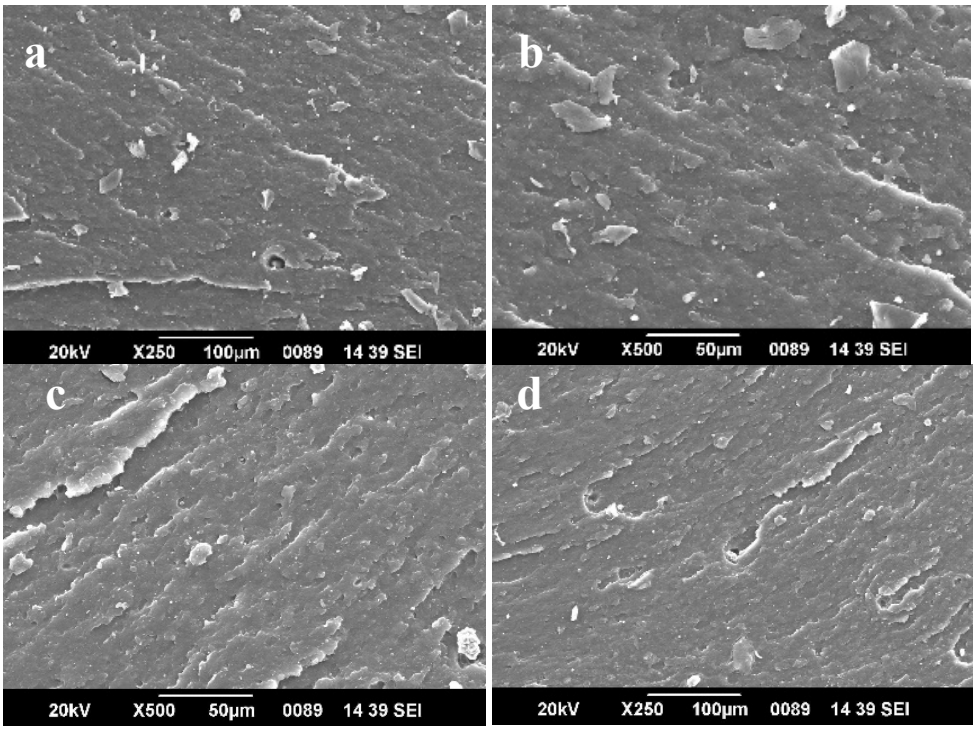

Figure 4.16-SEM images of tensile fracture surface of (a) and (b) NB20C3IL3; (c) and (d) NB20C5IL1

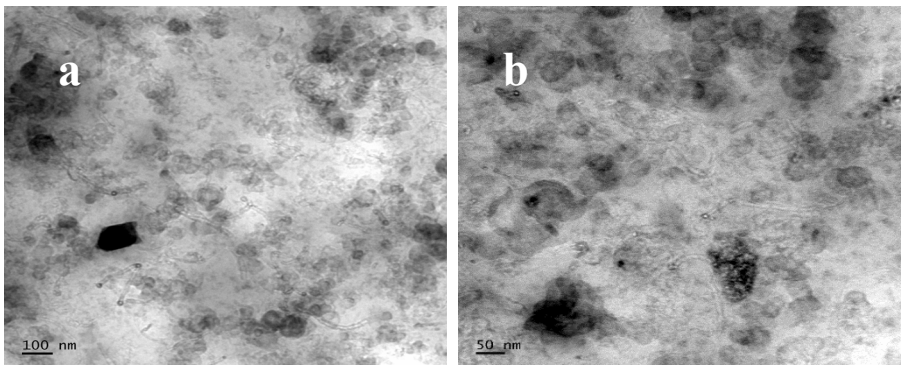

Figure 4.17-HRTEM images of NB20C3IL3 (a) high and (b) low magnifications

4.3.4.2. Dynamic mechanical analysis (DMA)

Figure 4.18(a) illustrates the storage modulus values of NR/CCB-ILCNT hybrid filler systems plotted against temperature. The composite NB20C5IL3 exhibits the highest storage modulus among the tested compositions. For the composite material containing 5 phr of ILCNT at a CNT to IL ratio of 1:3, the storage modulus at -70°C is 6763 MPa. Conversely, for the composite with a CNT to IL ratio of 1:1, the storage modulus is slightly lower, 6726 MPa.

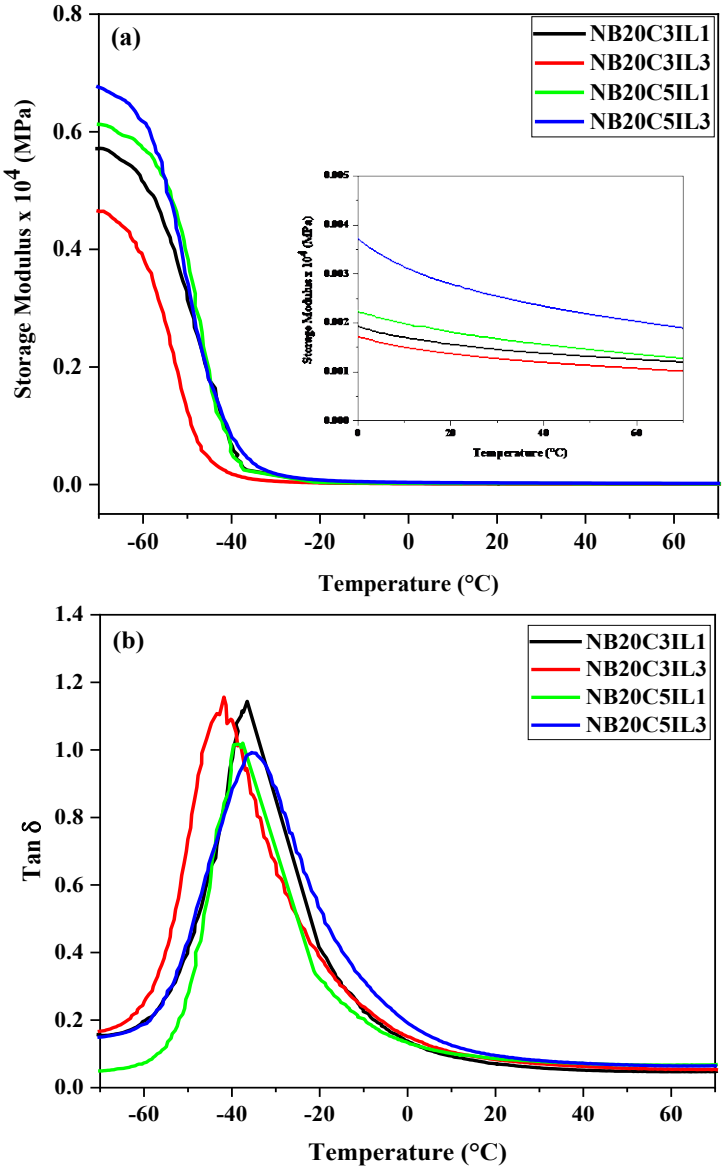

Figure 4.18-(a) Storage modulus [Inset: Storage modulus above 0°C] and (b) Loss tangent of NR/CCB-ILCNT hybrid filler systems

The inset of **Figure 4.18 (a)** clearly shows the storage modulus values above 0°C. The storage modulus increases linearly with the amount of CNT and IL at room temperature. Also, NB20C5IL3 exhibits the highest storage modulus values. **Figure 4.18-(b)** shows the loss tangent of NR/CCB-ILCNT hybrid filler systems plotted against temperature. The intensity of the loss tangent peak decreases with increasing amount of CNT. At 3 phr of ILCNT loading, a significant decrease is not observed despite increasing the filler to IL ratio from 1:1 to 1:3. However, a considerable change in peak intensity is observed when the amount of ILCNT is increased to 5 phr.

Theoretical parameters computed from DMA data are presented in **Table 4.9.** A lower β_f value is obtained for NB20C5IL3, which suggests improved effectiveness and dispersion of fillers in the NR matrix. Entanglement density and volume of constrained regions are increasing with CNT and IL content. This shows the enhanced interaction of CCB and IL modified CNT with NR matrix. Reinforcing efficiency has decreased by 17% for NB20C3IL1. However, NB20C5IL3 has increased by 69% compared to unfilled composites.

Table 4.9-Various theoretical parameters of DMA analysis

Sample	β_f	N (mol/dm^3)	C	r
NB20C3IL1	0.19	0.99×10^{-2}	7.63×10^{-2}	27.72
NB20C3IL3	0.16	1.03×10^{-2}	7.45×10^{-2}	22.91
NB20C5IL1	0.18	1.20×10^{-2}	1.01×10^{-2}	30.54
NB20C5IL3	0.11	1.92×10^{-2}	1.06×10^{-2}	46.93

4.3.5. NR/CCB-CNT-RGO hybrid filler systems

4.3.5.1. Mechanical properties and morphological analysis

Mechanical strength of the composites was evaluated after hybrid filler incorporation. Mechanical properties of the composites are presented in **Table 4.10.** The combination of three reinforcing fillers is expected to improve the mechanical strength of the matrix. The combination of CCB, CNT and RGO has reinforced the NR matrix effectively. However, there is no remarkable change in tensile strength with an increase in the weight percentage of CNT. Modulus values at 100, 200 and 300% elongation are higher for NB20C5R1 than NB20C1R1. Filler characteristics such as the nature of filler, concentration, orientation, filler-matrix interaction, filler-filler wettability and aspect ratio play a significant role in determining the mechanical

properties of the composites. (32) Various theoretical models are applied to predict the mechanical properties by considering the above-mentioned factors. Nicolais-Narkis model suggests that the area fraction scales in proportion to the volume fraction raised to the power of two-thirds. When the stress concentration factor decreases, the adhesion between the filler and the polymer matrix increases. This is because a lower stress concentration factor leads to more uniform stress distribution throughout the material, reducing the probability of stress concentrations at the interface between the filler and the matrix. Turcsanyi model proposed a direct method for calculating the tensile stress in unfilled and filled polymers. This method also relates the tensile strength of the composite material with volume fractions to describe the composition dependence of the tensile strength.

Table 4.10-Mechanical properties of NR/CCB-CNT-RGO hybrid filler systems

Sample	Elongation at break (%)	Tensile strength (MPa)	Modulus at 100% (MPa)	Modulus at 200% (MPa)	Modulus at 300% (MPa)
NB20C1R1	872 ± 38.9	21.57 ± 0.34	1.48 ± 0.02	2.7 ± 0.02	4.23 ± 0.02
NB20C5R1	909 ± 34.8	21.55 ± 0.61	2.1 ± 0.01	4.0 ± 0.03	6.5 ± 0.07

Theoretical prediction of tensile strength by the Nicolais-Narkis, Knori-Geil and Turcsanyi model and experimental tensile strength values are presented in **Table 4. 11.** Theoretical values exhibit only minor deviations from the experimental results, indicating that the hybrid filler network effectively reinforces the NR matrix. The k value of the Nicolais-Narkis model is -0.94, which suggests a better reinforcement mechanism.

Table 4.11 – Experimental and theoretical prediction of tensile strength (MPa) of NR/CCB-CNT-RGO hybrid filler systems

Sample	Experimental	Nicolais-Narkis model	Knori-Geil model	Turcsanyi model
NB20C1R1	21.57 ± 0.34	21.35	20.58	21.13
NB20C5R1	21.55 ± 0.61	21.76	21.14	21.93

SEM images of the tensile fracture surface of NB20C1R1 at different magnifications are shown in **Figure 4.19(a) and (b)**. RGO sheets are visible in **Figure 4.19 (a)** which

is marked in circle. **Figure 4.19 (c) and (d)** show the FESEM images of the tensile fracture surface of NB20C5R1 at different magnifications.

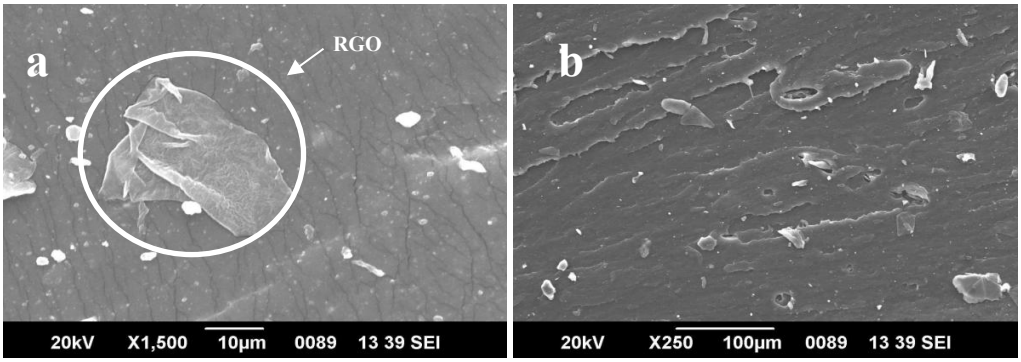

Figure 4.19-(a) and (b)-SEM images of tensile fracture surface of NB20C1R1

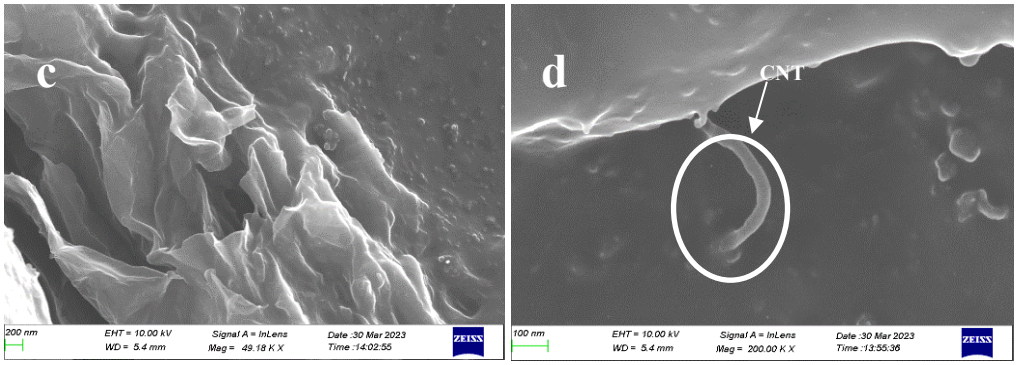

Figure 4.19-(c) and (d)-FESEM images of tensile fracture surface of NB20C5R1

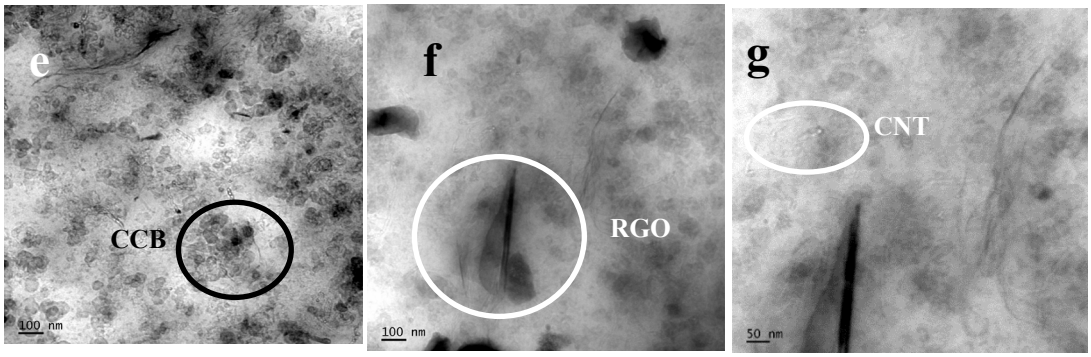

Figure 4.19 (e-g)-HRTEM images of NB20C1R1 at different magnifications

Notably, **Figure 4.19 (d)** reveals the presence of tubular CNT incorporated in the composite marked in a circle. The fracture topography appears to be influenced by the structure and reinforcing qualities of the fillers. Through morphological analysis, it has been determined that the hybrid fillers are successful in transferring stress within the matrix. The presence of surface roughness in the images suggests that the composites

have a denser crosslinking. Furthermore, the rougher section morphology corresponds to stronger mechanical properties. (33) **Figure 4.19 (e-g)** shows the TEM images of NB20C1R1 at different magnifications. CCB aggregates and CNT tubes are seen in the TEM images. The individual RGO sheets are also clearly visible at low and high magnifications.

4.3.5.2. Dynamic mechanical analysis (DMA)

Figure 4.20(a) demonstrates the variation of storage modulus with temperature from -70°C to 70°C for NB20C1R1 and NB20C5R1.

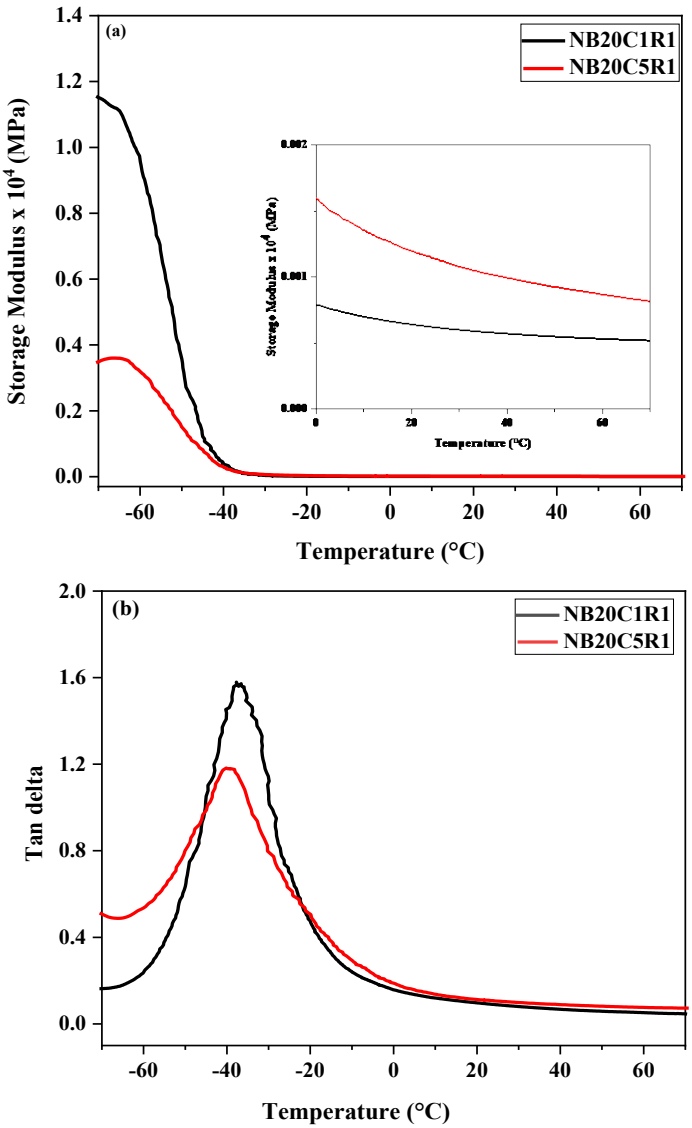

Figure 4.20 –(a) Storage modulus [Inset: Storage modulus above 0°C] and (b) Loss tangent of NR/CCB-CNT-RGO hybrid filler systems

The glassy region is characterised by higher storage modulus owing to the restricted mobility of the polymer chains. The reinforcement imparted by the hybrid fillers increased the storage modulus at temperatures above 0°C. Combination of three hybrid filler systems has created a strong and stiff interface in the NR matrix, resulting in increased storage modulus. In the glass transition region, the mobility of the polymer chains increases, leading to a significant decrease in storage modulus. The rubbery region shows minimum storage modulus. However, in the rubbery region a pronounced increase in storage modulus is observed at higher CNT loading as the percentage of CCB and RGO remains the same. Loss tangent or damping of the composites can be described as the ratio of the viscous to elastic response of a viscoelastic material. Tan δ associates with the damping due to the vibration and molecular segmental dynamics of polymer chains. Moreover, the area under the tan δ peak is directly proportional to the molecular mobility and energy dissipation ability.

Tan δ plot of the hybrid filler systems is given in **Figure 4.20 (b).** Hybrid fillers dispersed in the NR matrix restrict the polymer chain mobility and decrease the tan δ value. In the present study, NB20C5R1 has lower tan δ value and diminished area under the tan δ curve; lower tan δ signifies the higher energy storage potential and elastic response of the composites. Tan δ plot helps to identify the glass transition temperature (T_g) of the composites. T_g identified from **Figure 4.20 (b)** is -33.28 and -39.51°C for NB20C1R1 and NB20C5R1 respectively. Natural rubber is reported to have the highest damping factor because of the inherent motions of the isoprene backbone. (34) Addition of fillers can reduce the damping significantly due to the restriction in the segmental mobility. Tan δ_{max} obtained at Tg is used to locate the damping or loss factor, whichis observed at 1.48 and 1.18 for NB20C1R1 and NB20C5R1, respectively. The better dispersion and improved interfacial interactions of the hybrid filler system in polymer matrix are reflected in the DMA plots. Hybrid filler network in composites effectively restricts the segmental mobility of polymer chains through strong intermolecular interactions.

Impact of fillers on the modulus of composites can be assessed through the utilisation of the coefficient β_f, which is presented in **Table 4.12**. A lower β_f value indicates that the filler is reinforcing the NR matrix. The β_f has decreased from 0.6 to 0.1 upon increasing the concentration of CNT. This indicated that the hybrid filler system is

effectively dispersed in the rubber matrix, and interfacial interactions increased upon the addition of CNT. To better understand the role of confined polymer chains in improving the mechanical properties of NR composites, it is important to quantitatively estimate the volume fraction of the constrained region. The amount of constrained region can be determined by the decrease in the height of the tan δ peak. **Table 4.12** shows that the volume fraction of the constrained region increases in the presence of hybrid fillers, indicating the strong interfacial interaction of hybrid fillers with the rubber chain. Network formation of CCB, CNT and RGO immobilizes the polymer chains on the surface, leading to a larger constrained region. Entanglement density, N refers to the level of interaction and interlocking between polymer chains and are presented in **Table 4.12.** Computed N suggests the strong interfacial interaction with hybrid fillers and NR matrix. Degree of entanglement depends on the characteristics of the polymer matrix and the filler materials. Higher N value signifies a greater extent of entanglement between the NR chains and the filler system. Ternary filler system in NR matrix is effective in improving interfacial interaction as a result of immobilisation of more NR chains on the surfaces of CCB and CNT particles. The spherical surface of CCB and high aspect ratio of CNT allows more surface interaction with NR chains. The layered structure of RGO also facilitates interaction with NR chains. Another parameter to understand the filler-rubber interaction from storage modulus data is the reinforcing efficiency. **Table 4.12** presents the calculated values of reinforcing efficiency, r for the fillers used in the composites and obvious increase is obtained for NB20C5R1 than NB20C1R1. Reinforcing efficiency of fillers refers to their ability to improve the mechanical properties of the composite, and it depends on various factors, such as their shape, size, surface area, and interfacial interaction with the rubber matrix. It is proportional to its modulus relative to that of the rubber matrix (i.e., E_c/E_m). From the equation, it is clear that as the modulus of the filler increases, the reinforcing efficiency also increases and vice versa. The obtained DMA data indicates that several parameters, such as the effectiveness of the filler, the volume fraction of the constrained region, the degree of entanglement, and the reinforcing efficiency, support the fact that the hybrid filler network effectively enhances the interfacial interaction and reinforces the natural rubber matrix.

Table 4.12-Various theoretical parameters from DMA analysis

Sample	β_f	N (mol/dm^3)	C	r
NB20C1R1	0.60	0.40 x10^{-2}	2.92 x10^{-2}	7.35
NB20C5R1	0.10	0.93 x10^{-2}	7.12 x10^{-2}	18.06

4.4. Comparative analysis of properties

Table 4.13 presents the comparison of mechanical properties of NR incorporated with various filler systems.

Table 4.13-Comparative analysis of mechanical properties of NR hybrid filler systems

Sample	Elongation at break (%)	Tensile strength (MPa)	Modulus at 100% (MPa)	Modulus at 300%(MPa)
NB0	1184 ±22	17.1 ±0.9	0.9 ±0.01	2.0±0.00
NB20	893 ±25	26.3 ±0.9	1.6 ±0.02	4.5 ±0.08
NB20C1	699 ±7	24.0 ±0.1	2.2 ±0.06	6.6±0.24
NB20C5	561 ±33	21.3 ± 0.5	3.1 ±0.06	9.7±0.04
NB20IL1	886 ± 29	15.92 ± 0.08	1.19 ± 0.1	3.17 ± 0.24
NB20C3IL3	642 ± 41	11.7 ± 0.68	1.558 ± 0.02	4.54 ± 0.02
NB20C5R1	909 ± 34.8	21.55 ± 0.61	2.1 ± 0.01	6.5 ± 0.07

Introduction of a hybrid filler system has increased the tensile strength of NR matrix. The tensile strength of unfilled NR is 17 MPa, while CCB filler alone could increase the tensile strength to 53%. Modulus at 300% elongation is increased significantly from 4.5 to 9.7 MPa when 5 phr CNT is added to NB20. Ionic liquid modification has a detrimental effect on the tensile strength of the NR matrix. The ILCCB is effective in reinforcing NR than ILCNT-CCB filler system. The average tensile strength of CCB-CNT-RGO filler composites is 21.5 MPa which is approximately 27% higher than that of unfilled NR. Incorporation of carbon and boron nitride nanotubes as reinforcements in NR reports an 11.07% and 8.01% increase in the tensile strength respectively. (35) Elongation at break (%) is higher for NB20C5R1 than all other filler composites.

Table 4.14 presents the storage modulus of NR hybrid filler systems at 25°C. DMA analysis provides insights into the viscoelastic behaviour of the composites. The storage modulus of NB20 is measured at 7.07 MPa. Previous studies on vulcanised

NR incorporating 20 phr of CB report a storage modulus of approximately 5 MPa at 25°C. (36) Also, the room temperature storage modulus of NR filled with 15 phr of multi-walled carbon nanotubes alone is reported to reach only 6.11 MPa, which is 600% higher than unfilled NR. (37) In our study, a combination of 20phr CCB and 5 phr CNT could achieve a 1543% increase in storage modulus than unfilled NR. NB20C5 composite exhibits highest modulus than IL modified composites. Storage modulus of all hybrid filler reinforced composites is higher than unfilled NR at room temperature. IL modified fillers could achieve only a 478% and 473% increase in storage modulus for NR/ILCCB and NR/CCB-ILCNT systems respectively.

Table 4.14-Comparative analysis of storage modulus of NR hybrid filler systems at 25°C

Sample	Storage modulus (MPa)
NB0	1.99
NB20	7.07
NB20C5	32.7
NB20IL3	11.5
NB20C5IL3	26.5
NB20C5R1	11.4

4.5. Conclusion

Present chapter discusses the mechanical, morphological and dynamic mechanical properties of NR hybrid filler systems. The enhanced tensile strength and tensile modulus confirmed the reinforcement effect of CCB in the NR matrix. Ionic liquid modification of fillers has shown improvements in modulus at various strains. The role of ionic liquid in preventing CNT and CCB agglomeration has resulted in homogeneous dispersion of fillers in NR. Morphological analysis of the tensile fracture surface supports the same. The combination of CCB, CNT and RGO synergistically enhances the properties in the NR matrix.

4.6. References

1. Alshangiti DM. Impact of a nanomixture of carbon black and clay on the mechanical properties of a series of irradiated natural rubber/butyl rubber blend. E-Polymers. 2021;21(1):662–70.
2. Guth E. Theory of filler reinforcement. Journal of Applied Physics. 1945;16(1):20–5.
3. Tripathi D, Dey TK. Effect of particle size distribution on thermo-mechanical properties of NiO filled LDPE composites. Bulletin of Materials Science. 2019;42(4).

4. E. H. Kerner. The elastic and thermo-elastic properties of composite media. Proceedings of the Physical Society Section B. 1956;69:808–13.
5. Mott PH, Roland CM. Limits to Poisson's ratio in isotropic materials. Physical Review B - Condensed Matter and Materials Physics. 2009;80(13):1–4.
6. Nicolais L, Narkis M. Stress-strain behavior of styrene-acrylonitrile/glass bead composites in the glassy region. Polymer Engineering & Science. 1971;11(3):194–9.
7. Valiya Parambath S, Ponnamma D, Sadasivuni KK, Thomas S, Stephen R. Effect of nanostructured polyhedral oligomeric silsesquioxane on the physical properties of poly(vinyl alcohol). Journal of Applied Polymer Science. 2017;134(43):1–10.
8. Kunori T, Geil PH. Morphology-Property Relationships in Polycarbonate-Based Blends. II. Tensile and Impact Strength. Journal of Macromolecular Science, Part B. 1980;18(1):135–75.
9. Turcsányi B, Pukánszky B, Tüdõs F. Composition dependence of tensile yield stress in filled polymers. Journal of Materials Science Letters. 1988 Feb 1;7(2):160–2.
10. Bindu P, Thomas S. Viscoelastic behavior and reinforcement mechanism in rubber nanocomposites in the vicinity of spherical nanoparticles. Journal of Physical Chemistry B. 2013;117(41):12632–48.
11. Joy J, George E, Thomas S, Anas S. Effect of filler loading on polymer chain confinement and thermomechanical properties of epoxy/boron nitride (h-BN) nanocomposites. New Journal of Chemistry. 2020;44(11):4494–503.
12. Rasana N, Jayanarayanan K, Deeraj BDS, Joseph K. The thermal degradation and dynamic mechanical properties modeling of MWCNT/glass fiber multiscale filler reinforced polypropylene composites. Composites Science and Technology. 2019 Jan;169:249–59.
13. Omnès B, Thuillier S, Pilvin P, Grohens Y, Gillet S. Effective properties of carbon black filled natural rubber: Experiments and modeling. Composites Part A: Applied Science and Manufacturing. 2008;39(7):1141–9.
14. Oliveira FA, Alves N, Giacometti JA, Constantino CJL, Mattoso LHC, Balan AMOA, et al. Study of the thermomechanical and electrical properties of conducting composites containing natural rubber and carbon black. Journal of Applied Polymer Science. 2007;106(file:///E:/Work Data/aa NR_CCB_CNT/references ccb cnt/natarajan2017.pdf):1001–6.
15. Zhu L, Tian X, Pan Y, Chang T, Wang K, Niu G, et al. Optimization of Serial Modular Continuous Mixing Process Parameters for Natural Rubber Composites Reinforced by Silica/Carbon Black. Polymers. 2020 Feb 11;12(2):416.
16. Litvinov VM, Steeman PAM. EPDM-carbon black interactions and the reinforcement mechanisms, as studied by low-resolution1H NMR. Macromolecules. 1999;32(25):8476–90.
17. Payne AR. The dynamic properties of carbon black loaded natural rubber vulcanizates. Part II. Journal of Applied Polymer Science. 1962 May 1;6(21):368–72.
18. Fan Y, Fowler GD, Zhao M. The past, present and future of carbon black as a rubber reinforcing filler – A review. Journal of Cleaner Production. 2020 Feb;247:119115.
19. MEDALIA AI, KRAUS G. 8 -Reinforcement of Elastomers by Particulate Fillers. In: Mark JE, Erman B, Eirich FR, editors. Science and Technology of Rubber (Second Edition) [Internet]. San Diego: Academic Press; 1994. p. 387–418. Available from: https://www.sciencedirect.com/science/article/pii/B9780080516677500135
20. Dannenberg E. Molecular slippage mechanism of reinforcement. Trans Inst Rubber Ind. 1966;42:26–32.
21. Liu Y, Li L, Wang Q, Zhang X. Fracture properties of natural rubber filled with hybrid carbon black/nanoclay. Journal of Polymer Research. 2011;18(file:///E:/Work Data/aa NR_CCB_CNT/references ccb cnt/natarajan2017.pdf):859–67.
22. Albano C, Perera R, Cataño L, Karam A, González G. Prediction of mechanical properties of composites of HDPE/HA/EAA. Journal of the Mechanical Behavior of Biomedical Materials. 2011;4(3):467–75.
23. Zare Y. Development of Nicolais–Narkis model for yield strength of polymer nanocomposites reinforced with spherical nanoparticles. International Journal of Adhesion and Adhesives. 2016;70:191–5.
24. Al-Hartomy OA, Al-Solamy F, Al-Ghamdi A, Dishovsky N, Ivanov M, Mihaylov M, et al. Influence of carbon black structure and specific surface area on the mechanical and dielectric properties of filled rubber composites. International Journal of Polymer Science. 2011;2011.

25. Roy K, Chandra Debnath S, Das A, Heinrich G, Potiyaraj P. Exploring the synergistic effect of short jute fiber and nanoclay on the mechanical, dynamic mechanical and thermal properties of natural rubber composites. Polymer Testing. 2018;67:487–93.
26. Asha AB, Vijayan P P, Thomas S, Parameswaranpillai J, Puglia D, Siengchin S, et al. Fabrication of water-resistant epoxy nanocomposite with improved dynamic mechanical properties and balanced thermal and dimensional stability: Study on dual role of graphene oxide nanosheets and barium oxide microparticles. Colloids and Surfaces A: Physicochemical and Engineering Aspects. 2021;617(March):126405.
27. Stephen R, Raju KVSN, Nair SV, Varghese S, Oommen Z, Thomas S. Mechanical and viscoelastic behavior of natural rubber and carboxylated styrene-butadiene rubber latex blends. Journal of Applied Polymer Science. 2003;88(11):2639–48.
28. Stephen R, Thomas S, Raju KVSN, Varghese S, Joseph K, Oommen Z. Dynamic mechanical and dielectric properties of nanocomposites of natural rubber (NR), carboxylated styrene butadiene rubber (XSBR) latices and their blends. Rubber Chemistry and Technology. 2007;80(4):672–89.
29. Le HH, Wießner S, Das A, Fischer D, Auf Der Landwehr M, Do QK, et al. Selective wetting of carbon nanotubes in rubber compounds -Effect of the ionic liquid as dispersing and coupling agent. European Polymer Journal. 2016;75:13–24.
30. Liang JZ. Reinforcement and quantitative description of inorganic particulate-filled polymer composites. Composites Part B: Engineering. 2013 Aug 1;51:224–32.
31. Abraham J, P. MA, Kailas L, Kalarikkal N, George SC, Thomas S. Developing highly conducting and mechanically durable styrene butadiene rubber composites with tailored microstructural properties by a green approach using ionic liquid modified MWCNTs. RSC Adv. 2016;6(39):32493–504.
32. Alshangiti DM. Impact of a nanomixture of carbon black and clay on the mechanical properties of a series of irradiated natural rubber/butyl rubber blend. E-Polymers. 2021;21(1):662–70.
33. Pandey KN, Setua D, Mathur GN. Material behaviour: Fracture topography of rubber surfaces: An SEM study. Polymer Testing. 2003 May 1;22:353–9.
34. James, C.G. and Ronald, A.L. New York: CRCPress Taylor & Francis Group, 2012. Engineering Designwith Polymers and Composites.
35. Cui J, Zeng F, Yuan B. A comparative study on the interfacial characteristics and tensile behaviors of natural rubber composites reinforced by carbon and boron nitride nanotubes. Polymer Composites. 2022 Sep 1;43(9):6624–36.
36. Bandyopadhyaya S, Kitey R, Upadhyay CS. The Effect of Carbon Black Content on Viscoelastic Properties of Vulcanized Natural Rubber. In: ICEM 2022 [Internet]. MDPI; 2022 [cited 2023 Nov 4]. p. 9. Available from: https://www.mdpi.com/2673-9984/4/1/9
37. Medupin RO, Abubakre OK, Abdulkareem AS, Muriana RA, Abdulrahman AS. Carbon Nanotube Reinforced Natural Rubber Nanocomposite for Anthropomorphic Prosthetic Foot Purpose. Scientific Reports. 2019 Dec 27;9(1):20146.

Chapter 5

Dielectric and EMI Shielding Properties of NR Hybrid Filler Systems

Summary

This chapter focuses on the dielectric properties, electromagnetic interference (EMI) shielding effectiveness, and DC conductivity of the natural rubber (NR) hybrid filler systems. These properties are evaluated in terms of the homogeneous dispersion of fillers, as well as the physicochemical interfacial interactions established between the fillers and the polymer matrix. Moreover, the role of ionic liquids as potential modifiers in enhancing the dielectric and conductive properties of the hybrid filler systems is discussed. Also, AC conductivity data obtained from the dielectric investigations is analysed through the framework of Jonscher's Universal Power Law. NR/CCB-CNT-RGO hybrid filler systems exhibit the highest EMI SE of 33.8 dB in the 9-10 GHz frequency range. Ionic liquid modified CNT imparts conductivity to the NR with high conductivity in 10-3. NR composites fabricated are suitable for commercial EMI shielding applications.

A part of this chapter is published in the Journal of Applied Polymer Science. Vol. 139., No.47., Pages e53197, 2022. https://doi.org/10.1002/app.53197

5.1. Introduction

Dielectric permittivity of NR composites refers to the ability of the material to store electrical energy when subjected to an electric field. It characterises the polarisation response of the material. Electromagnetic interference (EMI) shielding property refers to the effectiveness of a material or structure in attenuating or blocking electromagnetic (EM) radiation and preventing its interference with electronic devices or systems. NR composites integrated with conductive fillers can exhibit enhanced DC conductivity. DC conductivity of NR composites is significantly influenced by the filler characteristics such as nature, amount, and dispersion of conductive fillers within the rubber matrix.

5.1.1. Theoretical models for dielectric studies

Dielectric permittivity obtained from the impedance analyser can be used to calculate the AC conductivity of the NR composites. The AC conductivity data is fitted with Jonsher Universal Power Law(1) by the least square method.

$$\sigma(\omega) = \sigma_{DC} + A\omega^{s} \tag{5.1}$$

where σ(ω) is the measured frequency dependent AC conductivity. The equation takes into account the frequency-dependent behaviour of the conductivity, σ_{DC} representing the frequency-independent DC observed in the initial plateau region. The constant A reflects polarizability and is temperature-dependent, while ω represents the angular frequency and s is the exponent. The exponent value 1 corresponds to an ideal Debye dielectric dipolar type, while 0 represents an ideal ionic type crystal (2).

5.2. Results and discussion

5.2.1. NR/CCB systems

Impedance analysers measure the frequency dependence of electrical properties, offering insight into the electrical relaxation behaviour of conducting elastomers. Frequency dependence of the dielectric constant (ε', real part of dielectric permittivity) with the CCB loading in NR is given in **Figure 5.1(a)**. Dielectric permittivity of NR increases with the increase in the percentage of CCB. Dielectric permittivity at 100 Hz is 4.01 for unfilled NR and 46.3 for 20 phr of CCB incorporated NR. Moreover, at 1000 Hz, the dielectric constant values are 3.93 and 43, respectively, for NB0 and NB20.

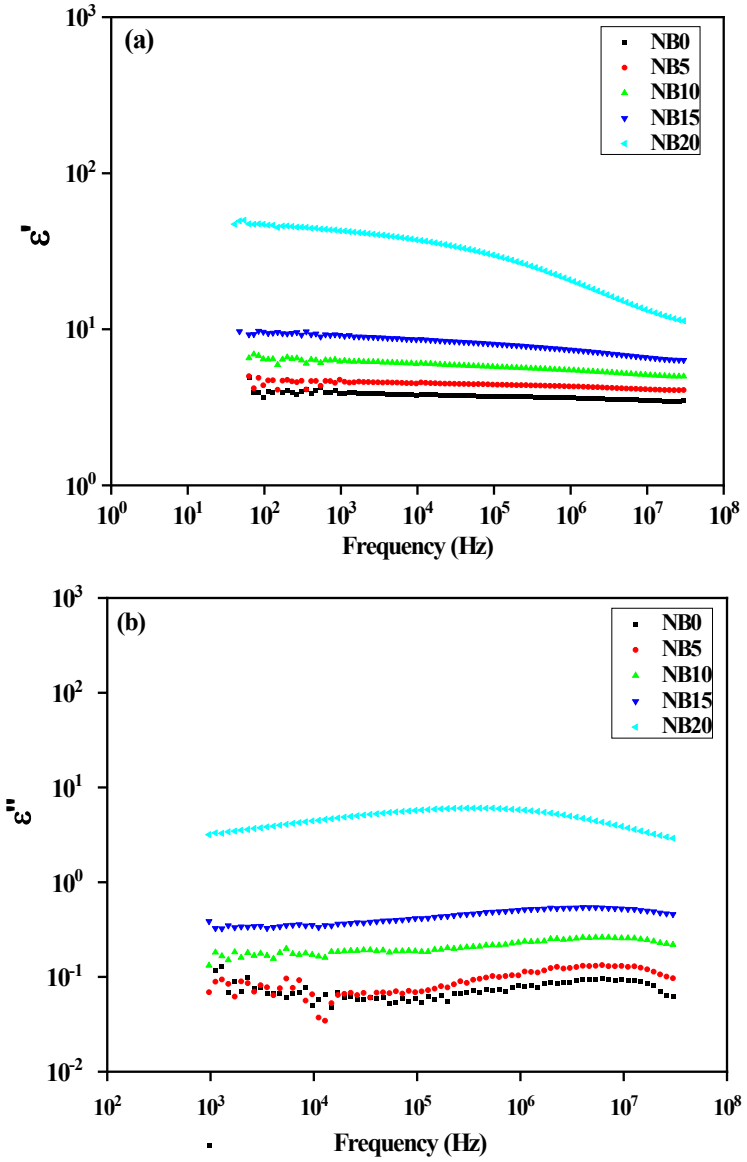

Figure 5.1-Frequency dependent (a) dielectric permittivity and (b) dielectric loss of NR/CCB systems

In NR composites, the dielectric permittivity typically depends on factors such as filler loading, filler type, the applied external electric field frequency, and temperature. As the filler loading increases, the dielectric permittivity of the composites generally increases due to enhanced polarization effects. Different types of polarizations can contribute to dielectric permittivity, including electronic, atomic, dipolar or orientational, and interfacial polarizations. (3,4) Electronic polarization occurs due to the displacement of electrons within the material when an external electric field is

applied. This kind of polarization is rapid and usually occurs at very high frequencies. Atomic polarization arises from the relative displacement between positive and negative ions in the material. When an electric field is applied, the ionic cores move, leading to a rearrangement, which, in turn, leads to this type of polarization. (4,5) Atomic polarization is fast, and it happens at somewhat lower frequencies than electronic polarization. Meanwhile, dipolar or orientation polarization arises from the alignment of permanent dipoles within the composites. In an external electric field, the polar molecules tend to align themselves with the field, resulting in orientation polarization. This process is slower and generally occurs at even lower frequencies. Space charge polarization or interfacial polarization is also known as Maxwell-Wagner Sillar (MWS) polarization and is prominent in composite or heterogeneous materials where there are interfaces or boundaries between two distinct materials or phases. When an external electric field is applied, charges accumulate at these interfaces, leading to polarization. (6) Interfacial polarizations have the longest response time. (7) Interfacial and orientation polarizations are also affected by the filler concentrations and distributions in composites. As filler concentration varies, it can alter the number of interfaces and their distribution or the volume of polar domains, which in turn can affect the overall dielectric response of the composite material. The response time for interfacial and dipolar polarization is longer compared to atomic and electronic polarizations. This makes them more significant in enhancing the dielectric constant under real-world application conditions. (8) The surface modifications on the filler particles make the orientational and interfacial polarizations relevant in NR hybrid filler composite systems. (9) Hence, by adjusting the filler concentrations, one can potentially tailor the dielectric properties of the composite to specific requirements.

Stockmayer (10) has identified dipoles and their relaxation behaviour in cis-polyisoprene based on vibration orientations. Normal mode relaxation or β relaxation corresponding to the parallel dipoles to the long chain is observed at low frequency owing to its longer time scale. Segmental mode relaxation or α relaxation related to the movement of local segments is observed at high frequency because of the shorter time scale. Broadened or shifted α relaxation peaks in filled composites may be associated with a change in glass transition temperature (11).

The dielectric constant directly depends on the polarizability of the material. The nature of interactions between rubber chains and CCB filler is still discussed and debated widely. The nature of interactions is found to be mainly physical. However, the mixing and curing of rubber chains with carbon black fillers can also introduce some covalent bonds. The surface area, aggregate structure and surface chemistry of carbon black affect the interfacial interactions with polymer chains (12).

Increased ε' suggests the increased conductivity of the composite. The increase in ε' of NB20 suggests the establishment of a continuous conduction pathway in the rubber matrix. At a lower percentage of filler, the aggregate distance is large, and as the distance decreases, polarizations like Maxwell-Wagner-Sillar polarizations come into play (13). Dielectric permittivity gradually decreases as the frequency is increased; the effect is prominent for NB20. Dielectric relaxation of orientation polarization explains the variation of dielectric permittivity at a higher frequency. At higher frequencies, the dipoles are out of phase while they are oriented in the alternating electric field, leading to a decrease in dielectric permittivity. The returning of dipoles to original random orientation take time more than the oscillating electric field, which result in energy absorption and dissipation as heat (14). In **Figure 5.1(b)**, the variation of dielectric loss (ε″, the imaginary part of dielectric permittivity) of NR/CCB systems with frequency across different filler loadings is depicted. The data clearly demonstrates that dielectric loss amplifies with an increase in filler loading, irrespective of the frequency. This enhancement in loss, especially at higher CCB loadings, points to a rise in the conversion of electrical energy to thermal energy, as indicated by the amplified dielectric loss (15). NB20 offers a superior balance with high dielectric constant and moderate dielectric loss. For capacitor applications, where a balance between high dielectric constant and minimal dielectric loss is essential, NB20 is preferable. **Figure 5.2 (a) & (b)** shows the frequency dependence of the real part of impedance (Z′) and imaginary part of impedance (Z″) of different filler loadings. Regardless of filler loading, Z′ gradually decreases with increasing frequency and levels off at higher frequency. However, for higher filler loading, Z′ is decreased and levelled off at a lower frequency. At lower frequencies, Z′ increases up to 10 phr and then starts decreasing for higher loading. Impedance is not frequency dependent at 25 phr filler loading. Impedance signifies the resistive part of the system in an AC circuit.

Impedance analysis shows that the system exhibits higher conductivity at high CCB loading. The imaginary part Z″ indicates the reactance, which is the resistance to the flow of current due to the capacitive or inductive nature of the NR/CCB composite, which is found to be lower at a higher percentage of CCB. At higher frequencies, it is independent of the filler loading. This is because of the electron hopping mode of conduction, which is more significant at higher frequencies.

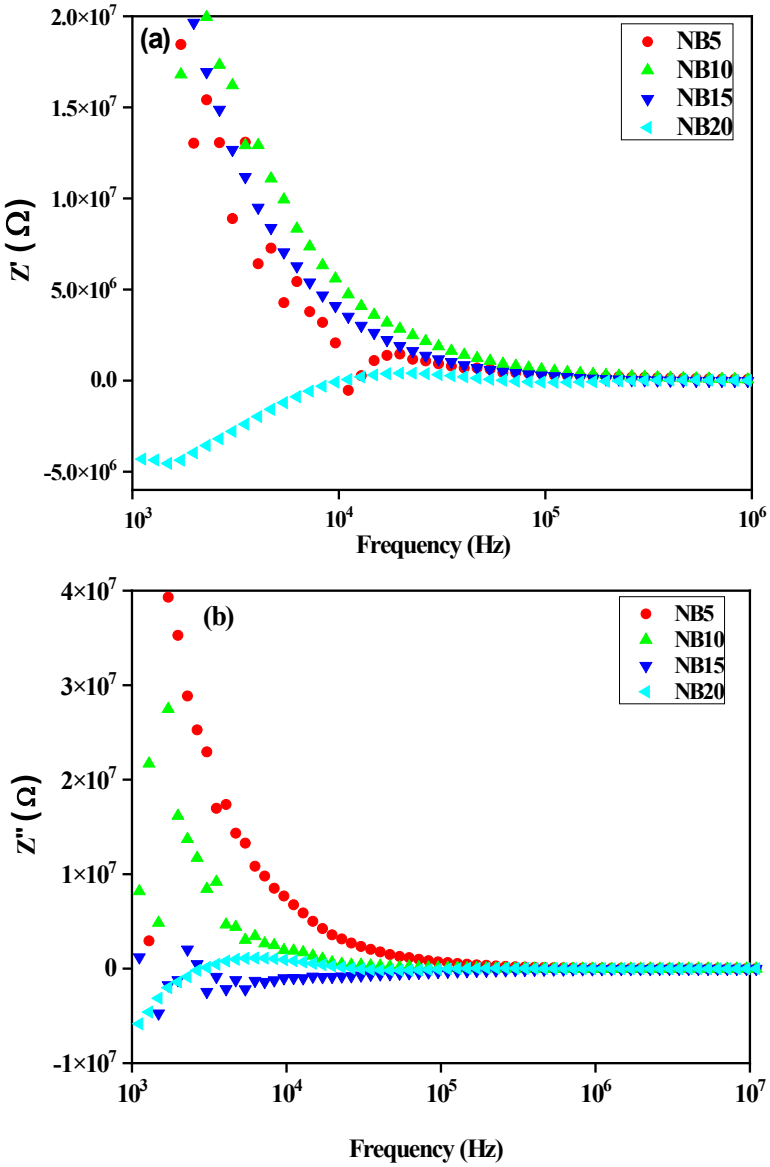

Figure 5.2-Frequency dependence of a) real part of impedance (Z′) and (b) imaginary part of impedance (Z″) of NR/CCB systems

Relaxation phenomena depend on the chemical crosslinks present in the viscoelastic NR as well as the physico-chemical interaction between NR and CCB. Crosslinking of polymers results in intermolecular chain restraint, which has a decisive role in the segmental dynamics of the polymeric matrix in composites (16). Conductive fillers like CCB can impart hydrodynamic interactions and complex physical and chemical interactions between solid filler surface and polymer matrix (17).

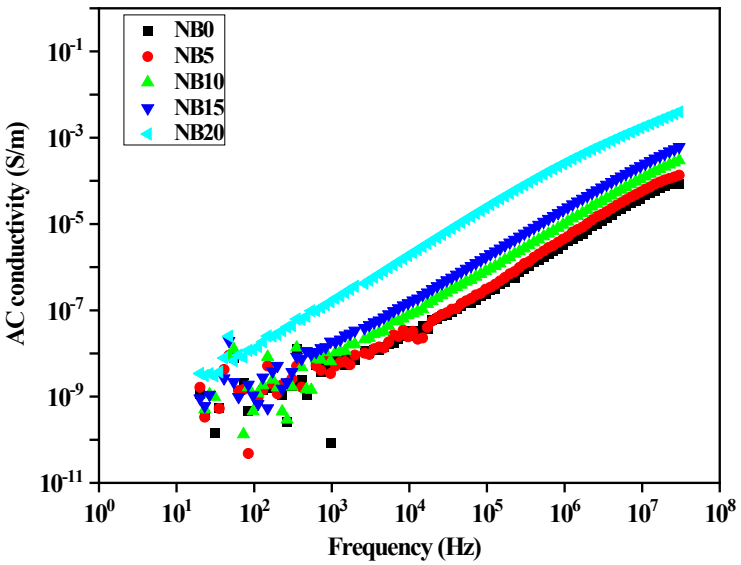

Figure 5.3-AC conductivity of NR/CCB systems

Figure 5.3 shows the deviation of AC conductivity with increasing frequency at various filler loadings of CCB in NR. AC conductivity of all composites increases with frequency, and maximum conductivity is observed for the 20 phr CCB system. AC conductivity gradually increases for NR/CCB systems up to 15 phr CCB, and a remarkable improvement in conductivity is obtained at 20 phr. The formation of a continuous conductive filler pathway in a polymer matrix causes a dramatic increase in conductivity for 20 phr filler loading. The experimental data was analysed using the Jonsher Universal Power law through the least squares method. This power law aligns well with the experimental observations, and the computed exponent values are tabulated in **Table 5.1**. Exponent values that fall between 0 and 1 suggest a hopping mode of conduction. (18) **Figure 5.4** shows the schematic representation of the conductive network formation of CCB aggregates in the NR matrix. Frequency dependent AC conductivity is due to the dipolar orientations and Maxwell-Wagner-

Sillar polarizations at the filler matrix interface. In addition to the interfacial interactions, the AC conductivity of composites also depends on several other factors: the conductivity of filler, dimension, nature, and orientation of filler in the polymer matrix.

Table 5.1- Frequency exponent of NR/CCB systems

Sample	s
NB0	0.92
NB5	0.93
NB10	0.98
NB15	0.94
NB20	0.77

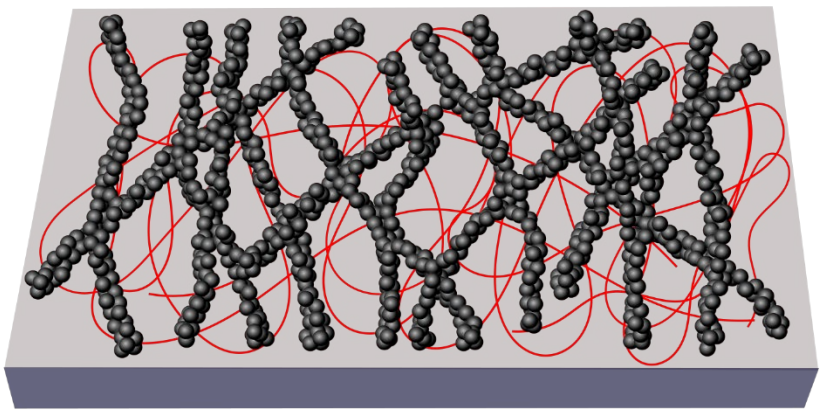

Figure 5.4-Schematic representation of conductive network formation of CCB aggregates in NR

Investigation of EMI shielding in composites is conducted in the frequency range of GHz, which aligns with the frequency requirements of commercial EM shielding devices. These shielding factors are commonly expressed in terms of shielding effectiveness (SE). Most EM radiation falling on the shielding material is either reflected or absorbed by the material. (19) Shielding by reflection is contributed by the surface reflection (SE_R) from free charge carriers in the system and by multiple reflections (SE_M) from the adjacent conducting layers. Shielding by reflection primarily occurs at the initial interface between the air and the shielding material. When EM radiation passes through the thickness of the material, absorption takes place. The absorbed EM waves within the shielding material are converted into heat.

This absorption process involves the dissipation of energy through ohmic losses in induced currents, losses associated with magnetic or dielectric polarizations, and hysteresis losses. Consequently, heat is generated within the composite material. The EM wave reflected from the second interface travels back to the first interface, leading to the occurrence of multiple reflections. These reflections can further contribute to the overall shielding effectiveness of the material. (20)

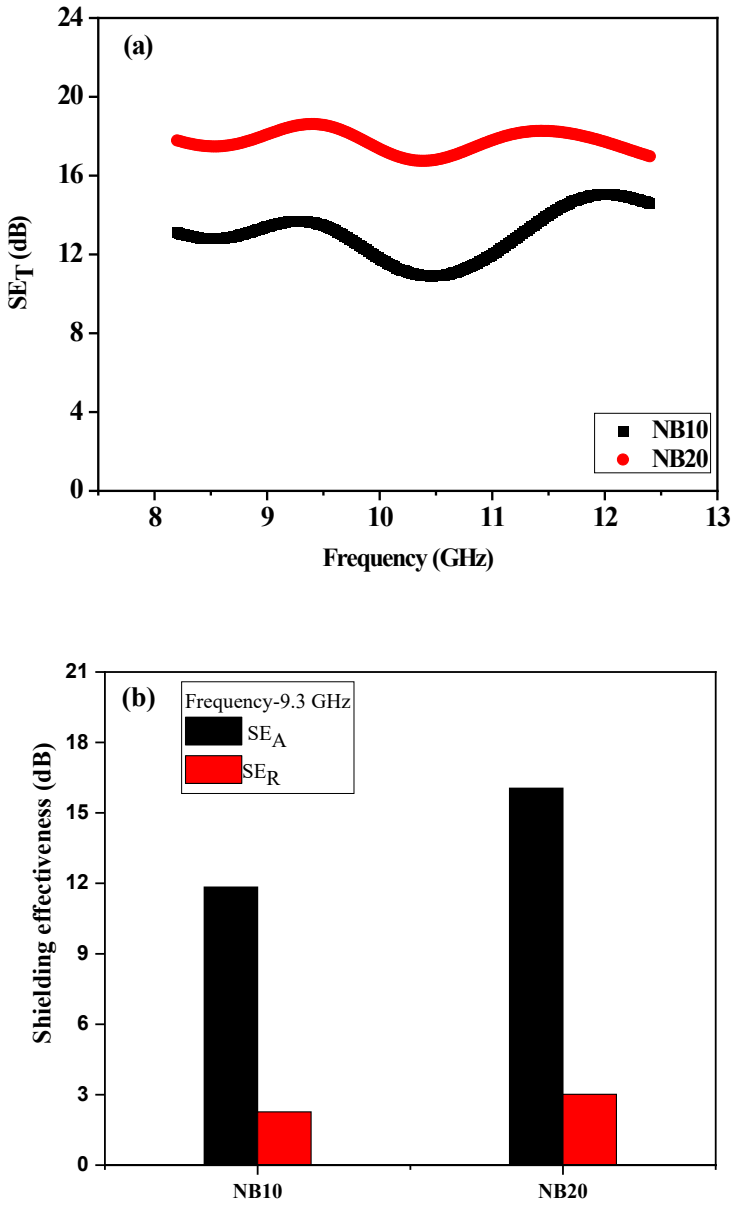

Figure 5.5-(a) SE_T and (b) SE_A and SE_R of NR/CCB systems

Additionally, the presence of a hybrid filler in the polymer matrix can create multiple interfaces within the composite material. This enhanced interface structure can improve the EMI shielding effectiveness of the material. When the EM wave interacts with a dielectric material, it induces dipole, ionic, electronic, and /or space charge polarizations within the material that align with the applied electric field. (21) **Figure 5.5 (a)** presents the plot of total shielding effectiveness (SE_T) against frequency for NR/CCB filled systems. The total shielding effectiveness increases with respect to CCB loading. At 9.3 GHz frequency, the values obtained for NB10 and NB20 are 14 and 19, respectively. This is lower than the commercial requirement for EMI shielding devices. The conductive filler network of CCB imparts some degree of EMI shielding property. The contribution of absorption and reflection in shielding of EMI is understood from **Figure 5.5 (b)**. The SE_A values are higher than SE_R for all composites, suggesting that most of the EM radiations are absorbed by the composite material.

DC conductivity of the NR/CCB systems with varying CCB content is given in **Table 5.2.** A higher DC conductivity can be correlated with greater reflection of EM radiation and, thereby enhancing the EMI SE. Formation of conductive network in polymer matrix due to the enhanced filler dispersion can improve the EMI SE. Also, the formation of conductive pathways can decrease the dielectric constant at low frequencies. As the CCB concentration increases, DC conductivity also increases. An increase in the conductivity of composites at higher concentration indicates the development of conductive network by the aggregates of CCB. Classical percolation theory (22) is applied to the DC conductivity data to estimate the electrical percolation threshold value of the NR/CCB systems. The scaling or power law equation is given by,

$$\sigma = \sigma_o(\varphi - \varphi_C)^t \tag{5.2}$$

where σ is the conductivity of the composite, φ is the volume fraction of the filler, φ_C is the electrical percolation threshold value and t is the critical exponent. The best linear fit of power law on the electrical data is given in **Figure 5.6.** The percolation threshold of CCB is 0.154 volume fraction and critical exponent is 5.4. The low percolation threshold value of CCB suggests the formation of continuous conductive network in the NR matrix.

Table 5.2-DC conductivity values of the NR/CCB systems

Sample	Conductivity (S/m)
NB10	2.00 x10^{-9}
NB15	1.62 x10^{-8}
NB20	4.01 x10^{-8}

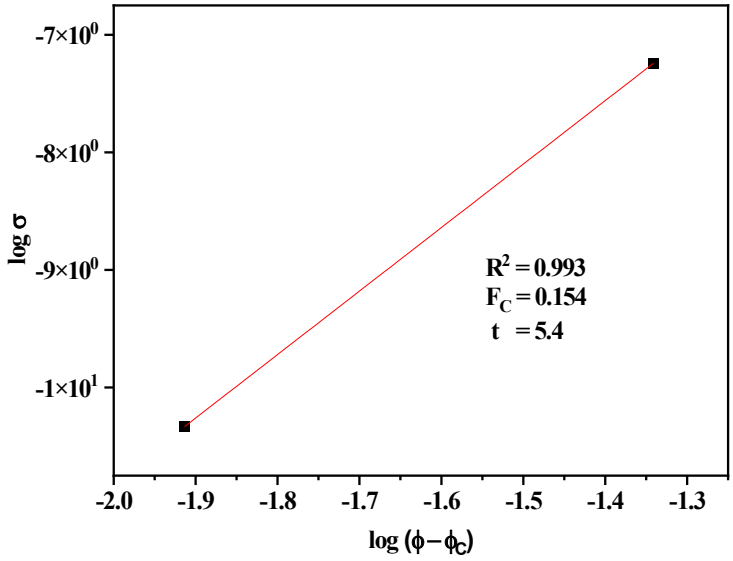

Figure 5.6-Best fit curve of power law of NR/CCB systems

5.2.2. NR/CCB-CNT hybrid filler systems

Figure 5.7 presents the frequency dependence of dielectric permittivity in relation to the CCB-CNT filler loading in NR. CCB-CNT hybrid filler systems enhance the dielectric permittivity of NR. Dielectric permittivity increases with filler loading as CNT loading increases from 0.5 phr to 1 phr, which is typical of conductive filler incorporated polymer composites. Increased permittivity is attributed to interfacial polarizations at heterogeneous phases with different electric conductivities. (23) Apart from MWS polarizations, space charge polarizations also play a role in enhancing dielectric constant. At low concentration of fillers, the isolated conducting fillers in insulated matrix results in low electron polarization due to the low chance of separation of charges. Meanwhile, at higher filler concentrations, electrons tunnel through the adjacent conducting fillers and lead to the separation of charges. This, in turn, increases the polarizations and results in a high dielectric constant. There is a remarkable increase in permittivity, which reaches a value of 1801 at low frequency for 1 phr

CNT. Below 10^4 Hz, the dielectric permittivity of NB20C3 and NB20C5 is lower than NB20C1, which is 998 and 1340, respectively. At higher filler loading, a higher concentration of conductive filler can cause the formation of the continuous conductive network in the NR matrix. This allows the continuous migration of electrons, leading to the lower dielectric constant. However, as the frequency increases, the contribution of dielectric polarizations to the dielectric constant decreases for NB20C1, resulting in decreased dielectric constant than NB20C3 and NB20C5. (24) As the frequency increases, the dielectric permittivity shows a steady increase with filler loading. As the frequency gradually increases, the dielectric constant decreases for the NR composites due to the lower contribution of interfacial polarizations. The observed enhancement in dielectric permittivity is attributed to the polarization mechanisms within the elastomer matrices filled with conductive material. Factors influencing the dielectric permittivity in these elastomers are (a) the intrinsic dielectric properties of both the polymer matrix and the filler, (b) the micro-capacitors formed within the matrix, and (c) the polarizations at the interfaces. Variation of ε″ of NR/CCB-CNT systems with frequency at different filler loadings is given in **Figure 5.7(b)**. Dielectric loss is the measure of electrical energy loss as thermal energy in the conduction pathways of hybrid filler systems. Dielectric loss increases with filler loading and decreases with frequency for NB20C0.5 and NB20C1. For composites with 3 and 5 phr CNT loading, dielectric loss shows different behaviour. It reduces with frequency and increases at a higher frequencies. Dielectric loss of NB20C3 and NB20C5 lowers even below NB20C1 between 10^3 and 10^6 Hz. NB20C3 and NB20C5 possess high dielectric permittivity and lower dielectric loss. Leakage currents within the conductive pathways of the composites explain the dielectric loss and the AC conductivity. The hybrid filler system introduces heterogeneity into the composites, leading to many filler-polymer interfaces with varying permittivity. This heterogeneity results in Maxwell-Wagner Sillar polarizations at lower frequencies, causing an increase in dielectric permittivity. The accumulation of free charges at these interfaces leads to interfacial polarizations, which account for the high dielectric permittivity observed at lower frequencies, which decreases with frequency. At higher frequencies the dipoles are unable to orient themselves according to the oscillating electric field. The time taken by the oscillating

dipoles to return to its original orientation is larger than that of alternating electric field. Thus, due to the dielectric relaxation of orientation polarization, an oscillating electric field cannot influence dipole rotation at higher frequencies. Here, the energy absorbed is dissipated as heat.

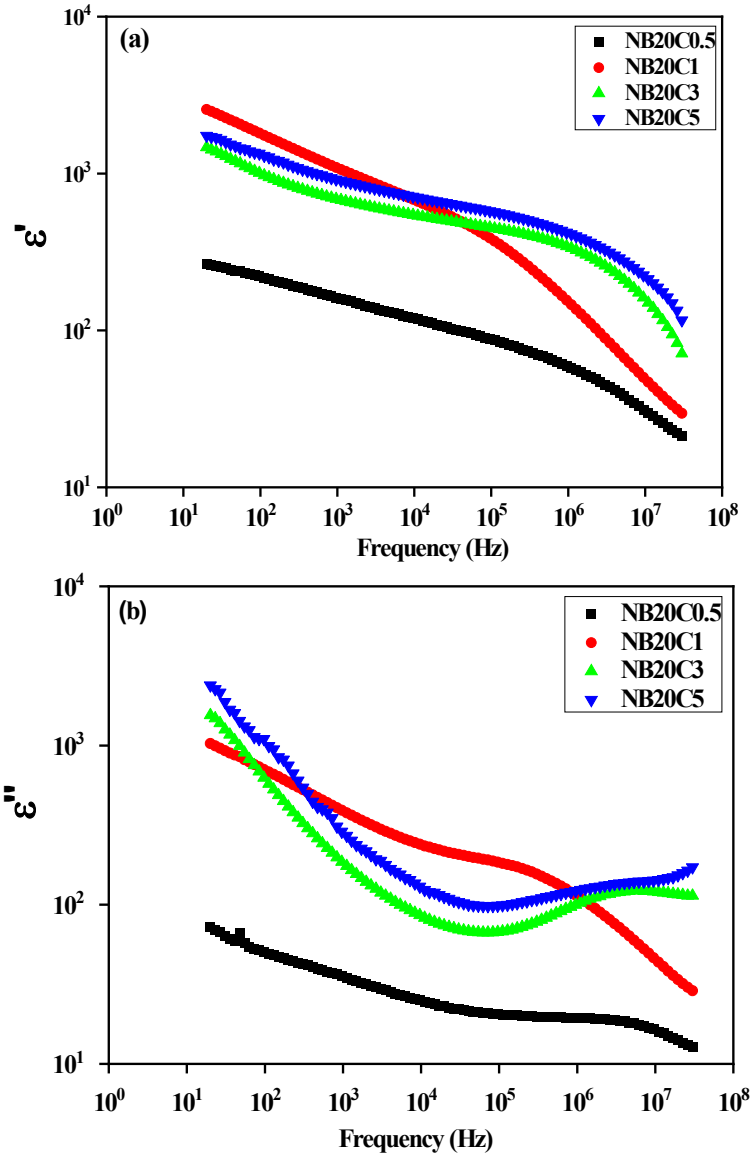

Figure 5.7-Frequency dependent (a) dielectric permittivity and (b) dielectric loss of NR/CCB-CNT hybrid filler systems

Frequency dependence of the real part of impedance (Z′) and the imaginary part of impedance (Z″) of different filler loadings are depicted in **Figure 5.8(a & b**. At lower frequencies real part impedance of NB20C3 and NB20C5 hybrid filler systems shows a marginal increase than NB20C1. However, impedance lowers as frequency increases

for NB20C3 and NB20C5. That is, at higher frequencies impedance decreases proportionally to filler loading. Correspondingly, imaginary impedance values are almost the same for NB20C3 and NB20C5 in the frequency range of analysis. Also, it is slightly higher than NB20C1 at a lower frequency. However, at high frequencies, the imaginary part of impedance proportionally decreases with frequency. Impedance values are found to be decreasing with increasing frequency in the investigated frequency range for all composites.

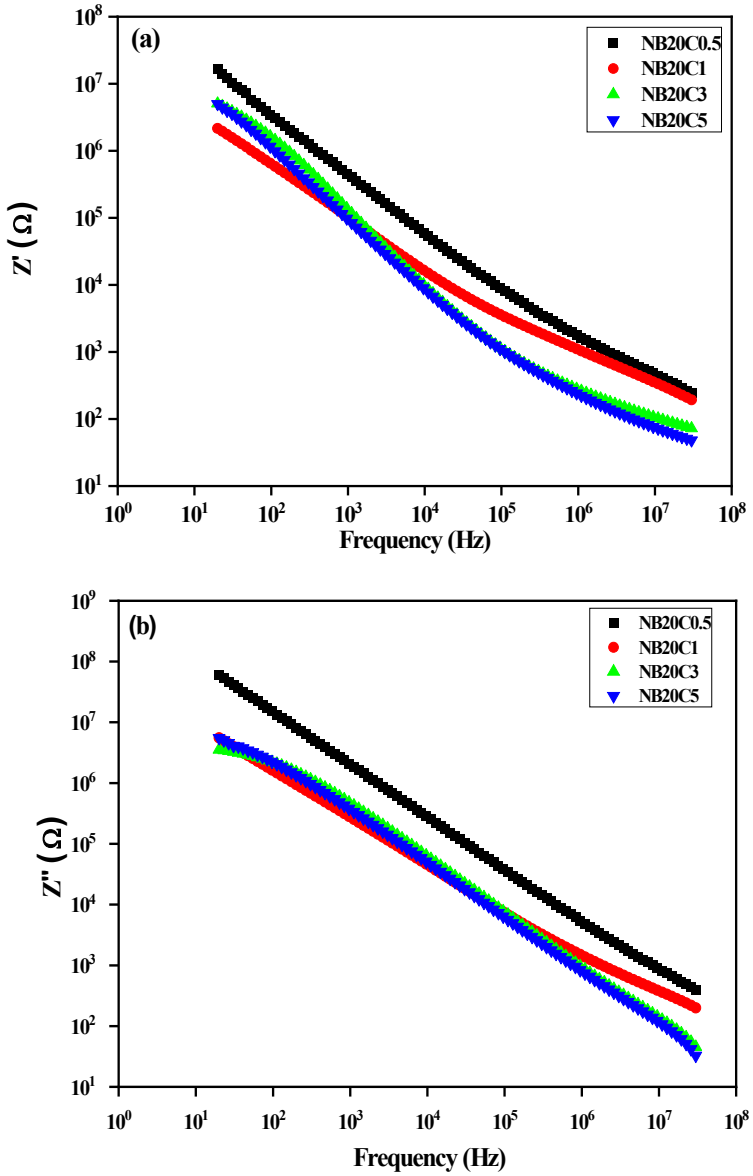

Figure 5.8-Frequency dependence of a) real part of impedance (Z′) and (b) imaginary part of impedance (Z″) NR/CCB-CNT hybrid filler systems

Impedance represents the resistive part of the system in an AC circuit. A decrease in impedance with filler loading suggests the formation of a conductive network of CCB and CNT in the matrix. Charge carrier transport inside the conducting elastomer matrix is through an electron hopping mechanism. This phenomenon is more significant at higher frequencies. This mechanism is responsible for the levelling off of impedance at higher frequency.

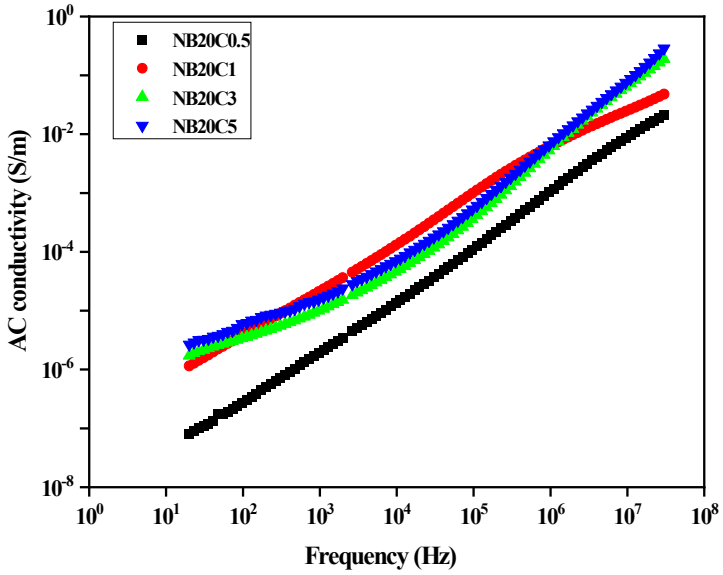

Figure 5.9-AC conductivity of NR/CCB-CNT hybrid filler systems

Figure 5.9 shows the variation of AC conductivity with increasing frequency at different filler loadings of NR/CCB-CNT hybrid filler systems. As mentioned earlier, the leakage current within the conductive network of the composites is responsible for the AC conductivity. NR/hybrid filler system shows a significant increase in AC conductivity up to 1 phr CNT. Higher loading of hybrid filler shows a marginal increase in conductivity. Generally, AC conductivity increases with frequency in conducting elastomers and is observed up to 1 phr CNT. However, the AC conductivity of NB20C3 and NB20C5 lowers in the frequency range of 10^3 to 10^6 Hz, where dielectric loss also exhibited the same trend. Increase in AC conductivity suggests the formation of the conductive pathway by CCB aggregates and CNT. The experimental data is fitted with Jonsher Universal Power Law by least square method. Jonsher Universal Power Law satisfactorily obeys the experimental data, and the

calculated exponent values are given in **Table 5.3.** The exponent values in the range $0<s<1$ indicate the hopping mode of conduction. The Maxwell- Wagner-Sillar polarizations at the interface affect the conduction mechanism. In the applied electric field, mobile charge carriers accumulate at the interface. Charge carriers are forced to drift large distances at low frequencies. At lower frequency the conductivity is independent of frequency, leading to the DC plateau limit, while conductivity increases exponentially at higher frequencies, according to $A\omega^s$ (25).

EMI shielding performance of hybrid filler composites is measured in the X-band frequency as it is important in modern wireless communication devices. The plot of SE_T against the frequency of NB20C3 and NB20C5 is given in **Figure 5.10 (a)**. Total shielding effectiveness increases up to 11 GHz when CNT loading increases from 3 to 5 phr. Moreover, total SE exceeds 22 dB in the investigating frequency range. Thus, both hybrid composites satisfy the requirement for commercial EMI shielding applications (20 dB). Shielding mechanism of polymer composites is more intricate compared to that of homogeneous conductive materials due to several reasons. Polymer composites present greater number of interfaces and a larger surface area for EM wave interaction (26). Effectiveness of EMI shielding depends on various factors, including the conductivity, dielectric properties, thickness, and frequency of the shielding materials. The conductivity, aspect ratio, dispersion, and loading of fillers all impact the overall shielding performance (27). Hybrid filler network formed by combining CNT and CCB provides additional free electrons, thereby facilitating high EMI shielding. Interconnected network of CNT and CCB also provides a large interface area for the interaction of EM radiation. Shielding effectiveness of polymer composites can be either due to the absorption mechanism (SE_A) or the reflection mechanism (SE_R). SE_T, SE_A and SE_R of polymer composites at 9.3 GHz are given in **Figure 5.10 (b)**. Increasing CNT content has caused more loss of EM radiation through absorption rather than reflection. Creation of conducting pathways in NR matrix by CNT-CCB hybrid system converts inherently dielectric elastomer to suitable candidate for EMI shielding devices. Interfacial polarizability and multiple conduction pathways generated in the composite matrix aid in the shielding of interacting EM radiation. DC conductivity values of the NR/CCB-CNT hybrid filler systems are given in **Table 5.3.** NR composites with 20 phr CCB have conductivity of 4.01×10^{-8} S/m due

to the conductive network formed by the CCB aggregates in the NR matrix. Conductivity increases with CNT loading and is found to be 1.41×10^{-6} S/m to 8.83×10^{-4} S/m, respectively, for 0.5 phr to 5 phr CNT. Thus, the presence of CNT helps in the formation of an effective conductive network in the matrix. CNT is able to connect the CCB aggregates in the NR matrix to form a conductive pathway. **Figure 5.11** shows the schematic representation of a conductive network of CCB-CNT hybrid filler in NR matrix.

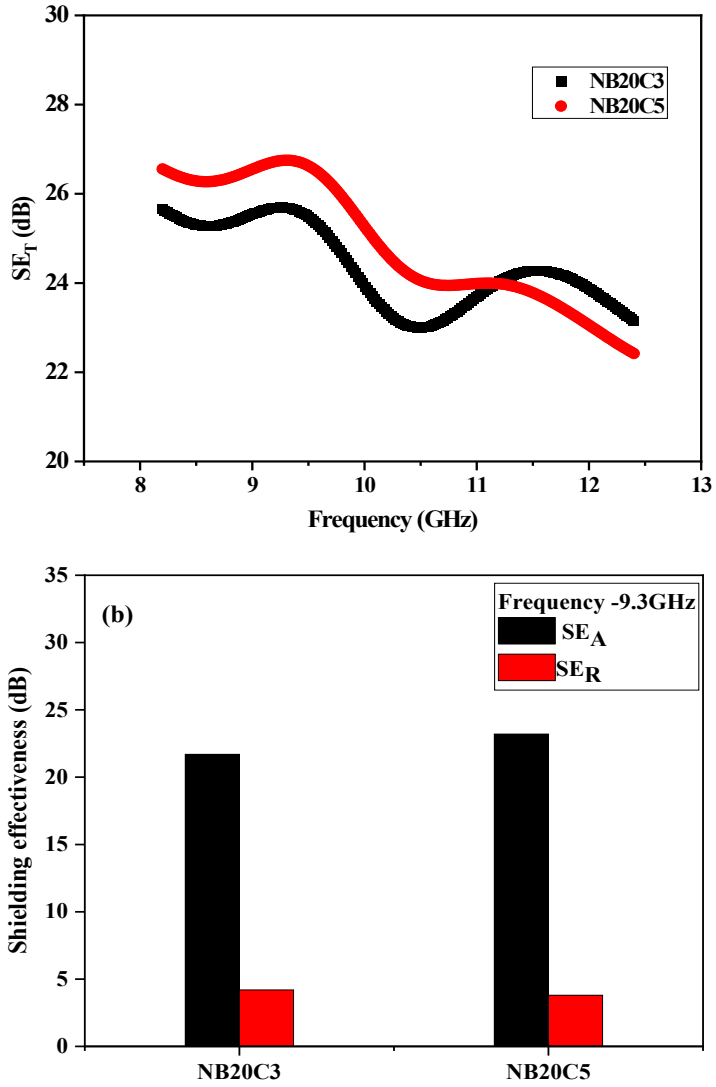

Figure 5.10-(a) SE_T and (b) SE_A and SE_R of NR/CCB-CNT hybrid filler systems

Table 5.3-DC conductivity values and frequency exponent of the NR/CCB-CNT hybrid filler systems

Sample	Conductivity (S/m)	s
NB20C0.5	1.41×10^{-6}	0.90
NB20C1	1.32×10^{-5}	0.78
NB20C3	1.18×10^{-4}	0.85
NB20C5	8.83×10^{-4}	0.82

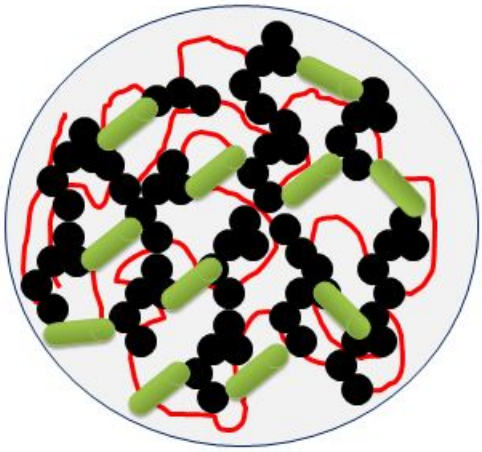

Figure 5.11-Schematic representation of conductive filler network formation of CCB-CNT in NR matrix

5.2.3. NR/1-ethyl-3-methylimidazolium chloride modified CCB (NR/ILCCB) systems

Variation of ε′ with the frequency of NR/ILCCB systems is presented in **Figure 5.12(a)**. In general, as is commonly observed, the dielectric permittivity of all composites decreases with increasing frequency. For ILCCB loading at two different ratios, the dielectric permittivity values are nearly identical. Ionic liquid modified CCB enhance the dielectric permittivity of NR by increasing the polarizability of the NR matrix and the dispersion of CCB. Distinct interphases are formed within the matrix through the combination of a hybrid filler network and ionic liquid modification. Charges accumulate at these interphases, leading to the emergence of Maxwell-Wagner-Sillar polarizations. All the aforementioned factors collectively contribute to the enhancement of dielectric permittivity. The variation of ε" with frequency is illustrated in **Figure 5.12(b).** The ε" decreases with frequency for both composites as

expected. However, NB20IL3 has a lower ε" at a higher frequency than NB20IL1. The higher imaginary part of the dielectric permittivity is contributed by the loss factors arising from the contributions of DC conductance (ε''_{DC}), interfacial polarizations (ε''_{MW}), and dipole orientations (ε''_{D}). (28) Mathematical relationship can be represented as,

$$\varepsilon'' = \varepsilon''_{DC} + \varepsilon''_{MW} + \varepsilon''_{D} \tag{5.3}$$

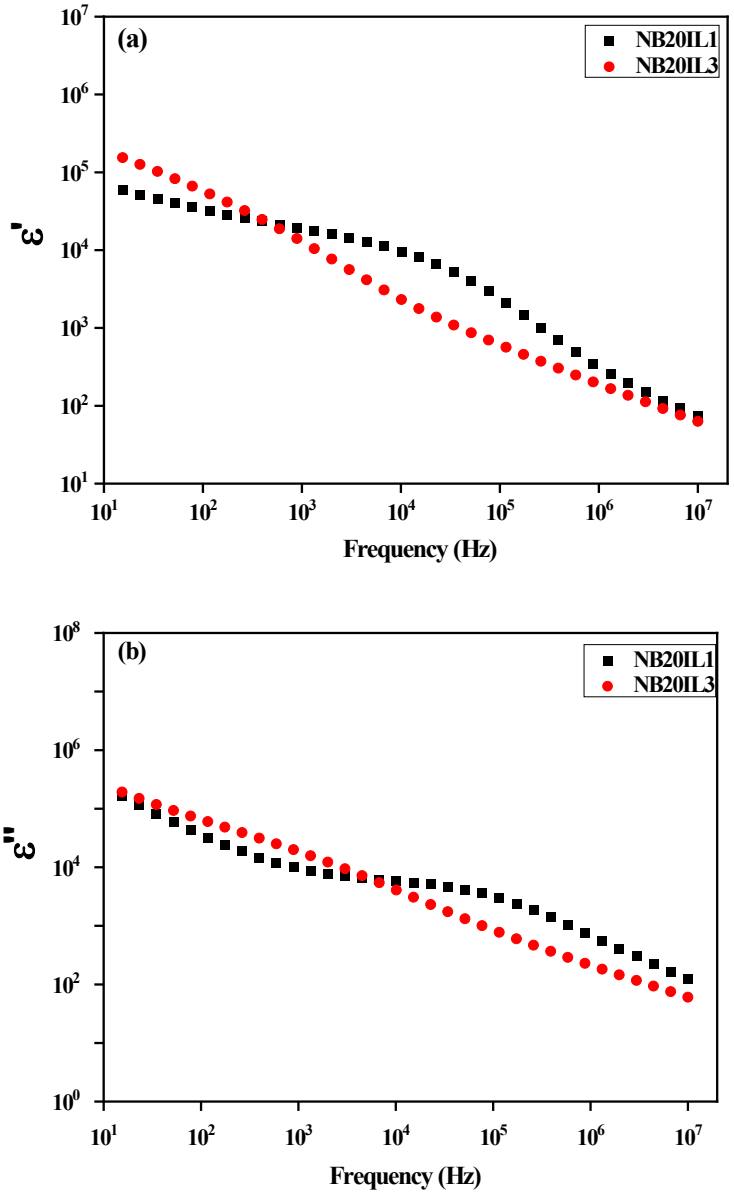

Figure 5.12-Frequency dependent (a) dielectric permittivity and (b) dielectric loss of NR/ILCCB systems

AC conductivity values of NR/ILCCB systems are plotted against frequency in **Figure 5.13.** AC conductivity of ILCCB reaches near 0.07 S/m in the investigated frequency range of 10 to 10^7 Hz. Here, NB20IL1 exhibited higher conductivity than NB20IL3. This is due to the formation of more conductive filler networks in NB20IL1 than NB20IL3, leading to the increase in leakage current at high frequency. In the literature, AC conductivity in the order of 10^{-4}-10^{-3} S/cm has been reported for epoxidized NR containing 50 mol% epoxide and 15-20 phr of CCB. Matchawet *et al.*(29) obtained AC conductivity in the order of 10^{-8}-10^{-7} S/cm at a frequency of 1 MHz for NR nanocomposites with 7.5 g of nanofibrillated cellulose.(30) Ionic liquid modification enables the creation of an interconnected conductive network of CCB in the NR matrix. The non-covalent interaction of the cationic part and aromatic π electrons of ionic liquid and π electrons of CCB reduces the chance for agglomeration of filler particles. Consequently, the dispersion of filler and its interaction with NR increases. Experimental data was analysed using Jonsher power law, and the exponents are given in **Table 5.4.** Frequency exponents are less than 1 and suggests hopping mode of conduction.

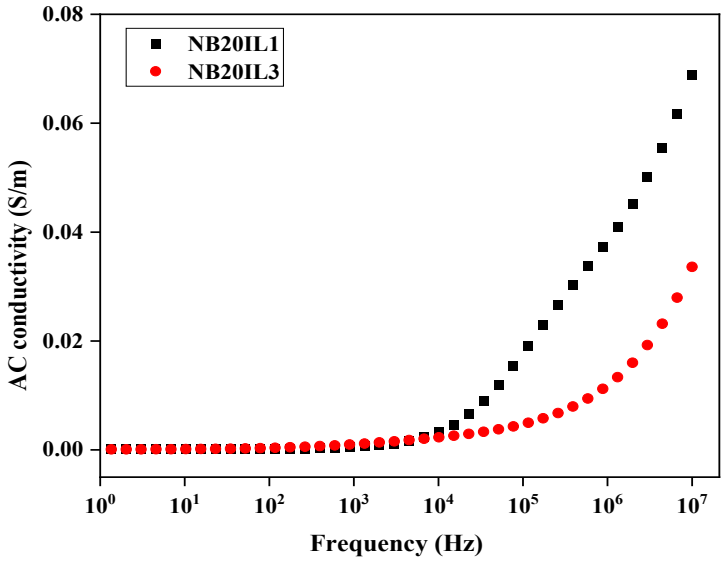

Figure 5.13-AC conductivity of NR/ILCCB systems

Figure 5.14(a) illustrates the SE_T in dB for NR/ILCCB systems across a range of frequencies. The total shielding effectiveness of the composites is almost similar for

both NB20IL1 and NB20IL3 within the frequency range under investigation. At 11GHz, the lowest total SE of nearly 20.3 dB is shown by ILCCB containing NR composites. The higher AC conductivity obtained for the composites can be related to the enhanced EMI shielding ability of composites.

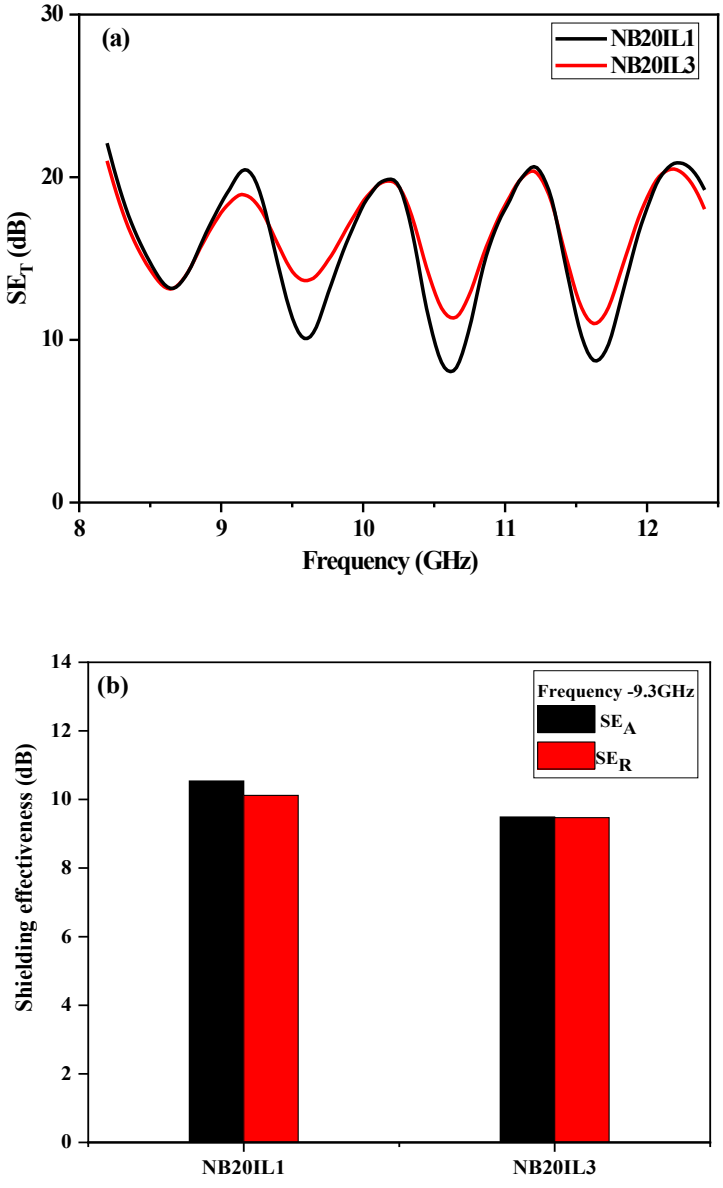

Figure 5.14-(a) SE_T and (b) SE_A and SE_R of NR/ILCCB systems

Higher amount of ionic liquid modified filler content in composites can lead to the formation of a more continuous conducting pathway for electron transport. This

increased conducting pathway enhances the electrical conductivity of the composite material. As a result, the composite exhibits higher AC conductivity. Also, the presence of IL and CCB in the composite introduces a large surface area, which allows for better interaction with incoming electromagnetic waves. This increased surface area enhances the absorption and scattering of EM waves, leading to higher electromagnetic interference shielding effectiveness. These composite acts as a barrier and effectively attenuates the EM waves, and thus possess the potential for EMI shielding devices. Presence of ionic liquid also plays a significant role in the EMI shielding of NR composites. It can act as a dispersant, facilitating the uniform dispersion of CCB within the NR matrix. This promotes better interfacial adhesion between filler and NR, enhancing the overall conductivity. The contribution of absorption and reflection in EM shielding is given in **Figure 5.14(b).** The plot clearly depicts that the absorption and reflection have almost equal contributions to the shielding of EM radiation. DC conductivity values of the composites are tabulated in **Table 5.4**. The conductivity values for NB20IL1 and NB20IL3 were observed to be in the range of 10^{-6}S/m. The observed conductive behaviour can be attributed to the chain-like structures formed by CCB filler particles. IL modification on CCB further creates extensive conductive networks in NB20IL1 and NB20IL3. Schematic representation of interaction of IL and CCB is given in matrix is given below **Figure 5.15**.

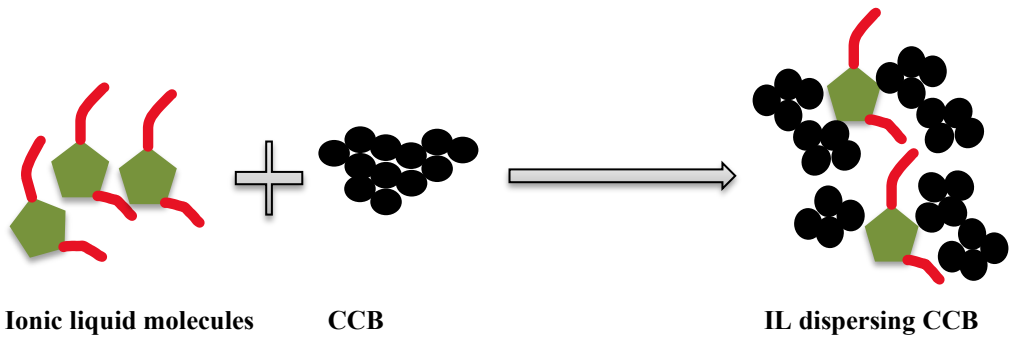

Figure 5.15- Schematic representation of interaction IL and CCB in NR

Table 5.4 -DC conductivity values and frequency exponent of NR/ILCCB systems

Sample	Conductivity (S/m)	s
NB20IL1	5.33 x 10^{-6}	0.38
NB20IL3	3.08 x 10^{-6}	0.45

5.2.4. NR/CCB-1-ethyl-3-methylimidazolium chloride modified CNT (NR/CCB-ILCNT) hybrid filler systems

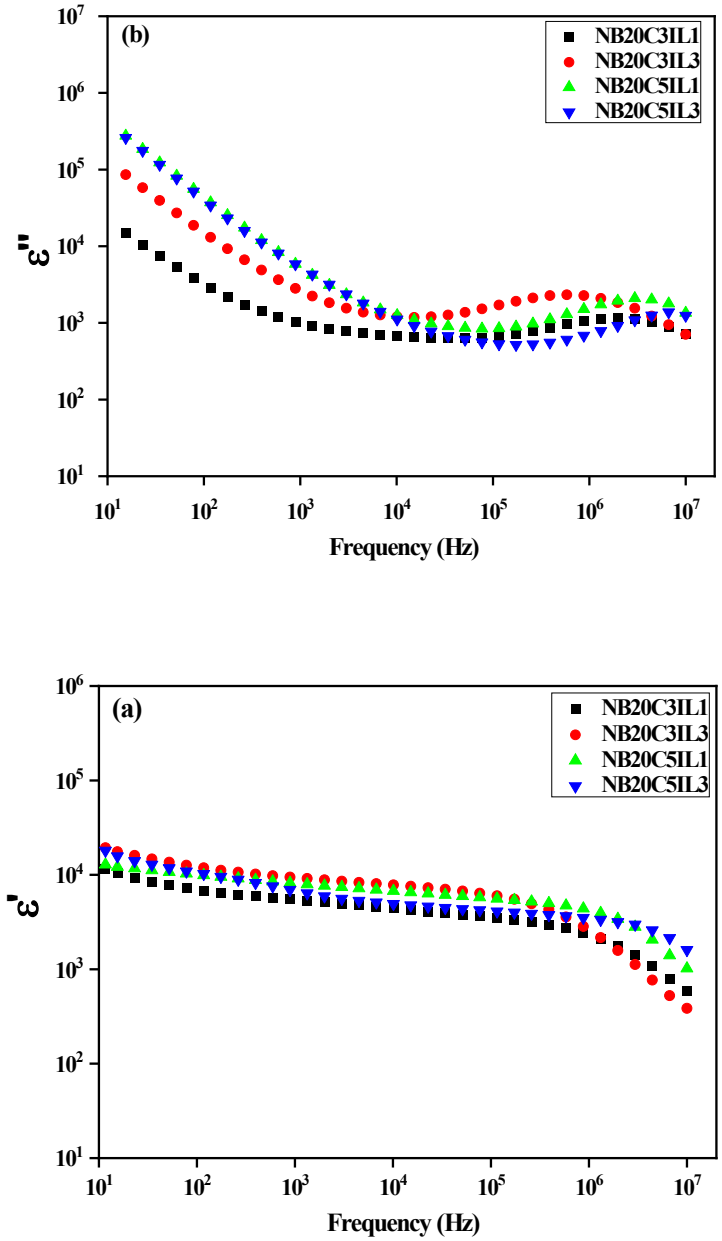

Figure 5.16-Frequency dependent (a) dielectric permittivity and (b) dielectric loss of NR/CCB-ILCNT hybrid filler systems

Figure 5.16 displays ε' and ε'' for NR/CCB-ILCNT hybrid filler systems. These composites consistently exhibit significant dielectric permittivity across the investigated frequency range, with values approximating 10^4. As CNT loading

increases from 3 to 5 phr, the dielectric permittivity increases subsequently. For NB20C3IL1 and NB20C3IL3, the permittivity increases with increasing amount of IL. However, for 5 phr CNT loading, variations in the amount of IL have minimal impact on dielectric permittivity. This enhancement in permittivity is attributed to the micro capacitor networks in the rubber matrix formed as a result of Maxwell-Wagner-Sillar polarizations (31). For NB20C5IL1 and NB20C5IL3, dielectric loss remains relatively consistent even though the amount of IL is varies. Importantly, the dielectric loss for composites at 3 phr ILCNT is less than that of the 5 phr ILCNT-loaded counterparts at frequencies under 10 KHz. A distinctive transition in behaviour is noted for the NB20C5IL3 composite around the 10 KHz mark: after this frequency, dielectric loss begins to decline and falls lower than that of NR composites with 3 phr ILCNT loading. However, NB20C3IL3 exhibits comparatively higher ε' with a combination of lower ε".

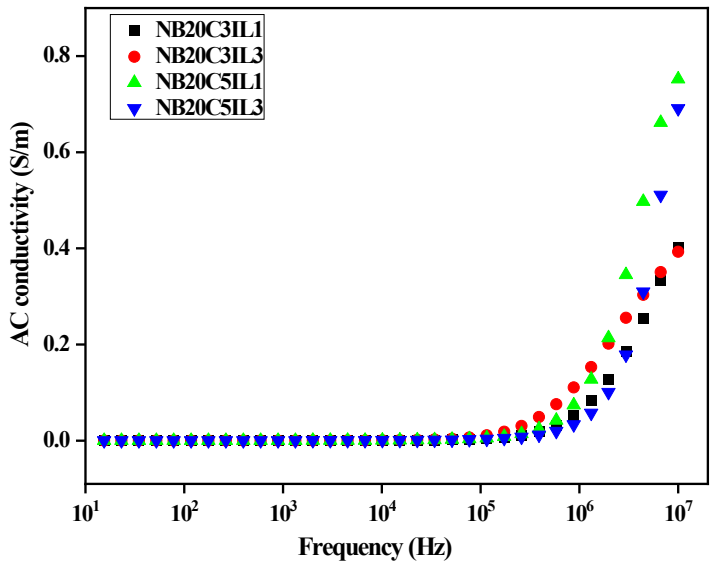

Figure 5.17-AC conductivity of NR/CCB-ILCNT hybrid filler systems

Figure 5.17 depicts the AC conductivity of NR/CCB-ILCNT hybrid filler systems against frequency. Modified CNT incorporated NR system shows a remarkable increase in AC conductivity. At 10^7 Hz, NB20C5IL1 and NB20C5IL3 show conductivity of 0.75 S/m and 0.69 S/m, respectively. Plateau region of the plot up to 10^5 Hz signifies the DC current. However, at higher frequency, a dramatic increase in

conductivity is observed. IL modified CNT and CCB form conductive pathways in the NR matrix which results in high AC conductivity. It can be explained in terms of the hopping mechanism, which is found to be higher for IL modified CNT. (32) The interconnected network of CNT allows hopping and tunnelling of charge carriers along the direction of the external electric field.(33) Also, the presence of strong π-π interaction between the aromatic imidazolium rings of ionic liquid and CNT can cause high conductivity.(34) Ionic liquid modification decreases the nanoscopic gap between tubes and results in the formation of percolating networks that indicate the homogeneous distribution of CNT and CCB in NR. This percolating network also allows easy movement of charge carriers across the matrix. (35) AC conductivity values are analysed using Jonscher power law by considering the initial DC plateau. Frequency exponent values are given in **Table 5.5.** All the values are less than 1.

Table 5.5-DC conductivity values and frequency exponent of NR/CCB-ILCNT hybrid filler systems

Sample	Conductivity (S/m)	s
NB20C3IL1	1.31×10^{-3}	0.50
NB20C3IL3	1.3×10^{-3}	0.69
NB20C5IL1	2.24×10^{-3}	0.33
NB20C5IL3	2.83×10^{-3}	0.29

The total shielding effectiveness of the NR/CCB-ILCNT hybrid filler systems are recorded and plotted against frequency which is presented in **Figure 5.18(a).** The SE_T values increase as a function of ILCNT within the frequency range under investigation. At 11GHz, NB20C5IL3 exhibits a SE_T of 26.4 dB. The higher AC conductivity obtained for the composites indicates of the enhanced EMI shielding ability of composites. NB20C5IL1 and NB20C5IL3 exhibit conductivity of 0.75 S/m and 0.69 S/m, respectively, at a frequency of 10^7 Hz. Ionic liquid modified filler can form a more continuous conducting pathway for electron transport. This increased conducting pathway enhances the electrical conductivity of the composite material. As a result, the composite exhibits higher AC conductivity. **Figure 5.18(b)** illustrates the contribution of absorption and reflection in EMI shielding. NB20C3IL1 predominantly relies on absorption for EM shielding. However, when the amount of

IL is increased, the contribution from reflection becomes dominant due to the formation of conducting pathway. When the concentration of CNT is increased, the significance of the absorption process in EMI shielding also increases. This implies a direct correlation between the amount of CNT and EMI shielding effectiveness through absorption.

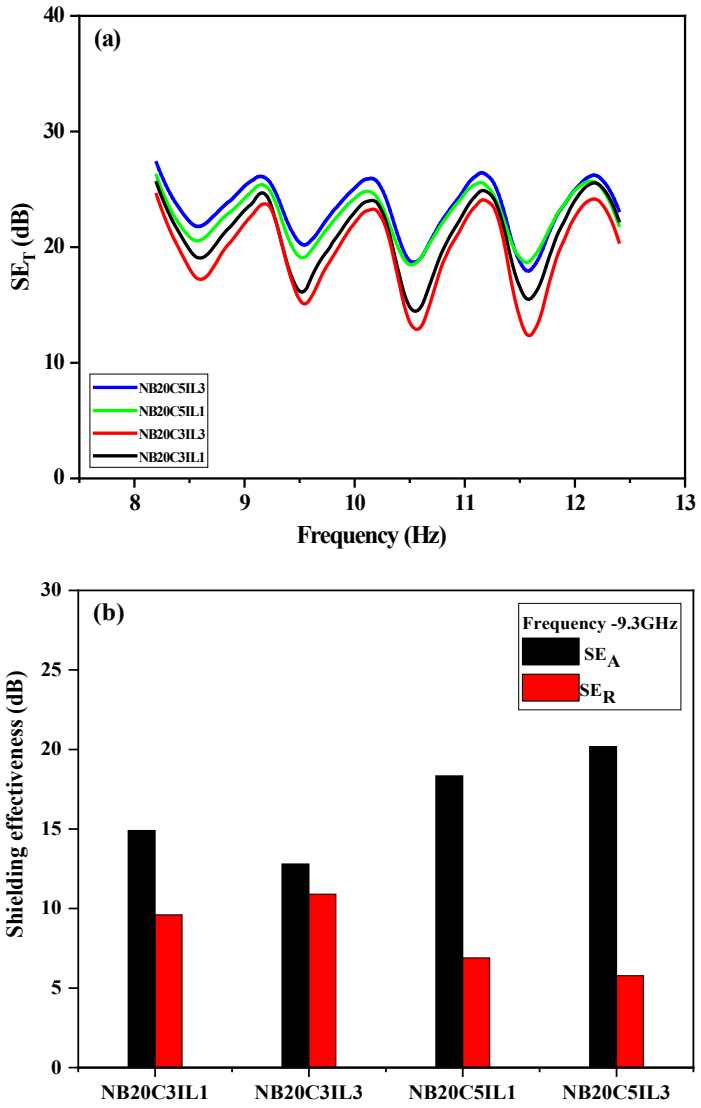

Figure 5.18-(a) SE_T and (b) SE_A and SE_R of NR/CCB-ILCNT hybrid filler systems

DC electrical conductivity data is tabulated in **Table 5.5.** When ILCNT and CCB are introduced, a significant enhancement in conductivity is observed, reaching approximately 10^{-3} S/m. This suggests that the ILCNT and CCB hybrid system has a

profound impact on improving conductivity compared to modified CCB. NB20C5IL1 exhibits a conductivity of 2.24 x 10^{-3} S/m, while NB20C5IL3 shows an increased conductivity of 2.83 x 10^{-3} S/m with CNT to IL ratio of 1:3. These findings indicate that the incorporation of 5 phr of CNT leads to further improvement in conductivity. In NR/CCB-ILCNT hybrid filler systems, the presence of ILCNT facilitates the formation of extensive conducting pathways, as evidenced by the data. The obtained DC conductivity values are in agreement with the AC conductivity data.

5.2.5. NR/CCB-CNT-RGO hybrid filler systems

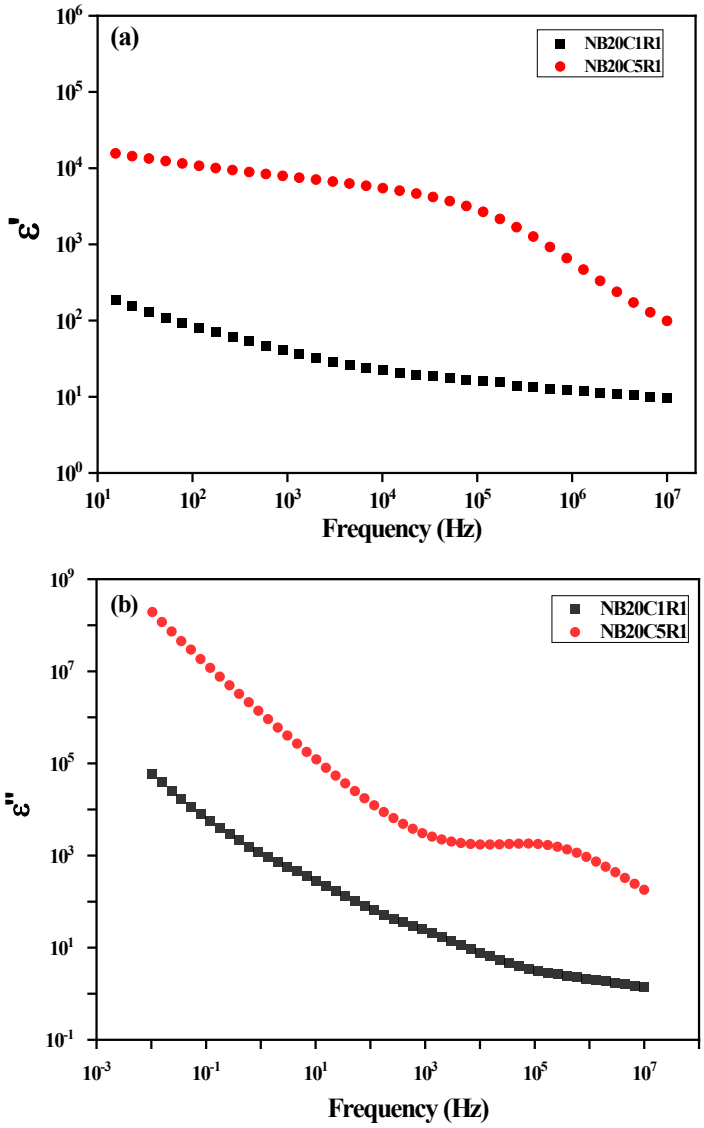

Figure 5.19-Frequency dependent (a) dielectric permittivity and (b) dielectric loss of NR/CCB-CNT-RGO hybrid filler systems

Frequency dependence of dielectric constant and dielectric loss of NR/CCB-CNT-RGO hybrid filler systems is given in **Figure 5.19**. The ε' and ε'' decreases with frequency for NB20C1R1 and NB20C5R1. ε' is higher for NB20C5R1 than NB20C1R1 at investigated frequency range. Increasing the CNT from 1 to 5 phr causes subsequent increase in ε' also. The ε'' is also proportional to CNT loading. Dielectric permittivity of NR composites arises due to different polarizations at the molecular level: dipolar, electronic, ionic and space charge polarizations. At lower frequencies, all polarizations contribute to the dielectric permittivity, resulting in a higher value. However, at higher frequencies, some polarizations may not be able to align with the frequency, causing a reduction in the dielectric permittivity.

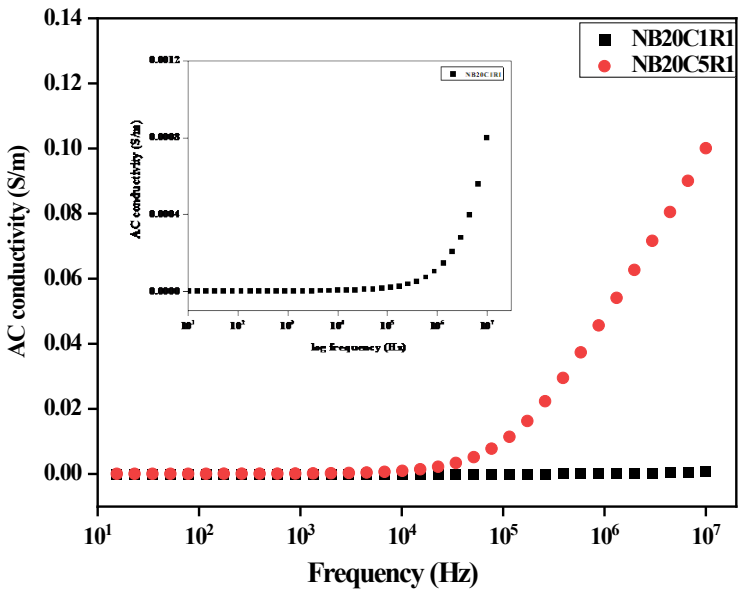

Figure 5.20-AC conductivity of NR/CCB-CNT-RGO hybrid filler systems

Figure 5.20 gives the AC conductivity of the hybrid filler systems. Inset of the plot depicts the variation of AC conductivity of NB20C1R1 with frequency. The investigated frequency range exhibits an increase in AC conductivity with increasing frequency. NB20C5R1 has attained AC conductivity value of 0.1 S/m at 10^7 Hz. Specifically, the AC conductivity demonstrates a more rapid increase at higher frequencies than lower frequencies. At lower frequencies, conductivity is independent of frequency, and it corresponds to DC current. At higher frequencies, frequency dependent AC component is seen, which is associated with the relaxation processes of

localised electric charge carriers on the filler surface. (36) The AC conductivity data obtained from experiments was analysed using the Jonsher Universal Power Law (1) equation, which was fitted to the data using the least square method. The exponent values obtained from the analysis are presented in **Table 5.6**, with values in the range of 0<s<,1 indicating a hopping mode of conduction. The results show that the Jonsher Universal Power Law equation satisfactorily explains the experimental data.

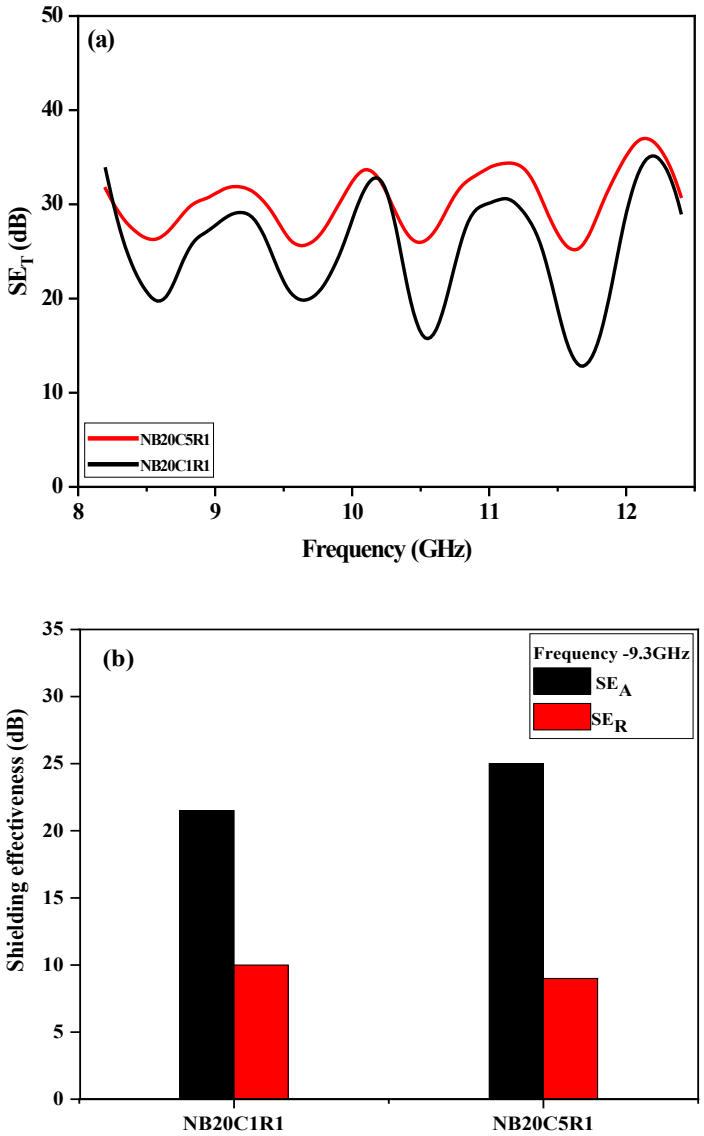

Figure 5.21 -(a) SE_T and (b) SE_A and SE_R of NR/CCB-CNT-RGO hybrid filler systems

EMI shielding of hybrid filler systems is investigated in the GHz range of frequency and is found to be in the range of commercial requirement of EMI shielding devices.(37) **Figure 5.21(a)** shows the SE_T values in dB of NR/CCB-CNT-RGO hybrid filler systems against frequency in GHz. Total SE of composites is increasing with filler loading in the investigated frequency range. Higher SE_T values observed are 37.4 and 35.3 dB at 12GHz for NB20C5R1 and NB20C1R1, respectively. Also, at 10 GHz, 33.8 and 32.9 dB is the total SE for NB20C5R1 and NB20C1R1, respectively. This EMI SE value is found to outperform some of the previously reported NR based composites with the same amount of CNT(38), CNT composite foams(39), a blend NR and ENR with CB(40), a hybrid system of CNT with non-carbon filler silica and a hybrid system of graphene with magnetic filler. (41) EMI shielding properties are directly related to the conducting network of fillers. Highly interconnected filler network permits increased interaction between EM radiation and conducting particles, which leads to increase in microwave (MW) absorption via electron transport through the conducting network. Thus, composites with higher AC conductivity show higher SE_T values. Interaction of RGO sheets, CCB and CNT allows the formation of multiple conducting pathways in the polymer matrix, which subsequently helps in improving the attenuation of EM radiation. **Figure 5.21(b)** illustrates the role of absorption and reflection in the EMI shielding effectiveness of the composites. The data prominently indicates a higher tendency for absorption of EM radiation. The pronounced absorption can be attributed to the synergistic effect of CNT, RGO and CCB hybrid filler systems. High surface area of the fillers can provide more interfaces for the interaction and dissipation of EM waves. Also, the enhanced charge carrier mobility in materials like CNT can result in increased interaction with the EM radiation, leading to its absorption. The layered structure of RGO and the tubular structure of CNT can cause multiple internal reflections of the EM waves, increasing the path length of these waves within the material. This extended interaction increases the chances of energy absorption. Also, RGO and CCB can contribute to dielectric loss of the EM energy. All these factors could lead to enhanced EMI shielding primarily through absorption. DC electrical conductivity data is given in **Table 5.6**. NB20C5R1 has high concentration of CNT. The well dispersed conductive fillers and their synergistic effect enhanced the electrical conductivity. Moreover, the π electrons present in CCB, CNT

and RGO layers also contribute to DC conductivity. Homogenous distribution of filler can create a conductive network of CCB aggregates, CNT and RGO layers. Schematic representation of the filler network is provided in **Figure 3.12 (Chapter 3)**.

Table 5.6-DC conductivity of NR/CCB-ILCNT hybrid filler systems

Sample	Conductivity (S/m)	s
NB20C1R1	2.28×10^{-7}	0.83
NB20C5R1	8.99×10^{-5}	0.47

5.3. Comparative analysis of properties

Dielectric permittivity of the NR hybrid filler systems increases gradually with filler incorporation. NR composites with IL modified fillers and hybrid filler systems of CCB, CNT and RGO have permittivity in the range of $10^4 – 10^6$. The total EMI SE and DC conductivity values of the different systems of fillers are given in **Table 5.7**. The shielding effectiveness is gradually increasing with the modification of fillers. The commercial requirement for EMI shielding devices is satisfied by all hybrid filler systems. NB20C5R1 has the highest EMI SE of 33.8 dB in the frequency range of 9-10 GHz. However, DC conductivity is highest for NB20C5IL3 in the order of 10^{-3}, which has an EMI SE of 26.2 dB. The shielding efficiency of a material is associated with the improved connectivity of conducting particles in the matrix rather than the overall conductivity. So NB20C5R1 has higher EMI shielding than NB20C5IL3 even though conductivity is higher for the latter. DC conductivity also shows notable improvement with hybrid filler systems.

Table 5.7-Comparative analysis of EMI SE and DC conductivity of NR hybrid filler systems

Sample	EMI SE in 9-10 GHz (dB)	DC conductivity (S/m)
NB20	18.9	4.01×10^{-8}
NB20C5	26.9	8.83×10^{-4}
NB20IL1	20.7	5.33×10^{-6}
NB20C5IL3	26.2	2.83×10^{-3}
NB20C5R1	33.8	8.99×10^{-5}

5.4. Conclusion

Dielectric permittivity of composites increases with the incorporation of conducting fillers. The investigation of EMI shielding effectiveness shows that NR/CCB-CNT-

RGO hybrid filler systems with 5 phr CNT have the highest EMI SE of 33.8 dB in the frequency range of 9-10 Hz. Ionic liquid plays a significant role in dispersing and stabilizing CNT within the composite, promoting better interfacial adhesion, and enhancing the conductivity of composites. DC conductivity is found to be higher for NB20C5IL3 in the order of 10^{-3}, which has an EMI SE of 26.2dB. For most NR systems, EMI shielding is primarily achieved through absorption. However, the presence of IL in the NR matrix increases the contribution of reflection to EMI shielding. In brief, the hybrid filler system makes NR highly suitable for commercial EMI shielding applications.

5.5. References

1. Jonscher AK. Dielectric relaxation in solids. Journal of Physics D: Applied Physics. 1999;32(14).
2. Ladhar A, Arous M, Kaddami H, Raihane M, Lahcini M, Kallel A, et al. Dielectric relaxation studies on nanocomposites of rubber with nanofibrillated cellulose. Journal of Non-Crystalline Solids. 2013;378:39–44.
3. Sreekumar PA, Saiter JM, Joseph K, Unnikrishnan G, Thomas S. Electrical properties of short sisal fiber reinforced polyester composites fabricated by resin transfer molding. Composites Part A: Applied Science and Manufacturing. 2012 Mar;43(3):507–11.
4. Fadel DS, Rajab MA, Ali AK. The effect of reinforcing with fibers and nanomaterials on the electrical properties of composite materials. Journal of Physics: Conference Series. 2021 Sep 1;1999(1):012134.
5. Chung DDL. 6 - Cement-Matrix Composites. In: Chung DDL, editor. Carbon Composites (Second Edition) [Internet]. Butterworth-Heinemann; 2017. p. 333–86. Available from: https://www.sciencedirect.com/science/article/pii/B9780128044599000063
6. Psarras G. Fundamentals of dielectric theories. In: Dielectric Polymer Materials for High-Density Energy Storage. Elsevier; 2018. p. 11–57.
7. Deshmukh K, Ahamed MB, Deshmukh RR, Pasha SKK, Bhagat PR, Chidambaram K. 3 - Biopolymer Composites With High Dielectric Performance: Interface Engineering. In: Sadasivuni KK, Ponnamma D, Kim J, Cabibihan JJ, AlMaadeed MA, editors. Biopolymer Composites in Electronics [Internet]. Elsevier; 2017. p. 27–128. Available from: https://www.sciencedirect.com/science/article/pii/B9780128092613000036
8. Niu C, Dong X, Qi M. Enhanced Electrorheological Properties of Elastomers Containing TiO2/Urea Core–Shell Particles. ACS Appl Mater Interfaces. 2015 Nov 11;7(44):24855–63.
9. Xie Z, Liu D, Xiao Y, Wang K, Zhang Q, Wu K, et al. The effect of filler permittivity on the dielectric properties of polymer-based composites. Composites Science and Technology. 2022 May 3;222:109342.
10. Stockmayer WH. Dielectric dispersion in solutions of flexible polymers. Pure and Applied Chemistry. 1967;15(3–4):539–54.
11. Huang M, Tunnicliffe LB, Thomas AG, Busfield JJC. The glass transition, segmental relaxations and viscoelastic behaviour of particulate-reinforced natural rubber. European Polymer Journal. 2015;67:232–41.
12. Robertson CG, Hardman NJ. Nature of carbon black reinforcement of rubber: Perspective on the original polymer nanocomposite. Polymers. 2021;13(4):1–28.
13. Xia X, Zhong Z. Maxwell–Wagner–Sillars mechanism in the frequency dependence of electrical conductivity and dielectric permittivity of graphene-polymer nanocomposites. Mechanics of Materials. 2017 Apr 5;109:42–50.
14. B S MS, Hiremath S, Kulkarni SM. Influence of conductive and dielectric fillers on the relaxation of solid silicone rubber composites. Materials Research Express. 2019;6(12):125308.

15. Wang X, Li Z, Chen Z, Zeng L, Sun L. Structural modification of carbon black for improving the dielectric performance of epoxy based composites. Advanced Industrial and Engineering Polymer Research. 2018;1(1):111–7.
16. Mohapatra S, Nando GB. Analysis of carbon black-reinforced cardanol-modified natural rubber compounDS. Rubber Chemistry and Technology. 2015;88(2):289–309.
17. Oliveira FA, Alves N, Giacometti JA, Constantino CJL, Mattoso LHC, Balan AMOA, et al. Study of the thermomechanical and electrical properties of conducting composites containing natural rubber and carbon black. Journal of Applied Polymer Science. 2007;106(file:///E:/Work Data/aa NR_CCB_CNT/references ccb cnt/natarajan2017.pdf):1001–6.
18. Gupta P, Mahapatra PK, Choudhary RNP. Investigation on structural and electrical properties of Co and W modified BaTiO3. Ceramics International. 2019;45:22862–71.
19. Peng M, Qin F. Clarification of basic concepts for electromagnetic interference shielding effectiveness. Journal of Applied Physics. 2021 Dec 14;130(22):225108.
20. Shukla V. Review of electromagnetic interference shielding materials fabricated by iron ingredients. Nanoscale Advances. 2019;1(5):1640–71.
21. Anderson L, Govindaraj P, Ang A, Mirabedini A, Hameed N. Modelling, fabrication and characterization of graphene/polymer nanocomposites for electromagnetic interference shielding applications. Carbon Trends. 2021 Jul;4:100047.
22. Kirkpatrick S. Percolation and Conduction. Reviews of Modern Physics. 1973 Oct 1;45(4):574–88.
23. Yang C, Song HS, Liu DB. Dielectric composites containing core@ shell structure particles. Advanced Materials Research. 2011;239:3113–8.
24. Zhou W, Zhang F, Yuan M, Li B, Peng J, Lv Y, et al. Improved dielectric properties and thermal conductivity of PVDF composites filled with core–shell structured Cu@CuO particles. Journal of Materials Science: Materials in Electronics. 2019 Oct 1;30.
25. Psarras GC. Conductivity and dielectric characterization of polymer nanocomposites. Physical Properties and Applications of Polymer Nanocomposites. 2010;31–69.
26. Luo JQ, Zhao S, Zhang HB, Deng Z, Li L, Yu ZZ. Flexible, stretchable and electrically conductive MXene/natural rubber nanocomposite films for efficient electromagnetic interference shielding. Composites Science and Technology. 2019;182(July):107754.
27. Poothanari MA, Abraham J, Kalarikkal N, Thomas S. Excellent Electromagnetic Interference Shielding and High Electrical Conductivity of Compatibilized Polycarbonate/Polypropylene Carbon Nanotube Blend Nanocomposites. Ind Eng Chem Res. 2018 Mar 28;57(12):4287–97.
28. Salaeh S, Nakason C. Influence of modified natural rubber and structure of carbon black on properties of natural rubber compounds. Polym Compos. 2012 Apr;33(4):489–500.
29. Matchawet S, Nakason C, Kaesaman A. Electrical and mechanical properties of conductive carbon black filled epoxidized natural rubber. Advanced Materials Research. 2014;844(file:///E:/Work Data/aa NR_CCB_CNT/references ccb cnt/natarajan2017.pdf):255–8.
30. Ladhar A, Arous M, Kaddami H, Raihane M, Kallel A, Graça MPF, et al. AC and DC electrical conductivity in natural rubber/nanofibrillated cellulose nanocomposites. Journal of Molecular Liquids. 2015;209:272–9.
31. Li B, Randall CA, Manias E. Polarization Mechanism Underlying Strongly Enhanced Dielectric Permittivity in Polymer Composites with Conductive Fillers. J Phys Chem C. 2022 May 5;126(17):7596–604.
32. Carabineiro SAC, Pereira MFR, Nunes-Pereira J, Silva J, Caparrós C, Sencadas V, et al. The effect of nanotube surface oxidation on the electrical properties of multiwall carbon nanotube/poly(vinylidene fluoride) composites. Journal of Materials Science. 2012;47:8103–11.
33. Abraham J, Arif P M, Xavier P, Bose S, George SC, Kalarikkal N, et al. Investigation into dielectric behaviour and electromagnetic interference shielding effectiveness of conducting styrene butadiene rubber composites containing ionic liquid modified MWCNT. Polymer. 2017 Mar;112:102–15.
34. Maiti S, Suin S, Shrivastava N, Khatua BB. A strategy to achieve high electromagnetic interference shielding and ultra low percolation in multiwall carbon nanotube–polycarbonate composites through selective localization of carbon nanotubes. RSC Advances [Internet]. 2014 [cited 2023 Aug 19]; Available from: https://www.semanticscholar.org/paper/A-strategy-to-achieve-high-electromagnetic-and-low-Maiti-Suin/3f5d9ab2e1a586684656b18283ea9039c2577680

35. Sahoo BP, Naskar K, Tripathy DK. Multiwalled Carbon Nanotube‐Filled Ethylene Acrylic Elastomer Nanocomposites: Influence of Ionic Liquids on the Mechanical, Dynamic Mechanical, and Dielectric Properties. :13.
36. Teusdea A, Malaescu I, Sfirloaga P, Marin CN. Electric and Dielectric Properties in Low-Frequency Fields of Composites Consisting of Silicone Rubber and Al Particles for Flexible Electronic Devices. Materials. 2022 Mar 21;15(6):2309.
37. Muringayil Joseph T, Mariya HJ, Haponiuk JT, Thomas S, Esmaeili A, Sajadi SM. Electromagnetic interference shielding effectiveness of natural and chlorobutyl rubber blend nanocomposite. Journal of Composites Science. 2022;6(8):240.
38. Jia LC, Yan DX, Yang Y, Zhou D, Cui CH, Bianco E, et al. High Strain Tolerant EMI Shielding Using Carbon Nanotube Network Stabilized Rubber Composite. Advanced Materials Technologies. 2017;2(7).
39. Zhan Y, Oliviero M, Wang J, Sorrentino A, Buonocore GG, Sorrentino L, et al. Enhancing the EMI shielding of natural rubber-based supercritical CO_2 foams by exploiting their porous morphology and CNT segregated networks. Nanoscale. 2019;11(3):1011–20.
40. Zhao H, Mazumdar S. Electron-electron interaction effects on the optical excitations of semiconducting single-walled carbon nanotubes. Physical review letters. 2004;93 15:157402.
41. Zhan Y, Wang J, Zhang K, Li Y, Meng Y, Yan N, et al. Fabrication of a flexible electromagnetic interference shielding Fe3O4@reduced graphene oxide/natural rubber composite with segregated network. Chemical Engineering Journal. 2018;344:184–93.

Chapter 6

Transport Properties and Kinetic Studies of NR Hybrid Filler Systems

This chapter focus on the solvent transport properties of natural rubber (NR) hybrid filler systems as a function of filler concentration and its comparison. Experimentally obtained transport data are evaluated using different kinetic models such as first-order kinetics, Higuchi, Korsemayer-Peppas, and Peppas-Sahlin models. Matrix-filler interactions are obtained from swelling studies and is evaluated using Kraus, Cunnen-Russel and Lorenz- Park plots. Incorporation of IL modified fillers and hybrid filler of CNT, CCB and RGO effectively restricts the diffusion of solvent molecules through the NR matrix.

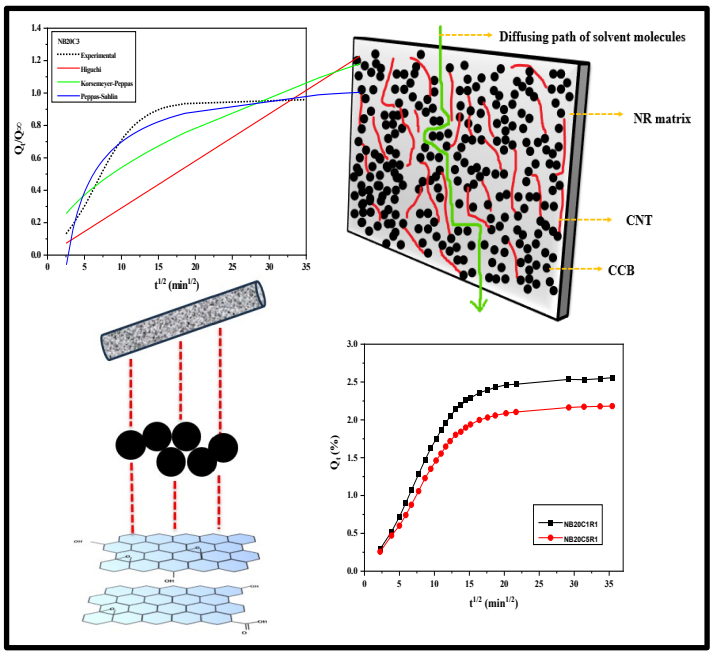

A part of this chapter is published in the journal Express Polymer Letters. *Vol. 17., No.10., Pages 1070-1080, 2023, DOI: 10.3144/expresspolymlett.2023.80*

6.1. Introduction

The transport properties of solvents in polymer composites are related to the distribution and reinforcement of fillers in the matrix. These are widely used as food packaging materials owing to their intrinsic qualities such as corrosion resistance, lightweight, and enhanced mechanical and thermal properties. (1) Incorporation of chemically modified fillers in polymer can improve the production of highly efficient membranes for pervaporation, ultrafiltration, reverse osmosis and gas separation. (2–8)

Natural rubber (NR) based polymer composites are widely used in the automotive, construction, and electrical industries and various engineering applications. Modifying rubber matrix by adding various fillers generates exciting changes in the properties of composites, including transport properties. Carbonaceous fillers such as carbon nanotubes (CNT), graphene, carbon black (CB), carbon fibres, etc., are used extensively in NR. Among the carbon nanofillers, graphene and its derivatives can refine the barrier characteristics of elastomer composites. Graphene-loaded fluoroelastomer shows decreased swelling rates in acetone compared to CB-filled fluoroelastomer composite. (9) Similarly, a hybrid filler combination of graphene with zinc oxide in NR shows the capacity to resist chemical attack. The mol % uptake for hybrid filler composites shows a remarkable decrease of 41.67% for kerosene, 4.44% decrease for diesel and 50% for polymethylsilane (PMS) and water, respectively, compared to CB-filled NR as control. (10) The incorporation of a hybrid filler system is effective in restraining the solvent penetration through the polymer matrix. (11) CNT/clay hybrid filler system improves the crosslink density of nitrile rubber (NBR)/NR blends. (12)

Theoretical understanding of the transport phenomena in rubber composites is beneficial in advanced research as well as in the fabrication of composite membranes. Empirical and semi-empirical mathematical models give a theoretical perspective of experimental transport data. This helps to elucidate the transport mechanism of solvents through the rubber matrix.

6.2. Theoretical models for transport and swelling studies

6.2.1. Kinetics of transport properties

Various theoretical models are employed for the kinetic analysis of transport properties of toluene in NR hybrid filler systems filled with hybrid fillers. This helps to provide a foundation for understanding the mechanisms involved. We have analysed the mode of transport and then employed first-order kinetics, Higuchi, Korsemayer-Peppas, and Peppas-Sahlin models to evaluate the transport properties.

6.2.1.1. Mode of transport

The mode of transport is analysed using the following equation,

$$log \frac{Q_t}{Q_\infty} = \log k + n \log t \tag{6.1}$$

where Q_t is the solvent uptake at time t, and Q_∞ is the equilibrium solvent uptake. The constants n and k are determined from the linear portion of the plot Q_t versus $\sqrt{t}$ through power regression analysis. The value of k depends upon the structural characteristics of polymer and polymer-solvent interaction, and n indicates the transport mechanism.

6.2.1.2. First-order kinetics

The first-order kinetic equation (13) is given below, where k is the first-order rate constant.

$$log Q_t = log Q_\infty - \frac{k\,t}{2.303} \tag{6.2}$$

6.2.1.3. Higuchi model

The Higuchi model proposed that diffusion is based on Fick's law and depends on the square root of time. This model is based on the following hypothesis:(14)

(a) diffusion is one dimensional
(b) the diffusing particles are much smaller than matrix systems
(c) diffusivity is a constant
(d) matrix swelling and diffusion are constant

Higuchi model is simplified as,

$$\frac{Q_t}{Q_\infty} = k_h\, t^{1/2} \tag{6.3}$$

where k_h is the Higuchi dissolution constant. Higuchi dissolution constant decreased linearly with increase in filler loadings.

6.2.1.4. Korsemeyer – Peppas model

Korsemeyer – Peppas (15) model helps to analyse the transport mechanism by the following exponential equation,

$$\frac{Q_t}{Q_\infty} = k\, t^n \tag{6.4}$$

where k is the kinetic constant, and n is the diffusional exponent that indicates the transport mechanism.

6.2.1.5. Peppas-Sahlin model

Peppas-Sahlin model is based on the theory that the transport mechanism has diffusional and relaxational contributions, which are additive in nature. (16) Peppas-Sahlin (17) equation is given by,

$$\frac{M_t}{M_\infty} = k_{\,1} t^m + k_2\, t^{2m} \tag{6.5}$$

where first and second term indicates the Fickian contribution and the case-II relaxational contribution. The diffusion exponent 'm' characterises purely Fickian diffusion in a controlled release device of any geometrical shape. Previous works on transport mechanisms of polymeric systems have shown that $k_1 > k_2$ implies diffusion-controlled mechanism, $k_1 < k_2$ implies matrix-controlled mechanism, and $k_1 = k_2$ implies a combination of diffusion-controlled and matrix-controlled mechanisms (18).

6.2.2. Theoretical prediction of rubber-filler interaction from swelling studies

Extent of interaction between rubber matrix and fillers can be analysed using Kraus (19), Cunneen-Russel (20) and Lorenz-Park (21) equations.

6.2.2.1. Kraus model

Kraus equation is given below,

$$\frac{V_{r0}}{V_{rf}} = 1 - m\left[\frac{f}{1-f}\right] \tag{6.6}$$

where V_{ro} is the volume fraction of rubber in the solvent-swollen gum vulcanizate, m is the polymer-filler interaction parameter, f is the volume fraction of filler and V_{rf} is the volume fraction of rubber in the solvent-swollen filled vulcanizate and is given by the Ellis and Welding equation (22) given below,

$$V_{rf} = \frac{\frac{d-fw}{\rho p}}{\frac{d-fw}{\rho p}+\frac{A_S}{\rho_S}} \tag{6.7}$$

where d is the deswollen weight of the sample, f is the weight fraction of filler, w is the initial weight of the sample, ρ_p is the density of the polymer, ρ_S is the density of solvent, and A_S is the amount of solvent absorbed. Plot of $\frac{V_{r0}}{V_{rf}}$ against $\frac{f}{1-f}$ gives a straight line whose slope m gives the direct measure of reinforcement by fillers.

6.2.2.2. Cunneen-Russel model

Cunneen-Russel equation is,

$$\frac{V_{r0}}{V_{rf}} = ae^{-z} + b \tag{6.8}$$

Plot of $\frac{V_{r0}}{V_{rf}}$ against e^{-z}, where z is the weight fraction of filler, gives a straight line with slope a and intercept b.

6.2.2.3. Lorenz and Park Model

Lorenz and Park equation(21) is given by,

$$\frac{Q_f}{Q_g} = ae^{-z} + b \tag{6.9}$$

where Q is the amount of solvent imbibed per unit weight, f and g refer to filled and gum rubber vulcanizates, a and b are the constants that depend on the filler activity, and z is the weight fraction of filler in the rubber composites.

6.3. Results and discussion

6.3.1. NR/CCB systems

6.3.1.1. Transport properties

The solvent uptake of polymer composites depends on the characteristics of fillers, temperature, morphology, type of solvent, free volume and processing conditions. (23)

Transport of solvents in polymers is also affected by crosslink density, free volume and structure of polymer. Polymer chain segmental motions have a significant influence on the processes associated with the diffusion of molecules through the polymer matrix. Variation in polymer composition and structure directly affects the free volume content and distribution, which in turn affects the transport of matter. The transport processes are interdependent with polymeric structure and segmental motion of polymer chains. (24)

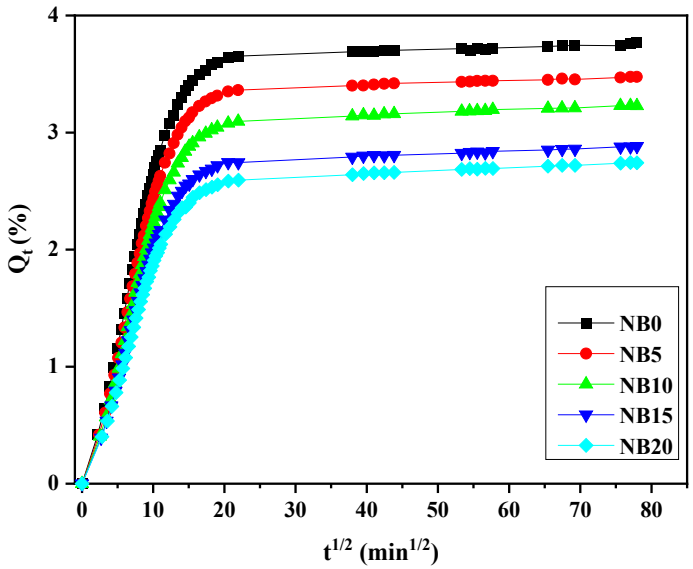

Figure 6.1–Sorption curves of NR/CCB systems

Transport properties of NR/CCB systems are analysed in toluene. The effect of filler on the solvent uptake of NR is depicted in **Figure 6.1**. Solvent absorption initially increases rapidly owing to the high concentration gradient of the solvent molecules in the NR matrix. Then, the sorption approaches equilibrium, as indicated by the plateau region of the sorption curve. From the plot of mol % uptake of toluene against $t^{1/2}$, it is clear that the solvent uptake of NR/CCB systems decreases

significantly as a function of weight percentage of filler. This can be described in terms of the formation of filler- filler and matrix- filler networks, which hinders the diffusion of solvent molecules. Diffusion coefficient and permeability coefficient values of the CCB loaded composite systems are given in **Table 6.1**. The diffusion coefficient gives the rate of diffusion of solvent molecules into the polymer matrix. The diffusion coefficient value decreases linearly with filler loading. Polymer- filler interaction has decreased the availability of free voids, thereby restricting the solvent diffusion through matrix. Sorption involves the initial penetration of solvent molecules and their diffusion across the rubber matrix. (25) Hence, the sorption coefficient depends on the solvent-rubber interaction. The permeability coefficient has both contributions from diffusion and sorption. Decreasing permeation coefficient with filler loading also suggests the improved filler-matrix interaction with increasing CCB content. Interaction of filler and rubber restricts the solvent swelling by the formation of crosslinks, which in turn reduces the segmental mobility of rubber chains. The decreased flexibility of the chains and the reduction in the number of voids in the matrix hinder the diffusion of solvent molecules.

Table 6.1 -Diffusion coefficient, permeability coefficient and parameter n of NR/CCB systems

Sample	D (cm^2/s)	P (cm^2/s)	n
NB0	2.14×10^{-6}	7.45×10^{-6}	0.62
NB5	1.96×10^{-6}	6.29×10^{-6}	0.62
NB10	1.74×10^{-6}	5.18×10^{-6}	0.63
NB15	1.45×10^{-6}	3.86×10^{-6}	0.64
NB20	1.22×10^{-6}	3.08×10^{-6}	0.61

The mode of transport is evaluated for the NR composites using **Equation (6.1)** and the n values are computed and tabulated in **Table 6.1.** The n value is between 0.5 and 1 for all composites, indicating the non-Fickian mode of transport. (26) For the non-Fickian mode, the chain relaxation is much slower than the solvent penetration. High degree of restriction produced by the filler particles reduces the segmental mobility of rubber matrix. (27) Thus, the polymer matrix requires more time for rubber chain rearrangement in response to swelling stress to accommodate solvent molecules. Moreover, incorporated CCB particles diffuse into the crosslinked polymer chains and restrict chain relaxation.

6.3.1.2. Kinetic studies

Various kinetic models are applied to the experimental transport data for a better understanding of the transport mechanism. The model constants and correlation coefficients are presented in **Table 6.2.**

Table 6.2-Correlation coefficients and kinetic model constants of NR/CCB systems

Sample		NB0	NB5	NB10	NB15	NB20
First order kinetics	K	0.0136	0.0134	0.0132	0.0163	0.0155
	R^2	0.8287	0.8390	0.8814	0.8861	0.8907
Higuchi model	k_h	0.0519	0.0518	0.0511	0.0512	0.0508
	R^2	0.8236	0.8226	0.8255	0.8201	0.8216
Korsemayer-Peppas model	K	0.1824	0.1814	0.1759	0.1807	0.1820
	N	0.2753	0.2760	0.2790	0.2745	0.2716
	R^2	0.9741	0.9878	0.9879	0.9864	0.9714
Peppas-Sahlin model	k1	19.7668	13.3063	12.6867	11.5134	19.8209
	k2	-20.2244	-13.8480	-13.1724	-12.0388	-20.3471
	M	-0.0131	-0.0214	-0.0211	-0.0242	-0.0137
	R^2	0.9821	0.9816	0.9829	0.9847	0.9891

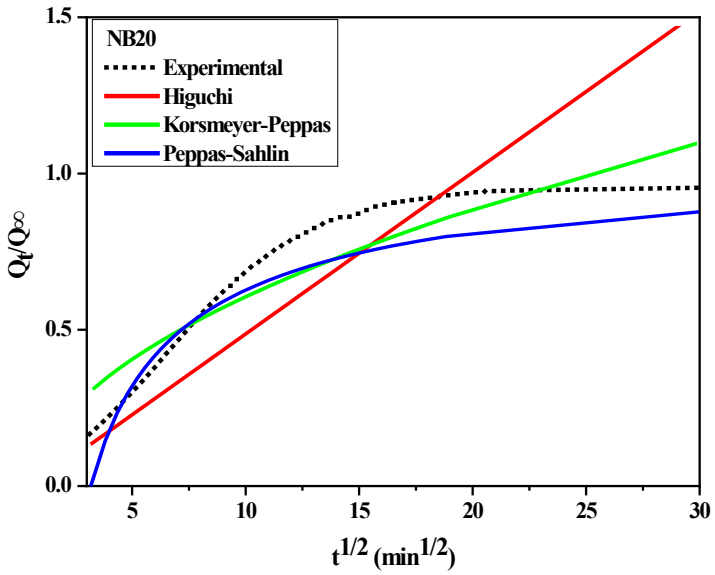

Figure 6.2-Model fitting of solvent permeation of NB20 using Higuchi, Korsmeyer-Peppas and Peppas-Sahlin models

First-order kinetic equation was applied, and the constant k is calculated. Correlation coefficient (R^2) obtained suggests that solvent diffusion in NR/CCB systems does not follow first-order kinetics. Peppas-Sahlin model fits well for the solvent diffusion of NR/CCB systems. In Peppas- Sahlin theoretical prediction, the k_1 values of all compositions are greater than k_2. The constant k_1 decreases with CCB addition up to 15 phr. NB20 has a k_1 value higher than NB0. The constant values obtained suggest a diffusion-controlled transport mechanism in all samples. The chemical potential gradient drives fickian diffusion of solvent molecules in the composites. Theoretical predictions of solvent permeation of NB20 using Higuchi, Korsemayer-Peppas and Peppas-Sahlin models are depicted in **Figure 6.2**.

6.3.1.3. Rubber-filler interactions

Degree of interaction between rubber matrix and CCB can be analysed using Kraus (19), Cunneen-Russel (20) and Lorenz-Park (21) equations. Kraus plot is given in **Figure 6.3(a)**. According to Kraus model, reinforcing fillers have negative slope. (28) $\frac{V_{r0}}{V_{rf}}$ signifies the extent of swelling restriction of the rubber matrix owing to the presence of incorporated filler. Here, as the CCB loading increases, the solvent uptake of the samples decreases. Consequently, the V_{rf} value increases leading to reduction in $\frac{V_{r0}}{V_{rf}}$ values as a function of CCB loading. Kraus plot gives a negative slope, signifying the reinforcement effect of CCB on the rubber matrix. Cunneen-Russel and Lorenz and Park plots of NR/CCB systems are given in **Figure 6.3 (b).** Positive slope indicates the reinforcement effect of filler in rubber matrix. Incorporation of CCB renders positive slope of Cunneen-Russel plot, which again supports the fact that filler effectively interacts with rubber matrix.[22] The $\frac{Q_f}{Q_g}$ values indicate the rubber-filler interaction. A decrease in $\frac{Q_f}{Q_g}$ with filler loading signifies a greater extent of filler-matrix interaction. The Lorenz-Park plot of $\frac{Q_f}{Q_g}$ against e^{-z} gives a straight line with a positive slope of 1.9267 and a y-intercept of - 0.9116 for NR/CCB systems

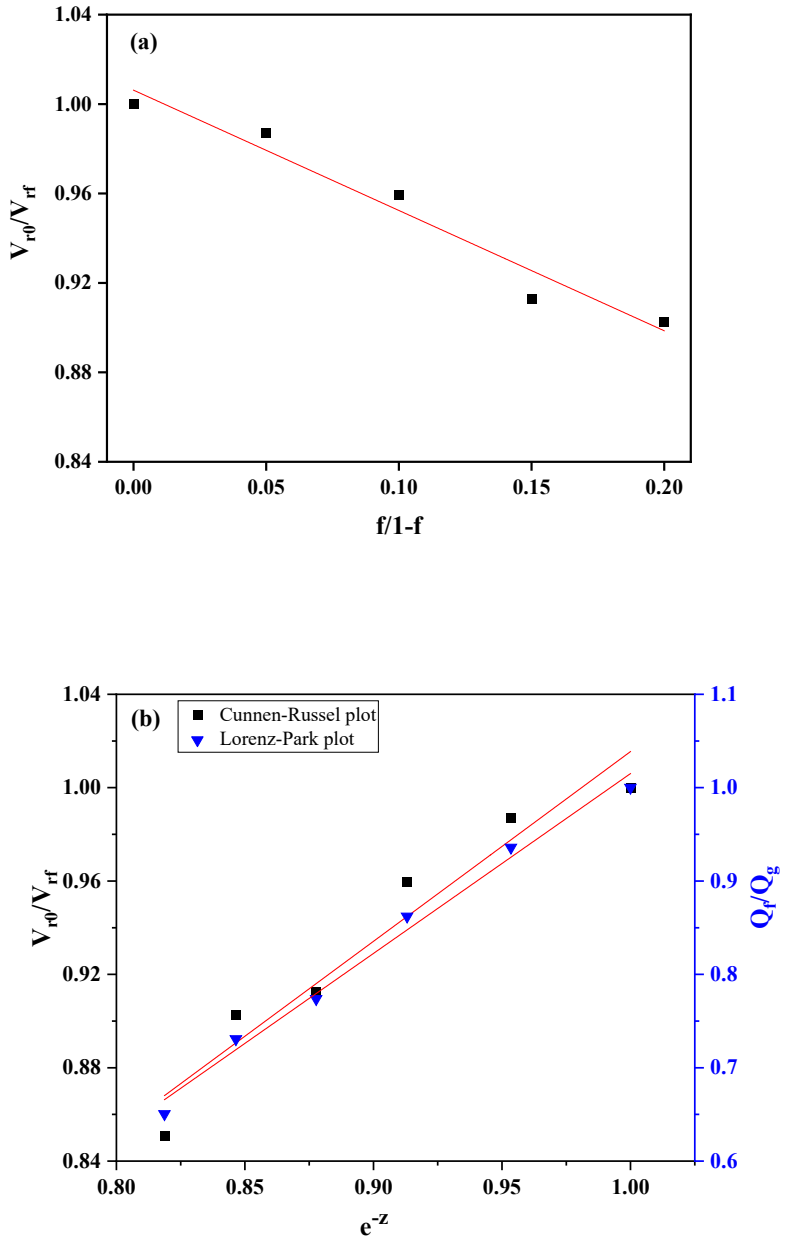

Figure 6.3-(a) Kraus (b) Cunneen-Russel and Lorenz and Park plots of NR/CCB systems

6.3.1.4. Swelling index and crosslink density

The swelling index (%) and swelling coefficient (∝) of NR/CCB systems are presented in **Table 6.3**. The swelling index (%) and swelling coefficient (∝) decrease linearly with an increase in filler loading, indicating the swelling restriction in the filled composites. Filler network formation restricts the movement of solvent particles through the polymer matrix. Swelling values give an insight into the

crosslink density of samples. CCB aggregates occupy the free volume of NR matrix resulting in the decrease in the voids in rubber matrix. The incorporation of fillers offers a tortuous path for diffusing solvent molecules. Thus, the solvent uptake of the filled composites decreases. The volume fraction of rubber in solvent-swollen composites (V_{rf}), apparent crosslink density ($\frac{1}{Q}$) and crosslink density ($\boldsymbol{v}$) of NR/CCB systems are presented in **Table 6.3**. The extent of crosslinking can be deducted from the V_{rf} values of the composites. V_{rf} values are gradually increasing with the filler loading, pointing towards the better interaction of rubber-filler and the formation of crosslinks. Apparent crosslink density values given by $\frac{1}{Q}$ also support the same. Similarly, the crosslink density of the composites also increases constantly with filler loading. It further supports the reinforcement effect of CCB in NR matrix. The values of crosslink density indicate the physical and chemical crosslinks in the system, such as sulfidic linkages, filler-filler and filler-rubber interactions. (29)

Table 6.3- Swelling index (%), swelling coefficient ($\propto$), volume fraction of rubber in solvent-swollen composites (V_{rf}), apparent crosslink density ($\frac{1}{Q}$) and crosslink density ($\boldsymbol{v}$) of NR/CCB systems

Sample	Swelling index (%)	Swelling coefficient, $\propto$	V_{rf}	$\frac{1}{Q}$	v (g/mol/cm^3)
NB0	340	3.92	0.2119	0.29	7.28×10^{-5}
NB5	318	3.67	0.2147	0.31	7.49×10^{-5}
NB10	293	3.38	0.2208	0.34	7.98×10^{-5}
NB15	263	3.03	0.2322	0.38	8.91×10^{-5}
NB20	248	2.86	0.2347	0.40	9.14×10^{-5}

6.3.2. NR/1-ethyl-3-methylimidazolium chloride modified CCB (NR/ILCCB hybrid filler systems

6.3.2.1. Transport properties

Sorption curves of NR composites with IL modified CCB is given in **Figure 6.4.** The initial rate of sorption is almost similar for both NB20IL1 and NB20IL3. Then, the sorption decreased tremendously for NB20IL3, where the ratio of IL is increased. Sorption involves the initial penetration of solvent molecules and the dispersion of toluene molecules across the rubber matrix. IL modified CCB thus decreases the

transport of toluene molecules through the NR matrix. The key factor contributing to the reduced sorption capacity is the increased crosslink density imparted by IL modification.

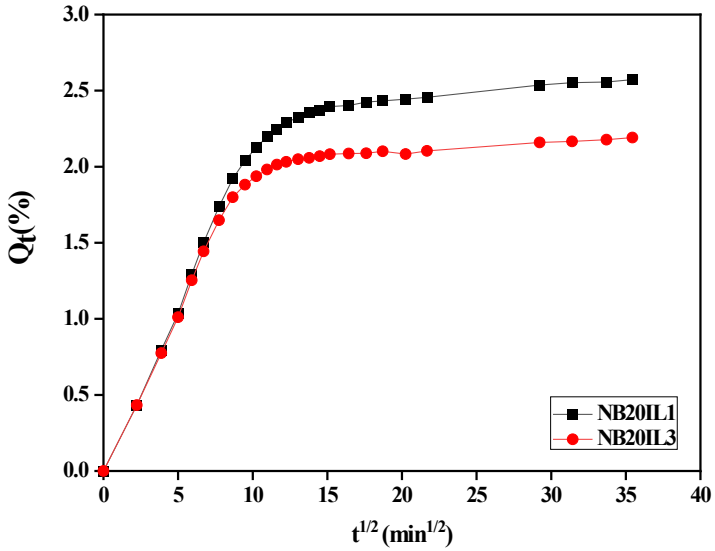

Figure 6.4 – Sorption curves of NR/ILCCB systems

Table 6.4 -Diffusion coefficient, permeability coefficient and parameter n of NR/ILCCB systems

Sample	D (cm^2/s)	P (cm^2/s)	n
NB20IL1	6.45 x 10^{-7}	1.53 x 10^{-6}	0.54
NB20IL3	7.33 x 10^{-7}	1.48 x 10^{-6}	0.51

The diffusion coefficient and permeability coefficient values are given in **Table 6.4.** Chemical interactions of filler and NR increased upon IL modification and caused a reduction in the diffusion of solvent molecules through the matrix. The analysis of the transport mechanism gives the parameter n, which is 0.54 and 0.51 for NB20IL1 and NB20IL3, respectively. This indicates non-Fickian mode of transport. Here, the rate of permeation of solvent molecules and polymer chain relaxation are similar. The presence of ionic liquid decreases the molecular chain relaxation of polymer chains. (27)

6.3.2.2. Kinetic studies

Table 6.5-Correlation coefficients and kinetic model constants of NR/ILCCB systems

Sample		NB20IL1	NB20IL3
First order kinetics	K	0.0137	0.0185
	R^2	0.9744	0.9784
Higuchi model	k_h	0.0762	0.0813
	R^2	0.9730	0.9543
Korsemayer-Peppas model	K	0.0825	0.0869
	N	0.5041	0.5249
	R^2	0.9959	0.9985
Peppas-Sahlin model	k1	-0.3249	-0.1091
	k2	0.3450	0.1737
	M	0.1604	0.2147
	R^2	0.9975	0.9988

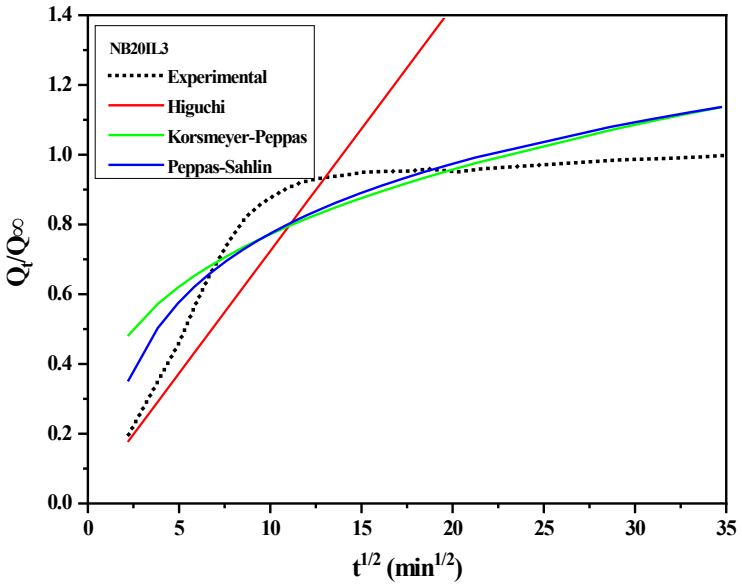

Figure 6.5- Model fitting of solvent permeation of NB20IL3 using Higuchi, Korsmeyer- Peppas and Peppas-Sahlin equations

Table 6.5 presents the model constants and the correlation coefficients obtained by comparing experimental transport data with various kinetic models. Higher correlation coefficient values determine the best fit kinetic model. The Peppas-Sahlin model gives the best fit for the experimental data. Here, k1<k2, which suggests matrix-controlled transport of solvent molecules in IL-modified systems. **Figure 6.5** gives the model fitting of solvent permeation of NB20IL3.

6.3.2.3. Swelling index and crosslink density

Table 6.6- Swelling index (%), swelling coefficient (∝), volume fraction of rubber in solvent-swollen composites (V_{rf}), apparent crosslink density ($\frac{1}{Q}$) and crosslink density (v) of NR/ILCCB systems

Sample	Swelling index (%)	Swelling coefficient ∝	V_{rf}	$\frac{1}{Q}$	v (g/mol/cm^3)
NB20IL1	207	2.39	0.2619	0.48	1.17×10^{-4}
NB20IL3	248	2.86	0.2186	0.40	7.80×10^{-5}

The swelling parameters of IL modified CCB incorporated NR composites are given in **Table 6.6.** As the percentage of IL in the filler increases, the swelling index (%) and swelling coefficient (∝) also increase due to the enhanced chemical interaction. The apparent crosslink density was measured as 1/Q, and the crosslink density estimated using the Flory-Rehner equation decreased as the amount of ionic liquid increased in filled NR composites.

6.3.3. NR/CCB-CNT hybrid filler systems

6.3.3.1. Transport properties

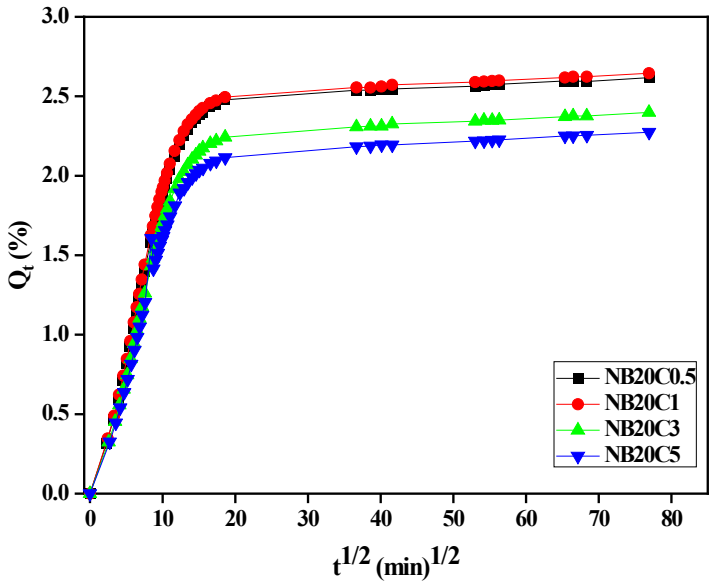

Figure 6.6 – Sorption curves of NR/CCB-CNT hybrid filler systems

Transport properties of NR-CCB/CNT hybrid filler systems are examined in toluene. **Figure 6.6** presents the sorption curves of hybrid filler-incorporated NR matrices. It

shows the rapid increase in toluene absorption, which then attains equilibrium as indicated by the plateau region. As the phr of CNT increases the solvent uptake decreases significantly. It can be attributed to the hybrid filler network formation of spherical CCB and CNT. This observation aligns with findings related to solvent transport in NR systems filled with halloysite nanotubes. (10) A schematic representation detailing the proposed hybrid filler network consisting of CCB and CNT is presented in **Figure 6.7**. **Table 6.4** presents the diffusion coefficient and permeability coefficient values of the NR/CCB/CNT hybrid filler systems. The diffusion coefficient gives the rate of diffusion of solvent molecules into the polymer matrix. Diffusion coefficient value decreases linearly with CCB-CNT loading. Polymer-filler interaction has reduced the availability of free voids, thereby restricting the solvent diffusion through the matrix.

CNT in NR matrix | CCB aggregates in the NR matrix | CNT-CCB network in NR matrix

Figure 6.7- Schematic illustration of hybrid filler network of CCB and CNT in NR matrix

Furthermore, the aspect ratio of CNT is high, and it offers a more tortuous path for the diffusion of solvent molecules compared to the NR/CCB system. **Figure 6.8** illustrates the tortuous path of diffusing solvent molecules in the NR/CCB-CNT hybrid filler systems. Permeability coefficient values decrease steadily with an increase in filler concentration. Permeation coefficient is decreased further upon the introduction of CNT to the single filler system. This is due to the improved filler-matrix interaction and the formation of crosslinks, which creates a hindrance to solvent transport.

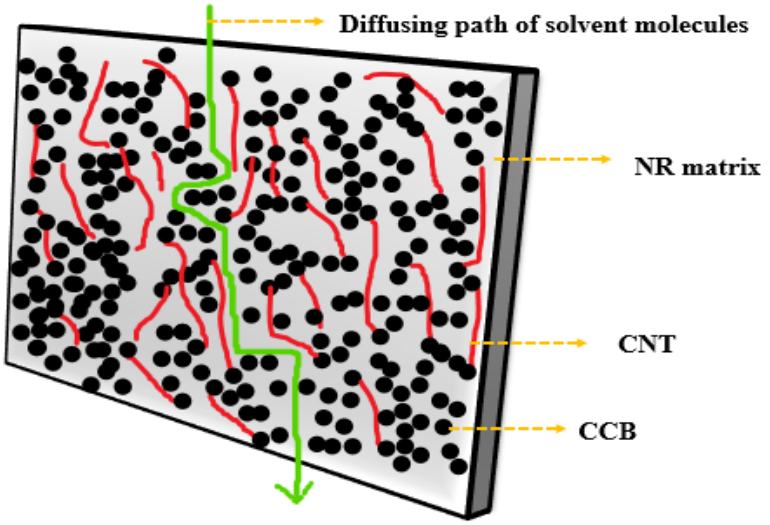

Figure 6.8. Schematic illustration of tortuous path of diffusing molecules in NR/CCB-CNT hybrid filler systems

Table 6.4 -Diffusion coefficient, permeability coefficient and parameter n of NR/CCB-CNT hybrid filler systems

Sample	D (cm^2/s)	P (cm^2/s)	n
NB20C0.5	1.16×10^{-6}	2.79×10^{-6}	0.62
NB20C1	1.10×10^{-6}	2.66×10^{-6}	0.62
NB20C3	1.01×10^{-6}	2.23×10^{-6}	0.62
NB20C5	0.90×10^{-6}	1.88×10^{-6}	0.62

The mode of transport of the composites is analysed, and n values are computed and presented in **Table 6.4**. The n value is 0.62 for all NR/CCB-CNT hybrid filler systems, indicating the non-Fickian mode of transport. (26) Hybrid filler network of CCB and CNT restricts the mobility of NR by physically restricting the movement of polymer chains. The presence of a CCB and CNT hybrid filler network thus restricts the deformation of NR and reduces its swelling capacity upon the penetration of solvent molecules. Thus, a reduced response of NR chains to the swelling stress occurs.

6.3.3.2. Kinetic studies

Constants of various kinetic models are given in **Table 6.5**. Peppas-Sahlin model fits well for the solvent diffusion of NR/CCB-CNT hybrid filler systems. In the Peppas-Sahlin model, the k_1 values of all compositions are greater than k_2. NR/CCB-CNT hybrid filler systems have almost similar k_1 values. The constant values obtained

suggest a diffusion-controlled transport mechanism in all samples. Fickian diffusion of solvent molecules in the composites is driven by the chemical potential gradient. Model fitting of solvent permeation of NB20C3 using Higuchi, Korsemayer-Peppas and Peppas-Sahlin models are depicted in **Figure 6.9**

Table 6.5- Correlation coefficients and kinetic model constants of NR/CCB-CNT hybrid filler systems

Sample		NB20C0.5	NB20C1	NB20C3	NB20C5
First order Kinetics	K	0.0156	0.0151	0.0148	0.0146
	R^2	0.8595	0.8621	0.8766	0.8727
Higuchi model	k_h	0.0293	0.0293	0.0290	0.0291
	R^2	0.9595	0.9656	0.9691	0.9523
Korsemayer- Peppas model	K	0.2189	0.2240	0.1544	0.1546
	N	0.2379	0.2341	0.2716	0.2716
	R^2	0.9846	0.9833	0.9863	0.9808
Peppas-Sahlin model	k1	19.7565	19.7498	19.7363	19.9999
	k2	-20.2367	-20.2425	-20.2549	-20.0001
	M	-0.0136	-0.0138	-0.0139	-0.0046
	R^2	0.9844	0.9868	0.9872	0.9864

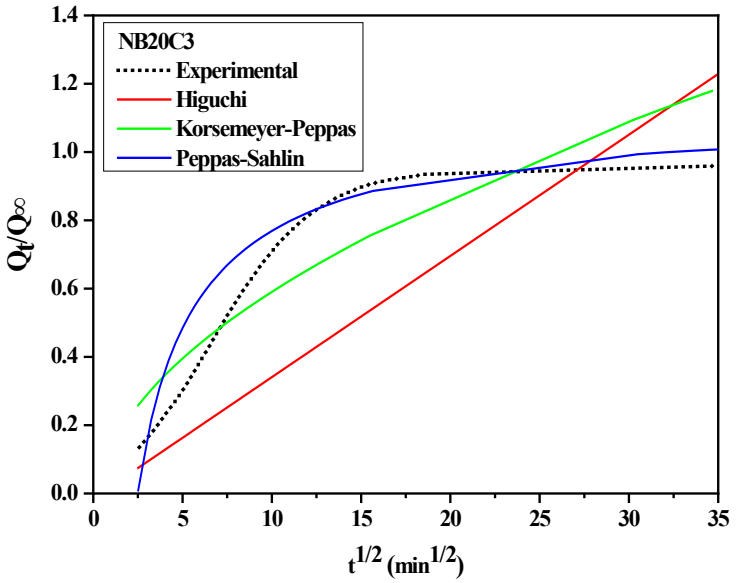

Figure 6.9 - Model fitting of solvent permeation of NB20C3 using Higuchi, Korsmeyer-Peppas and Peppas-Sahlin equations

6.3.3.3. Rubber-filler interactions

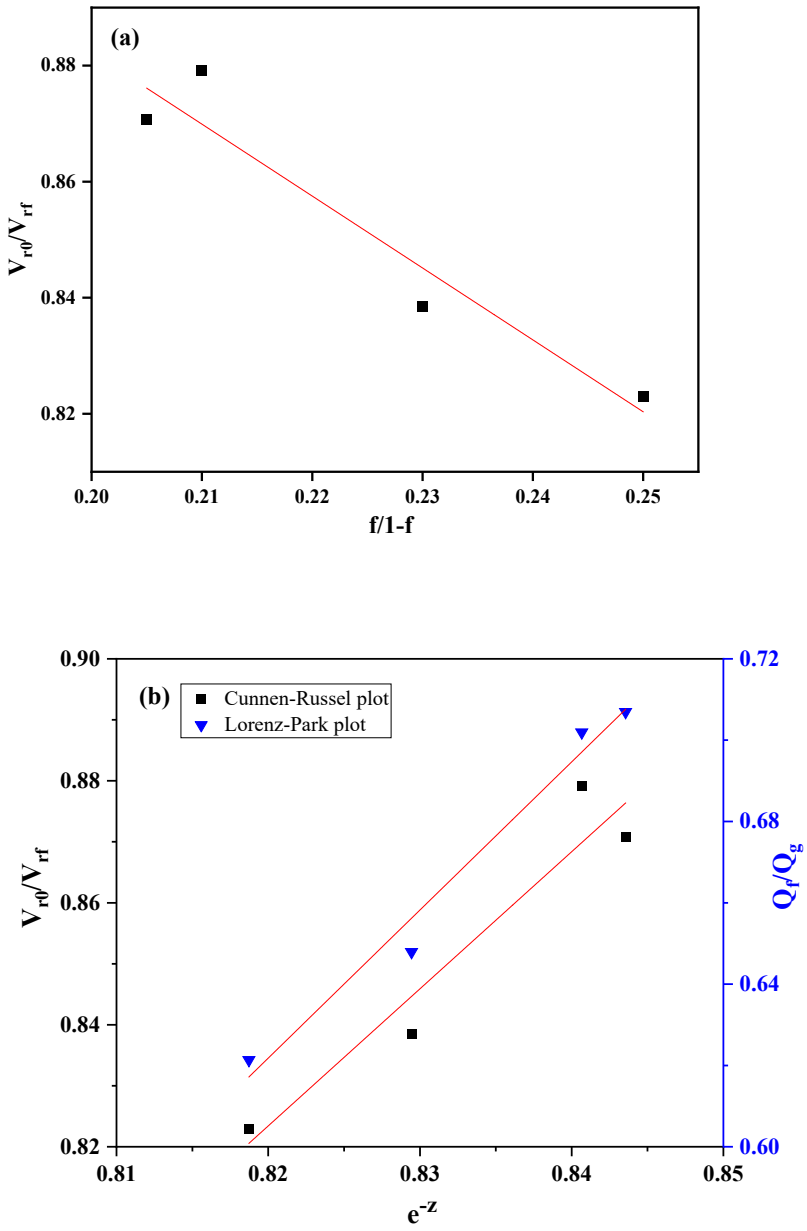

Figure 6.10-(a) Kraus (b) Cunneen-Russel and Lorenz and Park plots of NR/CCB-CNT hybrid filler systems

Figure 6.10 (a-b) presents the Kraus, Cunneen-Russel and Lorenz-Park plots of NR/CCB-CNT hybrid filler systems. Kraus plot of NR/CCB-CNT systems also gives a negative slope, suggesting the synergistic effect of hybrid filler system on the NR matrix. Well-dispersed CCB aggregates and hybrid filler networks of CCB and CNT

create stronger interfaces in the NR matrix. This leads to the restriction of solvent absorption in the NR. NR/CCB-CNT, hybrid filler systems, yield a positive slope of 3.6423 and y-intercept of -2.3649. A higher value of constant a and a lower value of constant b indicates the extent of polymer-filler interaction. (30) The value of constant 'a' increased for hybrid filler incorporated NR than single filler system, suggesting the enhanced polymer-filler interaction for the hybrid system. Higher differences between constant values 'a' and 'b' point towards the distinguished filler-rubber interaction.

6.3.3.4. Swelling index and Crosslink density

Swelling index (%) and swelling coefficient ($\propto$) of NR/CCB/CNT hybrid filler systems are presented in **Table 6.6**. Both swelling index (%) and swelling coefficient ($\propto$) decrease linearly with an increase in filler loading, indicating the swelling restriction in the filled composites. Hybrid filler network formation restricts the movement of solvent particles through the polymer matrix. Swelling values give an insight into the crosslink density of samples. CCB and CNT fillers occupy a free volume of the NR matrix, decreasing the voids in the rubber matrix. Incorporation of fillers offers tortuous path for diffusing solvent molecules. Thus, the solvent uptake of the filled composites decreases.

Table 6.6 -Swelling index (%), swelling coefficient ($\propto$), volume fraction of rubber in solvent-swollen composites (V_{rf}), apparent crosslink density ($\frac{1}{Q}$) and crosslink density ($\boldsymbol{v}$) of NR/CCB-CNT hybrid filler systems

Sample	Swelling index (%)	Swelling coefficient,$\propto$	V_{rf}	$\frac{1}{Q}$	$\boldsymbol{v}$(g/mol/cm^3)
NB20C0.5	240	2.77	0.2404	0.42	9.64×10^{-5}
NB20C1	238	2.75	0.2410	0.42	9.70×10^{-5}
NB20C3	220	2.54	0.2527	0.45	1.08×10^{-4}
NB20C5	211	2.43	0.2575	0.47	1.13×10^{-4}

The volume fraction of rubber in solvent-swollen composites (V_{rf}), apparent crosslink density ($\frac{1}{Q}$) and crosslink density ($\boldsymbol{v}$) of NR/CCB-CNT hybrid filler systems are summarised in **Table 6.6**. The extent of crosslinking in the composites

can be inferred from the V_{rf} values, which show a gradual increase with respect to CNT. This suggests improved interaction between the rubber and filler, along with crosslink formation. Similarly, the apparent crosslink density values obtained from $\frac{1}{Q}$ measurements also support this. The crosslink density of the NR/CCB/CNT hybrid filler systems was consistently enhanced as a function of CNT, providing further evidence of a synergistic effect from the combination of hybrid fillers within the NR matrix.

6.3.4. NR/CCB-1-ethyl-3-methylimidazolium chloride modified CNT (NR/CCB-ILCNT) hybrid filler systems

6.3.4.1. Transport properties

Transport behaviour of NR/CCB-ILCNT hybrid filler systems is depicted in **Figure 6.11**. The sorption of NR composites with 3 phr CNT does not vary with an increase in IL content. However, sorption decreases evidently for 5phr CNT-loaded composites. Also, the initial solvent uptake is lower for 5 phr CNT incorporated composites. Toluene uptake on NR composites decreases as the ratio of IL increases from 1:1 to 1:3.

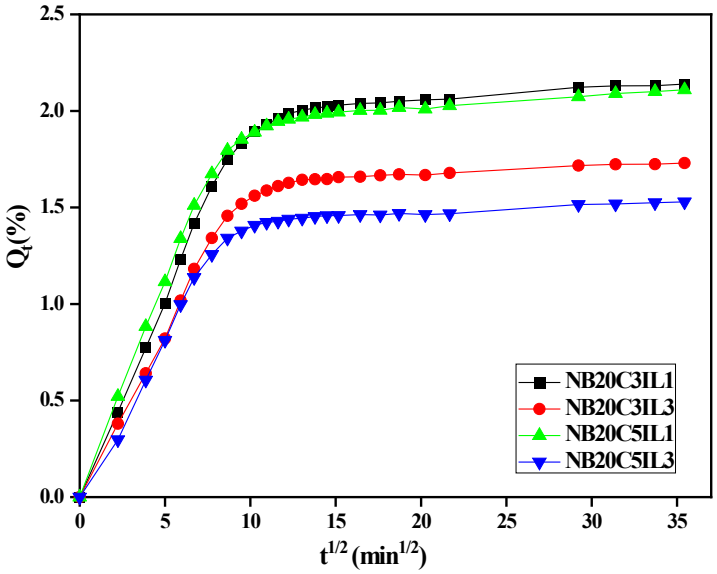

Figure 6.11 – Sorption curves of NR/CCB-ILCNT hybrid filler systems

Diffusion and permeability coefficient values of NR/CCB-ILCNT are summarised in **Table 6.7**.

These values agree with the obtained sorption behaviour; both decrease with increasing filler concentration. Analysis of the mode of transport gives the n value of 0.62. This suggests a non-Fickian mode of transport of solvent molecules across the polymer matrix.

Table 6.7 - Diffusion coefficient, permeability coefficient and parameter n of NR/CCB-ILCNT hybrid filler systems

Sample	D (cm^2/s)	P (cm^2/s)	n
NB20C3IL1	6.67×10^{-7}	1.62×10^{-6}	0.52
NB20C3IL3	6.16×10^{-7}	1.44×10^{-6}	0.50
NB20C5IL1	5.06×10^{-7}	1.34×10^{-6}	0.51
NB20C5IL3	4.72×10^{-7}	9.26×10^{-7}	0.54

6.3.4.2. Kinetic studies

Transport data of the NR/CCB-ILCNT hybrid filler systems are compared to various kinetic models. The model constants and the correlation coefficient values are presented in **Table 6.8**. The R^2 values indicate that the Peppas-Sahlin model best fits experimental transport data. The model fitting curve of experimental transport data of NB20C5IL3 with first-order kinetics, Higuchi, Korsemayer-Peppas and Peppas-Sahlin models are given in **Figure 6.12**.

Table 6.8- Correlation coefficients and kinetic model constants of NR/CCB-ILCNT hybrid filler systems

Sample		NB20C3IL1	NB20C3IL3	NB20C5IL1	NB20C5IL3
First order	k	0.0180	0.0178	0.0199	0.0242
Kinetics	R^2	0.9798	0.9809	0.9853	0.9788
Higuchi model	k_h	0.0960	0.0987	0.1056	0.1072
	R^2	0.9985	0.9981	0.9987	0.9974
Korsemayer-	k	0.0928	0.0953	0.1030	0.0897
Peppas model	n	0.5088	0.5092	0.5437	0.4802
	R^2	0.9984	0.9981	0.9966	0.9978
Peppas-Sahlin	k1	-0.1323	-0.0431	-0.1407	-0.5324
Model	k2	0.2001	0.1298	0.2373	0.5372
	m	0.2022	0.2335	0.1879	0.1486
	R^2	0.9987	0.9981	0.9991	0.9987

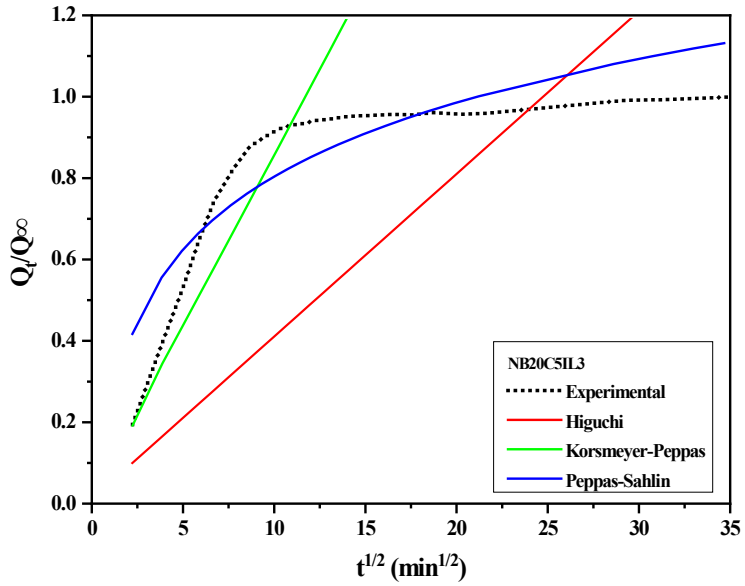

Figure 6.12- Model fitting of solvent permeation of NB20C5IL3 using Higuchi, Korsmeyer- Peppas and Peppas-Sahlin equations

6.3.4.3. Swelling index and crosslink density

Swelling index (%) and swelling coefficient (∝) values are presented in **Table 6.9**. NB20C3IL1 has the lower swelling index and swelling coefficient (∝). Crosslink density values calculated are in agreement with the result as mentioned above. NB20C3IL1 has the highest crosslink density which has least swelling index and swelling coefficient. This may be attributed to the effective filler network formed by the IL-modified CNT and CCB.

Table 6.9 - Swelling index (%), swelling coefficient (∝), volume fraction of rubber in solvent-swollen composites (V_{rf}), apparent crosslink density ($\frac{1}{Q}$) and crosslink density (v) of NR/CCB-ILCNT hybrid filler systems

Sample	Swelling index (%)	Swelling coefficient, ∝	V_{rf}	$\frac{1}{Q}$	v (g/mol/cm^3)
NB20C3IL1	162.1	1.87	0.3135	0.62	1.79 x 10^{-4}
NB20C3IL3	201.0	2.32	0.2676	0.50	1.23 x 10^{-4}
NB20C5IL1	198.2	2.29	0.2681	0.50	1.24 x 10^{-4}
NB20C5IL3	167.5	1.93	0.2987	0.60	1.59 x 10^{-4}

6.3.5. NR/CCB-CNT-RGO hybrid filler systems

6.3.5.1. Transport properties

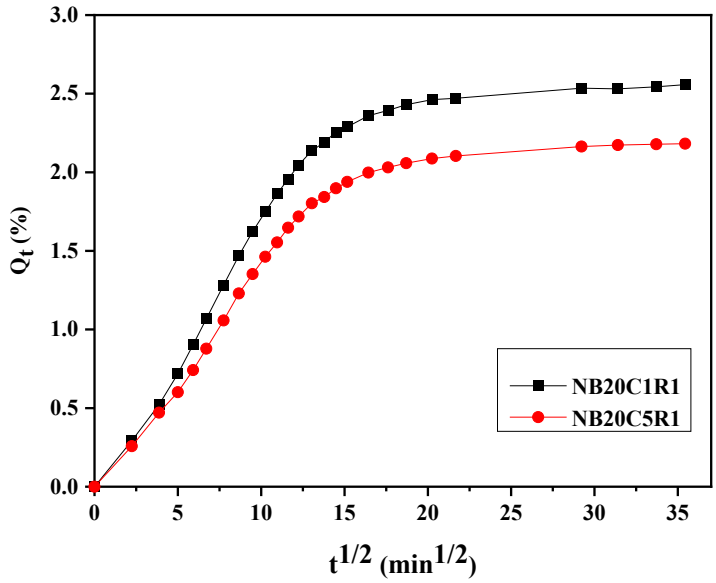

Figure 6.13 – Sorption curves of NR/CCB-CNT-RGO hybrid filler systems

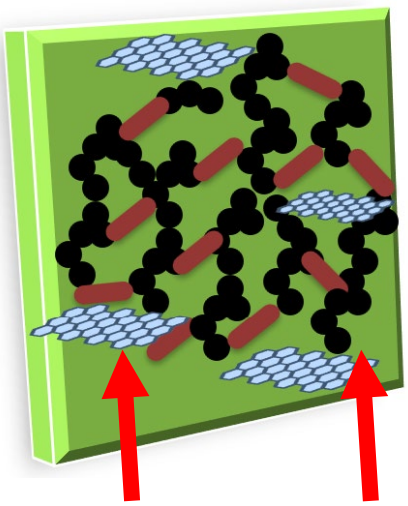

Figure 6.14-Schematic representation of barrier effect of filler network in NR/CCB-CNT-RGO composites

Sorption curves of NR/CCB-CNT-RGO hybrid filler systems are presented in **Figure 6.13.** The solvent uptake is found to depend on the amount of CNT. Toluene uptake is lower for NB20C5R1, with higher CNT content than NB20C1R1. The hybrid network formed by the CCB, CNT and RGO restricts the solvent transport across the polymer matrix. The high aspect ratio of CNT and RGO enhances the contact surface area of the filler and the matrix. The network of cylindrical CNT, spherical CCB, and

the planar graphitic structure of RGO provides a tortuous path for transporting solvent molecules. This hybrid network, with its complex structure, limits the initial solvent transport and leads to a decrease in solvent uptake as sorption progresses. **Figure 6.14** illustrates the schematic representation of filler network in NR/CCB-CNT-RGO hybrid filler systems that offer restriction to solvent diffusion. The diffusion and permeability coefficient values of the composites are presented in **Table 6.10.** Both diffusion and permeability coefficient decreases, indicating a restricted pathway for the solvent molecules across the polymer chain. The mode of transport analysed gives n value between 0.5 and 1, which indicates the non-Fickian mode of transport.

Table 6.10 - Diffusion coefficient, permeability coefficient and parameter n of NR/CCB-CNT-RGO hybrid filler systems

Sample	D (cm^2/s)	P (cm^2/s)	n
NB20C1R1	9.35×10^{-7}	2.20×10^{-6}	0.6
NB20C5R1	9.27×10^{-7}	1.86×10^{-6}	0.57

6.3.5.2. Kinetic studies

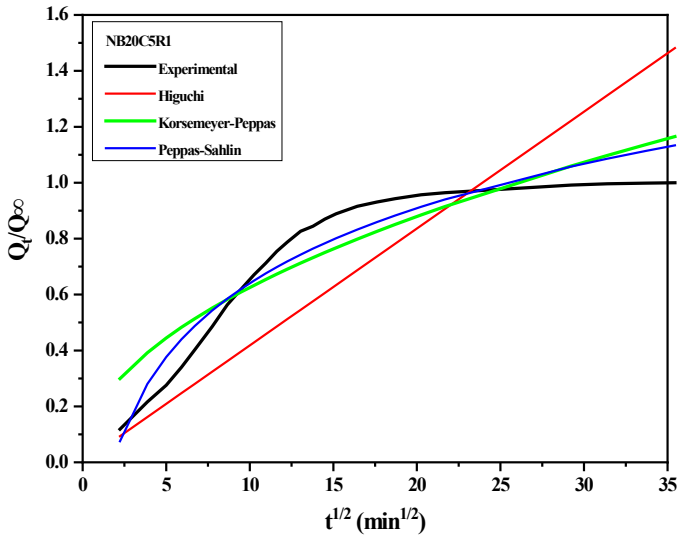

Figure 6.15- Model fitting of solvent permeation of NB20C5R1 using Higuchi, Korsmeyer- Peppas and Peppas-Sahlin equations

Table 6.11- Correlation coefficients and kinetic model constants of NR/CCB-CNT-RGO hybrid filler systems

Sample	Model parameters	NB20C1R1	NB20C5R1
First order kinetics	k	0.0100	0.0098
	R^2	0.9656	0.9668
Higuchi model	k_h	0.0596	0.0588
	R^2	0.9721	0.9753
Korsemayer-Peppas model	k	0.0477	0.0490
	n	0.5531	0.5445
	R^2	0.9837	0.9867
Peppas-Sahlin model	k1	-0.1687	-0.0904
	k2	0.1726	0.1134
	m	0.1985	0.2240
	R^2	0.9982	0.9983

Experimental transport data was computed theoretically by employing various models such as order kinetics, Higuchi, Korsemayer-Peppas and Peppas-Sahlin models. The Correlation coefficients and kinetic model constants obtained are plotted in **Table 6.11.** Peppas-Sahlin model fits well with experimental solvent transport data, as indicated by the R^2 value of 0.998. **Figure 6.15** shows the model fitting of experimental transport data of NB20C5R1 using First-order kinetics, Higuchi, Korsemayer-Peppas, and the Peppas-Sahlin model.

6.3.5.3. Swelling index and crosslink density

Swelling parameters like swelling index (%) and swelling coefficient ($\propto$) are given in **Table 6.12.**

Table 6.12 - Swelling index (%), swelling coefficient ($\propto$), volume fraction of rubber in solvent-swollen composites (V_{rf}), apparent crosslink density ($\frac{1}{Q}$) and crosslink density (ν) of NR/CCB-CNT-RGO hybrid filler systems

Sample	Swelling index (%)	Swelling coefficient, $\propto$	V_{rf}	$\frac{1}{Q}$	ν (g/mol/cm^3)
NB20C1R1	232	2.68	0.2446	0.43	1.00×10^{-4}
NB20C5R1	204	2.35	0.2634	0.49	1.19×10^{-4}

Swelling index (%) decreases from 232 to 204 when the amount of CNT increased. Similarly, the swelling coefficient also decreases as the amount of CNT increases in the hybrid filler system of CCB, CNT and RGO. Consistent reduction in both the swelling index and swelling coefficient as the CNT content is increased indicates the influence of CNT concentration on the swelling behaviour of NR hybrid filler systems. This can be attributed to the enhanced dispersion and improved interaction of filler in the polymer matrix. The high aspect ratio of CNT results in a large surface area for interaction with other fillers and matrix. The interconnected network between CNT, CCB and RGO offers a more effective barrier against penetration of swelling agents by reducing the free volume available for swelling molecules. RGO prevents the reagglomeration of CNT in matrix, while CNT and CCB can bridge the gap between RGO layers. Effective dispersion of hybrid fillers in the matrix, combined with crosslinking, results in the formation of a barrier that inhibits the penetration of solvents. (10) Well dispersed hybrid filler system of CCB, CNT and RGO within NR network creates hinderance for solvents to infiltrate the composite material. Also, increased interaction between the fillers within the composite leads to a higher crosslink density and strong network that acts as an obstacle to solvent uptake. This is supported by the apparent crosslink density and actual crosslink density values in **Table 6.12**. It is calculated using the Flory-Rehner equation and is higher for NB20C5R1, implying that the addition of CNT has created more crosslinks in the polymer matrix. This is attributed to the π electrons in the graphitic structure of CCB, CNT and RGO, which causes π-π interactions between the fillers. (**Figure 6.16**) This van der Waals interaction can increase the distribution of fillers in the matrix and establish a hybrid filler network.

6.4. Comparative analysis of transport properties

Table 6.13 presents the equilibrium solvent uptake and swelling index (%) of NR composites. Equilibrium solvent uptake decreased, and crosslink density increased by 27% of NB20 compared to unfilled NR. The addition of CNT further reinforced the composite, decreasing solvent absorption and swelling. Reinforcing fillers reduces the free voids present in the matrix. The presence of IL in the NR matrix caused slight reductions in solvent uptake and swelling, suggesting potential

interactions between IL and the rubber. Equilibrium solvent uptake has decreased by 40%, and crosslink density increased by 38% for NB20C5. NB20C5IL3 exhibits a 60% decrease in equilibrium solvent uptake and corresponding increase of 51% of crosslink density. The combination of spherical CCB, cylindrical CNT and layered RGO filler structures creates a complex and interconnected network in NR. The entanglement of polymer chains with the filler network inhibits their movement, increasing stiffness and reduced flexibility. This restricted mobility contributes to

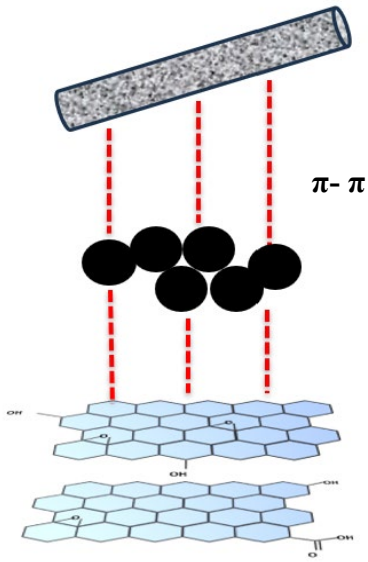

Figure 6.16- Schematic illustration of π-π interactions between CCB, CNT and RGO

reduced transport properties.

Table 6.13 -Equilibrium solvent uptake, Swelling index (%) and crosslink density (v) of NR hybrid filler systems

Sample	Equilibrium solvent uptake	Swelling index (%)	v (g/mol/cm^3)
NB0	3.77	339.6	7.28×10^{-5}
NB20	2.74	248.2	9.14×10^{-5}
NB20C5	2.27	211	1.13×10^{-4}
NB20IL3	2.19	248.2	7.80×10^{-5}
NB20C5IL3	1.52	167.5	1.59×10^{-4}
NB20C5R1	2.18	203.9	1.19×10^{-4}

6.5. Conclusion

Solvent transport of NR is observed to decrease for a hybrid filler system compared to the incorporation of a single filler. NR/CCB-ILCNT hybrid filler systems exhibit lowest swelling index (%) and highest crosslink density. Chemical and physical interactions of IL-modified CNT and CCB with NR increase the crosslink density of composites and restrict the solvent transport. NR/CCB-CNT-RGO hybrid filler systems also exhibit high crosslink density. The computation of kinetic parameters from transport data reveals that the Peppas-Sahlin model aligns well with experimental observations. This suggests that the transport mechanism is controlled by diffusion.

6.6. References

1. Zhang M, Biesold GM, Choi W, Yu J, Deng Y, Silvestre C, et al. Recent advances in polymers and polymer composites for food packaging. Materials Today. 2022 Mar 1;53:134–61.
2. Swapna VP, Jose T, George SC, Thomas S, Stephen R. Pervaporation separation of an azeotropic mixture of a tetrahydrofuran–water system with nanostructured polyhedral oligomeric silsesquioxane embedded poly(vinyl alcohol). Journal of Applied Polymer Science. 2019 Feb 15;136(7):47060.
3. Swapna VP, Thomas SP, Jose T, Moni G, George SC, Thomas S, et al. Mechanical properties and pervaporation separation performance of CTAB-modified cage-structured POSS-incorporated PVA membrane. Journal of Materials Science. 2019 Jun 1;54(11):8319–31.
4. Swapna VP, Nambissan PMG, Thomas SP, Vayyaprontavida Kaliyathan A, Jose T, George SC, et al. Free volume defects and transport properties of mechanically stable polyhedral oligomeric silsesquioxane embedded poly(vinyl alcohol)-poly(ethylene oxide) blend membranes. Polymer International. 2019 Jul 1;68(7):1280–91.
5. Swapna VP, Kaliyathan AV, Abhisha VS, Maria HJ, Nambissan PMG, Thomas S, et al. Changes in free volume and gas permeation properties of poly(vinyl alcohol) nanocomposite membranes modified using cage-structured polyhedral oligomeric silsesquioxane. Journal of Applied Polymer Science. 2021 Mar 10;138(10):49953.
6. Stephen R, Joseph K, Oommen Z, Thomas S. Molecular transport of aromatic solvents through microcomposites of natural rubber (NR), carboxylated styrene butadiene rubber (XSBR) and their blends. Composites Science and Technology. 2007;67(6):1187–94.
7. Thomas S, George SC, Jose T, editors. Polymer nanocomposite membranes for pervaporation. Amsterdam Kidlington Cambridge: Elsevier; 2020. 423 p. (Micro & nano technologies series).
8. Li D, Yan Y, Wang H. Recent advances in polymer and polymer composite membranes for reverse and forward osmosis processes. Progress in Polymer Science. 2016 Oct 1;61:104–55.
9. Liu M, Cataldi P, Young RJ, Papageorgiou DG, Kinloch IA. High-performance fluoroelastomer-graphene nanocomposites for advanced sealing applications. Composites Science and Technology. 2021;202:108592.
10. Ekebafe L, Nworie EC, Mahmud H. Mechanical and sorption indices of ZnO-rGO hybrid filled natural rubber nanocomposites.
11. Abhisha V, Augustine A, Joseph J, Thomas SP, Stephen R. Effect of halloysite nanotubes and organically modified bentonite clay hybrid filler system on the properties of natural rubber. Journal of Elastomers & Plastics. 2020 Aug;52(5):432–52.
12. Thomas S, Abraham J, George SC, Thomas S. Role of CNT/clay hybrid on the mechanical, electrical and transport properties of NBR/NR blends. Polymer Bulletin. 2020 Jan 1;77(1):1–16.

13. Maria HJ, Lyczko N, Nzihou A, Mathew C, George SC, Joseph K, et al. Transport of organic solvents through natural rubber/nitrile rubber/organically modified montmorillonite nanocomposites. Journal of Materials Science. 2013;48(15):5373–86.
14. Sambhudevan S, Shankar B, Appukuttan S, Joseph K. Evaluation of kinetics and transport mechanism of solvents through natural rubber composites containing organically modified gadolinium oxide. Plastics, Rubber and Composites. 2016;45(5):216–23.
15. Korsmeyer RW, Gurny R, Doelker E, Buri P, Peppas NA. Mechanisms of solute release from porous hydrophilic polymers. International Journal of Pharmaceutics. 1983;15(1):25–35.
16. Jose JP, Thomas S. XLPE based Al2O3–clay binary and ternary hybrid nanocomposites: self-assembly of nanoscale hybrid fillers, polymer chain confinement and transport characteristics. Phys Chem Chem Phys. 2014;16(37):20190–201.
17. A. Peppas N, J. Sahlim J. A simple equation for the description of solute release. III. Coupling of diffusion and relaxation. International journal of pharmaceutics. 1989;57:169–72.
18. Zachariah AK, Kumar Chandra A, Mohamed PK, Parameswaranpillai J, Thomas S. Mixed mode morphology in elastomeric blend nanocomposites: Effect on vulcanisation, thermal stability and solvent permeability. Polymer Composites. 2018;39:E1659–68.
19. Kraus G. Swelling of filler-reinforced vulcanizates. Journal of Applied Polymer Science. 1963 May 1;7(3):861–71.
20. Cunneen JI, Russell RM. Occurrence and Prevention of Changes in the Chemical Structure of Natural Rubber Tire Tread Vulcanizates during Service. Rubber Chemistry and Technology. 1970 Sep 1;43(5):1215–24.
21. Lorenz O, Parks CR. The crosslinking efficiency of some vulcanising agents in natural rubber. Journal of Polymer Science. 1961 Apr 1;50(154):299–312.
22. Ellis B, Welding GN. Estimation, from Swelling, of the Structural Contribution of Chemical Reactions to the Vulcanization of Natural Rubber. Part II. Estimation of Equilibrium Degree of Swelling. Rubber Chemistry and Technology. 1964 May 1;37(2):571–5.
23. Thomas S, Wilson R, Anil Kumar S, George SC, editors. Transport properties of polymeric membranes. Amsterdam, Netherlands ; Cambridge, MA, United States: Elsevier; 2018. 700 p.
24. Rogers CE, Semancik JR, Kapur S. Transport Processes in Polymers. In: Lenz RW, Stein RS, editors. Structure and Properties of Polymer Films: Based upon the Borden Award Symposium in Honor of Richard S Stein, sponsored by the Division of Organic Coatings and Plastics Chemistry of the American Chemical Society, and held in Boston, Massachusetts, in April 1972 [Internet]. Boston, MA: Springer US; 1973. p. 297–319. Available from: https://doi.org/10.1007/978-1-4615-8951-8_17
25. Danwanichakul P, Jaroenkarn S, Jumpathi P, Dechojarassri D. Sorption and desorption of toluene, m-xylene, p-cresol and water by natural rubber chips. 2006;12.
26. Kaliyathan AV, Rane AV, Jackson S, Thomas S. Analysis of diffusion characteristics for aromatic solvents through carbon black filled natural rubber/ butadiene rubber blends. Polymer Composites. 2021 Jan;42(1):375–96.
27. Therattil J. Transport Of Organic Solvents Through Ionic Liquid Modified Natural Rubber/MWCNT Composites. 2020;9(04):10.
28. Gobetti A, Cornacchia G, La Monica M, Zacco A, Depero LE, Ramorino G. Assessment of the influence of electric arc furnace slag as a non-conventional filler for Nitrile Butadiene Rubber. Results in Engineering. 2023 Mar 1;17:100987.
29. Fu W, Wang L, Huang J, Liu C, Peng W, Xiao H, et al. Mechanical Properties and Mullins Effect in Natural Rubber Reinforced by Grafted Carbon Black. Advances in Polymer Technology. 2019;2019:1–11.
30. Zachariah AK, Chandra AK, Mohammed PK, Parameswaranpillai J, Thomas S. Experiments and modeling of non-linear viscoelastic responses in natural rubber and chlorobutyl rubber nanocomposites. Applied Clay Science. 2016;123:1–10.

Chapter 7

Thermal Degradation and Kinetic Studies of NR Hybrid filler systems

Summary

This chapter evaluates the thermal degradation stability of natural rubber (NR) hybrid filler systems using thermogravimetric analysis (TGA) and discusses the thermal degradation mechanisms. Experimental data is analysed using the Coats-Redfern, Kissinger, Kissinger-Akahira-Sunose (KAS), and Flynn-Wall-Ozawa (FWO) model. Furthermore, this chapter gives an insight into the activation energy derived from the kinetic models of thermal degradation for NR composite systems.

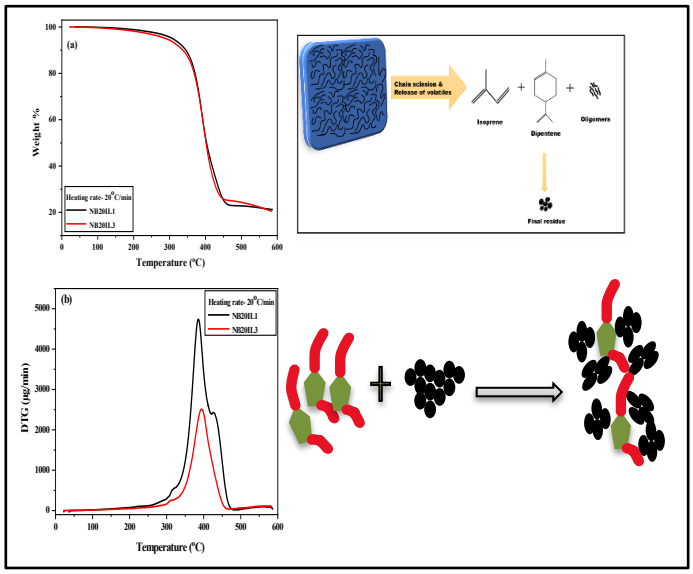

7.1. Introduction

Thermogravimetric analysis (TGA) is used to study the thermal degradation of composites with respect to variations in temperature and time. It also provides information about the thermal degradation stability of samples. This analysis can be performed under both isothermal and non-isothermal conditions. In the isothermal method, the temperature of the furnace is constant, and the degradation of the sample is determined over time, while in the non-isothermal method, the temperature of the furnace increases linearly with time due to the constant heating rate, and weight loss is measured with respect to both time and temperature.

Theoretical model analysis of thermal data helps to interpret the thermal behaviour of the polymer composites, offering keen insights into their degradation pathways and overall stability. To obtain accurate parameters, it is necessary to monitor heating curves at different heating rates. (5) Among the various kinetic models available, the one that aligns best with experimental data through a linear fit is often considered to be the suitable one.

7.2. Theoretical models for thermal analysis

Degradation kinetics of polymer composites can be comprehensively understood through various theoretical approaches. Among these approaches, the Coats-Redfern model is a model-based method that stands out as an exceptionally suitable and widely employed for the kinetic analysis of NR composites. There are also model-free methods and isoconversional methods such as the Kissinger method, the Kissinger-Akahira-Sunose (KAS) method and the Flynn- Wall-Ozawa (FWO) method to analyse the thermal degradation kinetics.

7.2.1. Coats-Redfern model

The Coats-Redfern equation for n= 1 is given below,

$$\log\left[\frac{-\log(1-\alpha)}{T^2}\right] = log\left(\frac{AR}{\beta E_a}\right)\left[\frac{1-2RT}{E_a}\right] - \frac{E_a}{2.303RT} \quad (7.1)$$

where α is the fractional mass loss at time t, T is the absolute temperature, A is the pre-exponential factor, R is the universal gas constant, β is the heating rate and E_a is the activation energy. A plot of $\log\left[\frac{-\log(1-\alpha)}{T^2}\right]$ as a function of $\frac{1}{T}$ gives a straight line with the slope equal to $\left[-\frac{E_a}{2.303RT}\right]$and the y-intercept is $log\left(\frac{AR}{\beta E_a}\right)\left[\frac{1-2RT}{E_a}\right]$. It is to be noted that in the employed Coats-Redfern equation, a reaction order of 1

was assumed. This choice could potentially account for the observed fluctuations in activation energy values across the data.

7.2.2. Kissinger method

The Kissinger method(6) which is based on the Arrhenius equation, provides a straight forward way to determine the apparent activation energy. Arrhenius equation for a simple thermal degradation reaction,

$$A_{solid} \rightarrow B_{solid} + C_{gas} \tag{7.2}$$

is given by,

$$k = Ae^{-E_a/RT} \tag{7.3}$$

The reaction rate is given by,

$$\frac{d\alpha}{dt} = kf[\alpha] \tag{7.4}$$

where t is the reaction time in seconds and α is the conversion degree. The α is calculated from the following equation,

$$\alpha = \frac{w_0 - w_t}{w_0 - w_\infty} \tag{7.5}$$

where W_o is the initial weight, W_t is the actual weight and W_∞ is the final weights of the composite samples in the TGA curves. $f[\alpha]$ depends on the specific degradation mechanism. Combining above equations gives,

$$\frac{d\alpha}{dt} = Ae^{-E_a/RT} f[\alpha] \tag{7.6}$$

In thermal degradation, the heating time determines the temperature, therefore,

$$\frac{d\alpha}{dt} = \frac{d\alpha}{dT}\frac{dT}{dt} = \beta\frac{d\alpha}{dT} \tag{7.7}$$

β is the heating rate given in K/min. From the above equations, we can write,

$$\frac{d\alpha}{dt} = \frac{A}{\beta} f[\alpha] e^{-E_a/RT} \tag{7.8}$$

Integration and rearrangement give,

$$g(\alpha) = \int_0^{\infty\Delta} \frac{d\alpha}{f(\alpha)} = \frac{A}{\beta}\int_0^T e^{-E_a/RT}\, dT = \frac{ART^2}{\beta E_a}\left(1 - \frac{2RT}{E_a}\right) e^{-E_a/RT} \tag{7.9}$$

where $g(\alpha)$ is the integral function of α. For different solid reactions of thermal degradations, $g(\alpha)$ has different expressions which is reflected in the thermal degradation curves.(7)

Kissinger method assumes that the maximum reaction rate occurs at the peak of the degradation rate with an increase in the reaction temperature. This method assumes a consistent activation energy throughout the conversion process.(8) The Kissinger method adopts the following equation:

$$\ln\left(\frac{\beta}{T_{max}^2}\right) = \ln\frac{AR}{E_a} + \ln[n(1-\alpha_{max})^{n-1}] - \frac{E_a}{RT_{max}} \quad (7.10)$$

T_{max} is the temperature at the inflection point of TGA curve and α_{max} is the conversion degree at the inflection point. Plotting $\ln\left(\frac{\beta}{T_{max}^2}\right)$ against $\frac{1}{T_{max}}$ gives a straight line and the slope of the straight line, $-\frac{E_a}{R}$ gives the apparent activation energy. The merit of this method is its ability to analyse complex thermally induced processes without prior knowledge of the underlying mechanism.

7.2.3. Kissinger-Akahira-Sunose (KAS) method

The Kissinger-Akahira-Sunose (KAS) method (6,9) relies on isoconversional analysis and calculate activation energy as a function of conversion degree at different heating rates. This is a non-isothermal method developed from the Arrhenius equation employing differential method. This method does not necessitate precise knowledge of thermal degradation mechanism.(10) The equation for the KAS method is given below,

$$\ln\left(\frac{\beta}{T^2}\right) = \ln\frac{AR}{E_a g(\propto)} - \frac{E_a}{RT} \quad (7.11)$$

where $g(\propto)$ is the integral conversion function indicating reaction model. At constant $\propto$, $\ln\left(\frac{\beta}{T^2}\right)$ versus $\frac{1000}{T}$ at different heating rates gives a straight line with slope $-\frac{E_a}{R}$, from which activation energy can be calculated.

7.2.4. Flynn- Wall-Ozawa (FWO) method

The Flynn-wall-Ozawa (FWO) method (11) also relies on isoconversional analysis to calculate the activation energy which varies with the conversion degree at various heating rates. The equation employed for FWO method is

$$\log\beta = \left\{\log\left[\frac{AE_a}{Rg(\alpha)}\right] - 2.315\right\} - \frac{0.457E_a}{RT} \quad (7.12)$$

At given α, plot of $\log\beta$ against $\frac{1}{T}$ gives fitted straight line. The activation energy can be determined from the slope $(-\frac{0.457E_a}{R})$. The activation energy calculated using FWO method is independent of thermal degradation reaction mechanism.

7.3. Results and discussion

The non-isothermal thermogravimetric analysis of the samples was conducted in the temperature range of 30°C to 580°C under the N_2 atmosphere, using multiple heating rates. Weight loss curves and differential thermogravimetric analysis (DTG) curves of the samples were plotted at a heating rate of 20°C min^{-1}. Additionally, TGA at 10°C min^{-1} and 15°C min^{-1} was employed to calculate the activation energy using kinetic degradation models.

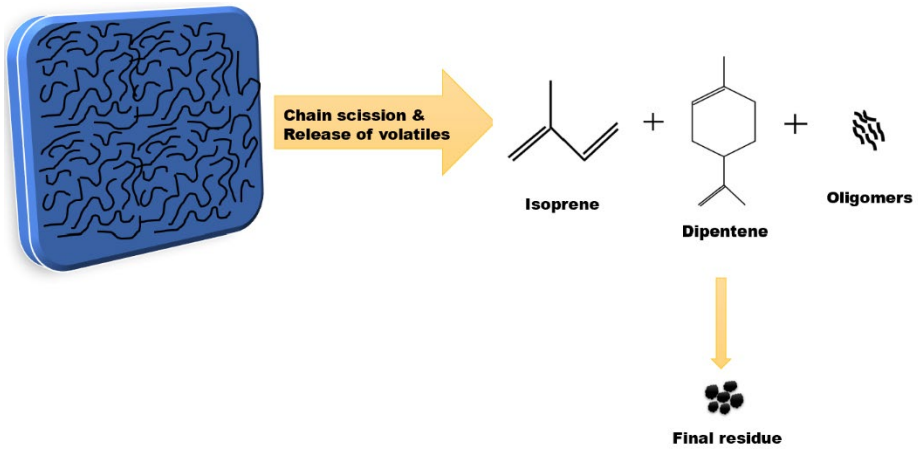

Figure 7.1- Schematic representation of thermal degradation of NR

Thermal decomposition of NR involves depolymerization through the radical mechanism, giving rise to compounds such as isoprene, dipentene and other oligomers.(1) The random scission kinetic model proposed for NR degradation postulates a chaotic cleavage of polymer backbone bonds, leading to the gradual formation of shorter molecular fragments. These fragments eventually vaporize when their size becomes sufficiently small, and this vaporization is directly detected through thermogravimetry. The process of random scission involves the generation of free radicals at various points within the polymer chains, resulting in the production of oligomers with diverse chain lengths. Moreover, the proportion of monomers to oligomers in the degradation products can be modulated by the temperature of decomposition.(2,3) Upon degradation, the primary products identified from the rubber are isoprene, dipentene, and various oligomers.(4) Post-degradation, the residual insoluble fraction predominantly contains recombined long-chain radicals, supplemented with fillers and other additive components. **Figure 7.1** illustrates the schematic representation of thermal degradation of NR.

Understanding the distinct phases of degradation, such as the diffusion of depolymerization products, is important for providing information on the intricate chemical and physical transitions that occur when a material undergoes thermal breakdown.

7.3.1. NR/CCB systems

7.3.1.1. TGA analysis and thermal stability

TGA and DTG patterns of unfilled NR and CCB filled NR composite systems at a heating rate of 20°C min^{-1} are presented in **Figure 7.2 (a)** and **(b)**, respectively. Thermograms show single-step degradation for NB0 and NB10, while NB20 has multi-stage decomposition as represented by the presence of shoulder peak in DTG. Weight loss percentage is higher for CCB filled samples compared to the unfilled NR at temperatures below 350°C. However, at temperatures above 350°C, the CCB filled composites exhibit higher stability. Also, thermal stability at high temperatures increases with CCB loading. DTG curves of NR/CCB systems show a major weight loss peak in the temperature range of 370-390°C. Peak intensity on the DTG curves signifies the rate at which weight loss occurs at a specific temperature during the thermal degradation process. A higher peak intensity indicates a more rapid decomposition of the material at that particular temperature range. Addition of CCB has led to a noticeable reduction in the DTG peak intensity, suggesting an enhancement in heat resistance. Moreover, increasing the CCB content to 20 phr has resulted in an additional improvement in the thermal stability of the NR composite.

Table 7.1 shows the degradation temperatures at 10, 50 and 75% weight loss and the maximum weight loss temperature (T_{max}). Temperatures for 75% weight loss gradually increase with CCB loading, indicating thermal stability. The temperature at which rubber composites experience a 50% weight loss during degradation is regarded as an indicator of their thermal stability. Inclusion of CCB has raised the T_{50}% to 397°C from 393°C (NB0), demonstrating an enhanced level of thermal stability. However, the introduction of 20 phr CCB and 10 phr CCB does not lead to significant alterations in thermal stability.

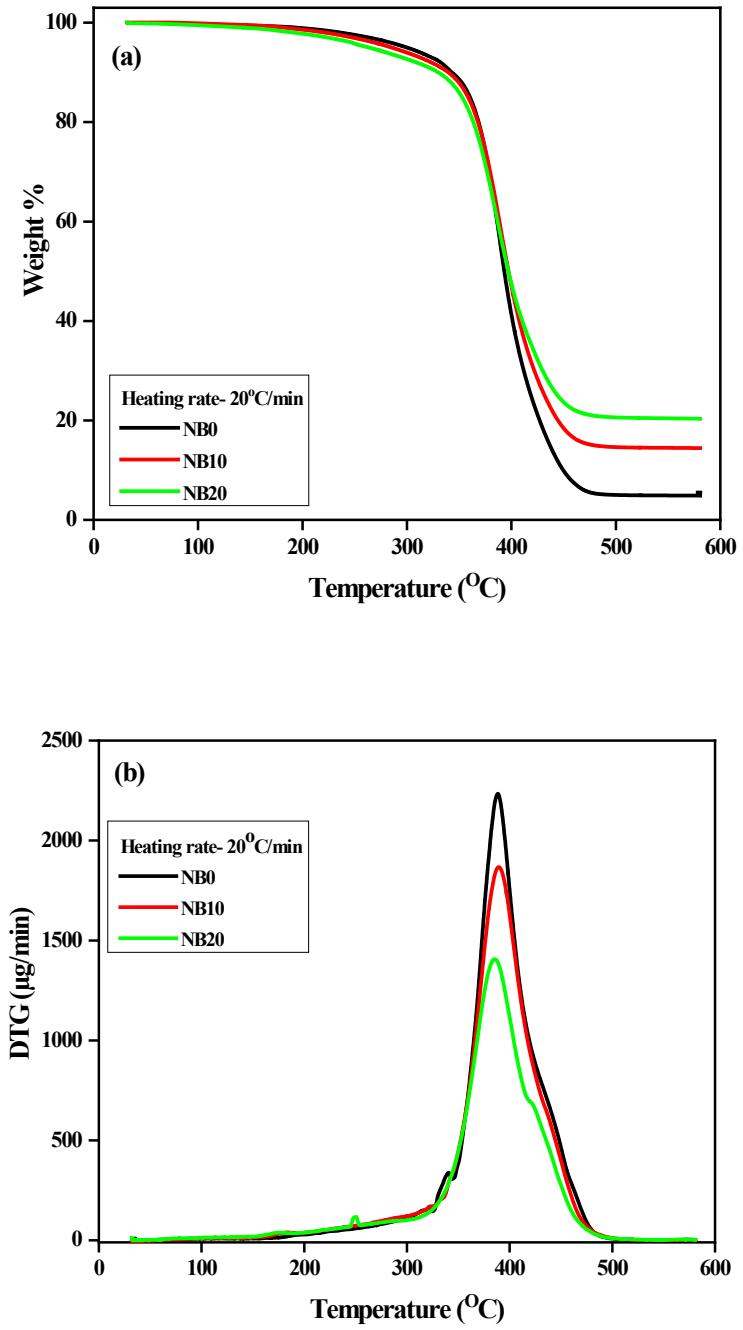

Figure 7.2-(a)TG and (b) DTG curves of NR/CCB systems

Table 7.1-Degradation temperatures of NR/CCB systems

Sample	$T_{10\%}$ (°C)	$T_{50\%}$ (°C)	$T_{75\%}$ (°C)	T_{max} (°C)
NB0	343	393	419	388
NB10	340	397	432	390
NB20	330	397	444	387

7.3.1.2. Kinetic studies

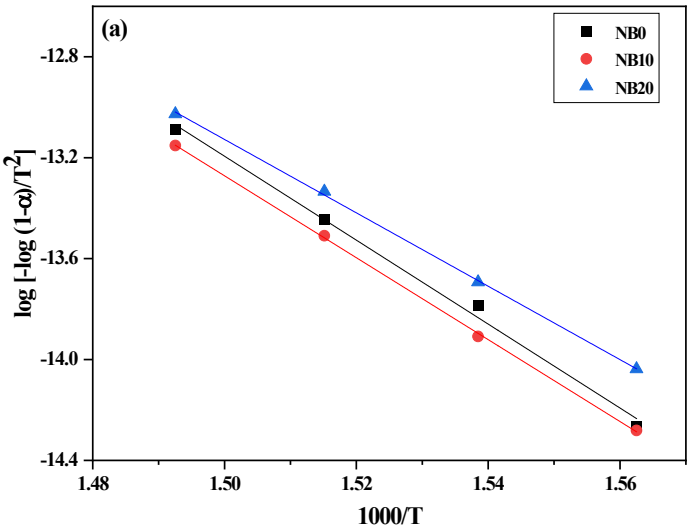

Figure 7.3(a) –Coats-Redfern plot of NR/CCB systems

Table 7.2- Activation energy from Coats-Redfern model for NR/CCB systems

Sample	E_a (kJ/mol)
NB0	123
NB10	135
NB20	121

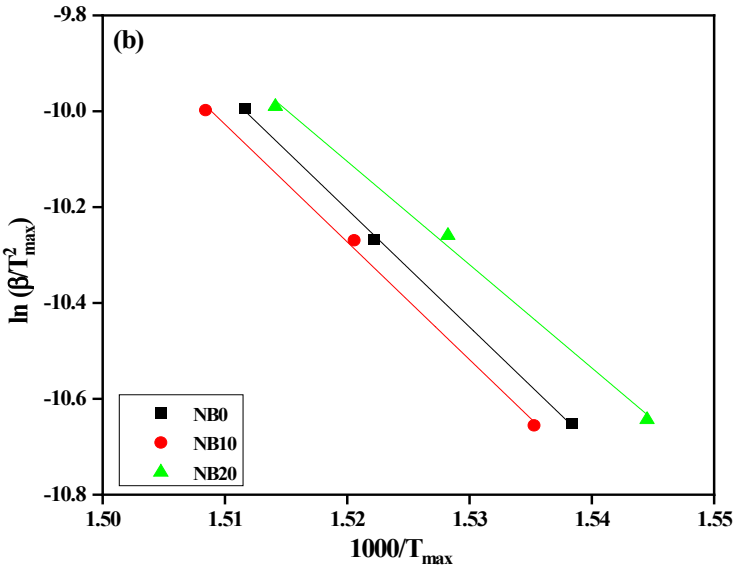

Figure 7.3(b)-Kissinger plot of NR/CCB systems

Coats–Redfern model is used to evaluate kinetic parameters from thermogravimetric data. Coats-Redfern plot of NR/CCB systems are given in **Figure 7.3(a).** The plot of $\log\left[\frac{-\log(1-\alpha)}{T^2}\right]$ as a function of $\frac{1}{T}$ gives a straight line with the slope equal to $\left[-\frac{E_a}{2.303RT}\right]$and the y-intercept is $\log\left(\frac{AR}{\beta E_a}\right)\left[\frac{1-2RT}{E_a}\right]$. The activation energy of degradation of rubber is calculated from the slope, which is$\left[-\frac{E_a}{2.303RT}\right]$. **Table 7.2** presents the activation energy results derived from the Coats-Redfern model. The findings of the model indicate that the introduction of 10 phr CCB led to an enhancement in the thermal stability of NR as inferred from the higher activation energy of NB10 than NB20.

Kissinger, KAS and FWO methods give further insight to the thermal degradation kinetics of NR/CCB systems. In the Kissinger method, the degree of conversion remains constant at the peak temperature (T_{max}) across multiple heating rates. **Figure 7.2(b)** gives the fitted straight line Kissinger plot of neat and CCB filled rubber composites. High linear correlation coefficient of the fitted straight line indicates the feasibility of the method. **Table 7.3** gives the activation energy calculated using the Kissinger method. Activation energy is only slightly increased upon CCB filler incorporation. At higher filler loading, activation energy is decreased according to Kissinger method. Iso conversional methods, KAS and FWO methods analyse thermal data at conversion degrees of 0.2, 0.4, 0.6 and 0.8. **Figure 7.3(c)** displays linearly fitted KAS model plots of NB10 at different conversion degrees: 0.2, 0.4, 0.6, and 0.8. The slopes of these plots are used to determine the activation energy of degradation of NR. FWO plots of NB10 with varying degrees of conversions are given in **Figure 7.3 (d).** Straight line obtained by plotting $\log\beta$ against $\frac{1000}{T}$ at different heating rates gives constant $\propto$ and permits the calculation of activation energy. Activation energy of this method is not influenced by the specific thermal degradation reaction mechanism.(7) **Table 7.3** summarises the activation energy values obtained from KAS and FWO models. It can be observed from **Table 7.3** that the Kissinger model calculates activation energy higher than the KAS model and lower than the FWO model.

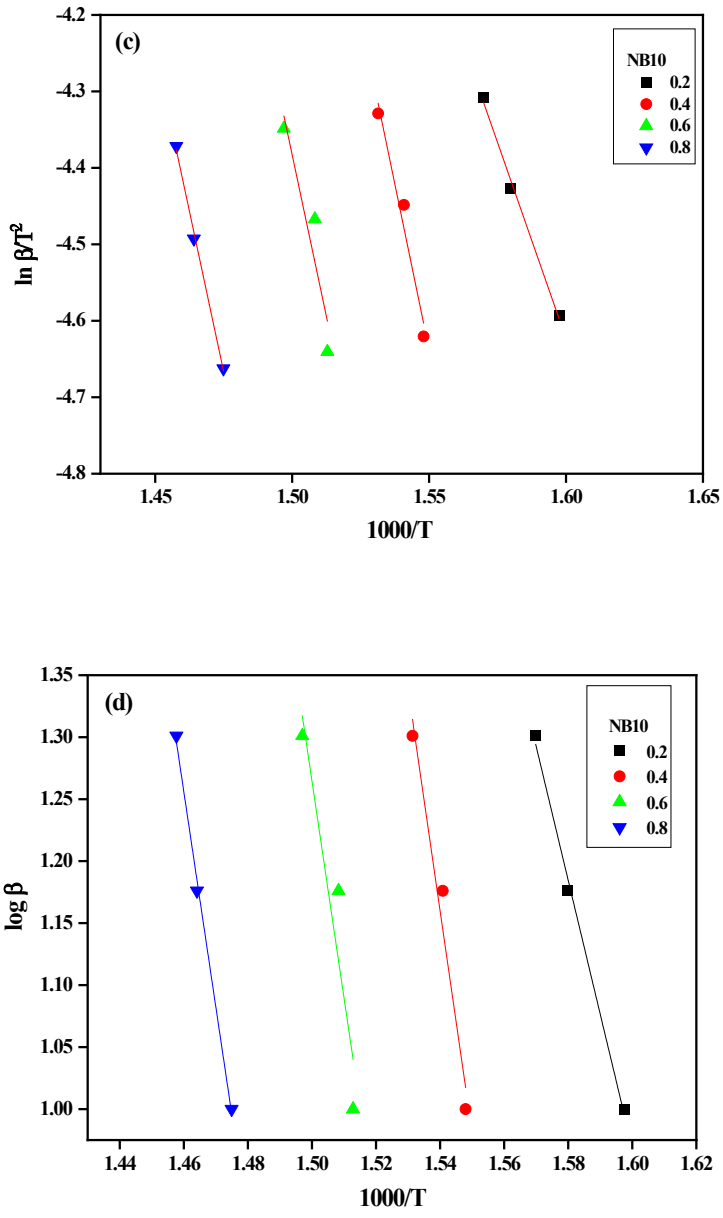

Figure 7.3-(c) KAS and (d) FWO plot of NB10

Table 7.3 -Activation energy (kJ/mol) of NR/CCB systems obtained from Kissinger, KAS and FWO models

	Kissinger model	**KAS model**				**FWO model**			
α	**0.4**	**0.2**	**0.4**	**0.6**	**0.8**	**0.2**	**0.4**	**0.6**	**0.8**
NB0	204	94	102	105	112	216	234	240	256
NB10	204	85	97	111	122	197	222	254	277
NB20	179	94	100	105	112	216	230	241	256

Kissinger model determines the activation energy based on the maximum degradation temperature. Activation energies calculated using KAS and FWO models increase with increasing conversion rates. This suggests the change of activation energy with filler incorporation is similar for KAS and FWO models. However, dissimilar activation energy values computed from both methods reflect the fact that the thermal degradation of NR composites does not follow simple one step mechanism.(8,12) KAS and FWO models are based on mathematical approximations and can be applied with linear variation of temperature and positive heating rates. Considering the average activation energy, KAS and FWO suggest NB10 to be thermally stable. Average activation energy of the hybrid filler systems predicted using model based and model-free isoconversional methods ranges from 103- 237 kJ/mol. Both Kissinger and Coats-Redfern models predict higher activation energy for NB10.

7.3.2. NR/1-ethyl-3-methylimidazolium chloride modified CCB (NR/ILCCB) systems

7.3.2.1. TGA analysis and thermal stability

TG curve depicted in **Figure 7.4(a)** elucidates distinct thermal degradation patterns between NB20IL3 and NB20IL1. The sample NB20IL3, characterised by a 1:3 filler-to-IL ratio, initiates its thermal decomposition at a temperature inferior to that of NB20IL1. Reference to **Table 7.4** reveals that NB20IL3 reaches its initial 10% weight loss at a comparatively reduced thermal threshold. Conversely, upon achieving a 50% weight reduction, the decomposition temperature of NB20IL3 exceeds that of NB20IL1. NB20IL3 also exhibits a higher decomposition temperature at a 75% weight loss. Notably, the thermal degradation stability of NB20IL3, as indicated by its Tmax, is at 395°C, whereas the unfilled NR has a Tmax of 388°C.

Ionic liquid (IL) has a significant role in determining the thermal stability and degradation mechanism of NR composites. Studies show that imidazolium based ionic liquids are more thermally stable than pyrrolidnium ring based ionic liquids. (13) Ionic liquids can also act as plasticisers, which can lead to low temperature degradation of NR composites. Decomposition of IL can also release some volatile compounds that can increase or decrease the degradation process.

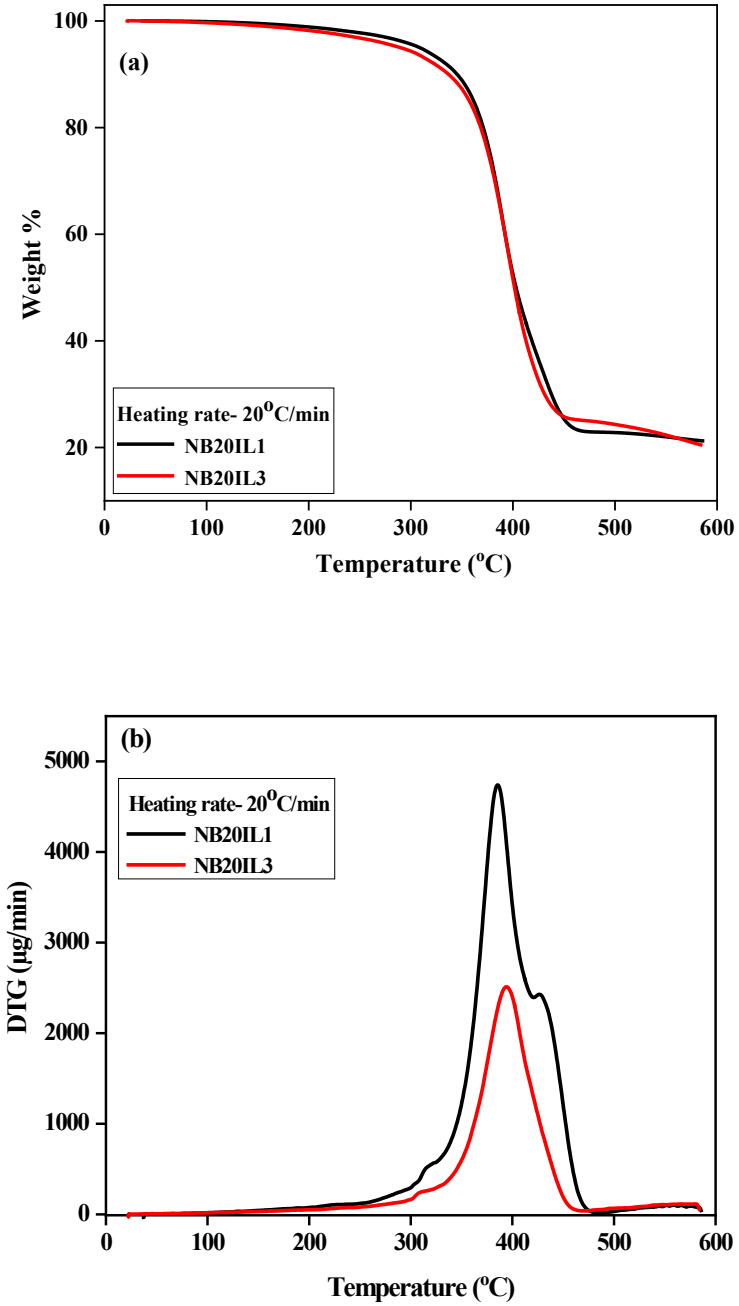

Figure 7.4- (a) TGA and (b) DTG curves of NR/ILCCB systems

Also, IL can slow down the degradation by forming the protective char layer during degradation or by inhibiting the evolution of volatile degradation products. However, TG curves show that IL imparts thermal stability to NR composites to a certain extent. Ionic liquid molecules can interact with the CCB agglomerates and aid in the uniform distribution of it in the NR matrix. CCB particles possess high

thermal conductivity, and the homogeneous dispersion of CCB in NR allows uniform heat transfer. The π-π interactions between the imidazolium ring of ionic liquid and the CCB particles evenly distribute the CCB and prevent the development of areas of localized high temperature. Schematic representation of ILCCB distribution in NR matrix is given in **Figure 5.15 (Chapter 5)**. The type and concentration of the ionic liquid, its interaction with the rubber matrix, and the presence of other fillers or additives have a role in determining the overall thermal behaviour of the composite. **Figure 7.4 (b)** displays the DTG curves of NR hybrid filler systems incorporated with CCB modified by IL. As the filler-to-IL ratio changes from 1:1 to 1:3, there is a marked decline in the DTG peak intensity. At lower IL content, an auxiliary peak, referred to as a shoulder peak, emerges between 400-500^{o}C on the DTG curve.

Table 7.4 shows the degradation temperatures of NR/ILCCB systems. Temperatures for 50% weight loss are almost similar for both composites, while temperature for 75% weight loss is higher for NB20IL3. Temperature for maximum degradation is also higher for NB20IL3.

Table 7.4-Degradation temperatures of NR/ILCCB systems

Sample	$T_{10\%}$ (°C)	$T_{50\%}$ (°C)	$T_{75\%}$ (°C)	T_{max} (°C)
NB20IL1	345	403	451	386
NB20IL3	337	402	473	395

7.3.2.2. Kinetic studies

Figure 7.6(a) illustrates the Coats-Redfern plot for the NR/ILCCB systems. The slope of this plot provides information on the activation energy, which has been documented in **Table 7.5**. Notably, NB20IL1 exhibits a greater activation energy compared to NB20IL3. Difference in activation energy between NB20IL1 and NB20IL3 suggests that the concentration and type of ionic liquid can have profound effects on the thermal properties of the composites. The change in activation energy could be attributed to varying interactions between the IL, CCB and the rubber matrix at different concentrations. Even a small change in the composition can lead to pronounced differences in their thermal behaviour.

Table 7.5 -Activation energy obtained from Coats-Redfern model for NR/ILCCB systems

Sample	E_a (kJ/mol)
NB20IL1	131
NB20IL3	126

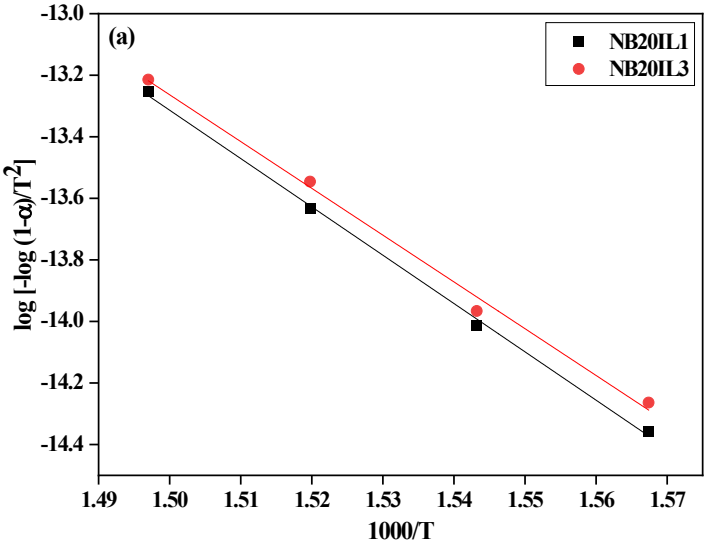

Figure 7.6(a)-Coats-Redfern plot of NR/ILCCB systems

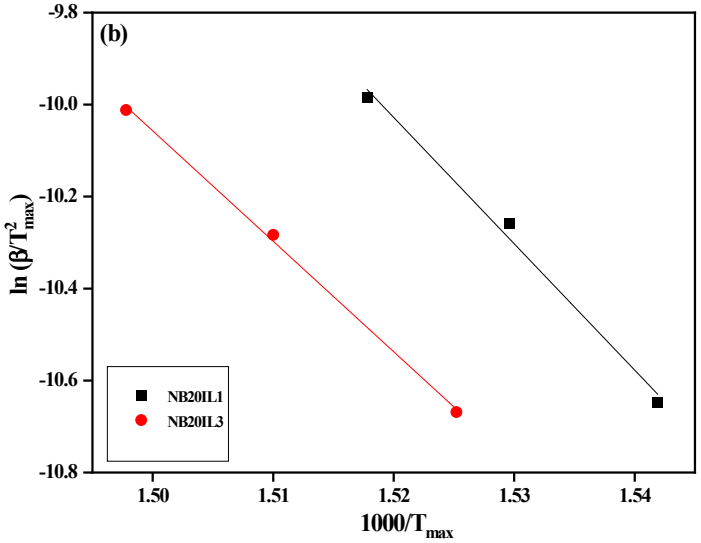

Figure 7.6(b) Kissinger plot of NR/ILCCB systems

Figure 7.6 (b), (c) and **(d)** illustrate the thermal behaviour of NR/ILCCB systems using Kissinger, KAS and FWO methods, respectively. Being a model-free method, the Kissinger method, allows for a direct comparison of the activation energies without the need to assume any specific reaction mechanism. This method is one of the commonly employed techniques to evaluate the activation energy of thermally stimulated processes.

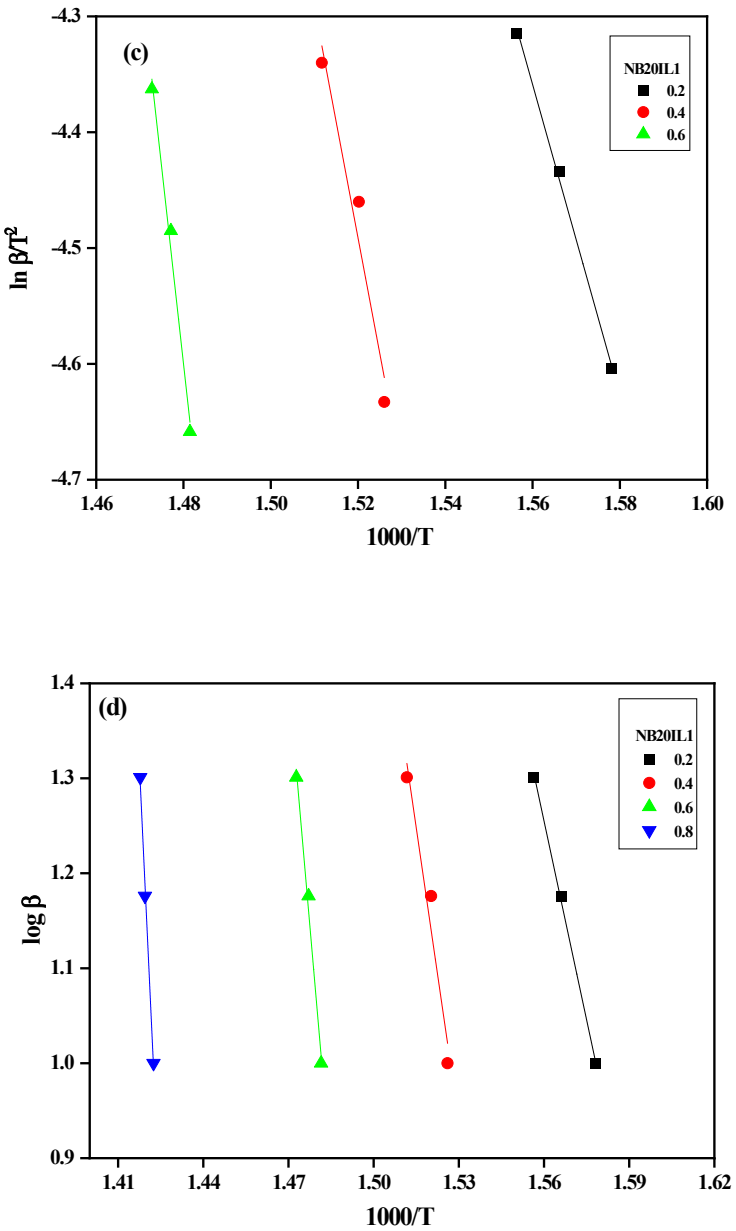

Figure 7.6-(c)KAS and (d) FWO plot of NR/ILCCB systems

Table 7.6 -Activation energy (kJ/mol) of NR/ILCCB systems obtained from Kissinger, KAS and FWO models

	Kissinger model	**KAS model**			**FWO model**		
	0.4	0.2	0.4	0.6	0.2	0.4	0.6
NB20IL1	228	111	166	282	259	330	553
NB20IL3	200	200	208	572	167	333	597

The KAS model works under the assumption of a constant reaction mechanism throughout the process, providing insight into how the system responds under varying temperature regimes. FWO also ascertain the activation energy without knowing the reaction mechanism. This method has been widely recognised for its reliability, especially when a single step reaction mechanism cannot be assumed. Each of these plots provides complementary information regarding the thermal stability, degradation kinetics, and behaviour of NR/ILCCB systems. Activation energy is computed from the slope of the plot, and the values have been documented in **Table 7.6.** Activation energy is calculated for conversion rates of 0.2, 0.4 and 0.6. Activation energy calculated from the Coats-Redfern, Kissinger and KAS model suggests NB20IL1 is more thermally stable. However, at a conversion degree of 0.8, the FWO model anticipates high activation energy for NB20IL3. The difference in computed activation energy can be attributed to the difference in approximation techniques adopted by models to obtain temperature integral. (14) This elevates the average activation energy of the sample, making it higher than that of NB20IL1.

7.3.3. NR/CCB-CNT hybrid filler systems

7.3.3.1. TGA analysis and thermal stability

Figure 7.7(a) and (b) illustrate the TGA and DTG curves of NR/CCB-CNT composite systems using a heating rate of 20°C per minute. TGA curve shows that NB20C3 degrades first compared to NB20C5. Increasing the CNT content has slightly improved the thermal stability, as observed in the weight loss curve. Also, NB20C5 exhibits higher residue than NB20C3. DTG curve of the NR/CCB-CNT hybrid filler systems exhibit an additional shoulder peak within the temperature span of 400°C to 450°C, implying a two-step degradation process. Initial degradation initiates around 300°C, with the peak weight loss occurring at approximately 384°C. Second degradation phase emerges around 400°C and can

be attributed to the degradation of fillers and other constituents present in the composite. DTG curves for NB20C3 and NB20C5 yield T_{max} values of 386°C and 385°C, respectively.

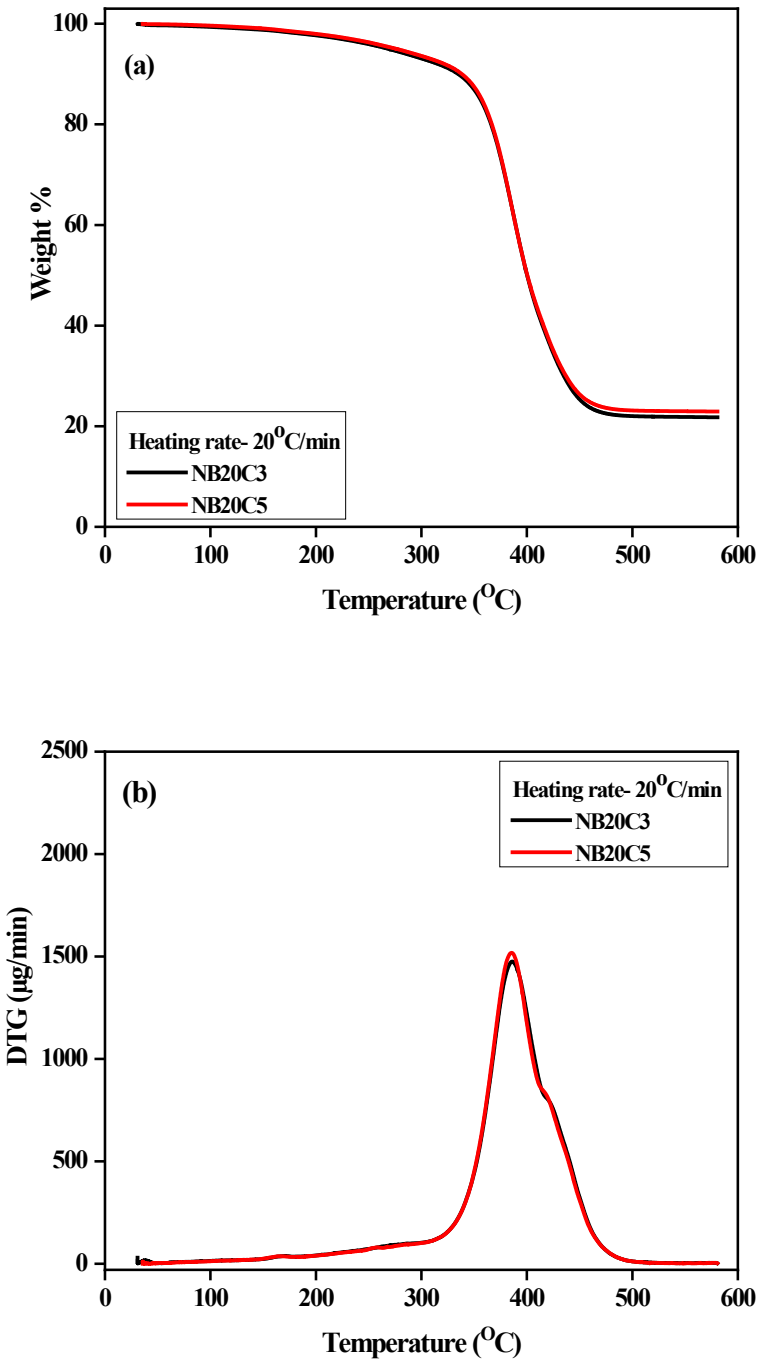

Figure 7.7-(a)TGA and (b) DTG curves of NR/CCB-CNT hybrid filler systems

Table 7.7- Degradation temperatures of NR/CCB-CNT hybrid filler systems

Sample	$T_{10\%}$ (°C)	$T_{50\%}$ (°C)	$T_{75\%}$ (°C)	T_{max} (°C)
NB20C3	334.8	399.9	451.5	386.1
NB20C5	338.3	400.3	458.5	385.4

7.3.3.2. Kinetic studies

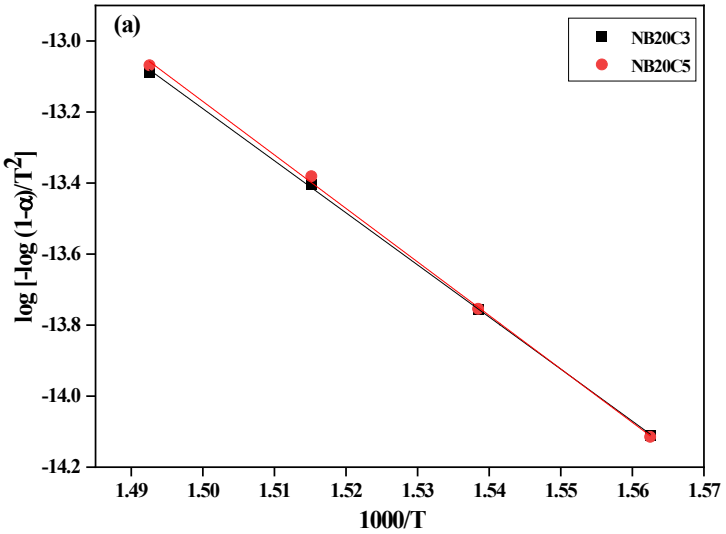

Figure 7.8(a)-Coats-Redfern plot of NR/CCB-CNT hybrid filler systems

Table 7.8- Activation energy obtained from Coats-Redfern model for NR/CCB-CNT hybrid filler systems

Sample	E_a (kJ/mol)
NB20C3	122
NB20C5	125

Activation energy calculated through the Coats-Redfern method is displayed in **Table 7.8**. As observed, the activation energy rises with an increase in CNT content. **Figure 7.8(a)** illustrates the Coats-Redfern plots, which have been linearly fitted. Kissinger, KAS, and FWO methods for kinetic analysis possess the advantage of determining the activation energy of degradation without necessitating the assumption of specific reaction models for the degradation steps. **Figure 7.8(b)** gives the fitted straight line Kissinger plot of hybrid filler CCB-CNT incorporated NR composites. Kissinger method is an integral, model-independent isonconversional approach used to determine the apparent activation energy of a system. Specifically, this method calculates the activation energy at a

consistent α value, typically where the maximum weight loss is observed in the DTG curve. This approach offers insight into the thermal stability and decomposition kinetics of materials without making assumptions about the reaction mechanism.

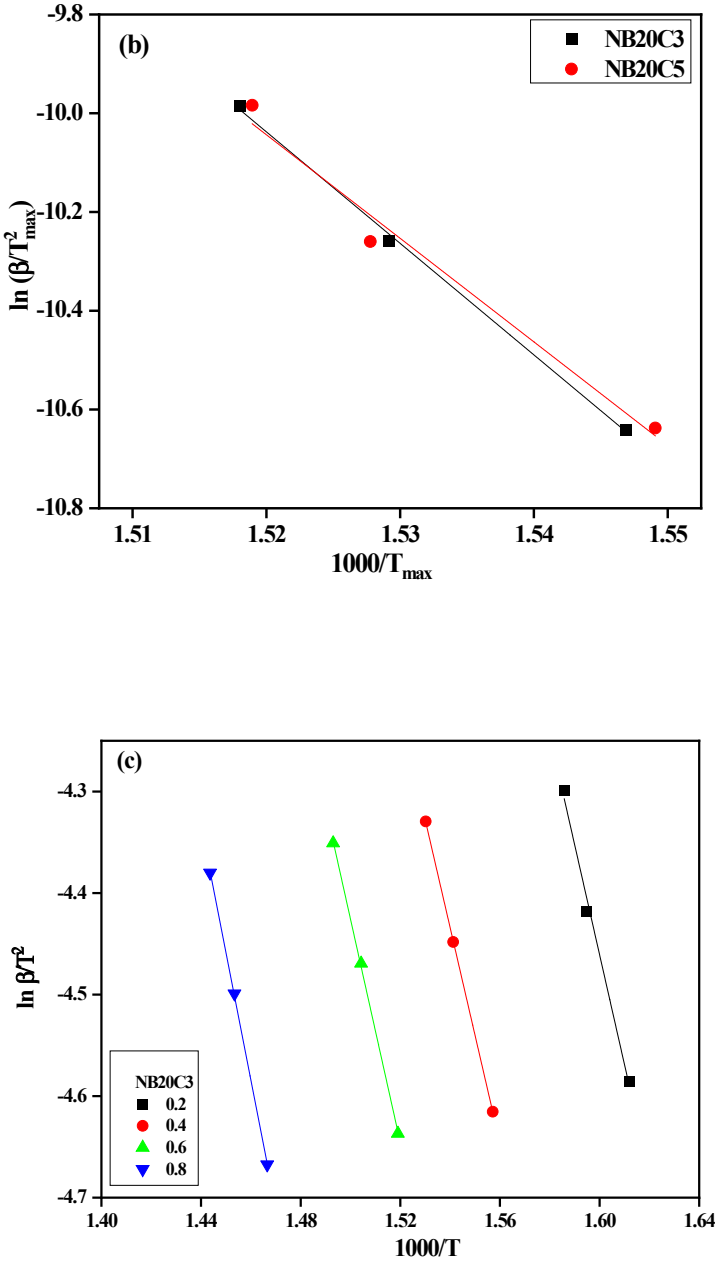

Figure 7.8(b)-Kissinger and (c)-KAS plot of NR/CCB-CNT hybrid filler systems

Activation energy obtained from Kissinger model is given in **Table 7.9**. **Figure 7.8(b)** shows the linearly fitted plots for the KAS model of NB20C3 at various conversion degrees: 0.2, 0.4, 0.6, and 0.8. By analysing the slopes of these plots, the activation energy required for the degradation of NR composites can be ascertained. The coefficient of correlation (R^2) for these linear fits is close to 0.99, indicating a strong linear correlation. Determined activation energy values are tabulated in **Table 7.9. Figure 7.8(c)** presents the FWO plot of NB20C5 at varying conversion degrees of 0.2, 0.4, 0.6 and 0.8.

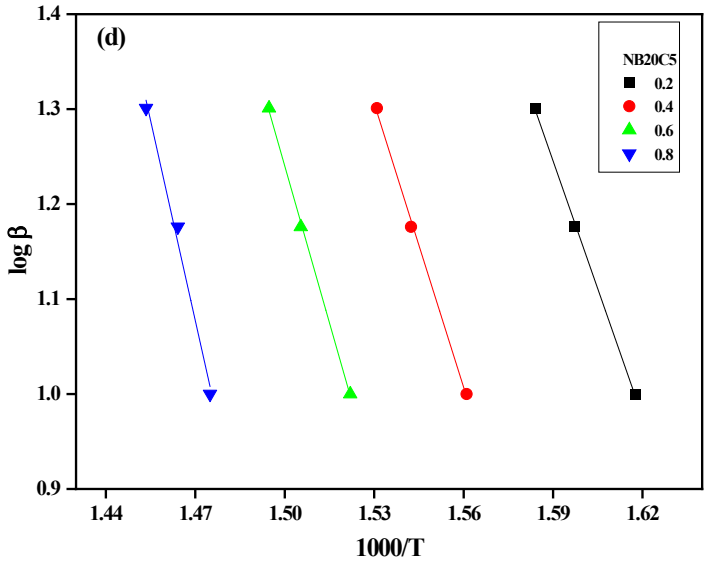

Figure 7.8(c)-FWO plot of NR/CCB-CNT hybrid filler systems

Activation energy values derived from isoconversional methods are influenced by both conversion rates and heating rates. As shown in **Table 7.9**., both the KAS and FWO models for NB20C3 exhibit a deviation from the expected trend, displaying a lower activation energy for the α value of 0.4. This does not agree with the general trend where activation energy increases as a function of α. Similar to NR/CCB systems, the FWO model reports the highest activation energy. All kinetic models indicate that NB20C3 exhibits superior thermal stability, as evidenced by a distinct difference in its average activation energy. However, when referencing the DTG curve, NB20C3 and NB20C5 show nearly identical T_{max} values.

Table 7.9 -Activation energy (kJ/mol) of NR/CCB-CNT hybrid filler systems obtained from Kissinger, KAS and FWO models

	Kissinger model	**KAS model**				**FWO model**			
α	**0.4**	**0.2**	**0.4**	**0.6**	**0.8**	**0.2**	**0.4**	**0.6**	**0.8**
NB20C3	192	90	88	92	104	207	203	211	239
NB20C5	173	70	78	87	103	163	181	200	235

7.3.4. NR/CCB-1-ethyl-3-methylimidazolium chloride modified CNT (NR/CCB-ILCNT) hybrid filler systems

7.3.4.1. TGA analysis and thermal stability

Figure 7.9(a) shows the TGA curves of NR hybrid filler systems incorporating CCB and IL-modified CNT. These curves suggest that merging IL-modified CNT with CCB offers consistent thermal stability, largely independent of the filler-to-IL ratio. Moreover, as the concentration of CNT changes from 3 phr to 5 phr, a marginal increase in thermal stability is observed. When analysing the thermal degradation behaviour of NB20C5IL3, it is observed that there is a rapid initial degradation with an increase in temperature. This can be attributed to the high thermal conductivity of the CNT present in the system.(15) CNT have exceptional thermal conductivity, which means they can effectively transport heat throughout a material. In the context of NB20C5IL3, a higher concentration of both CNT and IL can enhance the heat distribution within the composite, leading to more uniform and efficient heating. As a result, when the degradation temperature is reached, the entire sample undergoes thermo-oxidative degradation more quickly compared to composites with lower CNT or IL content.(16) Also, CNT can catalyse specific reactions or accelerate oxidative processes due to their nano-scale dimensions and high surface area, especially if they possess defects or functional groups on their surface. This catalytic effect, combined with efficient heat distribution, can contribute to the rapid initial degradation of the NB20C5IL3 composite. **Figure 7.9(b)** presents the DTG curve of NR/CCB-ILCNT hybrid filler systems. Degradation of NR exhibits distinctive decomposition occurring in two overlapping stages, indicating the involvement of a complex mechanism. (17,18) Initial stage of decomposition of NR encompasses radical depolymerisation of polymer chains. Second stage of NR degradation is marked by the diffusion of products that are formed during depolymerization reactions.

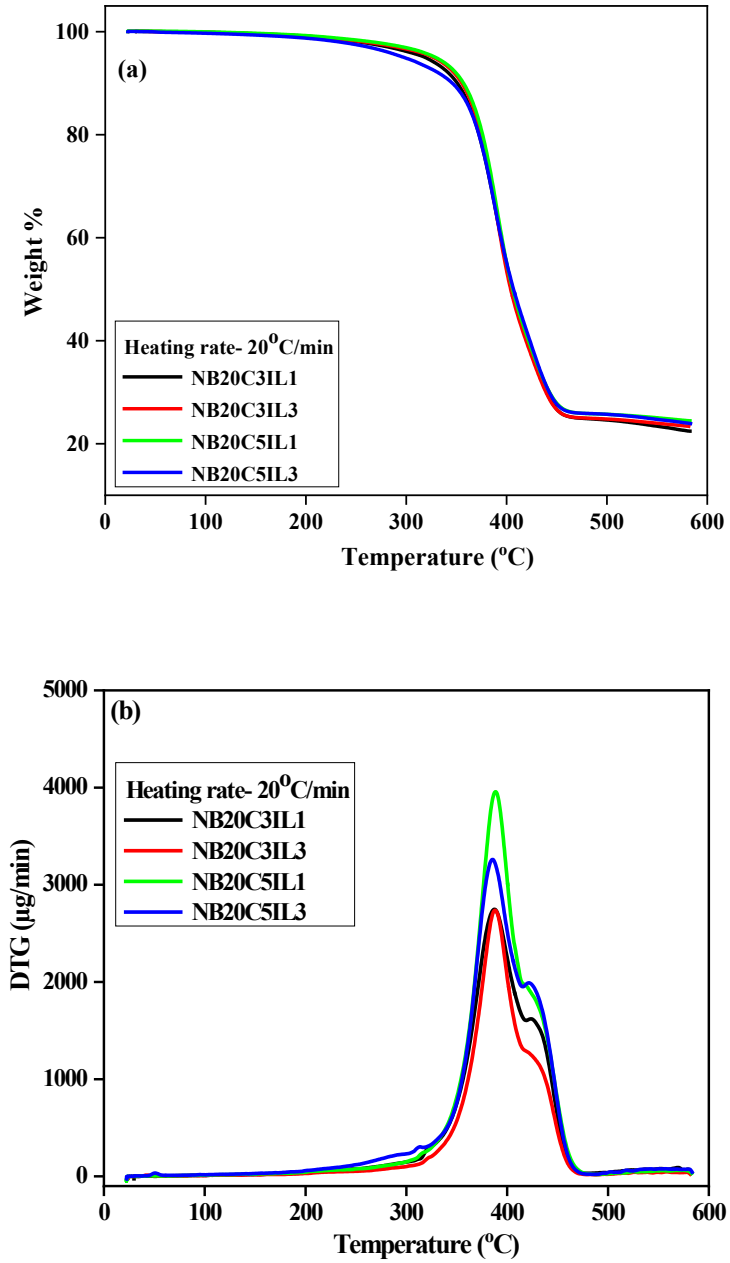

Figure 7.9(a)- TGA and (b) DTG curves of NR/CCB-ILCNT composite

Depolymerization involves the breaking down of polymer chains into smaller fragments, and in the case of NR, this results in the formation of dimers and trimers. These depolymerization products are often more volatile than the larger polymer chains. During the second stage, these products diffuse from the bulk of the polymer matrix towards its surface. This diffusion process is required for the overall degradation of the NR material. As the dimers and trimers move towards

the surface of the material, they can eventually evaporate or be released, contributing to the weight loss observed during thermal analysis. The rate at which these products diffuse can be influenced by factors such as temperature, heating rate, and the presence of any fillers or additives in the material. Presence of hybrid network of CCB and ionic liquid modified CNT can act as barriers in slowing down the diffusion of volatile compounds. Initial and following stages of degradation exhibit an overlapping nature due to the simultaneous depolymerization and diffusion of products.

Table 7.10-Degradation temperatures of NR/CCB-ILCNT hybrid filler systems

Samples	$T_{10\%}$ (°C)	$T_{50\%}$ (°C)	$T_{75\%}$ (°C)	T_{max} (°C)
NB20C3IL1	351	406	471	387
NB20C3IL3	355	404	478	388
NB20C5IL1	357	406	470	389
NB20C5IL3	345	407	539	386

The degradation temperatures of the NR/CCB-ILCNT hybrid filler systems are tabulated in **Table 7.10**. Initial degradation represented by the $T_{10\%}$ suggests that NB20C5IL1 begins its degradation later than the other samples, implying high initial thermal stability. NB20C5IL3 starts degradation at a lower temperature, suggesting reduced initial thermal stability. Temperatures for $T_{50\%}$ are comparable for all samples. NB20C5IL3 stands out with a significantly higher temperature for 75% weight loss, indicating better stability in advanced stages of degradation. This could be due to the possible formation of a protective char layer or any molecular interactions between CNT and IL components, which slow down further degradation.

7.3.4.2. Kinetic studies

Figure 7.10 (a) is the Coats-Redfern plot of NR systems with CCB and IL-modified CNT. **Table 7.11** summarises the activation energy values obtained from the linearly fitted curves. NB20C5IL1 is the most thermally stable composite, as indicated by the activation energy obtained from the Coats-Redfern plot. The thermal stability of composites decreases as the filler-to-IL ratio rises from 1:1 to 1:3, especially for NB20C5IL1 and NB20C5IL3. **Figure 7.10(b), (c) and (d)** are the Kissinger, KAS and FWO plots of the NR/CCB-ILCNT hybrid

filler systems. Activation energy values derived from the different models are consolidated in **Table 7.12**. KAS and FWO models were limited to conversion degrees of 0.2, 0.4, and 0.6 owing to the presence of a shoulder peak in the composite degradation profiles. Activation energy values are in the range of 100-200 kJ/mol across all models. For all NR/CCB-ILCNT systems, the activation energies determined by all theoretical models are consistent with each other and have only minor deviations.

Table 7.11-Activation energy obtained from Coats-Redfern model for NR/CCB-ILCNT hybrid filler systems

Sample	E_a (kJ/mol)
NB20C3IL1	117
NB20C3IL3	149
NB20C5IL1	151
NB20C5IL3	126

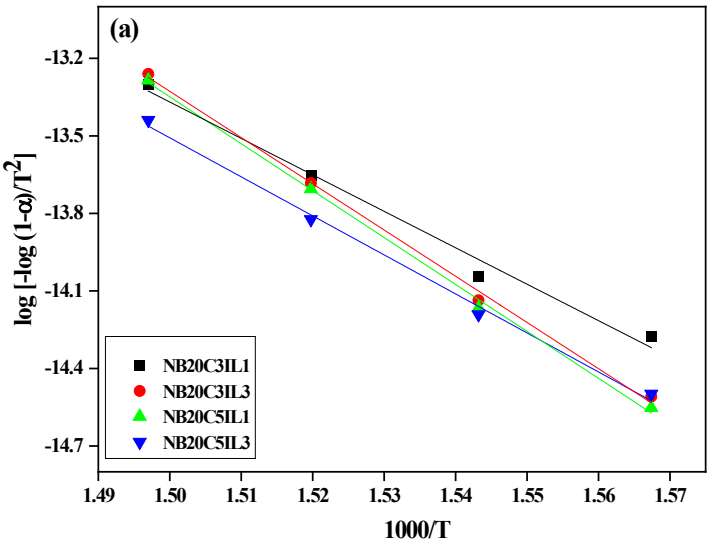

Figure 7.10(a)- Coats-Redfern plot of NR/CCB-ILCNT hybrid filler systems

Table 7.12 -Activation energy (kJ/mol) of NR/CCB-ILCNT hybrid filler systems obtained from Kissinger, KAS and FWO models

α	Kissinger model	KAS model			FWO model		
	0.4	**0.2**	**0.4**	**0.6**	**0.2**	**0.4**	**0.6**
NB20C3IL1	255	79	85	85	168	176	175
NB20C3IL3	196	68	76	18	184	168	172
NB20C5IL1	211	78	84	82	181	195	190
NB20C5IL3	157	83	91	97	191	210	224

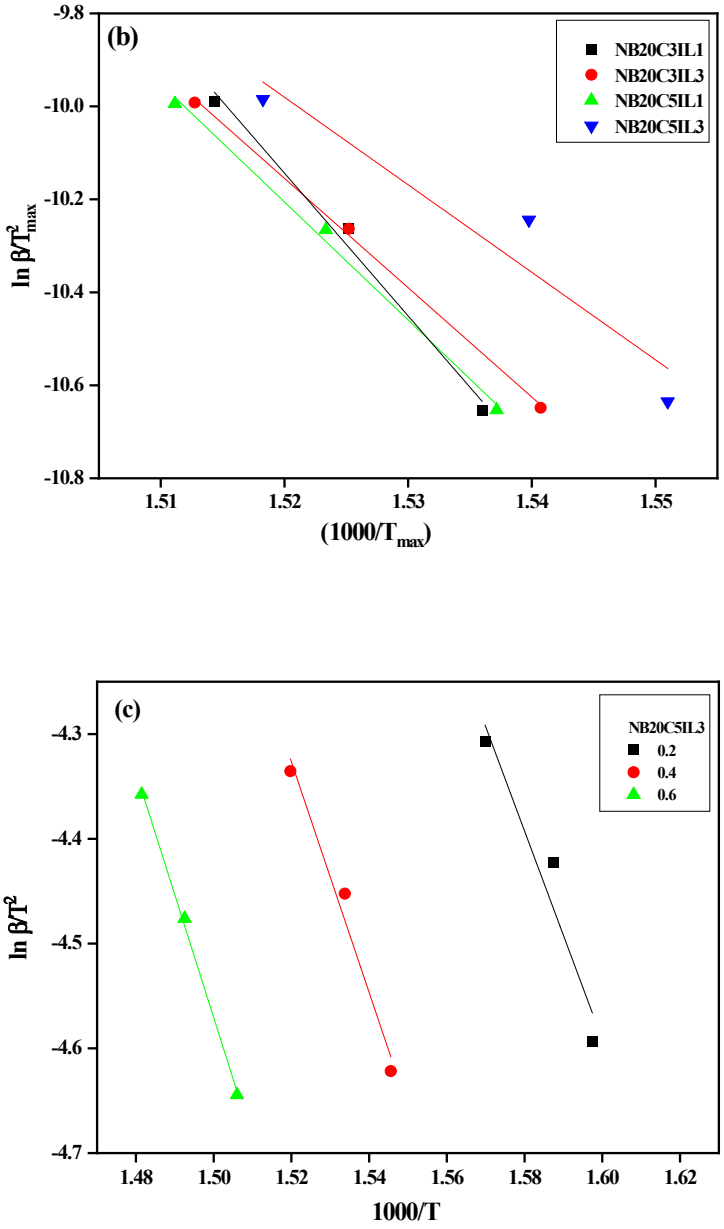

Figure 7.10(b)- Kissinger and (c) KAS plot of NR/CCB-ILCNT hybrid filler systems

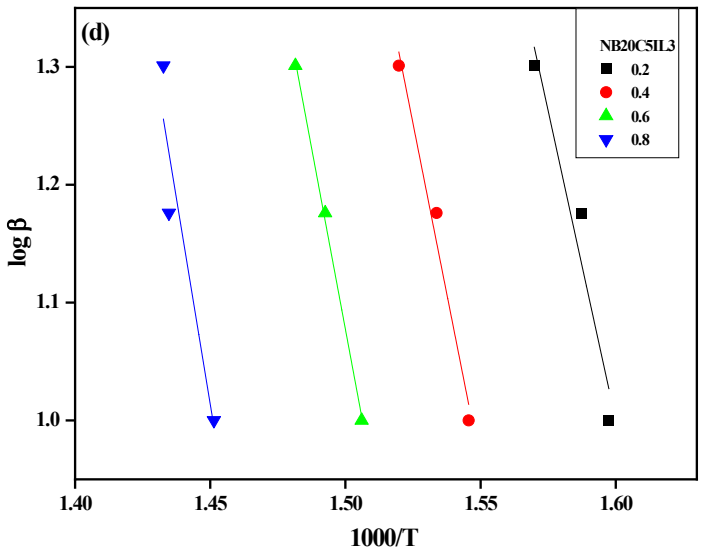

Figure 7.10(d)- FWO plot of NR/CCB-ILCNT hybrid filler systems

7.3.5. NR/CCB-CNT-RGO hybrid filler systems

7.3.5.1. TGA analysis and thermal stability

Figure 7.11(a) displays the TGA curve for hybrid filler systems incorporating a hybrid filler system consisting of CCB, CNT, and RGO. An observable enhancement in thermal stability is noted with higher phr CNT in the presence of RGO. **Figure 7.11(b)** presents the DTG curve of NR/CCB-CNT-RGO hybrid filler systems. DTG curves of NR/CCB-CNT-RGO hybrid filler systems also exhibit two peaks, which indicates a multi-stage decomposition process of NR. Perejón *et al.*(1) have addressed the intricate nature of NR decomposition, highlighting that it cannot be attributed to two distinct and independent stages of degradation.

Table 7.13- Degradation temperatures of NR/CCB-CNT-RGO hybrid filler systems

Sample	$T_{10\%}$ (°C)	$T_{50\%}$ (°C)	$T_{75\%}$ (°C)	T_{max} (°C)
NB20C1R1	357	405	466	391
NB20C5R1	356	407	570	389

Table 7.13 presents the degradation temperatures of NR/CCB-CNT-RGO hybrid filler systems at different % of weight loss. Thermal stability increases as the amount of CNT increases, as indicated by the $T_{50\%}$. This can be ascribed to the

elevated thermal conductivity of CNT, which provides uniform heat distribution and enhanced thermal stability. Temperature of maximum weightloss is slightly lower for NB20C5R1.

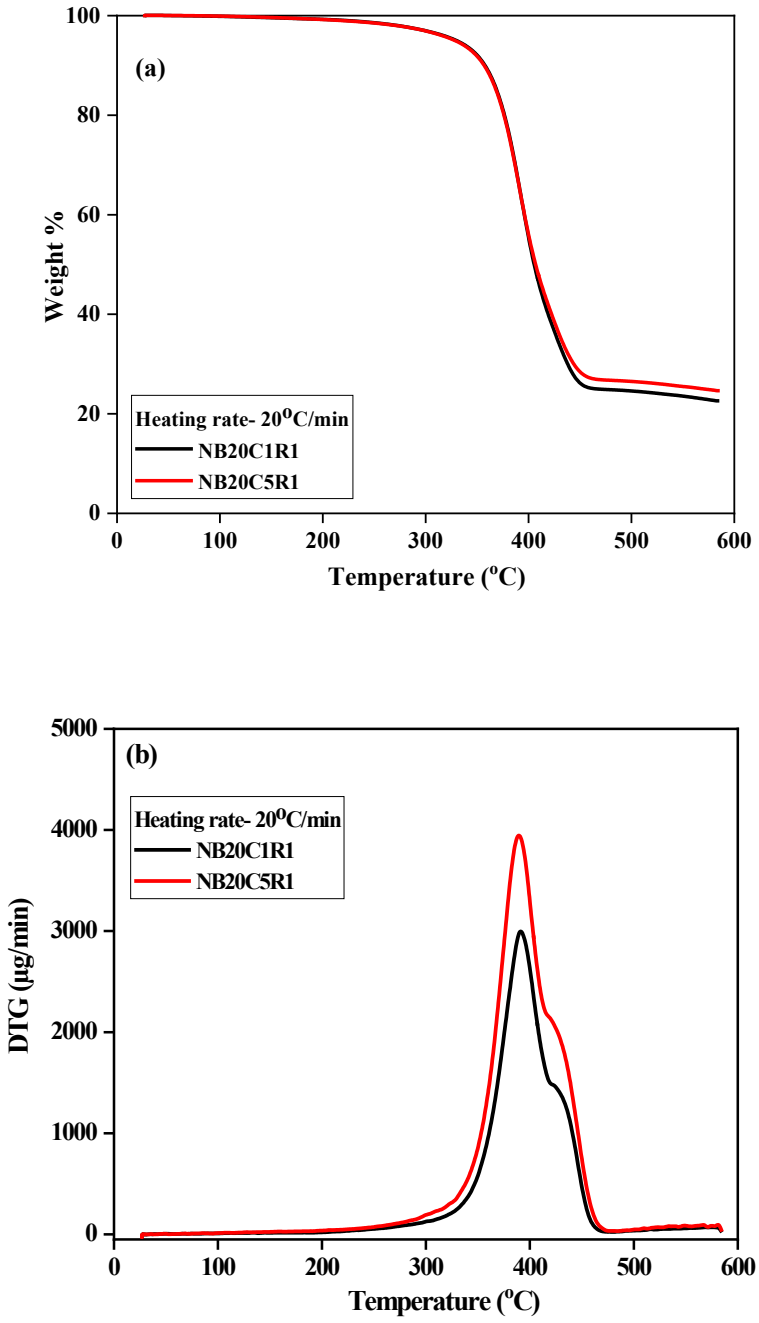

Figure 7.11(a)- TGA and (b) DTG curve at 20°C min^{-1} curves of NR/CCB-CNT-RGO hybrid filler systems

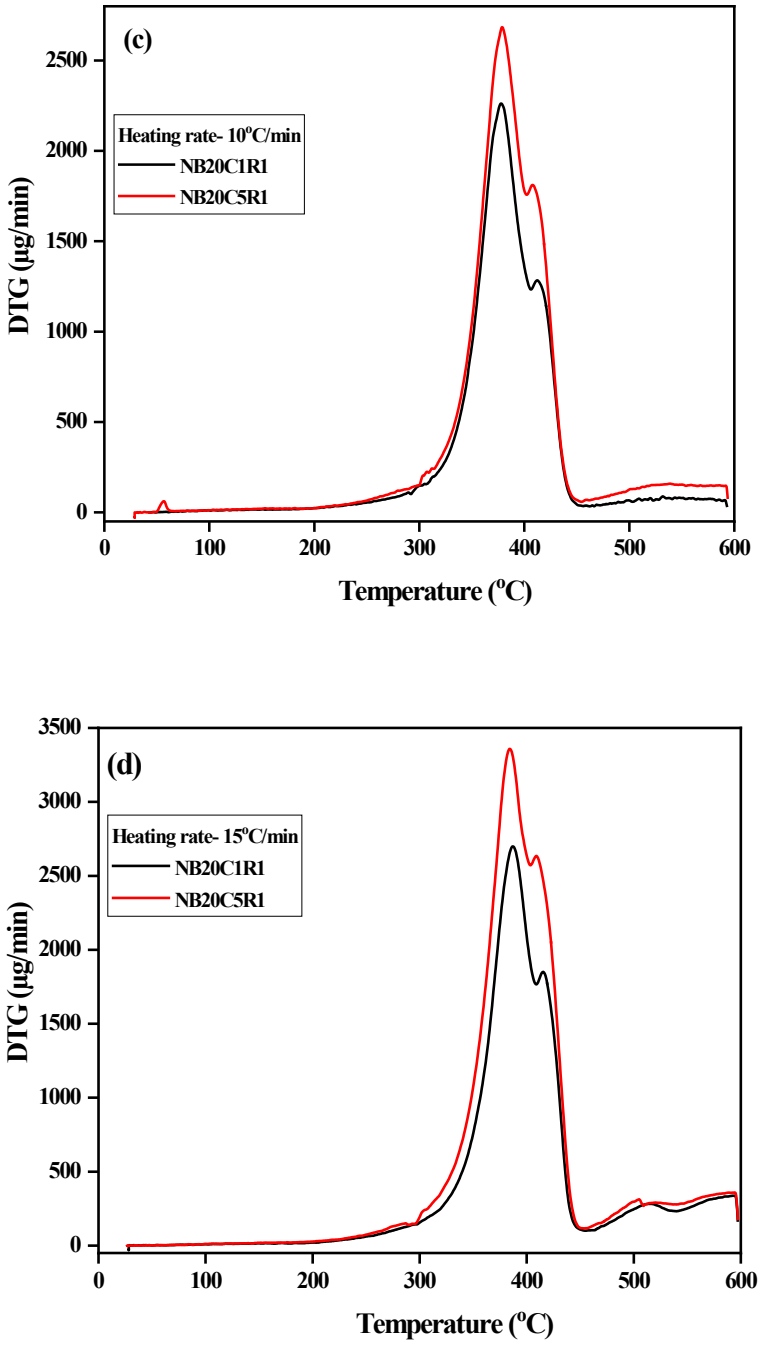

Figure 7.11-DTG curves (c) 10°C min^{-1} and (d)15°C min^{-1} of NR/CCB-CNT-RGO hybrid filler systems

Figure 7.11 (c) and (d) illustrate the DTG curves of NR/CCB-CNT-RGO hybrid filler systems at two distinct heating rates, 10°C min^{-1} and 15°C min^{-1}respectively. Notably, the intensity of the shoulder peak is observed to vary based on the heating rate. Intensity of the shoulder peak is more pronounced at lower heating

rate of 10°C min^{-1}. This phenomenon is linked to the formation of trimer and tetramer compounds during the NR decomposition process.(1) Lower heating rate encourages the formation of these compounds. Conversely, the peak intensity diminishes at a higher heating rate of 20°C min^{-1}. Thus, the degradation of NR/ hybrid filler systems involves non-independent two stage complex degradation processes. In the subsequent phase of NR degradation, the process involves the diffusion of the products resulting from depolymerization reactions, such as dimers and trimers. This diffusion mechanism, which proceeds from the bulk polymer matrix to its surface, constitutes the rate-limiting step in the comprehensive degradation of the NR composite. Inclusion of hybrid filler systems introduces a barrier effect that retards the overall degradation progression. As the heating rate increases, the degradation temperature also rises and consequently boosts the influence of random scission within the polymer chains. Depolymerization of NR chains produces polymer radicals, including isoprene units. Polymer radicals tend to form oligomers at low heating rates. Intramolecular cyclization or the recombination of monomers form oligomers, including dipentene, dimers, and trimers. (4,19,20) Primary phase of the thermal decomposition of NR is based on the principles of a random scission kinetic model. As the temperature lowers, the diffusion of the resulting species within the polymer matrix assumes a significant role. TGA at lower heating rates has thermal decomposition correspondingly at lower average temperatures, and the higher viscosity of the polymer matrix acts as a constraint on diffusion. This limitation emphasizes the relevance of diffusion as a key factor in describing the kinetics of the process. On the contrary, when high heating rates are employed, the time available for isoprene to engage in reactions that lead to the formation of oligomers, particularly trimers, becomes restricted. Moreover, at these elevated temperatures, the lowered viscosity of the polymer matrix facilitates the diffusion of species. (21)

7.3.5.2. Kinetic studies

Figure 7.12 (a) presents the Coats-Redfern plot for the NR/CCB-CNT-RGO hybrid filler systems. **Table 7.14** provides the activation energy values derived from the Coats-Redfern model. Activation energy values indicate that NB20C1R1

has greater thermal stability as indicated by the higher activation energy. On the other hand, NB20C5R1 exhibits lower activation energy.

Table 7.14 -Activation energy obtained from Coats-Redfern model for NR/CCB-CNT-RGO hybrid filler systems

Sample	E_a (kJ/mol)
NB20C1R1	139
NB20C5R1	134

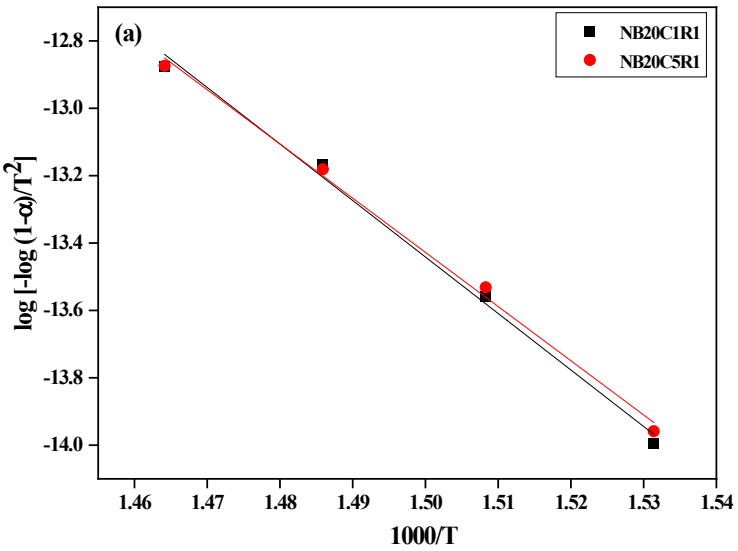

Figure 7.12(a)- Coats-Redfern plot of NR/CCB-CNT-RGO hybrid filler systems

Figure 7.12 (b), (c) and **(d)** presents the Kissinger, KAS and FWO plots of the NR/CCB-CNT-RGO hybrid filler systems. Activation energy values are presented in **Table 7.15.**

Table 7.15 -Activation energy (kJ/mol) of NR/CCB-CNT-RGO hybrid filler systems obtained from Kissinger, KAS and FWO models

	Kissinger model	**KAS model**				**FWO model**			
α	0.4	0.2	0.4	0.6	0.8	0.2	0.4	0.6	0.8
NB20C1R1	170	50	66	77	103	118	154	178	236
NB20C5R1	224	82	89	97	113	189	204	222	259

For NB20C1R1, the activation energy values increase as the conversion degree (α) progresses from 0.2 to 0.8 across all models. The presence of CNT and RGO at a ratio of 1:1 result in relatively lower activation energies compared to the NB20C5R1 sample. For NB20C5R1, with a higher concentration of CNT (5 phr), activation energies are generally higher across all models and conversion degrees.

This indicates that increasing CNT content improves the thermal stability of the composite. Kissinger model calculates activation energy at single conversion degree of 0.4 and the energy values lies between the activation energies of KAS and FWO models. Comparatively, NB20C5R1 demonstrates higher thermal stability than NB20C1R1 across all conversion degrees and models, which can be attributed to the increased CNT concentration.

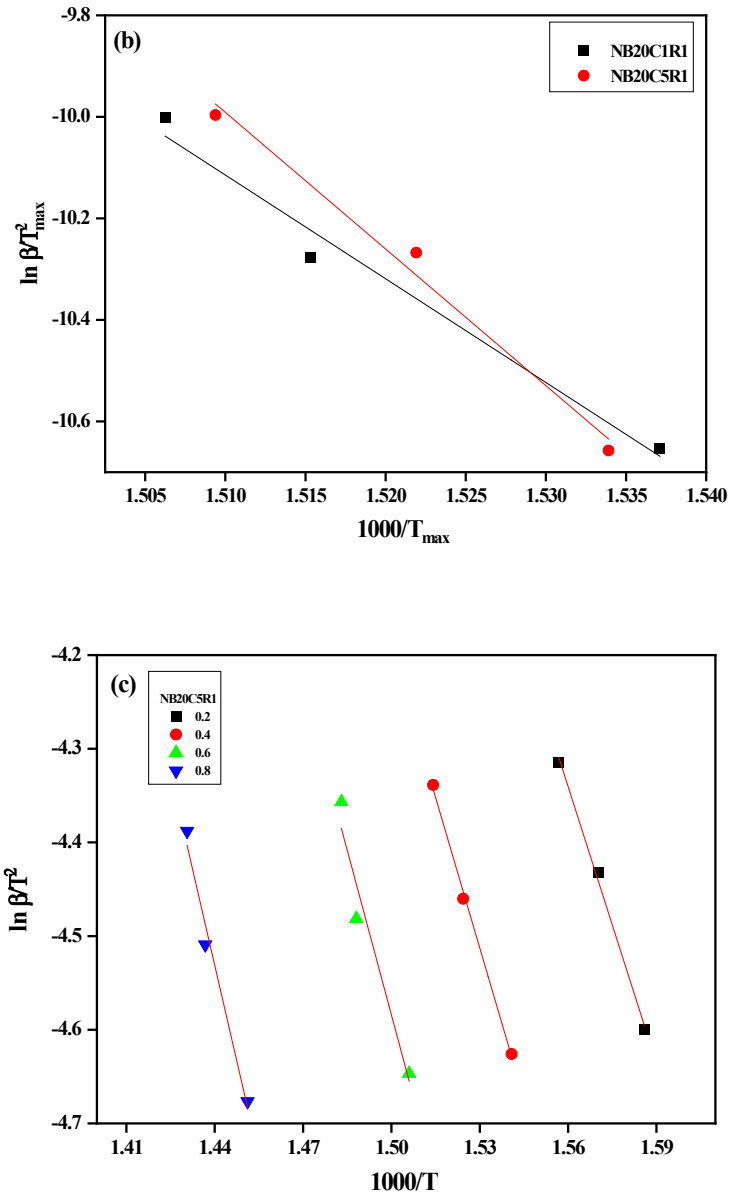

Figure 7.12 (b) Kissinger (c) KAS plot of NR/CCB-CNT-RGO hybrid filler systems

Activation energy obtained from the KAS model for both samples is found to be lower. This suggests that the degradation mechanisms or pathways estimated by the KAS model may differ from those estimated by the Kissinger and FWO models. Activation energies derived from the Kissinger and FWO models are nearly identical.

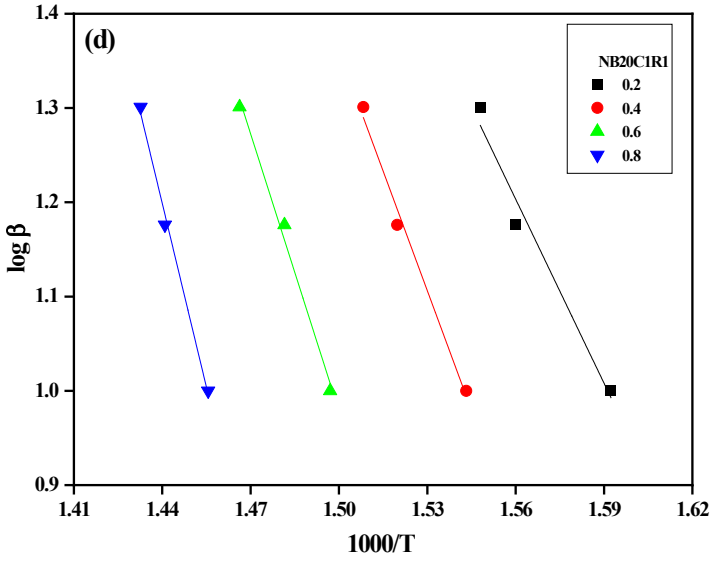

Figure 7.12(d)- FWO plot of NR/CCB-CNT-RGO hybrid filler systems

7.4. Comparative analysis of thermal degradation properties

Table 7.16 presents the $T_{50\%}$ of NR hybrid filler systems with various fillers. $T_{50\%}$ is the direct indication of thermal stability. All the filler incorporated composites has enhanced thermal stability. IL modified CNT-CCB and CCB-CNT-RGO incorporated composites exhibits higher thermal stability. **Table 7.17** presents the average activation energy of NR hybrid filler systems obtained from various models. NR containing IL-modified fillers and a hybrid system comprising CCB, CNT, and RGO exhibits elevated activation energy values. This suggests enhanced thermal stability for these systems. Improved thermal stability is attributed to the well-structured hybrid filler network within these composites. Aggregate structure of CCB chemically interacts with the ionic liquid and can also interact with NR chains. Optimal dispersion of fillers and the interaction of the polymer chains with these fillers play a pivotal role. Moreover, the barrier effect presented by the integrated filler system inhibits the migration of volatile

compounds to the surface. Such a phenomenon can decelerate the degradation process, further reinforcing the resistance of composite to thermal breakdown.

Table 7.16- Degradation temperatures of NR hybrid filler systems

Samples	$T_{50\%}$ (°C)
NB0	**393**
NB10	**392**
NB20IL1	**400**
NB20C5	**403**
NB20C5IL3	**407**
NB20C5R1	**407**

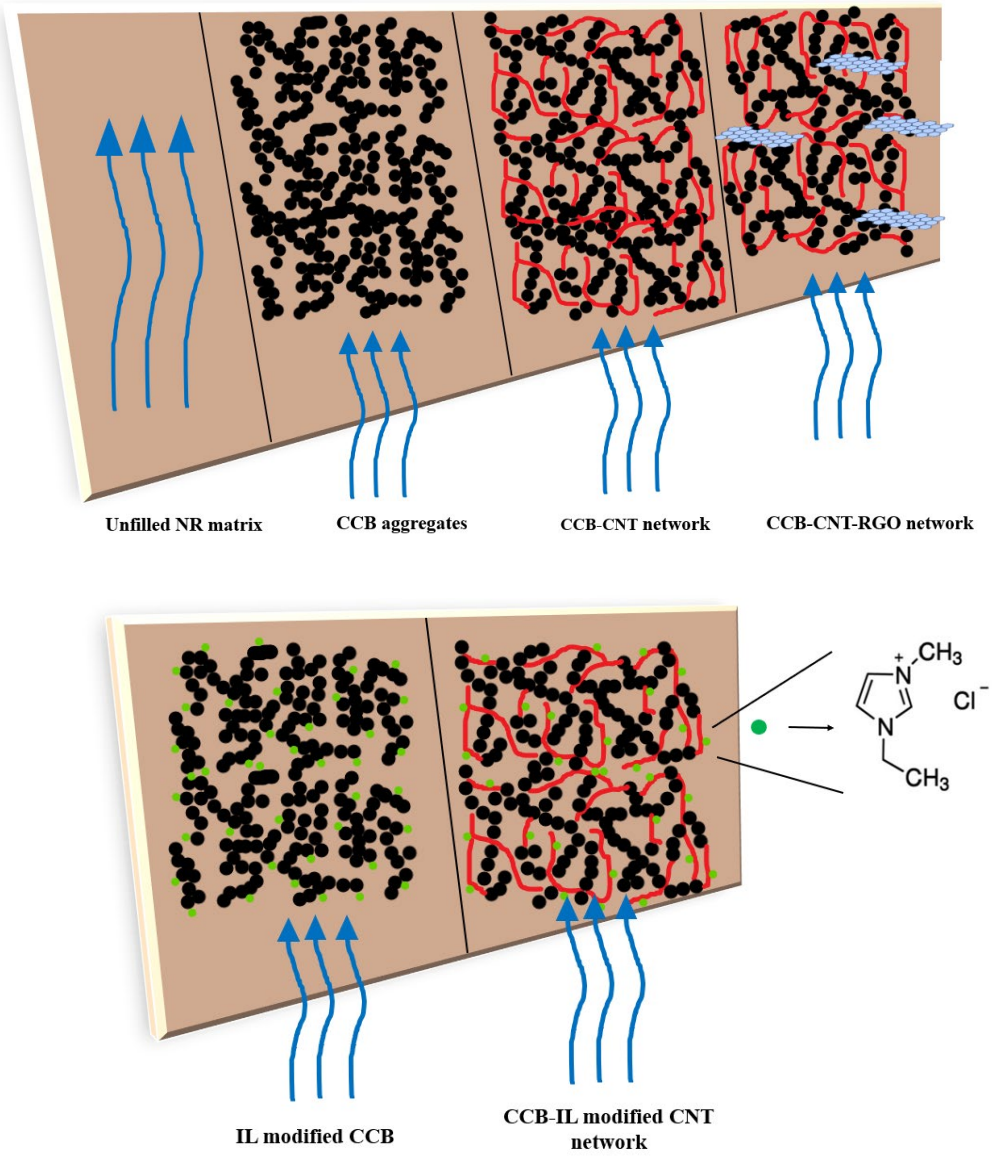

Figure 7.13- Schematic representation of barrier effect of filler network in NR matrix

Figure 7.13 shows the schematic representation of the barrier effect of different filler systems in resisting the thermal degradation of the NR matrix.

Table 7.17- Activation energy (kJ/mol) of NR hybrid filler systems

Sample	Coats-Redfern model	Kissinger model	KAS model	FWO model
NB0	123	204	102	234
NB10	135	204	97	222
NB20C3	122	192	88	203
NB20IL1	131	228	166	330
NB20C5IL1	151	211	84	195
NB20C5R1	134	224	89	204

7.5. Conclusion

Thermal studies of the NR hybrid filler systems provide information about the enhanced thermal stability of the from the IL modified CCB and CNT systems. Moreover, the hybrid filler combination of CCB-CNT-RGO also exhibits enhanced thermal stability, as indicated by the activation energy values deduced from the kinetic models. These models align closely with experimental findings, exhibiting high correlation values.

7.6. References

1. Perejón A, Sánchez-Jiménez PE, García-Garrido C, Pérez-Maqueda LA. Kinetic study of complex processes composed of non-independent stages: pyrolysis of natural rubber. Polymer Degradation and Stability. 2021 Jun;188:109590.
2. Galin-Vacherot M. Pyrolyse eclair de polyisoprenes. Essai de correlation entre les produits de degradation et la microstructure des polymeres. European Polymer Journal. 1971 Oct 1;7(10):1455–71.
3. Chien JCW, Kiang JKY. Polymer reactions—X thermal pyrolysis of poly(isoprene). European Polymer Journal. 1979 Jan 1;15(11):1059–65.
4. Groves SA, Lehrle RS, Blazsó M, Székely T. Natural rubber pyrolysis: Study of temperature-and thickness-dependence indicates dimer formation mechanism. Journal of Analytical and Applied Pyrolysis. 1991 Jul;19:301–9.
5. Sánchez-Jiménez PE, Pérez-Maqueda LA, Perejón A, Criado JM. Clarifications regarding the use of model-fitting methods of kinetic analysis for determining the activation energy from a single non-isothermal curve. Chemistry Central Journal. 2013 Feb 5;7(1):25.
6. Kissinger HE. Reaction Kinetics in Differential Thermal Analysis. Analytical Chemistry. 1957 Nov 1;29(11):1702–6.
7. Chen S, Yu H, Ren W, Zhang Y. Thermal degradation behavior of hydrogenated nitrile-butadiene rubber (HNBR)/clay nanocomposite and HNBR/clay/carbon nanotubes nanocomposites. Thermochimica Acta. 2009;491(1–2):103–8.
8. Heydari M, Rahman M, Gupta R. Kinetic study and thermal decomposition behavior of lignite coal. International Journal of Chemical Engineering. 2015;2015.
9. Akahira T, T. ST. Joint Convention of Four Electrical Institutes. Vol. 16. 1971.
10. Flores JJA, Quiñones JGR, Rodríguez MLÁ, Vera JVA, Valencia JE, Martínez SJG, et al. Thermal degradation kinetics and FT-IR analysis on the pyrolysis of pinus pseudostrobus, pinus leiophylla and pinus montezumae as forest waste in western Mexico. Energies. 2020;13(4).

11. Ozawa T. A New Method of Analyzing Thermogravimetric Data. Bulletin of the Chemical Society of Japan. 1965 Nov 1;38(11):1881–6.
12. Peterson JD, Vyazovkin S, Wight CA. Kinetics of the Thermal and Thermo-Oxidative Degradation of Polystyrene, Polyethylene and Poly(propylene). Macromolecular Chemistry and Physics. 2001 Mar 1;202(6):775–84.
13. Xue Z, Qin L, Jiang J, Mu T, Gao G. Thermal, electrochemical and radiolytic stabilities of ionic liquids. Phys Chem Chem Phys. 2018 Mar 28;20(13):8382–402.
14. Patidar K, Singathia A, Vashishtha M, Kumar Sangal V, Upadhyaya S. Investigation of kinetic and thermodynamic parameters approaches to non-isothermal pyrolysis of mustard stalk using model-free and master plots methods. Materials Science for Energy Technologies. 2022 Jan 1;5:6–14.
15. Han Z, Fina A. Thermal conductivity of carbon nanotubes and their polymer nanocomposites: A review. Progress in Polymer Science. 2011 Jul 1;36(7):914–44.
16. Krainoi A, Kummerlöwe C, Nakaramontri Y, Wisunthorn S, Vennemann N, Pichaiyut S, et al. Influence of carbon nanotube and ionic liquid on properties of natural rubber nanocomposites. 2019;22.
17. Danon B, Mkhize NM, Van Der Gryp P, Görgens JF. Combined model-free and model-based devolatilisation kinetics of tyre rubbers. Thermochimica Acta. 2015 Feb;601:45–53.
18. Brazier DW, Nickel GH. Thermoanalytical Methods in Vulcanizate Analysis II. Derivative Thermogravimetric Analysis. Rubber Chemistry and Technology. 1975 Sep 1;48(4):661–77.
19. Tamura S, Murakami K, Kuwazoe H. Isothermal degradation of cis-1,4-polyisoprene vulcanizates. Journal of Applied Polymer Science. 1983;28(11):3467–84.
20. Pielichowski K, Njuguna J, Majka TM. 7 - Thermal degradation of natural polymers. In: Pielichowski K, Njuguna J, Majka TM, editors. Thermal Degradation of Polymeric Materials (Second Edition) [Internet]. Elsevier; 2023 [cited 2023 Aug 11]. p. 149–70. Available from: https://www.sciencedirect.com/science/article/pii/B9780128230237000095
21. Statistical mechanical model for diffusion of simple penetrants in polymers. I. Theory - Pace - 1979 - Journal of Polymer Science: Polymer Physics Edition - Wiley Online Library [Internet]. [cited 2023 Aug 11]. Available from: https://onlinelibrary.wiley.com/doi/abs/10.1002/pol.1979.180170309

Chapter 8

Characterisation and Properties of Synthesised RGO Incorporated NR/ CCB-CNT Hybrid Filler Systems

Summary

This chapter explores the morphological and structural characteristics of thermally reduced graphene oxide, which is synthesised in the laboratory using Hummer's method (syTRGO). Also, the characterisation and properties of the syTRGO incorporated NR/CCB-CNT composites are discussed in detail. Finally, the properties of NR/CCB-CNT-syTRGO composites are compared with NR/CCB-CNT-RGO composites. NR/CCB-CNT-syTRGO composites exhibit a high tensile strength of 30.28 ± 0.76 MPa and DC conductivity of 10^{-3} S/m.

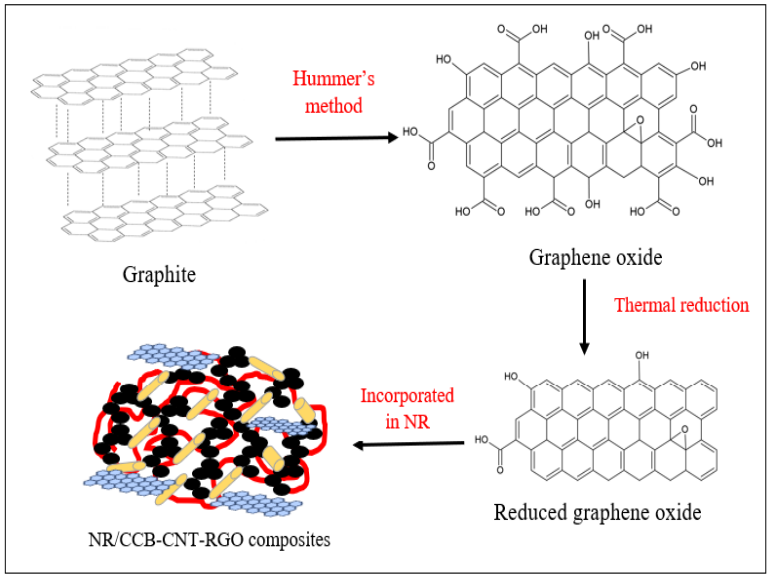

8.1. Introduction

Graphene is an elemental allotrope consisting of a hexagonal lattice arrangement of carbon atoms forming a single layer.(1) Graphene possesses notable physical properties, including high mobility of charge carriers (200,000 $cm^2V^- s^-)^1$, thermal conductivity (~5000 $Wm^{-1}K^{-1}$), Young's modulus (~1100 GPa) and surface area of 2630 m^2/g. (2,3) These distinctive features make graphene a promising one in materials science. Several methods are available for preparing graphene, each tailored to specific applications and desired characteristics. Exfoliation of graphite into single sheets of graphene by micromechanical cleavage, known as the Scotch tape method, was first reported in 2004. (4) Natural graphite flakes (NFG) are carbon arranged in hexagonal arrays, forming flat layers stacked in three dimensions. Within a plane, carbon atoms are held together by covalent bonds, while van der Waals forces act between adjacent layers, maintaining a separation of 0.337 nm. (5)

Oxidation-reduction methods for the large-scale synthesis of graphene from graphite include Hummer's method (6), Brodie's method (7), Staudenmaier's method (8) and modified and improved Hummer's method. (9) These methods, in general, utilise strong oxidising agents and acids to create graphite oxide, which has multiple layers. Exfoliation of graphite oxide produces graphene oxide, which is a few layers or a single layer. These oxidised layers are reduced thermally (10) or chemically (11) to obtain reduced graphene oxide (RGO).

In this study, natural graphite flakes are used to synthesise the graphene oxide (GO) using Hummer's method. Hummer's method is the fastest conventional method of producing graphite oxide/graphene oxide with a high C/O ratio. Oxidation of graphite-to-graphite oxide is accomplished by using an anhydrous mixture of sulphuric acid (H_2SO_4), potassium permanganate ($KMnO_4$) and sodium nitrate ($NaNO_3$). GO has many oxygen functionalities like carboxyl (COOH), carbonyl (C=O) and hydroxyl (OH) groups on the surface, which renders hydrophilicity to GO. GO can be efficiently reduced thermally in a muffle furnace, where the majority of the oxygen functionalities will be removed. (12)

8.2. Results and discussion

8.2.1. Morphology and structural analysis of the reduced graphite oxide (syTRGO)

Hummer's method is used to produce graphene, which is discussed in **Chapter 2**. GO obtained after drying has a sheet-like appearance and is brown in colour. After thermal reduction, there is a visible change in the appearance accompanied by a substantial increase in volume. Thermally reduced graphene oxide (syTRGO) is black in colour with fluffy nature which provides the first evidence of reduction of synthesised GO. **Figure 8.1** shows the XRD spectra of graphite, GO and syTRGO. The diffraction pattern of graphite shows a strong, narrow characteristic peak at 26.57° with d-spacing of 3.35A° corresponding to the lattice plane of (002). The incorporation of oxygen functionalities and intercalation of water molecules in GO has increased the interlayer spacing to 8.64A° and shifted the peak to 10.22° with low intensity. Graphite has narrow and high intensity peak compared to the peak of GO. Scherrer's analysis of the XRD diffraction pattern gives a crystallite size of 44.4 nm for graphite, which, upon oxidation, becomes 7.9 nm. Unlike the ordered and layered structure of graphite and GO, syTRGO is amorphous in nature, and this is confirmed by the absence of any characteristic peaks in the XRD data. (5,13) So here, the thermal reduction of GO has produced completely exfoliated, unstacked and amorphous syTRGO.

Figure 8.2(a-f) presents the TEM images of graphite, GO and syTRGO. **Figure 8.2(c)** shows the thin and highly exfoliated syTRGO sheets. Unlike GO, syTRGO has wrinkles and folds, which are indicated by the dark regions of the TEM image. SAED method allows for characterising the crystallographic structure of syTRGO. The lower intensity of crystallographic spots and diffused rings confirms the amorphous nature of reduced syTRGO **(Figure 8.2(f))**. SAED pattern of graphite flakes **(Figure 8.2 (d))** has bright hexagonal crystallographic spots indicating crystalline nature with AB stacking (14), and that of GO **(Figure 8.2(e))** has small spots making up a ring indicating its poly nanocrystalline nature.

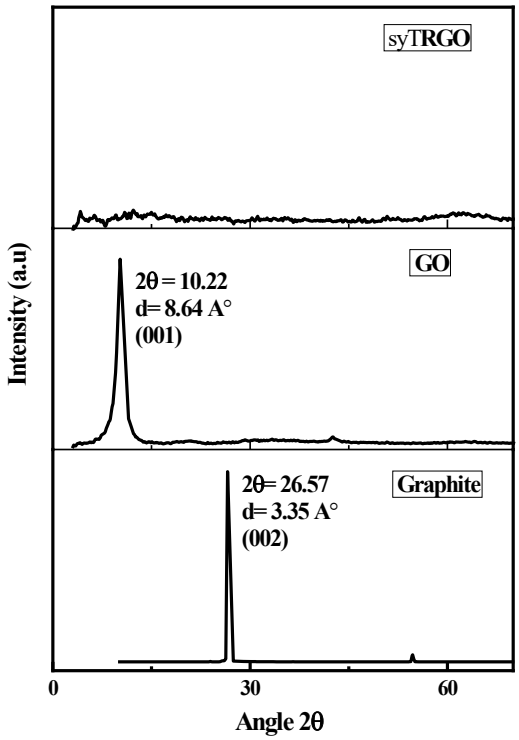

Figure 8.1- XRD spectra of graphite, GO and syTRGO

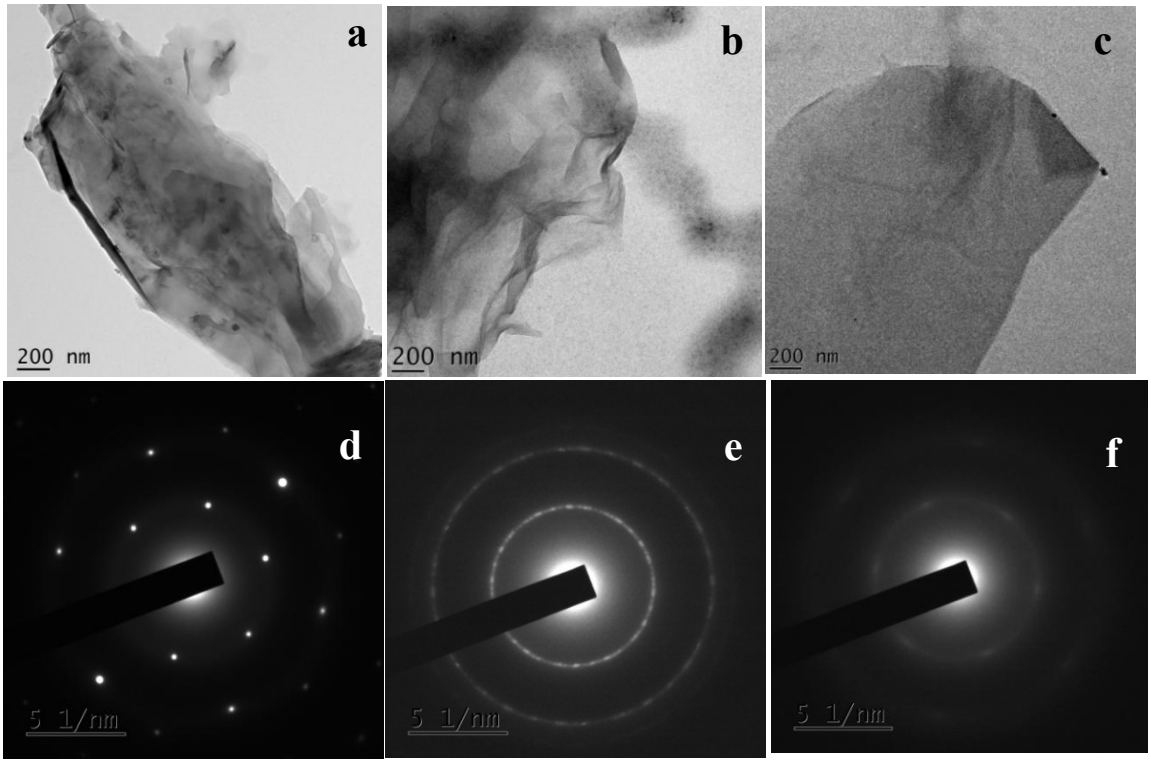

Figure 8.2- TEM images of (a) graphite, (b) GO and (c) syTRGO. SAED patterns of (d) graphite, (e) GO and (f) syTRGO

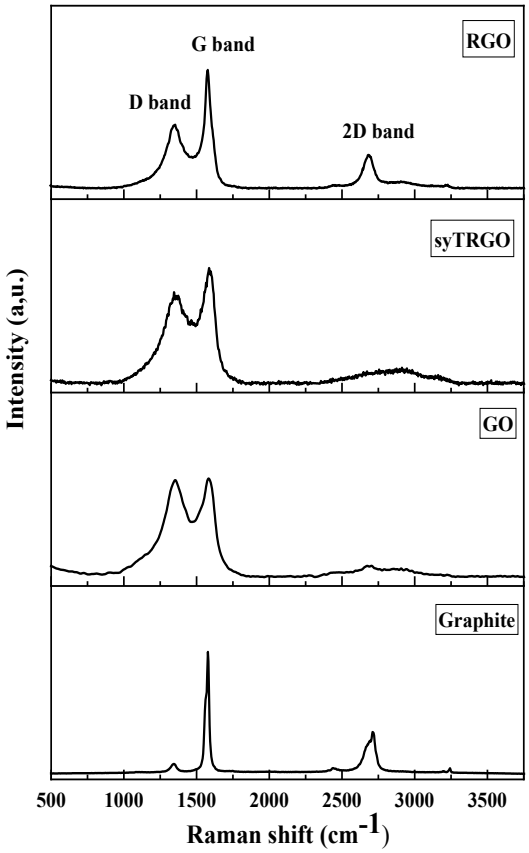

Figure 8.3- Raman spectra of graphite, GO, syTRGO and RGO

Raman spectroscopy gives information about the structural changes during the oxidation-reduction of graphite. Raman spectra of graphite, GO and syTRGO are shown in **Figure 8.3**. Raman spectrum of graphite shows three characteristic peaks at 1345, 1580 and 2714 cm^{-1}. The D band or 'disorder band' at 1345 cm^{-1} is associated with the disordered structure of the graphitic lattice. It indicates structural defects, edges and oxygen functionalities bonded to the carbon atoms. It is associated with the breathing mode of aromatic rings caused due to the defects present in the sample. (12)The sharp G band at 1580 cm^{-1} arises due to the in phase vibrations of the ordered crystal structure. The third band at 2714 cm^{-1} is the overtone of the D band, known as the 2D band. The ratio of the intensity of the D band to the intensity of the G band (I_D/I_G ratio) is 0.11 for graphite flakes indicating its ordered graphitic structure. Chemical oxidation of graphite flakes decreases the intensity of the G band (1581 cm^{-1}) and increases the intensity of the D band (1353 cm^{-1}) due to the destruction of the graphitic ordered structure. The deformation of graphitic structure is further confirmed by the broad and weaker 2D band at 2675cm^{-1}.

The incorporation of oxygen functionalities converts sp^2 carbon bonds to sp^3 and enhance the I_D/I_G ratio of GO to 0.98. After thermal reduction, the intensity of the D (1354 cm^{-1}) band is decreased only slightly, indicating the formation of syTRGO with defects. G band is observed at 1589 cm^{-1}. Sharp 2D band is associated with graphitic structure. The broad and weak 2D peak at 2862 cm^{-1} implies the amorphous nature of syTRGO. In addition, the I_D/I_G ratio has decreased only up to 0.76. This confirms that thermal reduction has completely exfoliated graphene layers and removed oxygen functionalities in GO. Raman spectra of RGO used for the studies in the previous chapter show a D band with low intensity and a sharp G band. Unlike synthesised syTRGO, RGO possesses a sharp 2D band. Compared to the laboratory synthesised TRGO, procured RGO has fewer defects and a more ordered graphitic structure. The 2D band of RGO and syTRGO doesn't represent the defects. However, the 2D position and shape of the 2D band can be used to measure graphene layers. (15,16)The 2D peak of RGO is at 2687, while syTRGO has a peak at 2872 $cm^{-1.}$ The shift of the 2D peak to a higher wavenumber indicates the increase in graphene layers. Thus laboratory synthesised syTRGO has more layers than RGO.

Figure 8.4 (a) & (b) presents the high resolution C1s XPS spectra of GO and syTRGO, which gives an insight into the reduction efficiency and chemical structural change associated with thermal reduction. **Figure 8.4** shows three characteristic peaks at ~284.8, ~286.9, and ~288.5 eV correspond to the binding energy of sp^2 C in C=C, C-O (hydroxyl and epoxy groups) and C=O (carboxyl and ketone groups) respectively. Increased intensity of C=C peak and decreased intensity of C-O and C=O peaks in syTRGO compared to GO confirms the effective removal of oxygen functionalities upon reduction. Atomic % of elements and C/O ratio of GO and syTRGO are given in **Table 8.1**. The thermal reduction has decreased the atomic % of oxygen from 30.2 to 13.6% while increasing the atomic % of C from 69.1 to 86.3 %. The C/O ratio of GO synthesised in the present study is 2.3, which is in agreement with the literature. (17) The C/O ratio of GO synthesised by Hummer *et al*. is 2.25. (6) Hummer's method introduces more oxygen functionalities than the modified Hummer's method. (18,19) Upon reduction of GO, the C/O ratio increases to 6.3, implying a decreased amount of oxygen functionalities. Thus, the low-

temperature reduction of GO is efficient in removing most of the oxygen functionalities from GO.

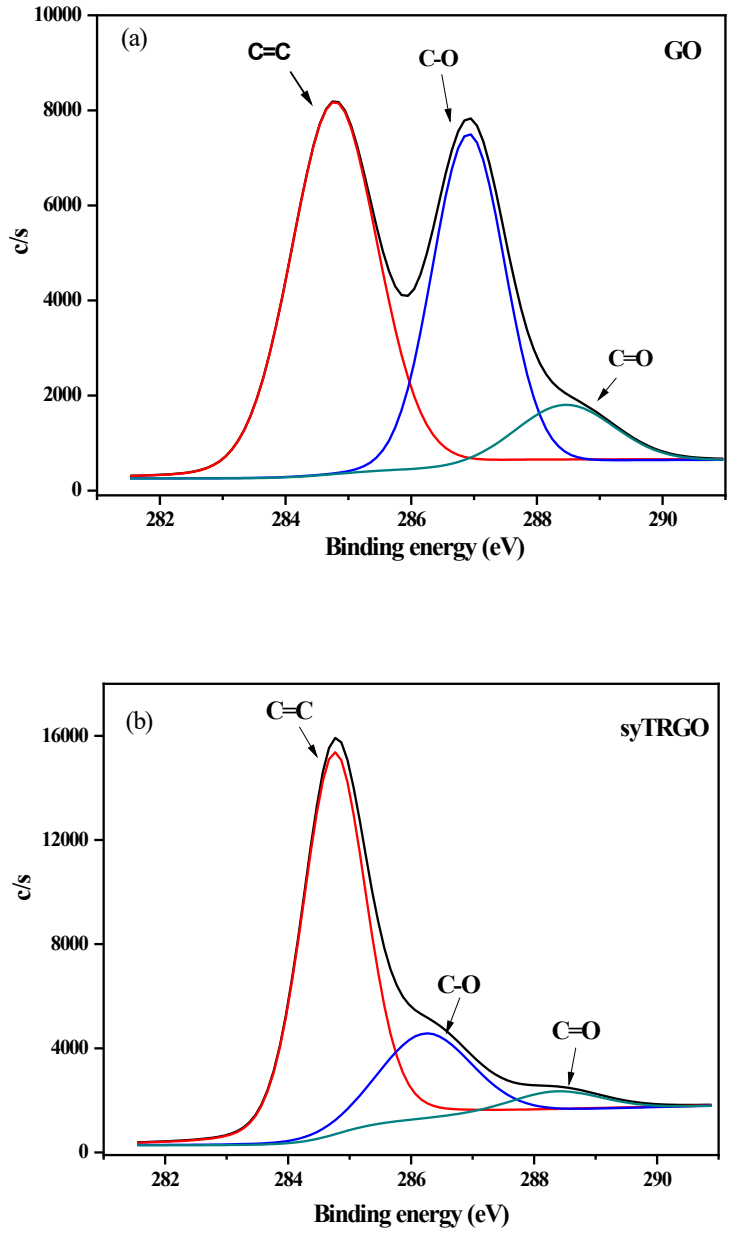

Figure 8.4- High resolution C1s XPS spectra of (a) GO and (b) syTRGO

Table 8.1- Atomic % and C/O ratio of GO and syTRGO

	Atomic % of		C/O
	C1s	O1s	
GO	69.1	30.2	2.3
syTRGO	86.3	13.6	6.3

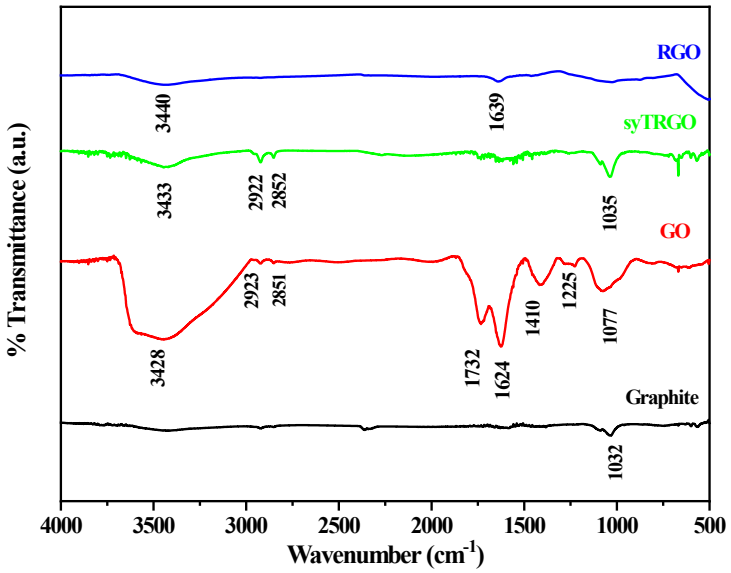

Figure 8.5- FTIR spectra of graphite, GO, syTRGO and RGO

Figure 8.5 shows the FTIR spectra of graphite, GO, syTRGO and RGO. FTIR spectra of graphite show no characteristic peaks except a weak peak at 1032 cm^{-1} corresponding to epoxide groups. Graphite oxide contains heavily oxygenated sheets bearing hydroxyl and epoxide functional groups on their basal planes, along with carbonyl and carboxy groups at the sheet edges. FTIR spectra illustrate the highly oxygenated GO in this work. Characteristic peaks of GO at 3428 cm^{-1} and 1624 cm^{-1} are due to O-H stretching vibrations and C=C symmetric vibrations of unoxidised graphitic domains, respectively. Oxidation of graphite is confirmed in the FTIR spectra of GO by the introduction of carboxylic C=O bond peak at 1732 cm^{-1}, epoxy C-O stretching peak at 1074 cm^{-1}, O-H deformation peak at 1410 cm^{-1} and weak stretching vibrations of C (sp^3)-H bonds at 2851 cm^{-1} and 2923 cm^{-1}. In contrast to GO, most of these peaks disappear or have decreased intensity in syTRGO. FTIR of purchased RGO shows only low intensity peaks at 3440 and 1639 cm^{-1}, indicating low amount of oxygen functionalities.

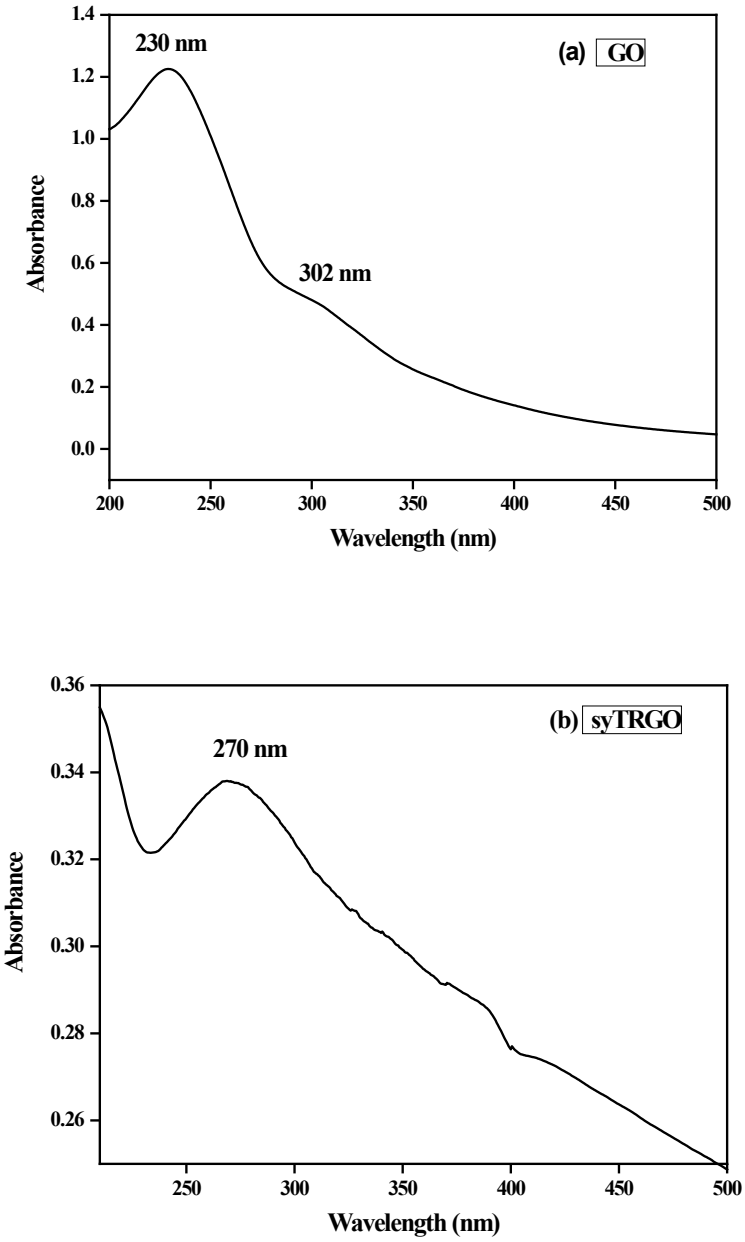

Figure 8.6- UV-Visible spectra of GO and syTRGO

Another important observation to be noticed is the shift in epoxide peak to a higher wavenumber in GO compared to graphite which again is shifted to low wavenumbers upon reduction. This confirms that electron withdrawing groups like carboxyl groups are introduced in GO, which is again removed in syTRGO. The intensity of the O-H stretching peak is decreased considerably in syTRGO and RGO. This proves that most of the adsorbed water is removed by thermal reduction. Epoxide peak at 1074 cm^{-1} is retained in the syTRGO with decreasing intensity, suggesting that thermal

reduction is effective in removing most of the oxygen functionalities and not all of the epoxide groups. This is supported by the XPS analysis of syTRGO and GO.UV-visible absorption spectra of GO and syTRGO are shown in **Figure 8.6 (a & b)** GO has a strong absorption peak at 230 nm, indicating τηε π–π* transition of aromatic carbons, accompanied by a shoulder peak at 302 nm, indicating the n- π* transition of CO groups. The thermal reduction has caused the redshift of the peak to 270 nm due to the restoration of sp^2 hybridized carbon atoms. (20) UV-visible spectra provide evidence for the oxidation of graphite flakes and its subsequent reduction.

8.2.2. Properties of NR/CCB-CNT-syTRGO composites

8.2.2.1. Cure characteristics

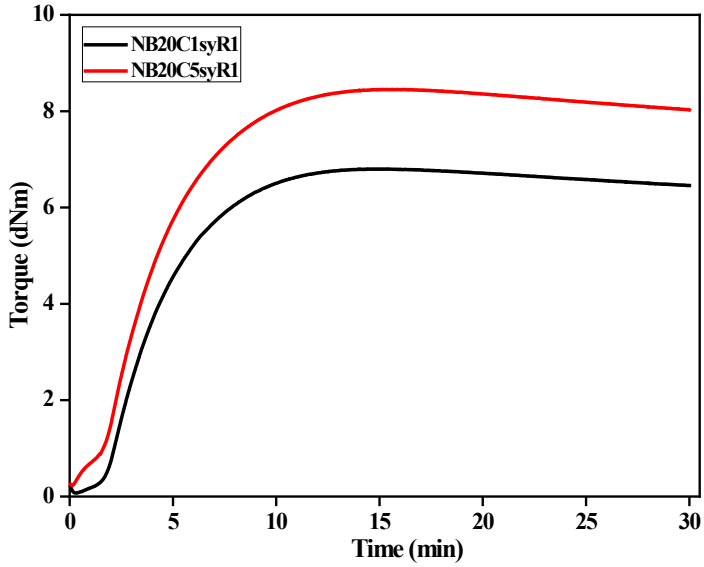

Figure 8.7- Torque-time curves of NR/CCB-CNT-syTRGO hybrid filler systems

Table 8.2- Cure characteristics of NR/CCB-CNT-syTRGO hybrid filler systems

Sample	M_L (dNm)	M_H (dNm)	ΔM	T_{90} (min)	$\propto_f$
NB0	0.12	10.41	10.29	6.14	-
NB20C1syR1	0.1	6.33	6.23	8.26	-2.12
NB20C5syR1	0.23	8.45	8.22	8.5	-0.97

Figure 8.7 presents the torque profile of NR/CCB-CNT-syTRGO composites. The torque experienced by the composite is directly proportional to the amount of CNT.

Table 8.2 provides the cure characteristics of the hybrid systems. The minimum torque exhibits a higher value for NB20C5syR1, and the elevated CNT concentration contributes to an increase in the initial viscosity of NR chains. Increased CNT concentration creates an extensive filler network that causes entanglement of NR chains. This causes resistance to the mobility of polymer chains and results in high viscosity. The torque difference also demonstrates an increase with respect to CNT content. Higher ΔM is associated with an increase in the crosslink density of the composites. (21) NB20C5syR1 has decreased rubber chain mobility due to the increased rubber-filler interaction.

8.2.2.2. Mechanical properties

Table 8.3 -Mechanical properties of NR/CCB-CNT-syTRGO hybrid filler systems

Sample	Density (g/cm^3)	Elongation at break (%)	Tensile strength (MPa)	Modulus at 100% (MPa)	Modulus at 200% (MPa)	Modulus at 300% (MPa)
NB20C1syR1	1.05	790 ±23	29.15 ±0.34	2.18 ±0.03	4.41 ±0.02	7.29±0.05
NB20C5syR1	1.07	729 ±36	30.28 ±0.76	2.99 ±0.16	6.12 ±0.29	9.89 ±0.45

Table 8.3 presents the mechanical properties of the composites. Tensile strength is 29.15 ±0.34 and 30.28 ±0.76 MPa for NB20C1syR1 and NB20C5syR1, respectively. Hybrid system of CCB, CNT and syTRGO exhibits strong filler-filler and filler-rubber interaction, contributing to the high reinforcement effect. The reinforcement mechanism of CCB is due to the strong rubber-filler interactions, while studies suggest that the reinforcement due to CNT can be attributed to the high aspect ratio and the physical interactions with rubber. (22,23) These physical interactions can aid in the effective and uniform stress transfer across the matrix and prevent the susceptibility of fatigue or failure. The oxygen functional groups present in syTRGO increase the chemical interactions with CNT and CCB and increase filler-filler interaction. The two-dimensional geometry of syTRGO also creates more interfaces with NR due to its large surface area to volume ratio and reinforces the polymer matrix. Orientation of fillers in a polymer matrix is also an important factor in reinforcing the composites. Presence of graphene layers in syTRGO allows the alignment of these along the direction of strain.(24) This, in turn, allows the stress transfer and prevents the localisation of stress. Thus, the hybrid filler system of CCB,

CNT and syTRGO effectively reinforces the NR matrix through interfacial interactions. This is also reflected in the modulus values at different elongations. **Table 8.4** presents the theoretically predicted tensile strength of NR/CCB-CNT-syTRGO hybrid filler systems Theoretical tensile strength predicted using the Nicolais-Narkis, Knori-Geil and Turcsanyi model gives values close to the experimental value. Tensile strength obtained using the Nicolais-Narkis model is in good agreement with experimental data.

Table 8.4- Theoretical comparison of tensile strength as a function of volume fraction of CCB

Sample	Experimental	Nicolais-Narkis model	Knori-Geil model	Turcsanyi model
NB20C1syR1	29.15 ±0.34	29.18	28.59	28.49
NB20C5syR1	30.28 ±0.76	30.32	30.80	30.87

8.2.2.3. Dielectric studies

Figure 8.8(a) and (b) show the frequency dependent dielectric permittivity and dielectric loss of syTRGO incorporated composites. The dielectric permittivity values lies between 10^4 -10^5 for both samples. The high dielectric permittivity indicates the conductive network of filler particles. The physical and chemical interactions of CCB-CNT and syTRGO establish a conductive network in the NR matrix. The oxygen functionalities in syTRGO help to increase the filler-filler and filler-matrix interactions. However, syTRGO incorporated composites exhibits comparatively high dielectric loss, which indicates the loss of electrical energy as thermal energy. **Figure 8.8 (c)** plots the AC conductivity of composites against log frequency. AC conductivity indicates the leakage current in dielectric materials. Both samples exhibit similar trends in AC conductivity indicating well established conductive network in NR matrix

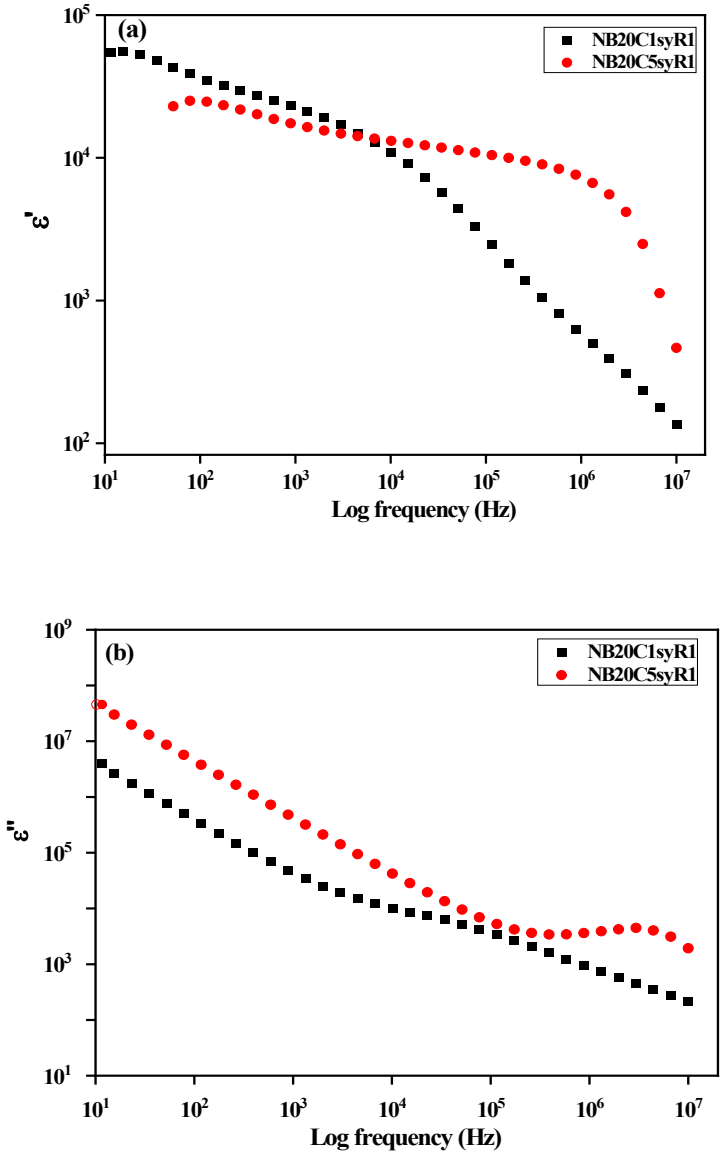

Figure 8.8- Frequency dependent (a) dielectric permittivity and (b) dielectric loss of NR/CCB-CNT-syTRGO hybrid filler systems

.

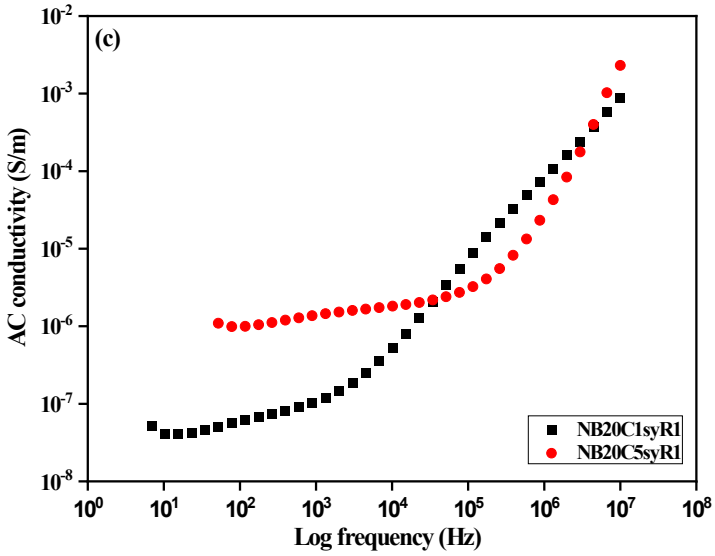

Figure 8.8- (c) AC conductivity of NR/CCB-CNT-syTRGO hybrid filler systems

8.2.2.4. DC conductivity

DC conductivity values of the NR/CCB-CNT-syTRGO hybrid filler systems are given in **Table 8.5.** The conductivity values are significantly improved by the incorporation of synthesised TRGO. NB20C5syR1 shows conductivity in the order of 10^{-3}. syTRGO forms a conductive network with CNT and CCB in the NR matrix. The functional groups in CCB, CNT and syTRGO can interact to form a conductive network. Since the thermal reduction has not completely removed all the oxygen functionalities in syTRGO, the hydroxyl and carboxyl groups present in syTRGO can interact with CCB and CNT.

Table 8.5 – DC conductivity of NR/CCB-CNT-syTRGO hybrid filler systems

Sample	DC conductivity (S/m)
NB20C1syR1	3.77×10^{-6}
NB20C5syR1	2.9×10^{-3}

8.2.2.5. Transport properties

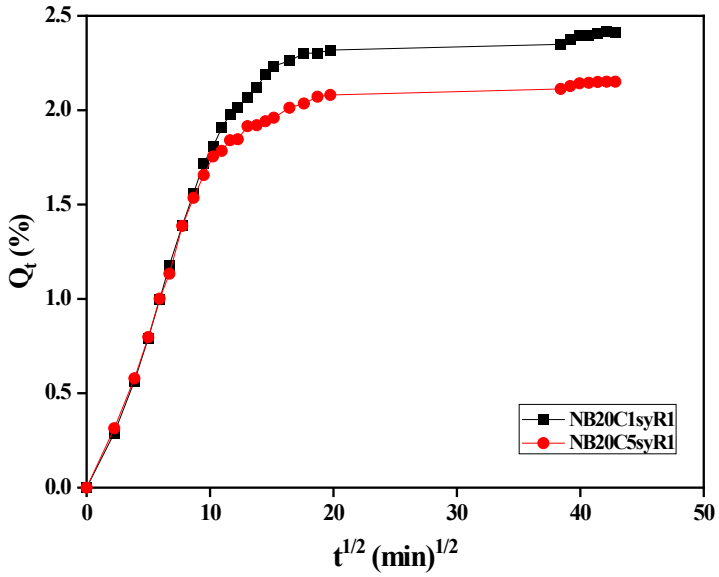

Figure 8.9- Sorption curves of NR/CCB-CNT-syTRGO hybrid filler systems

Table 8.6 - Diffusion coefficient, permeability coefficient and parameter n of NR/CCB-CNT-syTRGO hybrid filler systems

Sample	D (cm^2/s)	P (cm^2/s)	n
NB20C1syR1	8.65×10^{-7}	1.92×10^{-6}	0.59
NB20C5syR1	8.11×10^{-7}	1.61×10^{-6}	0.57

Figure 8.9 presents the sorption curves of NR/CCB-CNT-syTRGO hybrid filler systems. The filler network has effectively decreased solvent swelling as expected. **Table 8.6** presents the diffusion and permeability coefficients, which decrease as the toluene molecule has a tortuous path in the NR. The mode of transport was analysed and the parameter, n obtained is 0.59 and 0.57, which suggests non-Fickian mode of transport. The filler-filler interaction has restricted rubber chain mobility, which in turn reduces the sorption through the matrix.

Table 8.7- Correlation coefficients and kinetic model constants of NR/CCB-CNT-syTRGO hybrid filler systems

Sample		NB20C1syR1	NB20C5syR1
First order kinetics	k	0.0094	0.0086
	R^2	0.9656	0.9715
Higuchi model	k_h	0.0659	0.0753
	R^2	0.9730	0.9823
Korsemayer-Peppas model	k	0.1006	0.0940
	n	0.4151	0.4516
	R^2	0.9807	0.9853
Peppas-Sahlin model	k1	-0.7108	-1.2817
	k2	0.6520	1.2018
	m	0.1185	0.0869
	R^2	0.9957	0.9922

Kinetic models like First order kinetics, Higuchi, Korsemayer-Peppas and Peppas-Sahlin models were applied on transport data. The correlation coefficients and model constants are presented in **Table 8.7**. Among all the kinetic models, the Peppas-Sahlin model fits well for experimental data with the highest correlation coefficient. Here, the constant k1 is less than k2, and constant m decreases as CNT is increased. The constants k1 represent the Fickian contribution, and k2 represents the case II relaxational contribution. Higher value of k2 indicates that the transport is associated with polymer relaxation and swelling and is also associated with non-Fickian kinetics. The high negative value of k1 indicates the insignificant effect of Fickian diffusion mechanism. (25)

8.2.2.6. Swelling studies

Table 8.8 - Swelling index (%), swelling coefficient ($\propto$), volume fraction of rubber in solvent-swollen composites (V_{rf}), apparent crosslink density ($\frac{1}{Q}$) and crosslink density (v) of NR/CCB-CNT-syTRGO hybrid filler systems

Sample	Swelling index (%)	Swelling coefficient, $\propto$	V_{rf}	$\frac{1}{Q}$	v (g/mol/cm^3)
NB20C1syR1	227	2.62	0.2472	0.44	1.03×10^{-4}
NB20C5syR1	200	2.31	0.2648	0.50	1.2×10^{-4}

Swelling studies on the NR/CCB-CNT-syTRGO hybrid filler systems also suggests that the composites have decreased swelling in toluene. The filler-filler interaction has increased the crosslinks of the NR matrix, providing decreased free voids for the diffusion of toluene molecules. The composites exhibit increased crosslink density. The functional groups in fillers help to interact with the double bonds and sulfur in the NR matrix, creating crosslinks in the composites.

8.3. Comparative analysis of properties

Table 8.9 -Comparison of properties of NR/CCB-CNT-RGO and NR/CCB-CNT-syTRGO hybrid filler systems

Sample	v (g/mol/cm^3)	DC conductivity (S/m)	Tensile strength (MPa)	Modulus at 300% (MPa)
NB20C5R1	1.19×10^{-4}	8.99×10^{-5}	21.55 ± 0.61	6.5 ± 0.07
NB20C5syR1	1.2×10^{-4}	2.9×10^{-3}	30.28 ±0.76	9.89 ±0.45

Table 8.9 presents the comparison of properties of NR/CCB-CNT composites incorporated with commercial RGO and synthesized RGO. Both composites have 5 phr CNT and 1 phr RGO. The crosslink density of both composites is almost the same. However, DC conductivity, tensile strength and modulus at 300% elongation show a noticeable difference when laboratory synthesised syTRGO is used. DC conductivity of NB20C5R1 is in the order of $10^{-5,}$ while NB20C5syR1 is in the order of 10^{-3}.

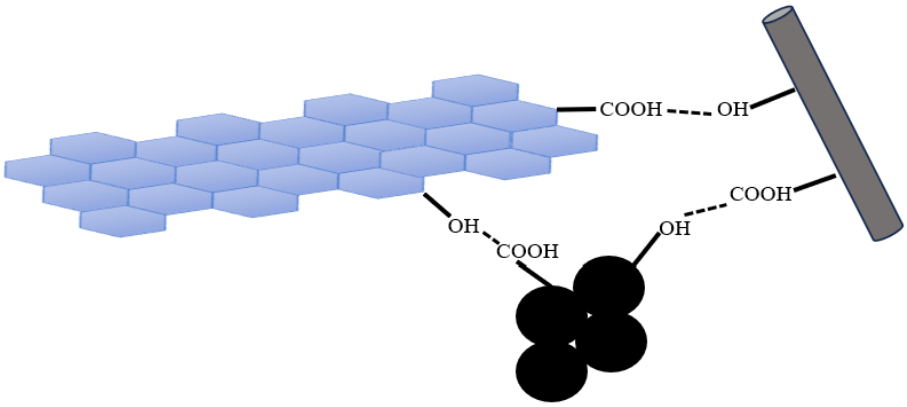

Figure 8.10- Schematic representation of interactions of fillers in NR/CCB-CNT-syTRGO hybrid filler systems

Tensile strength and modulus at 300% show a 40.5% and 52.2% increase, respectively, when synthesised TRGO is used. The oxygen functionalities present in the syTRGO can interact well with various functional groups of CCB and CNT and form an effective filler-filler network. This conductive filler network formation has helped in the easy transport of electrons, leading to increased conductivity. It also enhances the rubber-filler interfacial interaction, resulting in homogeneous dispersion of filler. Schematic representation of possible interaction between CCB, CNT and syTRGO is illustrated in **Figure 8.10**.

8.4. Conclusion

Graphene oxide was synthesised by Hummer's method and is characterised using various spectroscopic and microscopic techniques. GO was thermally reduced, and various studies such as Raman, FTIR, XRD and XPS analysis proved that thermal reduction removed the oxygen functionalities at an appreciable level. NR composites incorporated with synthesised TRGO exhibit enhanced properties. NR/CCB-CNT-syTRGO composites exhibit high tensile strength and DC conductivity. The remaining oxygen functional groups in the syTRGO help to form a filler network with CCB and CNT, resulting in enhanced filler-polymer interaction.

8.5. References

1. Geim AK, Novoselov KS. The rise of graphene. Nature Materials. 2007 Mar 1;6(3):183–91.
2. Lin Z, Yao Y, Li Z, Liu Y, Li Z, Wong CP. Solvent-Assisted Thermal Reduction of Graphite Oxide. J Phys Chem C. 2010 Sep 9;114(35):14819–25.
3. Randviir EP, Brownson DAC, Banks CE. A decade of graphene research: production, applications and outlook. Materials Today. 2014 Nov 1;17(9):426–32.
4. Novoselov KS, Geim AK, Morozov SV, Jiang D, Zhang Y, Dubonos SV, et al. Electric Field Effect in Atomically Thin Carbon Films. Science. 2004 Oct 22;306(5696):666–9.
5. Sadasivuni KK, Ponnamma D, Thomas S, Grohens Y. Evolution from graphite to graphene elastomer composites. Progress in Polymer Science. 2014 Apr;39(4):749–80.
6. Hummers WSJr, Offeman RE. Preparation of Graphitic Oxide. J Am Chem Soc. 1958 Mar 1;80(6):1339–1339.
7. Brodie BC. XIII. On the atomic weight of graphite. Philosophical Transactions of the Royal Society of London. 1997 Jan 1;149:249–59.
8. Staudenmaier L. Verfahren zur Darstellung der Graphitsäure. Berichte der deutschen chemischen Gesellschaft. 1898 May 1;31(2):1481–7.
9. Marcano DC, Kosynkin DV, Berlin JM, Sinitskii A, Sun Z, Slesarev A, et al. Improved Synthesis of Graphene Oxide. ACS Nano. 2010 Aug 24;4(8):4806–14.
10. Acik M, Lee G, Mattevi C, Chhowalla M, Cho K, Chabal YJ. Unusual infrared-absorption mechanism in thermally reduced graphene oxide. Nature Materials. 2010 Oct 1;9(10):840–5.
11. Gómez-Navarro C, Weitz RT, Bittner AM, Scolari M, Mews A, Burghard M, et al. Electronic Transport Properties of Individual Chemically Reduced Graphene Oxide Sheets. Nano Lett. 2007 Nov 1;7(11):3499–503.
12. Alam SN, Sharma N, Kumar L. Synthesis of Graphene Oxide (GO) by Modified Hummers Method and Its Thermal Reduction to Obtain Reduced Graphene Oxide (rGO)*. Graphene. 2017 Jan 10;6(1):1–18.

13. Iqbal MZ, Abdala AA. Thermally reduced graphene: synthesis, characterization and dye removal applications. RSC Adv. 2013;3(46):24455.
14. Jeong HK, Lee YP, Lahaye RJWE, Park MH, An KH, Kim IJ, et al. Evidence of Graphitic AB Stacking Order of Graphite Oxides. J Am Chem Soc. 2008 Jan 30;130(4):1362–6.
15. Kumar V, Kumar A, Lee DJ, Park SS. Estimation of Number of Graphene Layers Using Different Methods: A Focused Review. Materials. 2021 Aug 16;14(16):4590.
16. Hwangbo Y, Lee CK, Mag-Isa AE, Jang JW, Lee HJ, Lee SB, et al. Interlayer non-coupled optical properties for determining the number of layers in arbitrarily stacked multilayer graphenes. Carbon. 2014 Oct 1;77:454–61.
17. Gurzęda B, Buchwald T, Nocuń M, Bąkowicz A, Krawczyk P. Graphene material preparation through thermal treatment of graphite oxide electrochemically synthesized in aqueous sulfuric acid. RSC Adv. 2017;7(32):19904–11.
18. Ren PG, Yan DX, Ji X, Chen T, Li ZM. Temperature dependence of graphene oxide reduced by hydrazine hydrate. Nanotechnology. 2011 Feb 4;22(5):055705.
19. Dolbin AV, Khlistyuck MV, Esel'son VB, Gavrilko VG, Vinnikov NA, Basnukaeva RM, et al. The effect of the thermal reduction temperature on the structure and sorption capacity of reduced graphene oxide materials. Applied Surface Science. 2016 Jan;361:213–20.
20. Wong C, Lai C, Lee K, Hamid S. Advanced Chemical Reduction of Reduced Graphene Oxide and Its Photocatalytic Activity in Degrading Reactive Black 5. Materials. 2015 Oct 19;8(10):7118–28.
21. Abidin ZZ, Mamauod SNL, Sarkawi SS, Saimi NSB. Influence of Filler System on the Cure Characteristics and Mechanical Properties of Butyl Reclaimed Rubber.
22. Nah C, Lim J, Cho B, Hong C, Gent A. Reinforcing rubber with carbon nanotubes. Journal of Applied Polymer Science. 2010 Nov 5;118:1574–81.
23. Nah C, Lim J, Sengupta R, Cho B, Gent A. Slipping of carbon nanotubes in a rubber matrix. Polymer International - POLYM INT. 2011 Jan 1;60.
24. Papageorgiou DG, Li Z, Liu M, Kinloch IA, Young RJ. Mechanisms of mechanical reinforcement by graphene and carbon nanotubes in polymer nanocomposites. Nanoscale. 2020;12(4):2228–67.
25. Babu BR, Babu KN. Calculation of predominant drug release mechanism using Peppas-Sahlin model (substitution method): A linear regression approach.

Chapter 9
Conclusion

The present research work focuses on fabricating conducting natural rubber (NR) composites by incorporating various hybrid fillers. For the achievement of the goals, various conducting fillers such as conductive carbon black (CCB), carbon nanotubes (CNT), 1-ethyl-3-methylimidazolium chloride- modified CCB(ILCCB), CCB combined with -ethyl-3-methylimidazolium chloride -modified CNT(ILCNT), and hybrid filler systems of CCB, CNT, and thermally reduced graphene oxide (RGO) is employed. In order to get uniform dispersion of filler in the matrix, two processing steps were applied in the preparation of conducting NR. Thermally reduced graphene oxide is also synthesised in the lab and incorporated in the NR matrix. This comprehensive study involves experimental and theoretical modelling of the properties of the NR/hybrid filler systems and are compared.

The ionic liquid modification of conductive carbon black and carbon nanotubes is carried out for homogeneous dispersion and to enhance the conductivity of NR. The modified fillers were characterised using FTIR and Raman spectroscopy. The appearance of characteristic peaks of IL in IL-modified fillers confirms the successful modification of CCB and CNT. Morphological studies using SEM showed that IL modification had decreased the aggregation of CCB, decreased the tube length, and increased the wall thickness of CNT. The FTIR spectra of the NR hybrid filler systems were also recorded, and NR peaks were identified. Rheological analysis of NR/hybrid filler systems revealed that the NR get adsorbed on the surface of fillers, and these physical and chemical interactions decrease the mobility of the polymer chains. Consequently, the viscosity and torque increase. Among different filler-incorporated systems, NR/CCB-CNT exhibit high torque values. It can be attributed to the nanosize and high aspect ratio of CNT, which increase the contact surface area of filler with NR. Mechanical properties of the hybrid filler systems are measured, and the modulus values are compared with various theoretical models, viz, the Rule of mixtures, Einstein's, Guth and Kerner. The tensile strength of the hybrid filler systems is compared with theoretical predictions using Nicolais-Narkis, Knori-

Geil and Turcsanyi models. It is to be noted that NR/CCB-CNT-syTRGO composite has a 77% increase in tensile strength due to the synergistic effect of hybrid fillers. The oxygen functional groups in syTRGO aid in better filler-filler and filler-matrix interactions, thereby increasing the reinforcement effect. Morphological analysis of tensile fracture surface helps to understand the failure mechanisms and dispersion of fillers. Viscoelastic studies of the composites are essential for NR applications involving dynamic loading at various temperatures. Different parameters like volume fraction of constrained region, reinforcing efficiency, and degree of entanglement were computed to understand the filler-matrix interactions during dynamic loading. Higher storage modulus values were obtained for the CCB-CNT filler-incorporated NR system.

The dielectric permittivity of hybrid filler systems increases upon the incorporation of conducting fillers. Maxwell-Wagner-Sillar polarisations are primarily responsible for the high dielectric permittivity at lower frequencies in hybrid filler-incorporated NR composites. The electromagnetic interference (EMI) shielding efficiency of the hybrid filler systems was analysed in a VNA analyser in the GHz range. All the fabricated NR/hybrid filler systems have the values corresponding to the commercial requirements for EMI shielding devices. NR/CCB-CNT-RGO hybrid filler systems have the highest EMI SE of 33.8 dB, while IL-modified CNT incorporated NR has 26.2 dB. Materials with a continuous connection in the conductive pathway and high dielectric constant are essential for EMI shielding devices. The interaction of surface groups of CCB, CNT and RGO, and π-π electron cloud interactions of fillers, are responsible for the continuous electron transport. For most NR systems, EMI shielding is primarily achieved through absorption. EMI shielding through absorption depends on the polarizability of the composites. The high surface area and increased charge carrier mobility of fillers enhance their interaction with EM waves. However, the presence of IL in the NR matrix increases the contribution of reflection to EMI shielding. The DC conductivity values indicate the formation of conducting networks in the polymer matrix, reaching values as high as 10^{-3} S/m for the NR/CCB-ILCNT system.

The incorporation of hybrid fillers reduces the solvent uptake and swelling index of the NR matrix. Reduced swelling characteristics of the hybrid filler systems are related to increased crosslink density. The structural characteristics and geometrical shape of hybrid filler effectively decrease the free volume in the polymer matrix and provide a tortuous pathway for the diffusing molecules. Theoretical models were applied to the diffusion data for a better understanding of the transport mechanism. Upon the computation of kinetic parameters of transport data, it is found that the Peppas-Sahlin model is in good agreement with experimental observations, which suggests that the transport mechanism is diffusion-controlled. Rubber—filler interaction parameters are computed and analysed from the swelling experiments using Kraus, Cunneen-Russel and Lorenz-Park equations.

The thermogravimetric analysis combined with various kinetic modelling studies has been utilised to investigate the thermal behaviour of NR hybrid filler systems. This comprehensive analysis explores the degradation mechanisms specific to NR composites. On analysing the degradation temperatures of the composites, IL-modified CNT-CCB and CCB-CNT-RGO incorporated composites exhibit higher thermal stability. Models such as the Coats-Redfern, Kissinger, KAS, and FWO have been applied to understand the thermal stability of NR-hybrid filler systems. NR containing IL-modified fillers and a hybrid system comprising CCB, CNT, and RGO exhibit elevated activation energy values. This suggests enhanced thermal stability for these systems. The increased thermal stability is attributed to a well-structured hybrid filler network within these composites. The aggregate structure of CCB chemically interacts with the ionic liquid and can interact with NR chains. Moreover, the barrier effect presented by the integrated filler system inhibits the migration of volatile compounds to the surface, which can decelerate the degradation process.

Hummer's method was employed for synthesising graphene oxide (GO), followed by thermal reduction in a muffle furnace to obtain thermally reduced graphene oxide (TRGO). Synthesised TRGO was characterised using FTIR, UV-visible, XPS, and Raman spectroscopy, along with XRD and morphological analysis. These characterisations confirmed the successful synthesis of TRGO, featuring some

oxygen functionalities on the surface and a limited number of graphene layers. Evaluation of NR/CCB-CNT hybrid filler systems with RGO and syTRGO fillers indicates enhanced properties for syTRGO. NR/CCB-CNT-syTRGO, hybrid filler systems, demonstrate superior mechanical and dielectric properties. The presence of oxygen functionalities increases the interactions with functional groups of CCB and CNT, resulting in enhanced reinforcement and an extensive conducting pathway in NR.

Chapter 10
Recommendations

- Integrating ionic liquid-modified fillers and CCB-CNT-RGO into NR composites meets the commercial requirements for EMI shielding materials. The potential commercialisation of these composites could lead to the development of stretchable and flexible EMI shielding devices.
- NR containing synthesised thermally reduced graphene oxide (syTRGO), CNT and CCB demonstrates high conductivity and dielectric constants. It also shows excellent mechanical properties. The application of such composites in EMI shielding devices holds promising prospects and is yet to be explored. Due to the synergistic effect of fillers with various morphology, NR containing these hybrid systems exhibits good solvent resistance; the oil resistance of the systems is to be studied in detail.
- Ionic liquid modification of the synthesised thermally reduced graphene oxide may be explored to improve the properties of NR composites, such as solvent resistance and EMI shielding effectiveness.

CURRICULUM VITAE

ABHISHA V S

Research scholar
Department of Chemistry
St. Joseph's College (Autonomous). Devagiri
Calicut, 673008, Kerala, India.
Phone: +91 9544145753
Email: abhishasivadasan@gmail.com

Permanent Address : Vakkoottil house,
Narikundu post
Anappara, Ambalavayal,
Wayand-673593, Kerala, India.

Personal Information

Gender	:	Female
Date of birth	:	12/09/1992
Nationality	:	Indian
Marital status	:	Married

Educational Summary

Present (2017-2024)	:	PhD Thesis submitted on January 2024 Chemistry, University of Calicut, Kerala, India
Topic	:	Experimental and Modelling Studies on the Properties of Natural Rubber Reinforced with Conductive Hybrid Filler Systems
Supervisor	:	Dr. Ranimol Stephen, Associate Professor, Department of Chemistry St. Joseph's College (Autonomous), Devagiri, Calicut – 673 008, Kerala, India
2013-2015	:	**Master of Science,** Chemistry 5th rank in University of Calicut, 3.64 [4 point scale], 91% St. Joseph's College (Autonomous), Devagiri, Calicut – 673 008, Kerala, India

2010-2013	:	**Bachelor of Science**, Chemistry 4th rank in University of Calicut, 3.94 [4 point scale], 98.5% St. Joseph's College (Autonomous), Devagiri, Calicut – 673 008, Kerala, India

Academic Achievements

- **UGC-JRF**, Rank 56, June 2016.
- Qualified **GATE-2016** (Rank-1839, Score of 389).
- **3rd position** in Project Presentation Contest for the PG students of Chemistry under the University of Calicut.
- **5th rank** in the University of Calicut in MSc Chemistry.
- Did 3 months MSc project on "Synthesis and Characterization of Magnetic Nanoparticles Through Polyol Process" at Materials Science And Technology Division, National Institute for Interdisciplinary Science and Technology (NIIST), CSIR, Thiruvananthapuram under the guidance of Dr.Manoj Raama Varma.
- **4th rank** in the University of Calicut in BSc Chemistry.

Research Experience

- Experienced in preparation, characterisation and properties of micro and nanocomposites.
- Experience in the synthesis of nanoparticles.

Project work Co-guided

- Biodegradable Polymers from Natural Resources: Isolation and Characterization. (2019)
- Thermal degradation studies of Hybrid filler incorporated Natural Rubber. (2018)
- Synergistic Effect of Halloysite Nanotube and Surface Modified Nanoclay Hybrid Filler System on the Mechanical Properties of Natural Rubber. (2018)

Instrumental / Experimental Skills

- Demonstrable expertise in the operation and application of AT-IR, UV-spectroscopy, Probe-Sonicator and TGA.
- Expertise in the synthesis of nanoparticles and their characterisation.
- Experienced in the preparation of polymer nanocomposites through different techniques.

Publications

- **Abhisha VS,** Sisanth KS, Thomas S, Stephen R. Kinetic studies on the transport behavior of hybrid filler incorporated natural rubber (NR). Express Polymer Letters. 2023;17(10):1070–80. DOI: 10.3144/expresspolymlett.2023.80
- **Abhisha, V. S**., Sisanth, K. S., Parameswaranpillai, J., Pulikkalparambil, H., Siengchin, S., Thomas, S., Stephen, R., Comprehensive experimental investigations and theoretical predictions on the physical properties of natural rubber composites. Journal of Applied Polymer Science. 2022, 139(47), e53197.
- **Abhisha V**, Augustine A, Joseph J, Thomas SP, Stephen R. Effect of halloysite nanotubes and organically modified bentonite clay hybrid filler system on the properties of natural rubber. Journal of Elastomers & Plastics. 2020;52(5):432-452. doi:10.1177/0095244319865573
- **Abhisha VS,** Stephen R. Optical Properties of Carbon Nanotubes. In: Abraham J, Thomas S, Kalarikkal N, editors. Handbook of Carbon Nanotubes Cham: Springer International Publishing; 2021. p. 1–18.
- **Vakkoottil S. Abhisha**, Valiya P. Swapna, Ranimol Stephen. Modern Trends and Applications of Gas Transport Through Various Polymers. In: Thomas S, Wilson R, Kumar A, George SC, editors. Transport properties of polymeric membranes. Elsevier; 2017 Nov 20.
- Swapna VP, Kaliyathan AV, **Abhisha VS**, Maria HJ, Nambissan PMG, Thomas S, et al. Changes in free volume and gas permeation properties of poly(vinyl alcohol) nanocomposite membranes modified using cage-structured polyhedral oligomeric silsesquioxane. Journal of Applied Polymer Science. 2021 Mar 10;138(10):49953.
- Swapna VP, Krishnan M**, Abhisha VS**, Stephen R. Efficient cage structured polyhedral oligomeric silsesquioxane embedded poly(vinyl alcohol) membranes: Thermal degradation and mechanical stability in hydrated condition. Journal of Applied Polymer Science.2021 Dec 10;138(46):51377.
- Swapna VP, **Abhisha VS**, Stephen R. 9 - Polymer/polyhedral oligomeric silsesquioxane nanocomposite membranes for pervaporation. In: Thomas S, George SC, Jose T, editors. Polymer Nanocomposite Membranes for Pervaporation. Elsevier; 2020. p.201–29.

Research Awards

- **Best Paper Award** in the National Seminar "Frontiers in Chemical Sciences" (FCS 2024) organized by the Department of Chemistry, University of Calicut during 13th t0 15th February 2024.
- **Best Poster Award -Polymer** in 21st Prof. K.V. Thomas Endowment Seminar & 4th International Symposium on New Trends in Applied Chemistry sponsored by the ACS

Polymers on 7, 8 February 2023 Department of Chemistry, Sacred Heart College, Thevara, Kochi, India.

- **Second Prize in Poster Presentation** at the Third International Conference on "Nanomaterials: Synthesis, Characterization and Applications" by International and inter University Centre for Nanoscience and Nanotechnology, Mahatma Gandhi University, Kerala, India during 11, 12 and May 2018.
- **Rev.Fr.Kappulumakkal CMI endowment for Best Paper** published in the year 2019-2020 from St.Joseph's College (Autonomous), Devagiri, Calicut.
- **Best Poster Award** in the Emerging Frontiers in Chemical Sciences EFCS-2018 held during 23-25 November 2018 at Farook College, Calicut.

Papers Presented in Conferences

- **Presented poster** in the **Emerging Frontiers in Chemical Sciences EFCS-2023, International Conference** held on 19-21 December 2023 at Farook College, Calicut.
- **Presented a paper** at the **International Conference** on Advances in Material Science and Chemistry ICAMSC-2020 0n 10-12 August 2020 conducted by the Department of Chemistry, Amrita Viswha Vidyapeedam, Amritapuri Campus.
- **Presented poster** at the **107th Indian Science Congress 2020 (ISC-2020)** held from 3-7 January 2020 at the University of Agricultural Sciences in Bengaluru, Karnataka.
- **Presented a paper** at the **29TH Swadeshi Science Congress National Seminar** on Conductive Carbon Black Reinforced Natural Rubber Composites: Dielectric and Mechanical Properties **o**n 9-10 November 2019 at ICAR, Kasargod.
- **Delivered contributory lecture** at the RUSA funded Conference 'National Conference on Materials Chemistry NCMC-'19 on 9-10 December 2019 organized by the Department of Chemistry, St.Joseph's College (Autonomous), Devagiri, Calicut.
- **Presented poster** in the **Emerging Frontiers in Chemical Sciences EFCS-2019** held on 13-15 December 2019 at Farook College, Calicut.
- **Presented a paper** titled "Synergistic effect of Conductive Carbon Black (CCB)/Multiwalled Carbon nanotubes (MWCNT) hybrid filler system on the properties of Natural Rubber" at the RUSA-funded **International Conference on Frontiers of Material Science (FOMS-19)** 0n 16-18 December 2019 hosted by Department of Physics, St.Joseph's College (Autonomous), Devagiri, Calicut.
- **Presented poster** in the Emerging Frontiers in Chemical Sciences **EFCS-2017** held on 23-25 September 2017 at Farook College, Calicut.

Conferences and workshops attended

- Attended webinar on 'Macromolecular Evaluations Using Rheological Techniques' on 9th July 2020 organized by the Postgraduate and Research Department of Chemistry Farook college (Autonomous) Calicut.
- Participated in the webinar '100 Years of Polymer Science- From Past to Future' by Prof. (Dr.) Sabu Thomas, Hon'ble Vice Chancellor, Mahatma Gandhi University, Kottayam, Kerala, India organized by the Department of Chemistry, St. Joseph's College (Autonomous) Devagiri, Calicut, Kerala, India on September 9th, 2020.
- Participated at the International Virtual Conference on Advanced Nanomaterials Applications (VCAN 2020) organized by the Centre for Nanotechnology Research (CNR), Vellore Institute of Technology, Vellore, held during 17th-19th June 2020.
- Participated in the live webinar on Graphene- A wonder material organized by the Department of Science and Humanities, Vedavyasa Institute of Technology, Karad on 15th June 2020.
- Participated in the National webinar on Strategies to enhance the quality of research in the context of NAAC and NIRF jointly organized by Internal Quality Assurance Cell, Library Committee and Alumni of All Saints' College, Thiruvananthapuram on 5th June, 2020
- Participated in the Seminar on Technological Initiatives and Strategies: A Global Perspective organized by Department of Chemistry, St. Joseph's College (Autonomous), Devagiri, Calicut on 5th July 2019.
- Participated in the Preconference workshop in Research Methodologies in Chemistry on 21st August 2019 organized by the Department of Chemistry, MESMAC Centre for Interdisciplinary Studies, DGMMES Mampad College.
- Completed faculty development Programme on Functional materials and devices conducted from 10^{th} to 15^{th} September, 2018 by the Department of Chemistry, national Institute of Technology, Calicut.
- Participated in TEAM 2017- Three Day National Seminar on Theoretical and Experimental Approaches for Exploring Advanced Materials jointly organized by Department of Physics & Department of Chemistry, Govt. Arts & Science College, Kozhikode held on 13^{th}, 14^{th} & 15^{th} December 2017.

Express Polymer Letters Vol.17, No.10 (2023) 1070–1080
Available online at www.expresspolymlett.com
https://doi.org/10.3144/expresspolymlett.2023.80

Research article

Kinetic studies on the transport behavior of hybrid filler incorporated natural rubber (NR)

Vakkoottil Sivadasan Abhisha[1], *Krishanagegham Sidharathan Sisanth*[2], *Sabu Thomas*[2,3], *Ranimol Stephen*[1*]

[1]Department of Chemistry, St. Joseph's College (Autonomous), Devagiri, Affiliated to University of Calicut, 673008 Calicut, Kerala, India
[2]International and Inter University Centre for Nanoscience and Nanotechnology (IIUCNN), Mahatma Gandhi University, P.D. Hills, 686560 Kottayam, Kerala, India
[3]School of Energy Materials, Mahatma Gandhi University, P.D. Hills, 686560 Kottayam, Kerala, India

Received 5 April 2023; accepted in revised form 11 July 2023

Abstract. Conductive carbon black (CCB), carbon nanotubes (CNT) and its hybrids are introduced into the natural rubber (NR) matrix aiming to explore the effect of filler ratio on the transport properties. Solvent transport of NR is found to decrease for hybrid filler systems as compared to single filler incorporated systems. Kinetic parameters of solvent transport behavior of filled NR systems are analyzed using various kinetic models. Upon the computation of kinetic parameters of transport data, it is found that the Peppas-Sahlin model is in good agreement with experimental observations, which suggests that the transport mechanism is diffusion controlled. Rubber–filler interaction parameters are computed and analyzed from the swelling experiments using Kraus, Cunneen-Russel, and Lorenz-Park equations.

Keywords: *crosslinking, curing, elastomer, filler, natural rubber, vulcanization, carbon black, transport properties*

1. Introduction

The role of polymer composites in the field of membrane technology demands a comprehensive understanding and in-depth knowledge of the transport behavior of solvents in the composite matrix. The transport properties of solvents in polymer composites are related to the distribution and reinforcement of fillers in the matrix. Polymer composites are widely used as food packaging materials owing to their intrinsic qualities such as corrosion resistance, lightweight, enhanced mechanical properties, and thermal properties [1]. Polymer composites containing chemically modified fillers empower the production of highly efficient membranes for pervaporation, ultrafiltration, reverse osmosis, and gas separation [2–8].

The solvent uptake of polymer composites depends on the characteristics of fillers, temperature, morphology, type of solvent, free volume, and processing conditions [9]. The transport of solvents in polymers is also affected by crosslink density, free volume, and structure of the polymer. Polymer chain segmental motions have a crucial influence on the processes associated with the diffusion of molecules through the polymer matrix. Variation in polymer composition and structure directly affects the free volume content and distribution, which in turn affects the transport of matter. The transport processes are interdependent with the polymeric structure and segmental motion of polymer chains [10].

Natural rubber (NR) based polymer composites are widely used in the automotive, construction, and electrical industries and for various engineering applications. Modification of the rubber matrix by the addition of various fillers generates interesting changes

*Corresponding author, e-mail: ranistephen@gmail.com

Received: 3 May 2022 | Revised: 28 August 2022 | Accepted: 7 September 2022

DOI: 10.1002/app.53197

RESEARCH ARTICLE

Applied Polymer SCIENCE WILEY

Comprehensive experimental investigations and theoretical predictions on the physical properties of natural rubber composites

Vakkoottil Sivadasan Abhisha[1] | **Krishanagegham Sidharathan Sisanth**[2,3] | **Jyotishkumar Parameswaranpillai**[4] | **Harikrishnan Pulikkalparambil**[5] | **Suchart Siengchin**[5] | **Sabu Thomas**[2,6] | **Ranimol Stephen**[1]

[1]Department of Chemistry, St. Joseph's College (Autonomous), Devagiri, Affiliated to University of Calicut, Calicut, India

[2]School of Energy Materials and International and Inter University Centre for Nanoscience and Nanotechnology, Mahatma Gandhi University, Kottayam, India

[3]Department of Chemical Sciences, University of Johannesburg, Johannesburg, South Africa

[4]Department of Science, Faculty of Science & Technology, Alliance University, Bengaluru, India

[5]Department of Materials and Production Engineering, The Sirindhorn International Thai-German Graduate School of Engineering (TGGS), King Mongkut's University of Technology North Bangkok, Bangkok, Thailand

[6]School of Energy Materials and School of Chemical Sciences, Mahatma Gandhi University, Kottayam, India

Correspondence
Ranimol Stephen, Department of Chemistry, St. Joseph's College (Autonomous), Devagiri, Affiliated to University of Calicut, Calicut, Kerala-673008, India.
Email: ranistephen@gmail.com

Funding information
Rashtriya Uchchatar Shiksha Abhiyan, Grant/Award Number: A1/SJC/RUSA-SPD/MRP/42/2019; University Grants Commission (UGC), India

Abstract

Conducting elastomers are highly desirable in the present world because of their major applications in the electronic industry. Conductive carbon black (CCB) is a conventional reinforcing filler commonly used in elastomers to modify the mechanical as well as electrical properties. The present study focuses on the experimental and theoretical computation of filler reinforcement, dielectric, mechanical, dynamic mechanical, and surface morphology of natural rubber (NR)/CCB composites. Two step processing method is adopted to attain homogeneous dispersion of filler in the matrix: preparation of NR/CCB masterbatch through melt mixing using internal mixer followed by compounding in a two- roll mill. Improved DC conductivity in the order of 10^{-6} was obtained at higher filler loading indicating the formation of a continuous conductive network in the matrix. Percolation threshold was computed using Power law equation and obtained a value of 0.154 vol%. Theoretical predictions of mechanical modulus and tensile strength were done using rule of mixtures, Einstein, Guth and Kerner models and Nicolais-Narkis and Kuneri-Geil models respectively. A remarkable change in tensile strength is observed for NR as a function of the weight percentage of CCB; it is increased to 26.3 ± 0.9 MPa at 20 phr CCB from 17.1 ± 0.9 MPa for NR.

KEYWORDS

dielectric properties, glass transition, microscopy, molding, rubber

Article

JOURNAL OF ELASTOMERS & PLASTICS

Journal of Elastomers & Plastics
1–21

DOI: 10.1177/0095244319865573
journals.sagepub.com/home/jep
SAGE

Effect of halloysite nanotubes and organically modified bentonite clay hybrid filler system on the properties of natural rubber

Abhisha VS[1], Aneeta Augustine[1], Jesna Joseph[1], Selvin P Thomas[2] and Ranimol Stephen[1]

Abstract

The versatility and potential have framed natural rubber (NR) nanocomposites as the focal point in the polymer research field and industry. Currently, NR nanocomposites filled with hybrid nanostructures is an interesting area than single filler or conventional filler systems. Halloysite nanotube (HNT) and bentonite clay are well-studied potential fillers of polymers. This work is an attempt to study the effect of hybrid filler system of HNT and organically modified bentonite nanoclay (NC) in the properties of NR. NR/HNT-NC systems with varied filler concentrations were prepared in a two-roll mixing mill. Properties such as cure characteristics, morphology, mechanical, thermal, and transport behavior were analyzed in detail. The prepared composites had better wear properties than gum vulcanizates. Improvement in physical properties was observed due to the increased contact surface area between the filler and the matrix. The nanocomposite with 2 wt% hybrid filler shows a 31% decrease in abrasion loss compared to neat NR composite. Apparently, 4 wt% of hybrid filler could improve modulus at 300% strain and tear by approximately 57% and 14%, respectively. The ability to withstand high strain was evident from the improved crack growth resistance as observed in micrographs. Lorenz–Park plots were employed to analyze the rubber–filler interaction. The activation energy of thermal degradation was calculated using Coats–Redfern equation.

[1] Department of Chemistry, St. Joseph's College (Autonomous), Devagiri, Affiliated to University of Calicut, Calicut, Kerala, India
[2] Advanced Materials Laboratory of Yanbu Research Center and Department of Chemical Engineering Technology, Royal Commission for Yanbu-Colleges and Institutes, Yanbu Industrial City, Kingdom of Saudi Arabia

Corresponding author:
Ranimol Stephen, Department of Chemistry, St. Joseph's College (Autonomous), Devagiri, Affiliated to University of Calicut, Calicut 673 008, Kerala, India.
Email: ranistephen@gmail.com